IL
NUOVO CIMENTO
ORGANO DELLA SOCIETÀ ITALIANA DI FISICA
SOTTO GLI AUSPICI DEL CONSIGLIO NAZIONALE DELLE RICERCHE

VOL. XIII, N. 4 *Serie decima* 16 Agosto 1959

On the Lorentz-Invariant Approximation Method in General Relativity.

III. – The Einstein-Maxwell Field.

R. P. KERR

King's College - London

(ricevuto il 28 Novembre 1958)

Summary. — In this paper, the methods of the first two papers of this series have been extended to the Einstein-Maxwell field. It is shown that it is possible to set up a consistent Lorentz-invariant approximation procedure without it being necessary to expand the particle parameters, such as the mass and the charge. By using an invariant Green's function, we have calculated an integral expression for the field. This is a solution of the Einstein-Maxwell field equations, provided that the differential equations of motion, mass, charge, and spin are satisfied for each particle. The result does not depend on the degree of complexity of the first order solution. We have shown that the electromagnetic self forces which appear in the second approximation are significant, whereas it is necessary to go to the fourth approximation before it can be shown that the corresponding gravitational self forces are real and do not disappear in the higher approximations. Also, we have shown that the mass is conserved to the second approximation, but that the charge is not.

---

1. – Introduction.

In this paper we shall show that it is possible to set up a consistent Lorentz-covariant approximation procedure for solving the Einstein-Maxwell field equations. The method used will be completely analogous to that used in papers (I)

and (II) of this series for the pure gravitational field (*). We shall find that as well as the seven differential equations of motion, mass and spin, there is a further equation, that of charge, which must be satisfied by the parameters of each particle.

As in (I), we shall consider the field outside a set of particles whose parameters we label with a superscript p. We take a representative world line, $\overset{p}{z}{}^{\mu}(\overset{p}{s})$ (**), inside each particle, and then define the surfaces, S^p, by the following conditions: we define the functions $\gamma^{\mu}(x)$ and $s(x)$, in the vicinity of the p-th world line, by

$$x^{\mu} = z^{\mu}(s(x)) + \gamma^{\mu}(x)\,, \qquad v_p \gamma^p = 0\,, \tag{1.1}$$

and then S^p is defined by the equation

$$(\gamma, \gamma) \equiv \gamma_{\varrho}\gamma^{\varrho} \equiv \eta_{\alpha\beta}\gamma^{\alpha}\gamma^{\beta} = -a^2\,,$$

where a is the radius of the cylinders. We shall assume that the field is weak in the region, V, outside the S^p and that it is asymptotically Galilean at spatial infinity.

The Einstein-Maxwell field equations may be written as

$$\mathfrak{G}^{\mu\nu} = \mathfrak{T}^{\mu\nu}\,, \tag{1.2}$$

$$\varepsilon^{\mu\alpha\beta\gamma} F_{\underset{\sim}{\alpha\beta},\gamma} = 0\,, \tag{1.3}$$

$$\mathfrak{D}^{\mu} = (\sqrt{-g}\, F^{\underset{\sim}{\mu\alpha}})_{,\alpha} = 0\,, \tag{1.4}$$

where the electromagnetic energy-momentum tensor is given by

$$\mathfrak{T}^{\mu\nu} = \tfrac{1}{4}\mathfrak{g}^{\mu\nu} F_{\underset{\sim}{\alpha\beta}} F^{\underset{\sim}{\alpha\beta}} - \mathfrak{g}_{\alpha\beta} F^{\underset{\sim}{\mu\alpha}} F^{\underset{\sim}{\nu\beta}}\,. \tag{1.5}$$

Because we have assumed that the metric tensor is approximately Galilean

---

(*) R. P. KERR: *Nuovo Cimento*, **13**, 469, 492 (1959), referred to in the following as (I) and (II) respectively.

(**) The world line parameter, p, is defined by $(\mathrm{d}s)^2 = \eta_{\alpha\beta}\mathrm{d}z^{\alpha}\mathrm{d}z^{\beta}$, where $\eta_{\alpha\beta}$ is the Galilean metric tensor with signature $(+, -, -, -)$. We shall denote differentiation with respect to s by a dot, *e.g.* $\dot{v}_{\mu} = \mathrm{d}/\mathrm{d}s\,(v^{\mu})$, where $v^{\mu} = \dot{z}^{\mu}$.

in the region V, we may solve (1.3),

$$F_{\mu\nu} = \varphi_{\nu,\mu} - \varphi_{\mu,\nu} . \tag{1.6}$$

As the fundamental electromagnetic potential, we take

$$\Phi^{\mu} = \mathfrak{g}^{\mu\alpha}\varphi_{\alpha}$$

and then we may express $\mathfrak{D}^{\mu}$ as

$$\mathfrak{D}^{\mu} = (-\Box\Phi^{\mu} + \mathfrak{H}^{\mu}) + \mathfrak{Q}^{\mu} , \tag{1.7}$$

where

$$-\Box\Phi^{\mu} + \mathfrak{H}^{\mu} \equiv -g^{\alpha\beta}\Phi^{\mu}{}_{,\alpha\beta} - g^{\alpha\beta}\mathfrak{g}^{\mu\rho}{}_{,\alpha\beta}\varphi_{\rho} + \\ + (\sqrt{-g}_{,\nu}g^{\nu\alpha}g^{\mu\beta} + g^{\mu\alpha}{}_{,\nu}\mathfrak{g}^{\nu\beta} - \mathfrak{g}^{\alpha\beta}{}_{,\nu}g^{\mu\nu} + g^{\nu\alpha}\mathfrak{g}^{\mu\beta}{}_{,\nu})\varphi_{\beta,\alpha} , \tag{1.8}$$

$$\mathfrak{Q}^{\mu} \equiv -g^{\mu\alpha}\Phi^{\nu}{}_{,\nu\alpha} - \mathfrak{g}^{\beta\nu}{}_{,\nu\alpha}g^{\mu\alpha}\varphi_{\beta} - \mathfrak{g}^{\alpha\nu}{}_{,\nu}g_{\beta,\alpha} . \tag{1.9}$$

φ_{μ} is not defined uniquely by (1.5) since $F_{\mu\nu}$ is invariant under a *gauge transformation*

$$\varphi_{\beta} \to \varphi^{*}_{\beta} = \varphi_{\beta} + S_{,\beta} .$$

Provided that the field satisfies the usual boundary conditions at infinity and that $\mathfrak{g}^{\mu\nu}$ is weak in V, we can always choose S so that

$$\Phi^{\mu}{}_{;\mu} \equiv \Phi^{\mu}{}_{,\mu} = 0 . \tag{1.10}$$

This is not true for a general Riemannian manifold, but it does not restrict the generality of the solutions obtained by the method of this paper.

From (I), we may write the gravitational field equations as

$$-\tfrac{1}{2}\Box\mathfrak{g}^{\mu\nu} + \Lambda^{\mu\nu} + \tfrac{1}{2}Z^{\mu\nu} = \mathfrak{T}^{\mu\nu} , \tag{1.11}$$

where

$$\tfrac{1}{2}Z^{\mu\nu} \equiv \mathfrak{g}^{\alpha\varrho}{}_{,\varrho}P^{\mu\nu}_{\alpha} + \mathfrak{g}^{\alpha\varrho}{}_{,\varrho\beta}P^{\mu\nu;\beta}_{\alpha} .$$

If we restrict the co-ordinate system to satisfy the De Donder co-ordinate conditions.

$$\mathfrak{g}^{\mu\nu}{}_{,\nu} = 0 \,, \tag{1.12}$$

then the *reduced* gravitational field equations may be written as

$$-\tfrac{1}{2}\Box\mathfrak{g}^{\mu\nu} + \Lambda^{\mu\nu} = \mathfrak{T}^{\mu\nu} \,.$$

Similarly, since $\mathfrak{Q}^{\mu}$ is zero for fields satisfiyng (1.10) and (1.12), we may write the *reduced* electromagnetic equations as

$$\Box\Phi^{\mu} = \mathfrak{H}^{\mu} \,.$$

2. – Identities.

We shall need the following tensor identity equations, Firstly, we have the Bianchi identities,

$$\mathfrak{G}^{\mu\nu}{}_{,\nu} + \Gamma^{\mu}_{\alpha\beta}\,\mathfrak{G}^{\alpha\beta} \equiv 0 \,. \tag{2.1}$$

Also, from the definition of $\mathfrak{D}^{\mu}$ in (1.4) as a tensor density,

$$\mathfrak{D}^{\mu}{}_{;\mu} \equiv \mathfrak{D}^{\mu}{}_{,\mu} \equiv (\sqrt{-g}F^{\underset{\sim}{\mu\nu}})_{,\nu,\mu} \equiv 0 \,. \tag{2.2}$$

If we express $\mathfrak{T}^{\mu\nu}$ as a function of Φ^{μ} and $\mathfrak{g}^{\mu\nu}$, we have

$$\begin{aligned}\mathfrak{T}^{\mu\nu}{}_{;\nu} &\equiv \tfrac{1}{2}\,\mathfrak{g}^{\mu\nu}F_{\underset{\sim}{\alpha\beta};\nu}\cdot F^{\underset{\sim}{\alpha\beta}} - \mathfrak{g}_{\alpha\beta}F^{\underset{\sim}{\mu\alpha}}{}_{;\nu}\cdot F^{\underset{\sim}{\nu\beta}} - \mathfrak{g}_{\alpha\beta}F^{\underset{\sim}{\mu\alpha}}\cdot F^{\underset{\sim}{\nu\beta}}{}_{;\nu} \\ &\equiv \tfrac{1}{2}\,\mathfrak{g}^{\mu\nu}(F_{\underset{\sim}{\alpha\beta};\nu} + F_{\underset{\sim}{\beta\nu};\alpha} + F_{\underset{\sim}{\nu\alpha};\beta})F^{\underset{\sim}{\alpha\beta}} - \mathfrak{g}_{\alpha\beta}F^{\underset{\sim}{\mu\alpha}}F^{\underset{\sim}{\mu\beta}}{}_{;\nu} \,.\end{aligned}$$

The bracketed term is identically zero for an $F_{\underset{\sim}{\mu\nu}}$ given by (1.6), and so

$$\mathfrak{T}^{\mu\nu}{}_{;\nu} \equiv g_{\alpha\beta}F^{\underset{\sim}{\mu\alpha}}\mathfrak{D}^{\beta} \,, \tag{2.3}$$

for arbitrary Φ^{μ} and $\mathfrak{g}^{\mu\nu}$.

3. – Approximation method.

As shown in Sect. **1**, the Einstein-Maxwell field equations are equivalent to

$$\Box \mathfrak{g}^{\mu\nu} = 2(\Lambda^{\mu\nu} - \mathfrak{T}^{\mu\nu}) , \tag{3.1}$$

$$\Box \Phi^{\mu} = \mathfrak{H}^{\mu} , \tag{3.2}$$

$$\mathfrak{g}^{\mu\nu}{}_{,\nu} = 0 , \tag{3.3}$$

$$\Phi^{\mu}{}_{,\mu} = 0 , \tag{3.4}$$

and it will be this set of equations that we shall consider in the remainder of this paper. The right hand sides of (3.1, 2) are non-linear functions of Φ^{α} and $h^{\alpha\beta}$, where

$$\mathfrak{g}^{\mu\nu} = \eta^{\mu\nu} + h^{\mu\nu} .$$

If we write the field as a power series in an indeterminate parameter, λ,

$$\mathfrak{g}^{\mu\nu}(\lambda) = \eta^{\mu\nu} + \sum_{r>0} \lambda^r \underset{r}{h}{}^{\mu\nu} ,$$

$$\Phi^{\mu}(\lambda) = \sum_{r>0} \lambda^r \cdot \underset{r}{\Phi}{}^{\mu} ,$$

expand the *reduced* field equations, (3.1, 2), in powers of λ, and then equate the coefficient of λ^n to zero, we obtain the set of approximation equations,

$$\Box \underset{n}{h}{}^{\mu\nu} = 2(\underset{n}{\Lambda}{}^{\mu\nu} - \underset{n}{\mathfrak{T}}{}^{\mu\nu}) , \tag{3.5}$$

$$\Box \underset{n}{\Phi}{}^{\mu} = \underset{n}{\mathfrak{H}}{}^{\mu} . \tag{3.6}$$

$\underset{n}{\Lambda}{}^{\mu\nu}$ and $\underset{n}{\mathfrak{H}}{}^{\mu}$ are functions of the lower order fields. To each convergent set of solutions of these equations there corresponds a solution of (3.1, 2), *i.e.*

$$\mathfrak{g}^{\mu\nu} = \eta^{\mu\nu} + \underset{1}{h}{}^{\mu\nu} + \underset{2}{h}{}^{\mu\nu} + \ldots$$

$$\Phi^{\mu} = \underset{1}{\Phi}{}^{\mu} + \underset{2}{\Phi}{}^{\mu} + \ldots .$$

2249

However, this will only be a solution of the Einstein-Maxwell field equations provided that the coordinate and gauge conditions (3.3, 4) are satisfied. These may either be satisfied *exactly* in every approximation,

$$(3.7) \qquad \underset{n}{h}^{\mu\nu}{}_{,\nu} = 0\,, \qquad \underset{n}{\Phi}^{\mu}{}_{,\nu} = 0\,,$$

or else we may require the *total field to the n-th approximation*,

$$(3.8) \qquad \underset{(n)}{\mathfrak{g}}^{\mu\nu}{}_{,\nu} = \eta^{\mu\nu} + \underset{(n)}{h}^{\mu\nu} = \eta^{\mu\nu} + \sum_{1}^{n} \underset{r}{h}^{\mu\nu}\,, \qquad \underset{(n)}{\Phi}^{\mu} = \sum_{1}^{n} \underset{r}{\Phi}^{\mu}\,,$$

to satisfy them *to the same approximation*. We shall write this as

$$(3.9) \qquad \underset{(n)}{g}^{\mu\nu}{}_{,\nu} \sim 0\,, \qquad \underset{(n)}{\Phi}^{\mu}{}_{,\mu} \sim 0\,.$$

In Sect. 4, we shall show that it is possible to satisfy the « strong » gauge conditions, (3.7), in every approximation, but that we have to « expand » the mass, spin, dipole and charge parameters to do so. In the next section we shall show that this expansion is not necessary if we use the « weak » form of the co-ordinate and gauge conditions, (3.9) (*).

4. – The « strong » form of the gauge conditions.

Let us suppose that (3.5-7) are satisfied *exactly* for all $r < n$, and that $\overset{*}{\underset{n}{h}}{}^{\mu\nu}$ and $\overset{*}{\underset{n}{\Phi}}{}^{\mu}$ are particular solutions of the field equations in the n-th approximation. The most general solution of the field equations will then be

$$(4.1) \qquad \underset{n}{h}^{\mu\nu} = \overset{*}{\underset{n}{h}}{}^{\mu\nu} + 4\,\underset{n}{U}^{\mu\nu}\,, \qquad \underset{n}{\Phi}^{\mu} = \overset{*}{\underset{n}{\Phi}}{}^{\mu} + \underset{n}{\chi}^{\mu}\,,$$

where

$$(4.2) \qquad \Box \underset{n}{U}^{\mu\nu} = 0\,, \qquad \Box \underset{n}{\chi}^{\mu} = 0\,.$$

From the corollary to the theorem in Appendix A,

$$(\underset{n}{\Lambda}^{\mu\nu} - \underset{n}{\mathfrak{T}}^{\mu\nu})_{,\nu} = 0\,, \qquad \underset{n}{\mathfrak{H}}^{\nu}{}_{,\nu} = 0$$

(*) We shall refer to both the coordinate and gauge conditions as gauge conditions.

and so, if we take the ordinary divergence of (3.5, 6),

$$\Box \overset{*}{h}_{n}^{\mu\nu}{}_{,\nu} = 0 , \qquad \Box \overset{*}{\Phi}_{n}^{\nu}{}_{,\nu} = 0 .$$

In (I) we showed that this implies that

(4.3) (*)
$$\begin{cases} \overset{*}{h}_{n}^{\mu\nu}{}_{;\nu} = \sum_{p,t} \int \overset{p}{k}_{n}^{\mu:(\alpha)_t} D(r-z)_{,(\alpha)_t} \, \mathrm{d}s , \\ \overset{*}{\Phi}_{n}^{\nu}{}_{;\nu} = \sum_{p,t} \int \overset{p}{j}_{n}^{(\alpha)_t} \cdot D\,(r-z)_{,(\alpha)_t} \mathrm{d}s , \end{cases}$$

where the $\overset{p}{k}_{n}^{\mu:(\alpha)_t}$ and $\overset{p}{j}_{n}^{(\alpha)_t}$ are completely symmetric in the α_i, and

$$\overset{p}{v}_{\alpha_i} \overset{p}{k}_{n}^{\mu:\alpha_1 \ldots \alpha_t} = 0 , \qquad \overset{p}{v}_{\alpha_i} \overset{p}{j}_{n}^{\alpha_1 \ldots \alpha_t} = 0 .$$

We considered in detail in (I) the problem of whether we could satisfy the co-ordinate conditions for $h^{\mu\nu}$ by a suitable choice of $U^{\mu\nu}$. We found that if we take

(4.4) (**)
$$4 \overset{}{U}_{n}^{\mu\nu} = \sum_{p} \int (4 \overset{p}{m}_{n} \overset{p}{v}^{\mu} \overset{p}{v}^{\nu} - 8 \overset{p}{D}_{n}^{(\mu} \overset{p}{v}^{\nu)} - 4 \overset{p}{D}_{n}^{(\mu} \overset{p}{v}^{\nu)} - \overset{p}{k}_{n}^{(\mu;\nu)} -$$

$$- v_{\alpha} \overset{p}{k}_{n}^{\alpha:(\mu} \overset{p}{v}^{\nu)}) \, D(r-z) \mathrm{d}s + 4 \sum_{p} \int (2 \overset{p}{v}^{(\mu} \cdot \overset{p}{\underset{\sim}{S}}_{n}^{\nu)\alpha} + \overset{p}{D}_{n}^{\alpha} \cdot \overset{p}{v}^{\mu} \cdot \overset{p}{v}^{\mu}) D(r-z)_{,\alpha} \, \mathrm{d}s -$$

$$- \sum_{p,t} \int (\overset{p}{k}_{n}^{\mu:\varrho\nu(\alpha)_t} + \overset{p}{k}_{n}^{\nu:\varrho\mu(\alpha)_t} - \overset{p}{k}_{n}^{\varrho:\mu\nu(\alpha)_t}) D(r-z)_{,\varrho\alpha_t} \cdot \mathrm{d}s ,$$

where

(4.5)
$$\overset{p}{v}_{\alpha} \overset{p}{\underset{\sim}{S}}^{\mu\alpha} = 0 , \qquad \overset{p}{v}_{\alpha} \overset{p}{D}^{\alpha} = 0 ,$$

(*) As in (I), we use the following notation, $j^{(\alpha)_t} \cdot D_{,(\alpha)_t} = j^{\alpha_1 \ldots \alpha_t}$. $D_{,\alpha_1 \ldots \alpha_t} D(x)$ is an invariant Green's function.

(**) We use the notation, $2A^{[\mu}B^{\nu]} = A^{\mu}B^{\nu} - A^{\nu}B^{\mu}$, $2A^{(\mu}B^{\nu)} = A^{\mu}B^{\nu} + A^{\nu}B^{\mu}$.

then the co-ordinate conditions are satisfied exactly in the n-th approximation, provided that

$$\frac{\mathrm{d}}{\mathrm{d}s}\left(\overset{p}{m}\overset{p}{v}^{\mu}-\overset{p}{\dot{D}}^{\mu}-2\overset{p}{S}^{\mu\varkappa}\dot{\overset{p}{v}}_{\alpha}\right)=-\frac{1}{4}\overset{p}{k}^{\mu}+\frac{1}{4}\frac{\mathrm{d}}{\mathrm{d}s}\left(\overset{p}{v}_{\alpha}\overset{p}{k}^{\alpha;\mu}\right), \tag{4.6}$$

$$\frac{\mathrm{d}}{\mathrm{d}s}\left(\overset{p}{S}^{\mu\nu}\right)+2\cdot\overset{p}{S}^{\alpha[\nu}\overset{p}{v}^{\mu]}\cdot\dot{\overset{p}{v}}_{\alpha}=-\frac{1}{4}\overset{p}{k}^{[\mu;\nu]}-\frac{1}{4}\overset{p}{v}_{\alpha}\overset{p}{k}^{\alpha;[\mu}\overset{p}{v}^{\nu]}. \tag{4.7}$$

Similarly, if we write

$$\overset{}{\chi}^{\mu}=\sum_{p}\int\overset{p}{e}\cdot\overset{p}{v}^{\mu}D(r-z)\,\mathrm{d}s-\sum_{p,t}\int\overset{p}{j}^{\mu(\alpha)_t}\cdot D(r-z)_{,(\alpha)_t}\cdot\mathrm{d}s\,,$$

then

$$\Phi^{\mu}_{,\mu}=\sum_{p}\int\overset{p}{j}\cdot D(r-z)\,\mathrm{d}s+\sum_{p}\int\overset{p}{e}\cdot\overset{p}{v}^{\mu}\cdot D(r-z)_{,\mu}\,\mathrm{d}s=$$

$$=\sum_{p}\int\left(\overset{p}{j}+\frac{\mathrm{d}}{\mathrm{d}s}\left(\overset{p}{e}\right)\right)D(r-z)\cdot\mathrm{d}s\,,$$

so that the gauge conditions are satisfied, provided that the charge parameters satisfy the first order differential equations,

$$\frac{\mathrm{d}}{\mathrm{d}s}\left(\overset{p}{e}\right)=-\overset{p}{j}\,, \tag{4.8}$$

which gives the equation of charge in each approximation. Just as for $h^{\mu\nu}$, we cannot remove the monopole term in a purely algebraic way by the addition of a further solution of the wave equation.

5. – The « weak » gauge conditions and the equations of motion.

In (I) we showed that if we used the « weak » form of the gauge and co-ordinate conditions we did not need to expand the particle parameters. We shall now show that it is possible to prove the same theorem for the Einstein-Maxwell field, and we shall define the *physical* equations of motion, spin, mass and charge by induction on the reiteration order, n.

The most general solution of (3.5, 6), outside the surfaces, S^p, is

$$(5.1)\quad \underset{(r)}{h^{\mu\nu}} = \frac{1}{4\pi}\int_V 2(\underset{(r)}{\Lambda^{\mu\nu}} - \underset{(r)}{\mathfrak{T}^{\mu\nu}})(r')\cdot D(r-r')\,\mathrm{d}^4r' - \sum_p \int^p [\overset{p}{\underset{(r)}{k}}{}^{(\mu;\nu)} + \overset{p}{\underset{(r)}{k}}{}^{\alpha;(\mu}v^{\nu)}v_\alpha] D(r-z)\,\mathrm{d}s -$$

$$- \sum_{p\,t}\int^p [\overset{p}{\underset{(r)}{k}}{}^{\mu;\varrho\nu(\alpha)_t} + \overset{p}{\underset{(r)}{k}}{}^{\nu;\varrho\mu(\alpha)_t} - \overset{p}{\underset{(r)}{k}}{}^{\varrho;\mu\nu(\alpha)_t}]\, D_{,\varrho(\alpha)_t} + 4\,\underset{(r)}{U}{}^{\mu,\nu},$$

$$(5.2)\quad \underset{(r)}{\Phi^\mu} = \frac{1}{4\pi}\int \underset{(r)}{\mathfrak{H}^\mu}(r')\,D(r-r')\,\mathrm{d}^4r' - \sum_{p,t}\int^p \overset{p}{\underset{(r)}{j}}{}^{\mu(\alpha)_t}\cdot D(r-z)_{,(\alpha)_t}\mathrm{d}s + \underset{(r)}{\chi^\mu},$$

where

$$(5.3)\quad \begin{cases} \overset{p}{\underset{(r)}{k}}{}^{\mu;(\alpha)_t} = \dfrac{(-)^t}{2\pi t!}\cdot\displaystyle\int^p (\underset{(r)}{\Lambda^{\mu\nu}} - \underset{(r)}{Z^{\mu\nu}})\cdot\gamma^{(\alpha)_t}(1-(\dot v,\gamma))\,\mathrm{d}^2S_\nu\,, \\ \overset{p}{\underset{(r)}{j}}{}^{(\alpha)_t} = \dfrac{(-)^t}{4\pi t!}\cdot\displaystyle\int^p \underset{(r)}{H^\mu}\cdot\gamma^{(\alpha)_t}(1-(\dot v,\gamma))\cdot\mathrm{d}^2S_\mu\,. \end{cases}$$

d^2S_ν is a two dimensional surface element on the intersection of S^p and the plane, $s(r) = \text{const}$. It has the same direction as γ_ν and is orthogonal to v^μ. $\underset{(r)}{U^\mu}$ and $\underset{(r)}{\chi^\mu}$ are solutions of the wave equation. If we take the divergence of (5.1, 2), we have

$$\underset{(r)}{h^{\mu\nu}}{}_{,\nu} = \frac{1}{2\pi}\cdot\int_V (\underset{(r)}{\Lambda^{\mu\nu}}{}_{,\nu} - \underset{(r)}{\mathfrak{T}^{\mu\nu}}{}_{,\nu})(r')\cdot D(r-r')\mathrm{d}^4r' + \sum_p \int_{S^p} (\underset{(r)}{\Lambda^{\mu\nu}} - \underset{(r)}{Z^{\mu\nu}})D(r-r')\,\mathrm{d}^3S'^p_\nu -$$

$$- \sum_p \int^p (\overset{p}{\underset{(r)}{k}}{}^{(\mu;\nu)} + v_\alpha \overset{p}{\underset{(r)}{k}}{}^{\alpha;(\mu}v^{\nu)})\, D_{,\nu}\cdot\mathrm{d}s - \sum_{p,t>1}\int^p \cdot\, \overset{p}{\underset{(r)}{k}}{}^{\mu;(\alpha)_t} D_{,(\alpha)_t}\cdot\mathrm{d}s + 4\,\underset{(r)}{U}{}^{\mu\nu}{}_{,\nu}\,.$$

If we expand $D(r-r')$ as a function of the γ^μ, about the point $z^\mu(s)$, we obtain, as in (I),

$$(5.4)\quad \underset{(r)}{h^{\mu\nu}}{}_{,\nu} = \frac{1}{2\pi}\cdot\int_V (\underset{(r)}{\Lambda^{\mu\nu}}{}_{,\nu} - \underset{(r)}{\mathfrak{T}^{\mu\nu}}{}_{,\nu})\,D(r-r')\cdot\mathrm{d}^4r' + \sum_p \int^p \left(\overset{p}{\underset{(r)}{k}}{}^{\mu} - \frac{\mathrm{d}}{\mathrm{d}s}(v_\alpha \overset{p}{\underset{(r)}{k}}{}^{\alpha;\mu})\right)\cdot D(r-z)\,\mathrm{d}s +$$

$$+ \sum_p \int^p (\overset{p}{\underset{(r)}{k}}{}^{[\mu;\nu]} + v_\alpha \overset{p}{\underset{(r)}{k}}{}^{\alpha;[\mu}v^{\nu]})\, D(r-r')_{,\nu}\cdot\mathrm{d}s\,.$$

If we assume that

$$4\,\underset{(r)}{U}{}^{\mu\nu}{}_{,\nu} = \sum_p \int \overset{p}{\underset{(r)}{\hat{k}}}{}^{\mu} \cdot D(r-r')\,\mathrm{d}s + \sum_p \int \overset{p}{\underset{(r)}{\hat{k}}}{}^{\mu\nu}_{\smile} \cdot D(r-r')_{,\nu} \cdot \mathrm{d}s\,,$$

where $\overset{p}{\underset{(r)}{\hat{k}}}{}^{\mu\nu}_{\smile} \cdot v_\nu = 0$, then we have

$$\underset{(r)}{\mathfrak{g}}{}^{\mu\nu}{}_{,\nu} = \frac{1}{2\pi} \cdot \int_V (\underset{(r)}{\Lambda}{}^{\mu\nu}{}_{,\nu} - \underset{(r)}{\mathfrak{T}}{}^{\mu\nu}{}_{,\nu}) D \cdot \mathrm{d}^4 r' + \sum_p \int \overset{p}{\underset{(r)}{k}}{}^{\mu} \cdot D \cdot \mathrm{d}s + \sum_p \int \overset{p}{\underset{(r)}{k}}{}^{\mu\nu}_{\smile} \cdot D_{,\nu}\,\mathrm{d}s\,, \tag{5.5}$$

where

$$\begin{cases} \overset{p}{\underset{(r)}{k}}{}^{\mu} = \overset{p}{\underset{(r)}{\overset{*}{k}}}{}^{\mu} - \dfrac{\mathrm{d}}{\mathrm{d}s}\left(\overset{p}{v}_{\alpha}\, \overset{p}{\underset{(r)}{\overset{*}{k}}}{}^{\alpha;\mu}\right) + \overset{p}{\underset{(r)}{\hat{k}}}{}^{\mu}\,, \\ \overset{p}{\underset{(r)}{k}}{}^{\mu\nu}_{\smile} = \overset{p}{\underset{(r)}{\overset{*}{k}}}{}^{[\mu;\nu]} + \overset{p}{v}_{\alpha}\, \overset{p}{\underset{(r)}{\overset{*}{k}}}{}^{\alpha;[\mu} v^{\nu]} + \overset{p}{\underset{(r)}{\hat{k}}}{}^{\mu\nu}_{\smile}\, \overset{p}{v}_{\alpha}\, \overset{p}{\underset{(r)}{k}}{}^{\mu\alpha}_{\smile} = 0\,. \end{cases} \tag{5.5'}$$

Also, if

$$\underset{(r)}{\chi}{}^{\mu}{}_{,\mu} = \sum_p \int \overset{p}{\underset{(r)}{\hat{j}}} \cdot D(r-r') \cdot \mathrm{d}s\,,$$

then we have, in a completely analogous way,

$$\Phi^{\mu}{}_{,\mu} = \frac{1}{4\pi} \cdot \int_V \underset{(r)}{\mathfrak{H}}{}^{\nu}{}_{,\nu} D(r-r') \cdot \mathrm{d}^4 r' + \sum_p \int \overset{p}{\underset{(r)}{j}} \cdot D(r-r') \cdot \mathrm{d}s\,, \tag{5.6}$$

where

$$\overset{p}{\underset{(r)}{j}} = \overset{p}{\underset{(r)}{\overset{*}{j}}} + \overset{p}{\underset{(r)}{\hat{j}}}\,. \tag{5.6'}$$

Now, let us suppose that $\underset{(r)}{\mathfrak{g}}{}^{\mu\nu}{}_{,\nu}$ and $\underset{(r)}{\Phi}{}^{\nu}{}_{,\nu}$ are *O_r-functions* for all $r < n$. By this we mean that they consist of a linear sum of terms each of which contains a $\underset{(s)}{k}{}^{\cdot\cdot}$ or $\underset{(s)}{j}$ multiplied by a function of the $(r-s)$-th *approximation order*. Then, from Appendix A, we see that

$$(\underset{(n)}{\Lambda}{}^{\mu\nu} - \underset{(n)}{\mathfrak{T}}{}^{\mu\nu})_{,\nu} = O_n\text{-function}\,,$$

$$\underset{(n)}{\mathfrak{H}}{}^{\nu}{}_{,\nu} = O_n\text{-function}\,.$$

Consequently, if we define $\underset{(n)}{j}$ and $\underset{(n)}{k}{}^{\cdot\cdot}$ by (5.5, 6)′, $\underset{(n)}{\mathfrak{g}}{}^{\mu\nu}{}_{,\nu}$ and $\underset{(n)}{\Phi}{}^{\nu}{}_{,\nu}$ are both O_n-functions. By induction, this will be true for all n.

Provided that the solution, (5.1, 2), and the reiteration parameters, $\underset{(r)}{j}$ and $\underset{(r)}{k}^{\cdots}$, converge in the limit as $r \to \infty$, we obtain the exact equations of motion,

$$\overset{p}{\underset{(\infty)}{k}}{}^{\mu}, \quad \overset{p}{\underset{(\infty)}{k}}{}^{\mu\nu}, \quad \overset{p}{\underset{(\infty)}{j}} = 0 . \tag{5.7}$$

From this, we see that

$$\overset{p}{\underset{(r)}{k}}{}^{\mu} = - \overset{p}{\underset{r+1}{k}}{}^{\mu} - \overset{p}{\underset{r+2}{k}}{}^{\mu} - \ldots , \quad \text{etc.} ,$$

and so the r-th reiteration parameters are of the $(r+1)$-th approximation order. Consequently, from the definition of an O_n-function, $\underset{(n)}{g}{}^{\mu\nu}{}_{,\nu}$ and $\underset{(n)}{\Phi}{}^{\nu}{}_{,\nu}$ are of the $(n+1)$-th approximation order. This shows that the set of equations, (3.1-4), have been satisfied to the n-th approximation, without it being necessary to expand the mass, charge, spin or dipole moments.

The physical parameters are defined by the first order solution, $\underset{1}{U}{}^{\mu\nu}$ and $\underset{1}{\chi}{}^{\mu}$, and it will not reduce the generality of the solution if we take

$$\underset{(n)}{U}{}^{\mu\nu} = \underset{1}{U}{}^{\mu\nu} , \qquad \underset{(n)}{\chi}{}^{\mu} = \underset{1}{\chi}{}^{\mu} ,$$

for all n. However, we shall usually redefine the particle parameters in each approximation by changing U and χ. For instance, it was necessary in (II) to add on a $\underset{2}{U}{}^{\mu\nu}$ so that the mass would be a constant to the second approximation. Also, if we wished to take the limit as $a \to \infty$, we should have to add onto $\underset{1}{U}{}^{\mu\nu}$ and $\underset{1}{\chi}{}^{\mu}$ a non-zero solution of the wave equation, depending on the radius of S^p, a, in each approximation. Otherwise the limit would not exist.

If we define the representative world line by the conditions that the dipole moments, $\overset{p}{D}{}^{\mu}$, should be zero, then we may take for a simple particle,

$$\underset{1}{U}{}^{\mu\nu} = \int (mv^{\mu}v^{\nu} + 2\dot{v}_{\alpha} S^{\alpha(\mu}v^{\nu)}) D(r-z) \cdot \mathrm{d}s + \tag{5.8}$$

$$+ \int (S^{\mu\alpha}\overset{\circ}{v}{}^{\nu} + S^{\nu\alpha}\overset{\circ}{v}{}^{\mu}) D(r-z)_{,\nu} \mathrm{d}s + \underset{1}{U}{}^{\mu\nu}_{\text{ext}} ,$$

$$\underset{1}{\chi}{}^{\mu} = \int ev^{\mu} \cdot D(r-z) \cdot \mathrm{d}s + \underset{1}{\chi}{}^{\mu}_{\text{ext}} , \tag{5.9}$$

where $\underset{1}{U}^{\mu\nu}_{\text{ext}}$ and $\underset{1}{\chi}^{\mu}_{\text{ext}}$ is the external field. Therefore,

$$\underset{1}{k}^{\mu} = 4\cdot\frac{\mathrm{d}}{\mathrm{d}s}\,(m\cdot v^{\mu} - 2S^{\mu\alpha}\cdot\dot{v}_{\alpha}) = -\sum_{2}^{\infty}\underset{r}{k}^{\mu}, \tag{5.10}$$

$$\underset{1}{k}^{\mu\nu} = 4\cdot\frac{\mathrm{d}}{\mathrm{d}s}\,(S^{\mu\nu}) + 4(S^{\mu\alpha}\dot{v}_{\alpha}v^{\nu} - S^{\nu\alpha}\dot{v}_{\alpha}v^{\mu}) = -\sum_{2}^{\infty}\underset{r}{k}^{\mu\nu}, \tag{5.11}$$

$$\underset{1}{j} = 4\cdot\frac{\mathrm{d}}{\mathrm{d}s}\,(e) = -\sum_{2}^{\infty}\underset{r}{j}\,, \tag{5.12}$$

which gives the equations of motion, mass, spin and charge.

Since the spin parameters satisfy the equation,

$$v_{\alpha}\,S^{\mu\alpha} = 0\,, \tag{5.13}$$

we may introduce new parameters which behave like a covariant vector under infinitesimal Lorentz transformations,

$$S_{\mu} = \tfrac{1}{2}\varepsilon_{\mu\alpha\beta\gamma}v^{\alpha}S^{\beta\gamma}\,, \tag{5.14}$$

and then,

$$\varepsilon^{\mu\nu\varrho\sigma}v_{\varrho}S_{\sigma} = \tfrac{1}{2}\varepsilon^{\mu\nu\varrho\sigma}\cdot\varepsilon_{\sigma\alpha\beta\gamma}v^{\alpha}v_{\varrho}\cdot S^{\beta\gamma} = \tfrac{1}{2}\delta^{\mu\nu\varrho}_{\alpha\beta\gamma}\cdot v_{\varrho}v^{\alpha}S^{\beta\gamma} = -S^{\mu\nu}\,.$$

Therefore,

$$S^{\mu\nu} = \varepsilon^{\mu\nu\alpha\beta}\,v_{\beta}S_{\alpha}\,, \tag{5.15}$$

If we multiply (5.11) by $\frac{1}{8}\varepsilon_{\sigma\alpha\mu\nu}\,v^{\alpha}$, we have

$$-\tfrac{1}{2}\varepsilon_{\sigma\alpha\mu\nu}\,v^{\alpha}\varepsilon^{\mu\nu\varrho\beta}(\dot{v}_{\varrho}S_{\beta} + v_{\varrho}\dot{S}_{\beta}) = -\tfrac{1}{8}\,\varepsilon_{\sigma\alpha\mu\nu}v^{\alpha}\Big(\sum_{2}^{\infty}k^{\mu\nu}\Big)\,,$$

and so the left hand side may be written as

$$-\delta^{\varrho\beta}_{\sigma\alpha}(\dot{v}_{\varrho}S_{\beta} + v_{\varrho}\,\dot{S}_{\beta})v^{\alpha} = \dot{S}_{\sigma} - v_{\sigma}\dot{S}^{\alpha}\,v_{\alpha}\,.$$

Consequently,

$$\dot{S}_{\mu} - v_{\mu}\dot{S}_{\alpha}\,v^{\alpha} = -\tfrac{1}{8}\,\varepsilon_{\mu\alpha\varrho\sigma}v\Big(\sum_{2}^{\infty}k^{\varrho\sigma}\Big)\,, \tag{5.16}$$

$$v^{\alpha}S_{\alpha} = 0\,.$$

This corresponds to the equation of angular momentum for a classical Newtonian particle.

6. – Equations of motion and charge in the second approximation.

As our first order solution we shall take (5.8, 9). To obtain the equations of motion we shall have to calculate the right hand sides of (5.3). In the second order, $\underset{2}{A}{}^{\mu\nu}$ is independent of the electromagnetic field, and so will give the same contributions to the k from $\underset{2}{Z}{}^{\mu\nu}$.

In (II) we showed that the self forces from the gravitational field do not give a significant contribution to the equations of motion in the second approximation. The reason for this was that any such contributions must be linear, at least, in the equations of motion, mass or spin, *i.e.* $m\dot{v}^{\mu}$, $\dot{m}$ or $\dot{S}_{\mu}$, to the first approximation. Consequently, it is possible that in the higher approximations these terms might cancel when we use the equations of motion to the correct order. As we showed, we have to go to the fourth approximation before we can decide whether these self terms are significant or not. However, we shall see that these arguments do not apply to the electromagnetic self forces.

We shall not calculate the contributions to the equations of motion and spin in this paper since they have been done in essence in INFELD and WALLACE, 1940 [1]. They calculated the surface integrals,

$$\int \mathfrak{T}^{\mu\nu} \mathrm{d}^2 S_{\nu}, \tag{6.1}$$

which is the same as the electromagnetic part of our $\underset{2}{\overset{*}{k}}{}^{\mu}$, except for the factor $(1 - (\dot{v}, \gamma))$. If we carry out the calculations in precisely the same way that they calculated (6.1), we find

$$-\frac{1}{4}\underset{2}{k}{}^{\mu} = \text{grav. terms} + e\bar{F}^{\mu}_{\nu}v^{\nu} + b\cdot\frac{\mathrm{d}}{\mathrm{d}s}\left(\frac{e^2}{a}v^{\mu}\right) + \frac{2}{3}e^2(\ddot{v}^{\mu} + \dot{v}^2 v^{\mu}), \tag{6.2}$$

$$-\frac{1}{4}\underset{2}{k}{}^{\mu\nu} = \text{grav. terms},$$

where $\bar{F}^{\mu\nu}$ is the external field and b is a numerical constant. If we use the standing wave Green's function then we obtain the terms in front of the semicolon, but if we use the retarded potential, then we have the additional self terms. The only difference between (6.2) and the result of calculating (6.1)

---

[1] L. INFELD and P. R. WALLACE: *Phys. Rev.*, **57**, 797 (1940).

is that the constant b is different, but not zero. We may remove this term by redefining the mass in the second approximation. We add onto the solution of the second order field equations, (5.1, 2), a solution of the wave equation corresponding to a mass $+b\cdot e^2/a$. The reason that INFELD and WALLACE did not get this singular term in their calculations of (6.1) was that they deliberately omitted that part of (6.1) which depended on the surface of integration.

If we expand out $\underset{2}{\mathfrak{H}}{}^{\mu}$, we find that

$$(6.3)\qquad \underset{2}{\mathfrak{H}}{}^{\mu} = -4\underset{1}{U}{}^{\nu\beta}\underset{1}{\Phi}{}^{\mu}{}_{,\alpha\beta} + 2\underset{1}{U}{}^{\varrho}_{\varrho,\nu}(\underset{1}{\Phi}{}^{\mu,\nu} - \underset{1}{\Phi}{}^{\nu,\mu}) + \\ + 4\underset{1}{U}{}^{\mu\alpha}{}_{,\beta}\underset{1}{\Phi}{}^{\beta}{}_{,\alpha} - 4\underset{1}{U}{}^{\beta,\mu}_{\nu}\underset{1}{\Phi}{}^{\alpha}{}_{,\beta} + 4\underset{1}{U}{}^{\mu}{}_{\alpha}{}^{,\beta}\underset{1}{\Phi}{}^{\alpha}{}_{,\beta}.$$

Any self terms in $\underset{2}{j}$ must be proportional to $\dot{e}$, $\dot{m}$, $\dot{S}_{\mu}$, or $m\dot{v}^{\mu}$, and consequently they may cancel with terms of the third or higher orders through the equations of motion, etc. They will be omitted since we are only calculating the equation of charge to the second approximation. The calculations of the contributions to j from the external field is completely analogous to those of (II), and so well shall just give the result,

$$(6.4)\qquad \underset{2}{j} = e\left(\frac{2}{3}v^{\alpha}\cdot\overline{U}^{\beta}_{\beta,\alpha} + \frac{4}{3}\cdot v^{\alpha}v^{\beta}v^{\nu}\cdot\overline{U}_{\alpha\beta,\nu}\right) - 4mv^{\alpha}\Phi_{\alpha,\beta}v^{\beta} - 4S^{\underset{\sim}{\alpha\beta}}\cdot v^{\varrho}\cdot\Phi_{\alpha,\beta\varrho}$$

$$= \frac{\mathrm{d}}{\mathrm{d}s}\left(\frac{2}{3}e\cdot\overline{U}^{\alpha}_{\cdot\alpha} + \frac{4}{3}\cdot ev^{\alpha}v^{\beta}\cdot\overline{U}_{\alpha\beta} - 4mv^{\alpha}\Phi_{\alpha} + 2S^{\underset{\sim}{\alpha\beta}}\overline{F}_{\underset{\sim}{\alpha\beta}}\right) -$$

$$-\left(\frac{2}{3}\cdot\dot{e}\cdot\overline{U}^{\alpha}_{\cdot\alpha} + \frac{4}{3}\cdot\dot{e}v^{\alpha}v^{\beta}\overline{U}_{\alpha\beta} - 4\frac{\mathrm{d}}{\mathrm{d}s}(mv^{\alpha})\Phi_{\alpha} + 2\dot{S}^{\underset{\sim}{\alpha\beta}}\overline{F}_{\underset{\sim}{\alpha\beta}}\right) - \frac{8}{3}\cdot\dot{v}^{\alpha}v^{\beta}\overline{U}_{\alpha\beta} \quad (*).$$

The first term can be removed by redefining the charge in the second approximation, and the second term is an O_2-function, which may be neglected in the second approximation. However, if we replace $\dot{v}^{\alpha}$ by its value using the second order equations of motion, then the last term in (6.4) would give, among other things,

$$-\frac{8}{3}\cdot\frac{e^2}{m}\cdot v_{\varrho}v^{\beta}\overline{U}_{\alpha\beta}\overline{F}^{\underset{\sim}{\varrho\alpha}},$$

which cannot cancel with any terms from the third or higher approximations because of the factor, m^{-1}. Consequently, we have to the second approximation,

(*) $\overline{U}^{\mu\nu}$ is the external gravitational potential.

i.e. neglecting all O_2-functions,

$$\frac{\mathrm{d}}{\mathrm{d}s}(e) \stackrel{\text{gr}}{=} -\frac{8}{3}\cdot e\dot{v}^{\alpha}v^{\beta}\overline{U}_{\alpha\beta}\,. \tag{6.5}$$

From (6.2), we see that the equations of motion and spin are

$$\frac{\mathrm{d}}{\mathrm{d}s}(mv^{\mu}+2\varepsilon^{\mu\alpha\beta\gamma}\dot{v}_{\alpha}v_{\beta}S_{\gamma}) = \text{grav. terms} + e\overline{F}^{\nu\mu}\cdot v_{\nu} + \frac{2}{3}e^{2}(\ddot{v}^{\mu}+\dot{v}^{2}v^{\mu})\,, \tag{6.6}$$

$$\dot{S}_{\mu} - v_{\mu}v^{\alpha}\dot{S}_{\alpha} = \text{grav. terms}\,. \tag{6.7}$$

As we would expect, there is no couple on the charge. From (6.6) and the expression for the gravitational terms in (II), we see that the mass is a constant to the second approximation.

$$\frac{\mathrm{d}}{\mathrm{d}s}(m) = 0, \text{ to the second approximation.}$$

However, from (6.5) we see that the charge is not conserved in the second approximation. The only *significant* self forces are those from the electromagnetic field in (6.6), and these only appear if we use the retarded potential. If we use the standing wave Green's function, there are no significant self forces in the second approximation. Any gravitational self forces that appear in the second approximation may cancel with terms appearing in the higher approximations.

* * *

The author would like to thank the staff of the Mathematics Department, King's College, London, for their help while this paper was being written.

Appendix

Theorem. – If $\underset{(r)}{g}^{\mu\nu}{}_{,\nu}$ and $\underset{(r)}{\Phi}^{\beta\nu}{}_{,\nu}$ are O_r-functions for all $r < n$, then the divergences of the source functions, $(\underset{(n)}{\Lambda}^{\mu\nu} - \underset{(n)}{Z}^{\mu\nu}{}_{,\nu})$ and $\underset{(n)}{H}^{\nu}{}_{,\nu}$ are also O_n-functions.

We have already proved in Sect. 4 of (I) that

$$2\underset{(n)}{\Lambda}^{\mu\nu}{}_{,\nu} + \sum_{r} \underset{n-r}{\Gamma}^{\mu}{}_{\alpha\beta}(-\Box\, \underset{(r)}{h}^{\alpha\beta} + 2\underset{(r)}{\Lambda}^{\alpha\beta}) \equiv -\sum_{r=1}^{n-1} \underset{(r)}{h}^{\alpha\beta}{}_{,\beta}\cdot \underset{n-r}{P}^{\mu\nu}{}_{,\nu} - \dots\,. \tag{A.1}$$

This follows from the Bianchi identities, (2.1). The right hand side is linear in $\underset{(r)}{h}{}^{\alpha\beta}{}_{,\beta}$ and its derivatives, for $r < n$. Consequently, from our induction hypothesis, the r.h.s. is an O_n-function (*).

Since (2.3) is an identity, it must be true for the λ-series of Sect. 3. If we expand it out as a power series in λ, and equate the coefficients of λ^n, we have

$$\underset{n}{\mathfrak{T}}{}^{\mu\nu}{}_{,\nu} + \sum_s \Gamma^{\mu}_{\alpha\beta}\, \underset{s}{\mathfrak{T}}{}^{\alpha\beta} \equiv \sum_{r,s} g_{\alpha\beta}\, \underset{r}{F}{}^{\mu\alpha} (-\Box \underset{s}{\Phi}{}^{\beta} + \underset{s}{H}{}^{\beta} + \underset{s}{Q}{}^{\beta}) \cdot$$

Since the field equations, (3.6), are satisfied for all reiteration orders, we have, when we sum this equation from 1 to n,

$$\underset{(n)}{\mathfrak{T}}{}^{\mu\nu}{}_{,\nu} + \sum_s \underset{n-s}{\Gamma}{}^{\mu}_{\alpha\beta}\, \underset{(s)}{\mathfrak{T}}{}^{\alpha\beta} \equiv \sum_{r\,s} g_{\alpha\beta}\, \underset{r}{F}{}^{\mu\alpha} \cdot \underset{(s)}{Q}{}^{\beta} \,. \tag{A.2}$$

From the definition of $\mathfrak{L}^{\mu}$ in (1.9), we see that $\underset{(s)}{\mathfrak{L}}{}^{\mu}$ is linear in $\underset{(t.}{\mathfrak{g}}{}^{\mu\nu}{}_{,\nu}$ and $\underset{(t)}{\Phi}{}^{\nu}{}_{,\nu}$ and the derivatives of these functions. Consequently, from the induction hypothesis, the r.h.s. of (A.2) is an O_n-function.

From (A.1), (A.2), we have

$$\underset{(n.)}{\Lambda}{}^{\mu\nu}{}_{,\nu} - \underset{(n)}{\mathfrak{T}}{}^{\mu\nu}{}_{,\nu} + \sum_{r<n} \underset{n-r}{\Gamma}{}^{\mu}_{\alpha\beta} (-\tfrac{1}{2} \Box \underset{(r)}{\mathfrak{g}}{}^{\alpha\beta} + \underset{(r)}{\Lambda}{}^{\alpha\beta} - \underset{(r)}{\mathfrak{T}}{}^{\alpha\beta}) = O_n\text{-function} \,,$$

and so, from the field equations, (3.5),

$$(\underset{(n.)}{\Lambda}{}^{\mu\nu} - \underset{(n)}{\mathfrak{T}}{}^{\mu\nu})_{,\nu} \sim 0 \,. \tag{A.3}$$

Similarly, from the identity (2.2), we have

$$-\Box \underset{(n)}{\Phi}{}^{\mu}{}_{,\mu} + \underset{(n)}{\mathfrak{H}}{}^{\mu}{}_{,\mu} \equiv - \underset{(n.)}{\mathfrak{L}}{}^{\mu}{}_{,\mu} \,. \tag{A.4}$$

However, from the definition of $\mathfrak{L}^{\mu}$ in (1.9),

$$\underset{(n)}{\mathfrak{L}}{}^{\mu}{}_{,\mu} \equiv - \eta^{\mu\alpha} \underset{(n)}{\Phi}{}^{\nu}{}_{,\alpha\mu} - \sum_{r<n} \underset{n-r}{h}{}^{\mu\alpha} \underset{(r)}{\Phi}{}^{\nu}{}_{,\alpha\mu} - \ldots - \sum_{r,s<n} \underset{(r)}{h}{}^{\alpha\nu}{}_{,\nu} \underset{s}{g}{}^{\mu\beta} \underset{n-r-s}{\varphi}{}_{\beta,\alpha} \equiv \tag{A.5}$$

$$\equiv -\Box \Phi^{\mu}{}_{,\mu} + O_n\text{-function} \,.$$

Consequently, from (A.4), (A.5), we have

$$\underset{(n)}{\mathfrak{H}}{}^{\mu}{}_{,\mu} \sim 0 \,. \tag{A.6}$$

This has proved the second part of the theorem.

If the coordinate and gauge conditions are satisfied exactly in each approximation, then the r.h.s. of (A.1)-(A.4) and (A.6) are zero. Consequently, we have the following corollary.

(*) By definition, an O_r-function multiplied by a function of the s-th *approximation* order is automatically an O_{r+s}-function.

Corollary. – If the field equations, coordinate conditions, and gauge conditions are satisfied exactly in every previous approximation, then

$$(\underset{(n)}{\Lambda^{\mu\nu}} - \underset{(n)}{\mathfrak{T}^{\mu\nu}})_{,\nu} = 0\,, \qquad \underset{(n)}{\mathfrak{H}^{\mu}}_{,\mu} = 0\,.$$

This implies that

$$(\underset{n}{\Lambda^{\mu\nu}} - \underset{n}{\mathfrak{T}^{\mu\nu}})_{,\nu} = 0\,, \qquad \underset{n}{\mathfrak{H}^{\mu}}_{,\mu} = 0\,.$$

RIASSUNTO (*)

In questo articolo sono stati estesi al campo di Einstein-Maxwell i metodi adottati nei primi due articoli di questa serie. Si dimostra che è possibile stabilire un procedimento coerente di approssimazione dell'invariante di Lorentz senza che sia necessario sviluppare i parametri delle particelle, quali la massa e la carica. Abbiamo calcolato, usando una funzione invariante di Green, una espressione integrale per il campo. Tale espressione è una soluzione delle equazioni del campo di Einstein-Maxwell, supposto che siano soddisfatte, per ciascuna particella, le equazioni del moto, della massa, della carica e dello spin. Il risultato non dipende dal grado di complessità della soluzione del primo ordine. Abbiamo dimostrato che le autoforze elettromagnetiche che compaiono nella seconda approssimazione sono significative; è necessario invece giungere fino alla quarta approssimazione prima che si possa dimostrare che le corrispondenti autoforze gravitazionali sono reali e che non scompaiono nelle approssimazioni superiori. È stato anche dimostrato che la massa si conserva fino alla seconda approssimazione, la qual cosa non avviene per la carica.

(*) *Traduzione a cura della Redazione.*

IL NUOVO CIMENTO Vol. XIII, N. 4 16 Agosto 1959

The Interaction and Decay of K^- Mesons in Photographic Emulsion.

Part I.

General Characteristics of K^--Interactions and Analysis of Events in which a Charged π-Meson is Emitted.

(K^--Collaboration)

B. Bhowmik (*), D. Evans, D. Falla, F. Hassan, A. A. Kamal (**), K. K. Nagpaul (***) and D. J. Prowse

H. H. Wills Physical Laboratory - Bristol

M. René

Laboratoire de Physique Nucléaire, Université Libre - Bruxelles

G. Alexander (*•*), R. H. W. Johnston and C. O'Ceallaigh

Institute for Advanced Studies - Dublin

D. Keefe

University College - Dublin

E. H. S. Burhop, D. H. Davis, R. C. Kumar, W. B. Lasich, M. A. Shaukat (•*•) and F. R. Stannard

Physics Department, University College - London

G. Bacchella (†), A. Bonetti, C. Dilworth, G. Occhialini and L. Scarsi

Istituto di Scienze Fisiche dell'Università - Milano

Istituto Nazionale di Fisica Nucleare - Sezione di Milano

M. Grilli, L. Guerriero, L. von Lindern (§), M. Merlin (×) and A. Salandin

Istituto di Fisica dell'Università - Padova

Istituto Nazionale di Fisica Nucleare - Sezione di Padova

(ricevuto il 13 Gennaio 1959)

(*) Now at the University of Delhi, India.
(**) Now at the University of Hyderabad, India.
(***) On leave of absence from University of Punjab, Pakistan.
(*•*) Now at University of Rehovoth, Israel.
(•*•) Now at the Institute for Advanced Studies, Dublin.
(†) Now at C.I.S.E., Milan.
(§) Now at Max Planck Institut, für Physik and Astrophysik, München.
(×) Now at the Istituto di Fisica dell'Università, Bari.

Summary. — A total of 3480 K⁻-mesons has been observed. Of these 445 interact in flight, at a mean energy of 40 MeV and only their general characteristics have been studied. Little difference has been observed between the number of unstable charged particles ($\Sigma^{\pm}$-hyperons and $\pi^{\pm}$-mesons) in these interactions and those in the 3035 interactions at rest. The 3035 K⁻-interactions at rest have been studied in detail. In this paper (Part I) are given the results on those interactions in which π-mesons are emitted. An estimate of the Σ-hyperon nuclear potential is based on the energy spectrum of π-mesons emitted in the K⁻-interactions in which the only charged particles emitted are a π-meson and a Σ-hyperon. A detailed examination of the angular distribution of 2-pronged events, and of the sign ratio of the π-mesons, the prong distribution and energy release in all events has led to an estimate of the probabilities of absorption of positive and negative Σ-hyperons in the parent nucleus, and to a partition of the events between the various primary reactions (*).

(*) In Part II all the events will be examined in which a Σ-hyperon is emitted, and the results of the two papers combined to obtain an estimate of the number of multinucleon interactions and hence the $\Sigma : \Lambda^0$ ratio at production, the probability of absorption of the π-mesons and the relative intensities of the various types of reaction.

1. – Introduction.

1·1. *Statement of the problem.* – K⁻-mesons were first discovered as products of the cosmic radiation, and it is only recently that they have been produced at the Bevatron and Cosmotron in sufficient numbers for their properties to be studied in a systematic manner. Their existence was confirmed through the early experimental work in cloud chambers and emulsion stacks [1]. The apparent contradiction between the copious production of the strange particles and their slow decay, led to the postulate of the « associated production » [2]. The strangeness schemes proposed by GELL-MANN [3] and by NISHIJIMA [4] included within them the concept of associated production. It was a feature of this concept that it could be used to provide an empirical explanation of the relatively small number of K⁻-mesons produced whether

[1] K. H. BARKER: *Proceedings of the Duke Conference* (1953), p. 11-18; D. LAL, Y. PAL and B. PETERS: *Proc. Ind. Acad. Sci.*, **38**, 398 (1953); *Report of the Committee on K-particles*, Padua-Conference, in *Suppl. Nuovo Cimento*. **12**, 433 (1954).

[2] A. PAIS: *Phys. Rev.*, **86**, 663 (1952).

[3] M. GELL-MANN: *Phys. Rev.*, **92**, 833 (1953); M. GELL-MANN and A .PAIS: *Proc. Glasgow Conference* (1954).

[4] K. NISHIJIMA: *Proc. Theor. Phys.*, **10**, 581 (1953); **12**, 107 (1954).

by the cosmic radiation ([5]) or by the beams of high energy particles from the large accelerators. The results of cosmic-ray work ([6]) indicated that the capture at rest of a K^--meson very frequently led to the emission of a hyperon or hyperfragment from the resulting star. This observation was confirmed by work with machine produced K^--mesons ([7]). This early work was hampered by an unfavourable K^-/π^- ratio in the beam of particles available. Because of this, it was not possible to make a detailed investigation into all properties of the interactions which take place at rest or in flight. At about the same time, following the development of the 10 inch hydrogen bubble chamber at Berkeley ([8]), a direct investigation of the K^--proton interaction was initiated. The results obtained up to this time (1956), have been summarized by S. GOLDHABER ([9]). By then, the mean free path of the K^--mesons was known to be geometric or slightly less. A charged Σ-particle was emitted in about 15% of the stars, and a charged π-meson in about 30%. A few events representing the inelastic scattering of a K^--meson in flight in which the K^--meson re-emerged had been reported, but the strong absorptive reaction appeared to be predominant. It was suggested that some events could be explained as the charge exchange of a K^--meson with a proton. Several examples of the elastic scattering of K^--mesons from free protons had been reported, and the cross-section appeared very much greater than that for K^+-proton scattering ([10]).

When, therefore, the 0° separated beam of K^--mesons became available at the Bevatron, it was felt that by a concentrated collaborative effort, many finer details of the K^--interaction with nuclei would become apparent, and that new knowledge on other related subjects, such as the properties and interactions of hyperons, would follow from a careful study of the K^--interaction in emulsions. It was also hoped that such experimental information could be used in conjunction with the bubble chamber results ([11]), which were then

([5]) R. ARMENTEROS, B. GREGORY, A. LAGARRIGUE, L. LEPRINCE-RINGUET, F. MULLER and CH. PEYROU: *Suppl. Nuovo Cimento*, **12**, 324 (1954).

([6]) M. DI CORATO, B. LOCATELLI, G. MIGNONE and G. TOMASINI: *Suppl. Nuovo Cimento*, **12**, 270 (1954); M. F. FRIEDLANDER, Y. FUJIMOTO, D. KEEFE and M. G. K. MENON: *Nuovo Cimento*, **2**, 90 (1955).

([7]) W. CHUPP, G. GOLDHABER, S. GOLDHABER and F. H. WEBB: *Phys. Rev.*, **100**, 959 (1955); W. F. FRY, J. SCHNEPPS, G. A. SNOW and M. S. SWAMI: *Phys. Rev.*, **100**, 950 (1955); E. P. GEORGE, A. J. HERZ, J. H. NOON and N. SOLNSTEFF: *Nuovo Cimento*, **3**, 94 (1956); J. HORNBOSTEL and E. O. SALANT: *Phys. Rev.*, **102**, 502 (1956); D. M. FOURNET and M. WIDGOFF: *Phys. Rev.*, **102**, 929 (1956); D. M. HASKIN, T. BOWEN and M. SCHEIN: *Phys. Rev.*, **103**, 1512 (1956).

([8]) L. W. ALVAREZ: *Berkeley Bubble Chamber*, (1956), *CERN Symposium*.

([9]) S. GOLDHABER: *Report at Rochester Conference* (1956).

([10]) F. C. GILBERT, C. E. VIOLET and R. S. WHITE: *Phys. Rev.*, **103**, 1825 (1956).

([11]) L. W. ALVAREZ, H. BRADNER, P. FALK-VAIRANT, J. D. GOW, A. H. ROSENFELD, F. T. SOLMITZ and R. D. TRIPP: *Nuovo Cimento*, **5**, 1026 (1957).

becoming available, to study the interactions of K^--mesons with neutrons, a topic about which very little information had been published at the time [12].

The publication of the results of the present collaboration will be divided into a number of parts of which this is the first. In this paper (Part I), the general characteristics of K^--interactions are discussed, particular attention being paid to those in which a π-meson is observed to have been produced. Part II, publication of which will follow, deals with those stars in which a charged hyperon is produced. Characteristics such as the interaction cross-sections, life time and masses of K^--mesons and $\Sigma^{\pm}$-hyperons will be discussed in successive papers.

1·2. *The primary processes in* K^- *absorption.* – The absorption of K^--mesons by a nucleus may take place as a result of interaction of the K^--particle, either with a single nucleon or alternatively, with two or more nucleons.

Table I shows the interactions in which a π-meson may be produced in a process involving a single nucleon, the Q value of each reaction, the energy of each product ignoring the Fermi motion of the nucleons in the nucleus, and finally, limiting values of energies of products assuming a maximum Fermi momentum of 200 MeV/c. In this Table, an average of 20 MeV is assumed for the sum of the binding energy of the nucleon concerned and the excitation of the final nucleus [12].

TABLE I.

Interaction process	Q value (MeV)	Energy of products from Q (MeV)		Expected limits of energy of products (**) (MeV)			
		Hyperons	π-mesons	Hyperons		π-mesons	
				Max	Min	Max	Min
i) $K^- + p \rightarrow \pi^+ + \Sigma^-$	96	13	83	43	0	76	33
ii) $\rightarrow \pi^- + \Sigma^+$	103	14	89	45	0	83	38
iii) $\rightarrow \pi^0 + \Sigma^0$	110	15	95	47	0	90	43
iv) $\rightarrow \pi^0 + \Lambda^0$	182	29	153	71	1	161	91
v) $K^- + n \rightarrow \pi^0 + \Sigma^-$	101	13	88	44	0	81	37
vi) $\rightarrow \pi^- + \Sigma^0$	106	14	92	46	0	86	40
vii) $\rightarrow \pi^- + \Lambda^0$	179	29	150	70	1	158	89
viii) $K^- + p \rightarrow n + \bar{K}^0$	0 (*)	—	—	—	—	—	—

(*) Small, not known.

(**) Allowing for Fermi motion, binding energy and excitation of residual nucleus, but assuming zero nuclear potential for K, π, Σ and Λ^0.

[12] F. C. GILBERT, C. E. VIOLET and R. S. WHITE: *Phys. Rev.*, **107**, 228 (1957).

Table II gives similar details for possible interactions which may take place with two nucleons.

In addition to processes (xvi-xix), fourteen other processes of a similar type may be supposed to take place, if we envisage the association with reactions i) to vii) of a second nucleon which gains or loses energy as a result of the interaction.

TABLE II. – *Details of* K^-*-interaction processes with two nucleons* (*).

(*a*) *without* π*-meson emission.*

Interaction process	Q value (MeV)	Energy of products from Q (MeV)		Expected limits of energy of products (MeV)			
		Hyperon	Nucleon	Hyperons		Nucleons	
				Max	Min	Max	Min
ix) $K^- + p + p \rightarrow \Sigma^+ + n$	241	107	134	173	14	187	28
x) $\rightarrow \Sigma^0 + p$	245	108	137	177	14	191	28
xi) $\rightarrow \Lambda^0 + p$	317	147	170	232	35	242	45
xii) $K^- + p + n \rightarrow \Sigma^- + p$	237	105	132	169	14	183	28
xiii) $\rightarrow \Sigma^0 + n$	245	108	137	177	14	191	28
xiv) $\rightarrow \Lambda^0 + n$	317	147	170	232	35	242	45
xv) $K^- + n + n \rightarrow \Sigma^- + n$	237	105	132	169	14	183	28

(*) An average of 40 MeV has been assumed for the sum of the binding energies of the two nucleons concerned and the excitation energy of the final nucleus.

(*b*) *with* π*-meson emission.*

Interaction process	Q value (MeV)	Expected limits of energy of products (*)					
		Hyperon		Nucleon		π-meson	
		Max	Min	Max	Min	Max	Min
xvi) $K^- + p + p \rightarrow \Sigma^+ + n + \pi^0$	106	58	0	64	0	66	0
xvii) $\rightarrow \Sigma^0 + n + \pi^+$	106	58	0	64	0	60	0
xviii) $\rightarrow \Lambda^0 + n + \pi^+$	178	106	0	122	0	138	0
xix) $K^- + n + n \rightarrow \Sigma^- + p + \pi^-$	98	50	0	56	0	58	0

(*) Allowing for Fermi motion, binding energy of nucleons, and excitation of residual nucleus.

Processes of the type (xvi-xix) occur either directly in a single process, or as a combination of two processes, of which one is a one-nucleon process of the type i) to vii), and the other a charge exchange of a π^- or π^0-meson with another nucleon. Alternatively, some apparent two-nucleon interactions

may be due to a K^- charge exchange process of type viii), followed by the absorption of the K^0-meson by a second nucleon and the production of a hyperon and a π-meson.

1·3. *Exposure and processing.* – A stack of 100 6 in. × 8 in. × 600 μm emulsion sheets was exposed at the Bevatron to the separated K^--meson beam devised by Dr. W. BARKAS and his group ([13]). We are greatly indebted both to them and to Drs. R. W. BIRGE and E. J. LOFGREN for their care and attention in carrying out the exposure. The stack was not ideal for the analysis of K^--meson stars as its dimensions were inadequate to ensure the stopping of a sufficient proportion of the fast mesons emitted. The stack was exposed so that the momentum variation occured across each plate and was constant through the depth of the stack, the average momentun being ~ 300 MeV/c. The stack was processed at Bristol using standard techniques with a hot plate at a temperature of 27 °C and a development time of 1 hour. The value of grain density at minimum ionization was found to be low, about 16 grains/100 μm. This defect has made it difficult to observe the emission of fast mesons in stars and to follow them through the stack. No precaution had been taken to keep the stack at low temperature during the period between its delivery from Ilford Ltd., and its return after exposure to the refrigerator at the H. H. Wills Physical Laboratory. For this reason, it is felt that the low-grain density at minimum ionization may well have been a consequence of diminished sensitivity and fading of the latent image between pouring, exposure and processing ([14]).

2. – Indentification of K primaries.

Tracks lying within 5° of the direction of the incident beam, and having a grain density lying within narrow limits of that expected for a K-meson of the mean beam energy, were picked up 3 mm from the emulsion edge and followed to the end of their range or to a point where interaction or decay occurred.

Identification of K-mesons was established generally by the ionization-range method based on suitable calibration. All interactions in flight were discarded if less than 10 mm of track were available for measurements and efficient discrimination in the presence of background protons. In certain cases, identification of the primary track was open to doubt. Such were interactions and disappearances in flight and events of the type K_ϱ and one-prong K_σ. For these, it was necessary to make scattering measu-

([13]) W. BARKAS: *Report at 7-th Rochester Conference* (1957).

([14]) G. OCCHIALINI: *Premier Colloque de Photographie Corpusculaire, Strasbourg* (1957). B. BHOWMIK, J. H. DAVIS, D. EVANS and D. J. PROWSE: *Nuovo Cimento*, **7**, 712 (1958).

rements in order to reduce to a negligible proportion the number of cases of proton contamination within our samples of K-mesons at rest and in flight. Details of the ionization and scattering measurements are given in the following Section 3·4.

Figs. 1*a* and 1*b* represent a random sample of the ranges of K-mesons which entered the high and low momentum half of the plates and were brought to rest. There appears no significant difference in range distribution between those K-mesons which produce ϱ-stars and those which produce σ-stars. Indeed, the appearance of these histograms is consistent with the absence of any significant proton contamination within the sample.

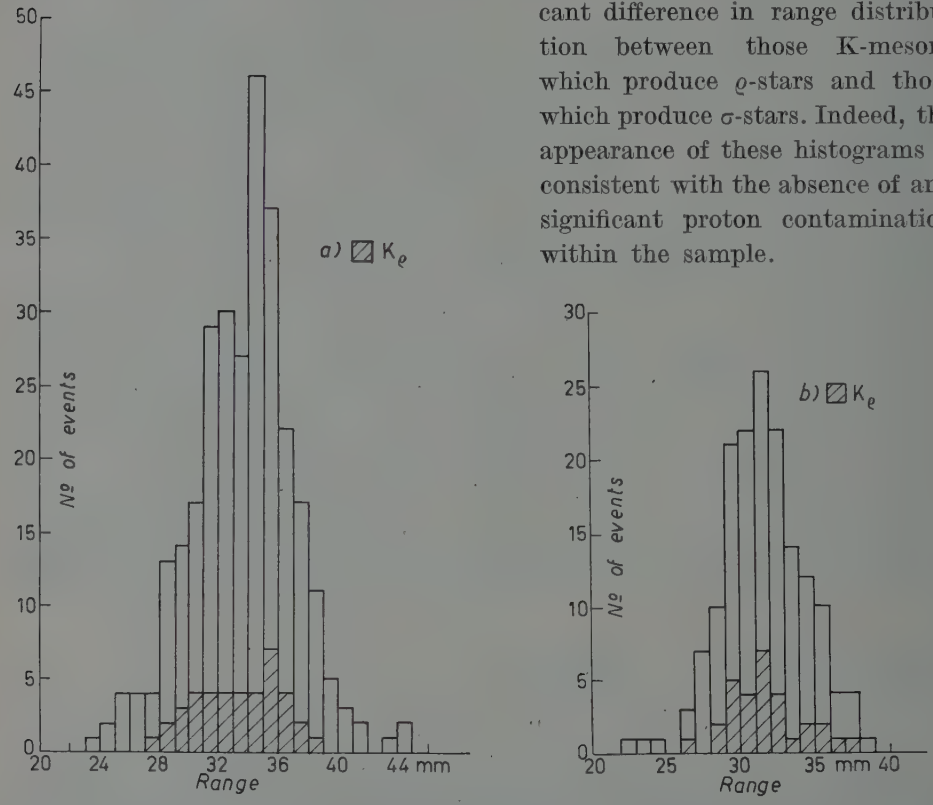

Fig. 1. – Range distribution of K^--mesons followed to rest discriminating between K_ϱ and K_σ events. *a*) Upper momentum range. *b*) Lower momentum range.

3. – Analysis of K-meson interactions.

3·1. *General procedure.* – After careful examination of the end point of each K-particle which either came to rest, or interacted, or disappeared in flight in the emulsion, the following characteristics were noted:

1) The height of the end point from glass.

2) The presence of a slow electron, blob or recoil (the last defined as a track shorter than 5 μm).

3) The number of prongs.

4) The ionization of prongs. These were divided into two groups, one containing « black » and « grey » tracks, the other « light » tracks.

5) The existence of a second star connected with the first by a shorter track, or of a double centre in the star.

The value of the ionization chosen as the bounding value between the two groups corresponds to a π-meson of energy ~ 30 MeV, or to a proton of ~ 200 MeV. Most of these tracks have been followed to their point of rest or of exit from the stack (see below). Sharp angles of scattering and sudden changes in grain density were recorded, and all track endings, whether in flight or at rest, were scrutinised for visible evidence of interaction.

The end-point of all K-mesons lying within 20 μm (unprocessed emulsion) of the surface or glass having been excluded from the analysis, there remained a total of 3 035 captures at rest and 445 interactions or decays in flight.

3·2. *Captures at rest. Identification of « black » and « grey » prongs.* – All « grey » and « black » tracks, irrespective of dip, were followed to their end or their point of exit from the stack. A negligible number of these tracks was lost through the cut edge or in distorted regions of the plates.

Most of the denser tracks have been followed to the point of arrest, decay, or interaction in the stack, and their classification as « baryons » or π-mesons did not give rise to any difficulty. Ability to discriminate was not lost, even when the particles left the stack, since in this case, variation of ionization with range provides an adequate criterion.

On the other hand, the identification of charged hyperons among baryons is acceptable only if the decay or interaction products are clearly seen, and if it can be excluded that the event is a case of scattering or interaction of a stable particle.

The sources of ambiguity in the identification of hyperons are discussed fully in Part II. In the present paper we confined our attention to « clearly defined » Σ-hyperons, *i.e.*, $\Sigma \to \pi$ at rest or in flight, $\Sigma \to p$ at rest, $\Sigma \to p$ in flight where no other interpretation is plausible, Σ^--interactions at rest giving stars of one or more prongs which leave no reasonable doubt as to their nature, or interactions in flight in which the visible energy release in the star produced exceeds the kinetic energy of the baryon before interaction. Many events in which a charged hyperon is produced elude detection. In Part II we shall attempt to arrive at an estimate of the true number emitted. The particles causing baryon prongs which either came to rest, interacted in flight or which left the stack and which were not clearly recognizable as hyperons, may be expected to include unidentified hyperons, protons, deuterons, tritons, α-particles, and a few heavier fragments. No attempt has been made to establish such a detailed classification, and throughout this paper such « stable »

prongs have been considered to be due to protons, the energy release in the star being calculated on this assumption.

A small number of short dense tracks interconnect some K-stars with secondary stars. In a few cases it was possible to attribute the track to a hyperfragment. In other cases, either the nature of the particle could not be determined, or its length was so short that the event could be described only as a double-centred star (D.S.).

The errors in the estimates of energy of baryons interacting or decaying in flight, or leaving the stack, depend mainly on the available length of track, and increase greatly for low velocities and for dipping tracks. Clearly, when the track was short, only a rough estimate of the velocity of the particle could be made.

3·3. *Captures at rest. Identification of « light » tracks.* – « Light » tracks, when making an angle of less than 20° to the plane of the unprocessed emulsion, were followed as far as was practicable (*).

The identification of the particles which gave rise to « light » tracks was based, either on the inspection of the end of the track, or on combined ionization-range or ionization-scattering measurements over an adequate segment of track (see Sect. 3·4).

All but 3 of the identified « light » particles were π-mesons.

Of the three fast baryons, two were protons which were followed to rest. The third fast baryon was followed for more than 7 cm before leaving the stack and it is therefore unlikely that it was a hyperon. Assuming that it was a proton, its kinetic energy was (235 ± 20) MeV. On the other hand, the maximum energy of a proton or hyperon emitted in a K-meson absorption is expected to be not larger than 270 MeV (see Section 1·2), which corresponds in ionization to a π-meson of about 40 MeV. One would expect therefore, among the π-mesons in the energy interval 30 to 40 MeV, of which the tracks have not been followed because the angle of dip was larger than 20°, a contamination of approximately 6 baryons. If one takes all the unidentified « light » tracks as being due to π-mesons, the proportion among them of fast baryons is little more than one per cent of the observed number of 764, and must be negligible among the π-mesons of energy greater than 40 MeV.

On the other hand, in the conditions of development of our stack, « light » tracks can easily escape observation, so that a loss of the fastest π-mesons is to be expected and hence, the number of observed « light » particles must be considered as an underestimate of those emitted. An attempt to find the factor of loss will be made in Section 3·5.

(*) Measurements on a small proportion of these tracks emitted in the direction of the K-beam had to be abandoned because of the danger of confusion with the background tracks of near minimum grain density. Others became difficult to follow, either because they passed through a region of low grain density (see later), or because of a scattering in the vertical plane which caused the track to dip excessively.

Misidentification of « light » tracks may occur due to occasional errors in tracing the tracks from one plate to another or across the cut-edges. Normal precautions were taken in following, such as positioning of the field using neighbouring tracks, and verifying consistency in grain density and track inclination. In addition, however, a check was made by following a sample of π-tracks back from the end-point to the parent stars. Errors in following were found to be negligible.

3·4. *Energy measurement.* – When the full range of the particle was available, the energy was deduced on the assumption that all the « stable » prongs were protons, using the range-energy relation given by BARKAS ([15]). Normalization of the curve to the local stopping-power of the emulsion by range measurements on μ-mesons arising in π-μ-e decay was used only in cases where precise mass estimates were required.

Ionization measurements were made on those tracks which either interacted, or decayed in flight, or left the stack.

Different techniques were used in different laboratories, *e.g.* reciprocal mean gap-length, grain density and blob density. These parameters were related to the velocity of the particles by means of measurements on tracks of K-mesons followed from the point of arrest to a residual range-point of about 3 cm, and of π-mesons up to a residual range of about 9 cm, using π-secondaries originating in $\Sigma \to \pi$ decay at rest. For greater velocities, it was necessary to extrapolate the experimental ionization-velocity curves as the only available experimental point was the « plateau » value

TABLE III. – *Comparison of values of grain-density corresponding to minimum* ($g_{\min}$) *obtained by different groups within the collaboration.*

Plates	$g_{\min}$ /100 μm	Laboratory
3 – 22	16.3 16.4	U.C. London Dublin
23 – 42	15.8 15.2	U.C. London Dublin
43 – 50	16.1	U.C. London
41 – 70	15.7	Brussels-Milan
53 – 92	15.3	Bristol
71 – 100	15.8	Padua

([15]) W. BARKAS, P. H. BARRET, P. CÜER, H. H. HECKMAN, F. M. SMITH and H. K. TICHO: *Phys. Rev.*, **102**, 583 (1956).

obtained from the π-μ-e decay electrons. Curves relating the ionization parameters to the velocity of the particles in G-5 emulsions have already been published ([16]). Their applicability to the present work was verified by calibration using the tracks of stopping particles of which the identity was established. The results obtained by the various collaborating groups are compared in Table III, and the agreement will be seen to be satisfactory.

In order to minimize the effects of corrosion in the surface layers and of underdevelopment in the bottom layers, only the central part of the emulsion was used. Whenever possible, measurements of ionization were made in several successive plates, in order to reduce the effect of fluctuation of grain density from plate to plate. In general, the variation of minimum ionization was found to be small. Fig. 2 shows

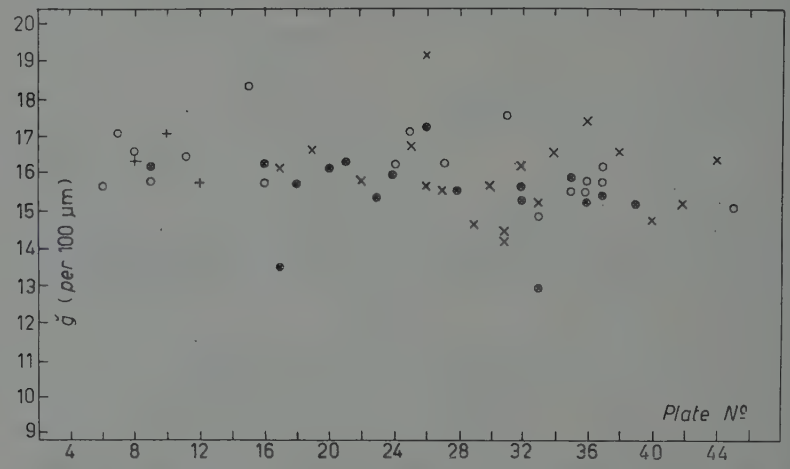

Fig. 2. – Plate to plate variation in g for a sample of 40 plates. ○ $\check{g}$ deduced from blob measurements on π-mesons of known energy using $\alpha = 0.85$ μm in the relation $b = ge^{-g\alpha}$ (based on (800÷1000) blobs in each plate). +, × and ⊗ $\check{g}$ deduced from blob and hole measurements on K^--meson tracks, with $\check{g} \sim 3$ (based on 400 blobs and 50 holes).

values of $g_{\min}$ measured in plates Nos. 3-45. In this figure, the open circles were obtained from measurements of π-meson tracks of known energy, based on a measurement of 800-1000 blobs in each plate. The solid circles and crosses were obtained from blob and gap measurements on K-meson tracks: in this case, 400 blobs and 50 gaps were counted in each plate.

In addition to a reduction of $g_{\min}$ near the surface and bottom of the plates, local variations were sometimes found within a plate. For example, the value of $g_{\min}$ tended to be lower in regions near the uncut border of the plates. These regions were not used in the ionization estimates unless appropriate calibration was made.

For π-mesons up to 90 MeV, a determination of ionization at one point of the track was usually considered sufficient. For π-mesons of greater energy

([16]) G. Alexander and R. H. W. Johnston: *Nuovo Cimento*, **5**, 363 (1957).

if sufficient length of track was available, two determinations were made at different levels of grain density.

If, however, the track-length available was insufficient to establish the existence of a variation in grain density, a measurement of scattering was also made, if it appeared advantageous to do so. In a residue of cases, due to an increase in dip of the track, or to heavy distortion in the plates through which it passed, or simply because the track was too short, it was not found possible to obtain more than a single estimate of the energy.

3·5. *Loss of light particles.* – The faster particles may easily escape observation, particularly in a stack with low minimum grain density such as the present. Accordingly, as soon as a first analysis of material had been completed, the end of every K-track was re-examined in order to detect any associated light tracks which might have escaped observation in the first scan. An attempt was also made to detect any loss which was a function of the angle of dip of the track or of its depth in the emulsion. The largest sample of light tracks available was that of the π-mesons emitted in K^--interactions at rest. A frequency distribution of the angle of dip, θ_π, of all those π-mesons of energy greater than 30 MeV ($g^* < 2.5$) is shown in Table IV. There seems to be no significant departure from isotropy. The distribution in depth in the emulsion of the K^--interaction giving rise to these π-mesons is shown in Table V *a*). Here, there is some evidence for a tendency for tracks to escape detection when originating near the suiface or the glass.

TABLE IV. – *Distribution of angles of dip of π-meson tracks (energy of π-mesons* > 30 MeV).

Interval of solid angle	0°–14°.5	14°.5–30°	30°–48°.6	48°.6 – 90°
No. of events	181	194	182	193

Since it is to be expected that such a loss will be greatest for the tracks of lowest grain density, the material was further subdivided, and a comparison was made of the depth distribution for π-mesons of energy less than 30 MeV, between 30 ÷ 60 MeV, greater than 60 MeV, and finally, of undetermined energy. For π's of energy up to 60 MeV, the distribution was flat (see Table V *b*)), indicating negligible loss. The distribution for π's of energy greater than 60 MeV, and of unknown energy, showed marked evidence of loss. The combined distribution of the latter categories is given in Table V *c*), and shows an overall loss $22 \pm 7\%$. The number of π-mesons of energy known to be high (*e.g.* > 90 MeV) was too few to allow a separate analysis of their distribution. Those π-mesons in the category « unknown energy » will tend to be of higher

TABLE V. - *Depth distribution of* π*-emitting* K^-*-captures.* K_π/K *means the ratio of the number of* π*-emitting to the total number of stars in a given layer of the emulsion.*

a) All π-mesons.
b) Kinetic energy of π-mesons $\leqslant 60$ MeV.
c) Kinetic energy of π-mesons > 60 MeV or unknown.

Depth in the emulsion (μm above glass)		$0 \div 100$	$100 \div 200$	$200 \div 300$	$300 \div 400$	$400 \div 500$	$500 \div 600$
$K_\pi/K \times 100$	*a*)	22.6 ± 1.1	28.4 ± 1.2	28.6 ± 1.3	36.1 ± 1.4	28.8 ± 1.3	25.9 ± 1.3
	b)	10.4 ± 1.5	13.4 ± 1.7	10.9 ± 1.4	13.1 ± 1.7	12.7 ± 1.7	10.4 ± 1.6
	c)	12.2 ± 1.6	15.0 ± 1.8	17.7 ± 2.0	23.0 ± 2.3	16.1 ± 1.9	15.5 ± 2

energy, chiefly due to difficulty in following. It seems clear, therefore, that the energy spectra obtained are biassed in the direction of low energy on account of observational loss of the faster π-mesons. Since, however, due to insufficient statistics, the energy dependence of the scanning-loss could not be established precisely, it was not considered feasible to attempt a correction to the shape of the experimental spectrum.

The method described above, of correcting for observational loss, assumes in effect that there is no loss of particles in the central regions of the emulsion strips. We may expect, however, that there will be some failure to observe tracks at all depths, particularly in the case of the faster particles. If this is the case, the corrections which have been adopted for the total π/K ratio (Section 5·2) and for the loss of π-secondaries from Σ-hyperons (Part II), will have been underestimated (*).

3·6. *Analysis of* K*-interactions in flight.* – Because of the difficulty of analysing the interactions in flight due to the dimensions of the stack and the small number of events available, the main interest of the present work has been directed to the study of capture at rest. The analysis of interactions in flight has been restricted, therefore, to the estimation of the mean free path, the evaluation of a lower limit for the life time, and a general picture of the salient experimental facts, without attempting a detailed identification of the « light » particles emitted.

(*) *Note added in proof.* - That this is so has been shown in a successive study of K^--stars in a more favourable stack (M. C. AMERIGHI, F. BALDASSARE, M. BENISTON, A. BONETTI, D. H. DAVIS, M. DI CORATO, C. DILWORTH, E. FERREIRA, E. FROTA-PESSOA, W. B. LASICH, N. RAINA, M. RENÉ, J. SACTON and A. C. SICHIROLLO: *Nuovo Cimento*, **12**, 91 (1959)).

4. – General results on K⁻-interactions in flight and at rest.

4·1. *Prong distribution.* – Interactions with hydrogen nuclei of the emulsion leading to the production of $\Sigma^{\pm}$-hyperons and $\pi^{\pm}$-mesons are easily identified by testing for conservation of momentum and energy. 11 out of the 3 035 interactions at rest, and 17 out of the 445 interactions and decays in flight, were established as having taken place on free protons. These events are discussed in Part III, where the cross-section for interaction on free protons and the mass difference between Σ^{+} and Σ^{-}-hyperons are estimated. They do not appear in any of the tables and discussion of the present paper. In 3 cases only did the K⁻-meson re-emerge after interactions in flight: these events are not described here.

TABLE VI. – *Total prong distribution for* K⁻ *interaction at rest in complex nuclei* (*).

Type of events	No. of prongs											
	0	1	2	3	4	5	6	7	8	9	10	Total
(π, Σ) events (**)	—	—	146	19	9	5	1	—	—	—	—	180
(π, D.S.) events	—	—	6	15	14 (2)	9 (1)	1	1 (1)	—	—	—	46
π-events without Σ	—	149	251 (12)	134 (16)	59 (5)	49 (5)	22 (3)	3	—	—	—	667 (43)
Σ-events (**) without π	—	39	33 (10)	26 (5)	27 (6)	21 (3)	2	—	—	—	—	148 (24)
D.S. events without π	—	8	16	29 (7)	24 (2)	12 (6)	9 (0)	3 (1)	1	1	—	103 (16)
Stable prongs only	509	350 (52)	333 (80)	289 (80)	233 (51)	98 (20)	41 (6)	14 (0)	9 (1)	3	1	1880 (290)
Total	509	546 (52)	785 (102)	512 (108)	366 (66)	194 (35)	76 (9)	21 (2)	10 (1)	4	1	3024

(*) The numbers given in brackets under each row refer to the number of events of each category containing a proton of energy > 60 MeV.

(**) Only unambiguously identified Σ's are included. Σ^{-}-hyperons which interact at rest without producing any visible prongs are not included here. A small number of Σ's identified by interactions in flight is included. In these, the visible energy of the star exceeded the kinetic energy of the Σ before interaction. Stops in flight are not included.

The prong distribution of the stars produced by K^--interactions at rest and in flight in G-5 nuclei are shown in Table VI and Table VII respectively. (In these investigations any track longer than 5 μm is defined to be a prong).

TABLE VII. – *Total prong distribution for* K^- *interaction in flight in complex nuclei.*

Type of event	No. of prongs											
	0	1	2	3	4	5	6	7	8	9	10	Total
(π, Σ)	—	—	8	10	5	—	2	—	1	—	—	26
(π, D.S.)	—	—	1	1	1	1	1	—	—	—	—	5
π no Σ	—	(**)6	12	20	12	2	2	1	2	1	—	(*) 58
Σ no π	—	4	6	5	1	4	2	1	—	—	—	24
D. S. no π	—	2	3	3	6	1	—	2	2	1	—	20
Stable only	66	54	40	34	25	13	3	2	5	2	2	246
Total	66	66	70	73	50	21	10	6	10	5	2	379

(*) This figure is deficient in π-mesons because the whole sample was not rescanned. The percentage of π-mesons on the rescanned sample is 33 ± 3 %.

(**) Includes 3 events with blob and 3 events with secondary ionization $> 1.4 \times g_{min}$.

These tables give the numbers of events actually observed in each category. As shown in Section **3**·5, the number of π-mesons is underestimated, due to scanning loss. From the depth distribution of the stars at rest containing a π-meson, it is estimated that, corresponding to 893 π-mesons seen, 110 escaped observation in the layers near surface and glass in the plates. The π/K^- ratio in stars at rest, should be raised therefore from the experimental value of 29.6 ± 1.1 to 33.2 ± 1.2. However, this corrected ratio is likely to be an underestimate (*).

In Table VII the one-prong events which have been classified as « π no Σ » are those in which the ionization of the prong emerging from the supposed interaction exceeds $1.4\, g_{min}$, or if there is associated with it a blob, an Auger electron or a recoil. It seems reasonable to suppose that nearly all events not fitting into the above categories, but in which there is a sudden deflection of

(*) *Note added in proof.* - The value of the π/K^- ratio obtained by AMERIGHI *et al.* (*Note added in proof*, Sect. **3**.5) is in fact 39.2 ± 2.

the incoming K^--track, the emergent track being lightly ionizing, are cases of K^--decay in flight. On this assumption, the ratio π/K^- for stars in flight ([18]) is $(33 \pm 3)\%$ (after partial rescan but not corrected for scanning loss).

As explained in Section 3·5 a detailed discussion of the factors, leading to loss of hyperons, and the corrections to be applied to the observed numbers is given in Part II. The overall Σ/K^- ratio, observed in stars at rest is $(10.5 \pm 0.6)\%$; when all corrections are applied one obtains $(20 \pm 5)\%$. The Σ/K^- ratio observed in stars in flight is $(13 \pm 2)\%$. There were too few stars in flight to allow a separate estimate of the corrections to be applied in this case. As a first approximation, since the mean energy of the particles is not greatly changed, corrections similar to those for stars at rest may be applied.

Many of the identified hyperfragments produced in K^--interactions are of very short range (see Fig. 3). This fact leads to difficulties in estimating their total number. The identification of the event as a hyperfragment is uncertain when no estimate of charge or mass can be made on the interconnecting track (see Section 3·2). Further, when the range of the hyperfragment is less than 2 or 3 μm, its track can not be distinguished against the general blackening at the centre of the K^--star, and the event appears as a double-centred star. Such events are always difficult to recognise, and some of those classified as being many-pronged, may be in fact double-centred, of which the centres lie so close together that they can not be resolved in G-5 emulsion even under the most careful scrutiny.

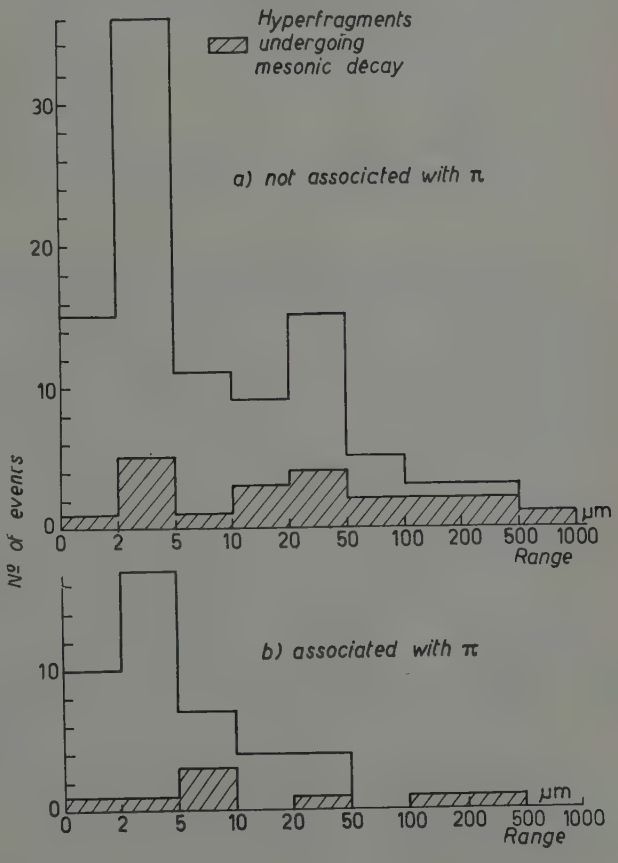

Fig. 3. – Range distribution of the linking track in double stars (D.S.).

Considerable modification to Tables VI and VII may therefore be required to obtain the true distribution of events. Such a modification, however, would require a more precise knowledge of the velocity-dependence of the corrections and of the energy spectra of the particles in each category and, in consequence, the analysis of a much larger number of events.

4·2. *Comparison of stars produced by* K*-interactions in flight and at rest.* – The comparison of Tables VI and VII shows:

a) No great change in the observed percentage of unstable particles (see Table VIII). This is to be compared with the results obtained by the Berne group ([17]) at a higher mean energy, 86 MeV instead of 40 MeV.

TABLE VIII. – *Observed percentage of unstable particles.*

Ratio of No. of unstable particles to No. of K^--stars	Stars in flight Mean $E_K = 40$ MeV	Stars at rest	Bern group Stars in flight Mean $E_K = 86$ MeV
π/K^-	$(33 \pm 3)\%$	$(29.6 \pm 1.2)\%$	$(21.7 \pm 2.4)\%$
Σ/K^-	$(13.3 \pm 2)\%$	$(10.5 \pm 0.6)\%$	$(7.9 \pm 1.2)\%$
D. S./K^-	$(6.7 \pm 1.4)\%$	$(5.5 \pm 0.5)\%$	$(4.0 \pm 1.0)\%$

b) The mean number of stable prongs and their association with π and Σ are rather different. In flight, the fraction of (π, Σ) events without stable prongs is reduced to less than half of that found at rest.

Further, in interactions in flight, there seems to be no appreciable increase in kinetic energy of the Σ hyperons due to the residual energy of the K^--meson.

The mean energy of the identified hyperons is 32 MeV in interactions at rest, and 22 MeV in interactions in flight.

In our stack, detailed measurements of energy of the π-mesons emitted in interactions in flight were not made.

From previous experiments ([18]), and from the present work and in successive papers, it appears that for hydrogen the cross-section for elastic scattering is about three times that for absorption. It is a little difficult therefore, to explain the very few events (3 in 445, see above) in which a K-meson re-emerges from

([17]) Y. EISENBERG, W. KOCH, E. LOHRMANN, M. NIKOLIC, M. SCHNEEBERGER and H, WINZELER: *Nuovo Cimento*, **9**, 745 (1958).

([18]) M. CECCARELLI: *Report at the 7-th Rochester Conference* (1957).

an interaction in flight. ALLES *et al.* [19] have treated the problem in some detail by means of a Monte Carlo calculation.

They conclude that an attractive potential must exist between the nucleus and the K-meson. This conclusion is dependent on the assumption that the ratio of absorption to scattering for neutrons is not very different from that for protons. As mentioned above, a comparison between the prong distribution for the (π, Σ) events and the mean energy of Σ and π in flight and at rest would indicate that a not inconsiderable part of the extra 50 MeV kinetic energy appears as additional prongs rather than in increased energy of the π-mesons or Σ-hyperons. It would thus appear that frequently the K-meson is elastically scattered by a nucleon, transferring some of its energy to it, before capture takes place in a subsequent process. The probability of capture rises rapidly as the K-meson energy decreases. The second interaction therefore is more likely to result in capture than is the first. If, however, this is the case, the proportion of K_ϱ-endings among the stars in flight should be smaller than among those at rest. Experimentally, however, there appears to be no significant difference between these proportions. This observation could, perhaps, be explained if the cross-section of the charge-exchange interaction

$$K^- + p \rightarrow K^0 + n$$

occurring in competition with the first scattering, were about 15% of that for scattering.

An increase in number of stable prongs could also be associated with an enhanced elastic scattering of π-mesons produced with higher energy than in stars at rest, possibly in more central collisions. If such were the case, it would seem strange that the total number of π-mesons escaping from the nucleus is not reduced, as in the stars of higher energy. However, this effect may be due to a compensatory mechanism. As will be seen later (Part II) (*), there is an appreciable number of K^--interactions at rest which appear to involve two or more nucleons, and in which a π-meson is not emitted. If this fraction is reduced in interactions in flight, there will be a higher fraction of π-meson-producing interactions. An increased π-absorption might then be compatible with an unchanged probability of π-emission.

---

[19] W. ALLES, N. N. BISWAS, M. CECCARELLI and J. CRUSSARD: *Nuovo Cimento*, **6**, 571 (1957).

(*) See contribution to Kaplon Report: *Geneva Conference* (1958).

5. – K⁻-interactions at rest in which π-mesons are emitted.

5·1. *General characteristics and nomenclature.* – The general characteristics of the 893 stars from which the emission of a π-meson was observed are displayed in Table IX. The mean energies given are obtained from those stars in which the emergent π-meson had a dip less than 20°. The observed ratio of π^- to π^+ obtained from π's brought to rest in the emulsion, is given for each type of event. The separation of the (π, Σ) events into the categories (π^+, Σ^-) and (π^-, Σ^+), is based on the classification of particles set out in Section 5·2.*a*.

The nomenclature employed to indicate the various types of stars is as follows:

(π, Σ, n) denotes an event containing π-meson and identified Σ-hyperon and n stable prongs.

(π, n) an event containing π-meson, n stable prongs and no identified hyperon.

(π, D.S.) an event in which is observed a π-meson and a secondary star. This category includes hyperfragments, double stars with short unidentified linking tracks, and double-centred stars.

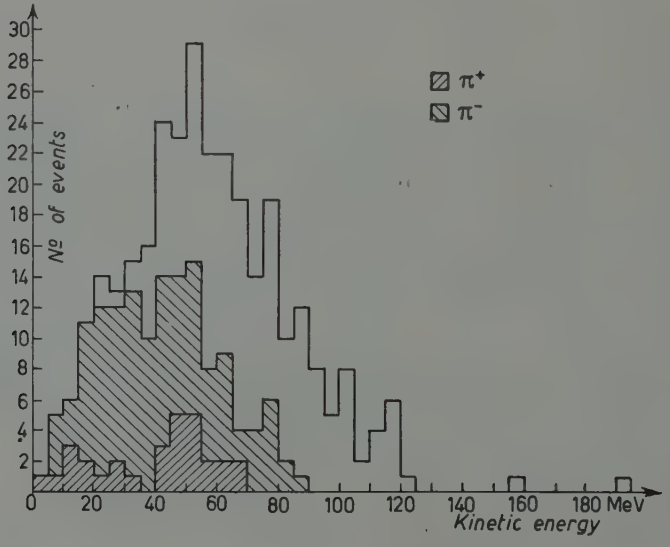

Fig. 4. – Total energy spectrum of π-mesons (angle of dip $\leqslant 20°$).

5·2. *Energy spectrum and sign ratio of all π-particles.* – The energy spectrum for all π-mesons of dip angle less than 20° is shown in Fig. 4. Shading indi-

TABLE IX. – *Characteristics of stars in which a charged π-meson is emitted.*

Star type	No. of events observed	Mean energy of π-meson T_π (MeV)	Mean energy of Σ-hyperon T_Σ (MeV)	Mean energy in stable prongs T_P (MeV)	Total visible energy $T_\pi + T_\Sigma + T_P$ + binding energy	Sign ratio of π mesons observed $\pi^- : \pi^+$
1 Total	**893**	—	—	—	—	191 : 49
2*a* $\pi + \Sigma + 0$	**146**	52 (59 events)	24 (141 events)	0	80 (58 events)	28 : 7
Σ^+, π^-	99	51 (38 »)	24 (98 »)	0	77 (37 »)	—
Σ^-, π^+	25	55 (10 »)	19 (21 »)	0	76 (10 »)	—
$\Sigma^\pm$, $\pi^\pm$	22	60 (11 »)	25 (22 »)	0	81 (11 »)	—
2*b* $\pi + \Sigma +$ prongs	**34**	38 (10 events)	21 (34 events)	9 (32 events)	78 (10 events)	11 : 2
Σ^+, π^-	27	39 (9 »)	19 (26 »)	8 (25 »)	79 (9 »)	—
Σ^-, π^+	7	—	25 (7 »)	12 (7 »)	—	—
2 Total $\pi + \Sigma$	180	—	—	—	—	39 : 9
3 π + D.S.	**46**	76 (11 events)	—	28 (43 events)	130 (10 events)	8 : 1
4*a* $\pi + 0$	149	79 (51 events)	—	—	79 (51 events)	19 : 7
4*b* $\pi + 1$	251	53 (94 »)	—	19 (251 events)	79 (88 »)	38 : 16
4*c* $\pi + 2$	134	50 (51 »)	—	28 (131 »)	92 (50 »)	48 : 10
4*d* $\pi + \geqslant 3$	133	47 (39 »)	—	41 (133 »)	129 (38 »)	39 : 6
4 Total $\pi + n$	**667**	—	—	—	—	144 : 39

TABLE X. – *π-Meson secondaries from* K^-*-meson capture* (Energy > 100 MeV).

Laboratory	Event number	Type of event	Angle of dip	No. of grains	Mean distance of count from emission (mm)	Energy from ionization (MeV)	Length of cell (μm)	No. of cells	Mean distance of scattering from emission (mm)	Energy from scattering (MeV)	Energy adopted (MeV)	Remarks
Brussels-Milan	371	π only	+13°	1025	5.2	112 ± 15	—	—	—	—	112 ± 15	Potential path = 33 mm.
	335	π only	+12°	—	—	96 ± 8	50	136	3.4	95 ± 20	96 ± 8	Stops in flight.
	658	π only	− 6°	1000	5.7	114^{+15}_{-12}	—	—	—	—	113^{+10}_{-7}	
				504	31.5	112^{+11}_{-8}	—	—	—	—		
	269	π only	−11°	1000	4.9	100 ± 10	—	—	—	—	100 ± 10	
	240	π+1	−14°	1000	30.2	116^{+10}_{-8}	—	—	—	—	116^{+10}_{-8}	Scattering unreliable owing to dip.
	375	π+n	+15°	700	4.5	190 ± 40	—	—	—	—	190 ± 40	Toward external border. Corroded region. Potential path = 20 mm.
	543	π+n	− 1°	1000	4.7	104 ± 12	50	272	6.8	119 ± 15	110 ± 10	Potential path = 40 mm.
Dublin	12/20/19	π only	−20°	1000	4.0	156^{+35}_{-30}	—	—	—	—	156^{+35}_{-30}	Parallel to the beam and hard to follow.
	24/30/24	π+1	+17°	800	4.0	—	—	—	—	—	97 ± 8	Scattering unreliable owing to dip.
				800	12	97 ± 8	—	—	—	—		
				800	20	—	—	—	—	—		
	14/28/24	π+n	+ 4°	800	3	119^{+17}_{-15}	—	—	—	—	91 ± 7	
				1000	27	91 ± 7	—	—	—	—		
	10/8/14	π+n	+ 8°	1000	4	120^{+16}_{-13}	—	—	—	—	101 ± 8	

	Padua	289	π only	12	1100		$-\frac{}{}$					
2283	U. C. London	2307	π+HF	+20°	666	3	115^{+10}_{-13}	—	—	—	—	115^{+20}_{-12}	
		2418	π+HF	− 4°	1000	4	101^{+8}_{-7}	100	45	2.2	103^{+13}_{-17}	101^{+8}_{-7}	Scattering unreliable owing to dip.
		3010	π+HF	− 6°	2000	8	—	100	43	2.1	106^{+20}_{-18}	117 ± 2	
					1000	13	117 ± 2	—	—	—	—		
					1000	102	—	—	—	—	—		
		3313	π only	− 2°	1000	4	102 ± 5	100	40	2	106^{+21}_{-19}	102 ± 5	
					800	19.6							
		1009	π only	+15°	650	3	112 ± 12	—	—	—	128^{+26}_{-24}	110 ± 6	
					600	10.6	96 ± 8	—	—	—	—		
					600	16.5	122 ± 12	—	—	—	—		
		2109	π only	− 6°	1083	4	100 ± 4	100	21	1	136^{+20}_{-35}	100 ± 4	
					1000	13.3							
		2715	π only	+ 8°	741	3	105^{+11}_{-8}	—	—	—	—	105^{+11}_{-8}	
		2815	π only	− 6°	800	3	116 ± 8	—	—	—	—	110 ± 8	
					545	11							
		6802	π only	+17°	504	2	102 ± 14	—	—	—	—	102 ± 14	Scattering unreliable owing to dip.
		7853	π only	+19°	1120	4	105^{+10}_{-8}	—	—	—	—	105^{+10}_{-8}	Scattering unreliable owing to dip.
		6053	π only	+ 4°	1045	4	115^{+12}_{-10}	100	55	2.8	124^{+20}_{-18}	116^{+12}_{-10}	
		5656	$\pi+n$	+20°	1193	4	118^{+12}_{-10}	—	—	—	—	118^{+13}_{-10}	Scattering unreliable owing to dip.

cates π-mesons the sign of which was determined by following the tracks to the end of their ranges. The mean error in energy determination is 2% for tracks followed to their end and between 4 and 8% where energy is estimated from ionization. On the faster tracks the estimated error is greater, generally about 12% for energies above 100 MeV. Details of the measurements made on these high energy π-mesons are given in Table X (*). As discussed in Section 3·5, this spectrum is subject to bias arising from the higher scanning loss of the faster π-mesons.

The observed π^-/π^+ ratio is 3.9 ± 0.7. As has already been pointed out [20], this is not necessarily the true overall ratio, if there is a difference between the energy spectra of the π^- and π^+ mesons, since the chance of following a π-meson track to the end of its range, and so of determining its sign, decreases rapidly as its energy increases. In our stack, it was possible to follow to rest 94% of π's of energy less than 30 MeV, 55% between 30 MeV and 60 MeV, 26% between 60 MeV and 90 MeV, and none above 90 MeV. Before considering the overall experimental π^-/π^+ ratio, one should estimate first its value in given intervals of energy, since, in an energy interval suitably chosen, there should be negligible bias in favour of either sign. This has been done in Table XI.

TABLE XI.

Energy of π	No. π^-	No. π^+	Sign ratio π^-/π^+
0÷30 MeV	95	25	3.8 ± 0.8
30÷60	76	19	4.0 ± 0.9
60÷90	20	5	4.0 ± 1.6
> 90	—	—	—

There is no statistically significant evidence for a variation of the ratio with energy. We take therefore, an overall π^-/π^+ ratio $= 3.9 \pm 0.7$, over the energy interval (0÷90) MeV. On this basis the total number of π-mesons observed, corrected for observation loss, will be as set out in Table XII.

(*) The two highest values, 156 and 190 MeV respectively, are subject to considerable doubt due to difficulty in measurement (see Table X).

(20) C. DILWORTH: *Report at 7-th Rochester Conference* (1957). Also contribution to Kaplon Report: *Geneva Conference* (1958).

TABLE XII.

Energy range	0÷90 MeV		> 90 MeV
Sign of π	−	+	±
Number observed	628	161	104
Number corrected for observational loss	690	179	134

The numbers of charged π-mesons of each sign created in the primary interaction of the K^--meson with one or more nucleons, could be deduced from the total number of π-mesons, emitted, the π^-/π^+ ratio, and the relative probabilities, if known, of absorption of π^+ and π^- mesons in the parent nucleus (Part II).

In this experiment, however, the total number of π-mesons emitted is uncertain since it is likely that the observation-loss has been underestimated (see Section 3·5). Moreover, the π^-/π^+ ratio is unknown for π-mesons of energy greater than 90 MeV. Although there is no evidence for a variation of this ratio up to 90 MeV, it remains possible that it changes at higher energies.

5·3. (π, Σ) *events.*

a) Associated signs in (π, Σ) events. – In 893 events, there are 180 in which both hyperon and π-meson are seen. Among them, there are 35 in which the sign of both π and Σ is known, and 123 in which the sign of either Σ or π is recognised.

Table XIII gives the number of events in each category.

TABLE XIII.

Class	$\pi^+ \Sigma^-$	$\pi^- \Sigma^+$	$\pi^\pm \Sigma^-$	$\pi^\pm \Sigma^+$	$\pi^- \Sigma^\pm$	$\pi^+ \Sigma^\pm$	$\pi^\pm \Sigma^\pm$	Total
π, Σ, 0	3	22	18	71	6	4	22	146
π, Σ, n	0	10	5	16	1	2	0	34

No clearly identified hyperon was found to be associated with a π-meson of the same sign, so that it is reasonable to assume that such an occurrence is very infrequent. In constructing Table IX, therefore, it has been assumed that when the sign of the charge of either the π-meson or the hyperon is known,

its partner is of opposite charge. In this way there remain only 22 $(\Sigma^{\pm}, \pi^{\pm})$ events. The division of these events between (Σ^{+}, π^{-}) and (Σ^{-}, π^{+}) can be obtained by use of the branching ratio $\Sigma^{+} \to p/\Sigma^{+} \to \pi^{+}$ (see Part II). The total number of observed (Σ, π) events can thus be divided into 145 (Σ^{+}, π^{-}) and 35 (Σ^{-}, π^{+}) (*).

b) The loss of energy of Σ-hyperons and π-mesons in collisions within the nucleus in which they are produced. – The fact that only 34 out of 180 (π, Σ) are associated with prongs, indicates that the loss of energy of π's and Σ's in leaving the nucleus is rather small. Since, on the average, the mean energy of the π is 14 MeV lower in (π, Σ, n) than in $(\pi, \Sigma, 0)$ events, and the energy of the Σ is about the same in both, it seems that it is the loss of energy of the π-meson which is the principal cause of emission of stable prongs. For this reason it is of interest to estimate in how many of the $(\pi, \Sigma, 0)$ events energy loss occurred which resulted in the emission of neutrons.

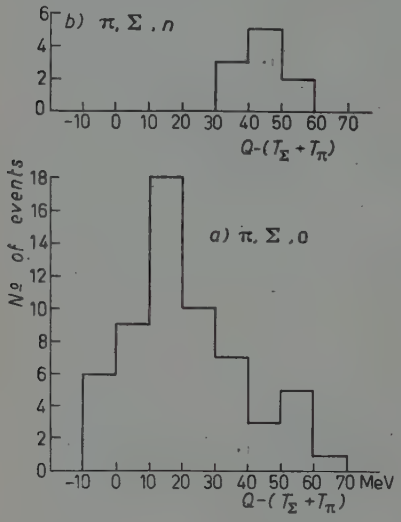

Fig. 5. – Distribution of the residual energy $Q-(T_{\Sigma}+T_{\pi})$ in: *a*) $(\pi, \Sigma, 0)$ events, *b*) (π, Σ, n) events.

As already pointed out by GILBERT *et al.* [10], the spread in total energy $(T_{\pi}+T_{\Sigma})$ in (π, Σ) events is small. In our sample, the mean energy observed is 80 MeV, and 88% of the events lie in the range 60 to 110 MeV. The distribution of the quantity $Q-(T_{\pi}+T_{\Sigma})$ (Fig. 5*a*) extends to negative values, because of statistical fluctuations in the estimates of kinetic energy. This is consistent with a mean excitation energy of about 15 MeV, with about 15% of the events showing a higher energy loss, resulting in the emission of neutral particles. The corresponding distribution for (π, Σ, n) events (Fig. 5*b*) shows a grouping of the value of $Q-(T_{\pi}+T_{\Sigma})$ between 30 and 60 MeV, similar to the tail of the distribution

(*) On the other hand, the evidence given in Table XIII is not sufficient to rule out the occurrence of charge exchange or of 2 N interactions with emission of a π-meson. Interactions of this type, leading to stars in which a π and Σ of the same sign are ejected, will be characterized in most cases by the emission of at least one stable prong, and the number of (π, Σ, n) events, in which both signs are known, is small. One event was observed in which there was a negative π-meson, a possible negative Σ-hyperon, and 2 short stable prongs. Since however, the identification of the Σ-hyperon was open to doubt, it has not been included among the clearly identified hyperons.

for $(\pi, \Sigma, 0)$. The comparison of these two distributions leads us to consider that in the majority (about 80%) of the $(\pi, \Sigma, 0)$ events, apart from the 15 MeV excitation energy given up to the nucleus, no furthear ppreciable energy is lost in collisions by the emerging π or Σ.

These considerations imply that both the π-meson and Σ-hyperon spectra are largely free from distortion due to energy loss by collisions of the particles in the parent nucleus. A distortion due to scanning loss of the faster π-mesons may, however, be present. In Fig. 6*a* are given the spectra for π^-, π^+ and $\pi^\pm$ for $(\pi, \Sigma, 0)$ events, and in Fig. 6*b*, the corresponding spectra for (π, Σ, n) events. The larger proportion of low energy π's in (π, Σ, n) events is evident. At the high energy end, the spectra are limited at 90 MeV.

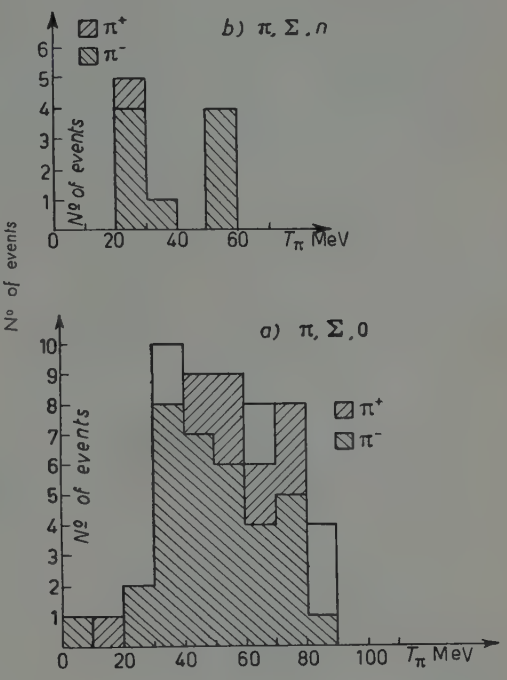

Fig. 6. – Energy distribution of π-mesons from (π, Σ) events. (Angle of dip $\leqslant 20°$).

c) The effective nuclear interaction of Σ^--hyperons. – The absorption of K^--mesons by nuclei has been discussed by CAPPS ([21]) in terms of the optical model. He supposed the hyperon and π-meson to be produced in potential wells of depth V_Σ, V_π respectively, and took the total energy inside the nucleus to be

$$(M_K + M_\pi - M_\Sigma - M_\pi)c^2 + V_\Sigma + V_\pi - V_N ,$$

where M_K, $M_\mathcal{N}$, M_Σ, M_π respectively refer to the masses of the K, nucleon, Σ and π, and V_Σ, V_π to the depth of the Σ and π potential wells. V_N is the sum of the binding energy of the nucleon and the mean excitation energy of the product nucleus. This energy is supposed to be shared between the product particles, just as would be the case if it were the Q-value of an interaction between the K-particles and the nucleon outside nuclear matter. The parti-

([21]) R. H. CAPPS: *Phys. Rev.*, **107**, 239 (1957).

cles, in escaping from the nucleus have to pass through the barrier produced by a combination of the nuclear and Coulomb potential. Their chance of emerging depends, not only on the height of the barrier, but also on their angle of incidence to it (*i.e.*, on their angular momentum about the centre of the nucleus).

CAPPS showed that this model gives quantitative agreement with the energd distribution of hyperons produced inside nuclei by K^--capture. He showey further, that the form of the observed hyperon spectra was rather insensitive to the value of $|V_\Sigma|$ for values between 10 and 30 MeV.

The theoretical spectra do not take into account the effect of interactions of the particles in the nucleus but, as discussed in the preceding section, there is reason to suppose that such interactions do not commonly involve large energy losses.

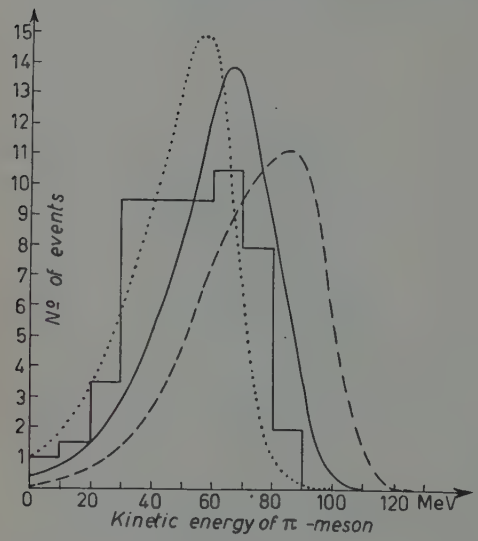

Fig. 7. – Energy distribution of π^--mesons in $(\Sigma^+, \pi^-, 0)$ events. The histogram represents the combined distributions obtained by GILBERT *et al.* [12] and the present work. The curves represent the theoretical distribution for $|V_\Sigma| = 0$(·····), 15 (——) and 30 MeV (– – –). Average experimental errors are folded in.

It would seem to be of interest, therefore, to compare the observed π-meson spectra with those calculated from the model. The spectrum of negative π-mesons obtained here (Fig. 6) has been combined with that given by GILBERT *et al.* [12] in order to furnish a sample sufficiently large to allow comparison with the calculations. In Fig. 7 therefore, the combined histogram is compared with that calculated from Capps model for $|V_\Sigma|$ 0, 15 MeV and 30 MeV respectively with the experimental errors folded in (*).

In performing this calculation, $|V_\pi|$ was taken to be 40 MeV, while $|V_N|$ was taken to be 20 MeV. The value obtained for $|V_\Sigma|$ will depend on that assumed for V_π and V_N. If there were small energy loss by all π's in collisions, the value of $|V_\Sigma|$ should be increased. Further, any scanning bias leading to a loss of fast π-mesons will tend to lead to an underestimate of $|V_\Sigma|$. However, there is little reason to suppose that the value of $|V_\Sigma|$ is larger than 15 MeV, so that the effective hyperon-nucleus well is not very deep.

(*) We are indebted to Dr. DELL'ANTONIO, Dr. PAROLINI and Mr. UNDERHILL for calculating these distributions.

d) The energy visible in stable prongs. – As shown above (Section 5·3.*b*), the energy visible in stable prongs in (π, Σ) events can be attributed mainly to the inelastic scattering of the π-mesons.

As seen in Table VI, 56% of the (π, Σ, n) events have one stable prong only, and none have more than 4 prongs. The distribution of total energy (kinetic energy+binding energy) of these prongs is given in Table XIV.

In no (π, Σ, n) event, is there more than 60 MeV in stable prong energy. The maximum energy of a single prong in this sample is 25 MeV.

TABLE XIV. – *Energy visible in stable prongs in* (π, Σ, n) *events* (*Kin. En.*+*Bind. En.*).

Total energy in stable prongs MeV	0÷10	10÷20	20÷30	30÷40	40÷50	50÷60
No. of events	7	11	12	4	0	1

5·4. $(\pi$, D.S.) *events*. – As will be seen from Table IX, the 46 events falling within this category are characterized by:

i) A mean energy of the π-meson (77 MeV), higher than the average of other types of event. The energy distribution extends up to 120 MeV.

ii) A mean total visible energy release of 130 MeV, also higher than the average of other types of event.

Three of these events may be interpreted as involving the emission of a hyperfragment. As pointed out however in Section 4·1, the linking track in the majority of the cases is very short and identification of its nature is generally difficult, and often impossible (see also Fig. 3). Considerations based on the shape of the total π-meson energy spectrum, and also the fact that only 2 out of 3 024 K^--stars have been seen to contain 2 π-mesons, would appear to rule out the hypothesis that these double stars should be attributed to slow negative π-mesons.

A certain fraction, however, of these interconnecting tracks could be short negative hyperons. The appearance of the secondary stars is very similar to that of the stars produced by Σ^- at rest, exception being made of the mesonic decays which are clearly attributable to hyperfragments. The percentage of fast protons (about 30%) is the same in both cases.

However, the high mean energy of the π-mesons, and the large visible energy release, would indicate that the process involved in this class of event is essentially different from those in the (π, Σ) events. This would render plausible the supposition that most of the $(\pi$, D. S.) events are due in fact to hyperfragment emission.

The high mean total visible energy is to be attributed in part to the presence of fast π-mesons, but also to a large energy release in stable prongs (see Table XV) related to the presence (20%) of «fast» protons of energy greater than 30 MeV, which was the maximum energy observed in (π, Σ, n) events.

TABLE XV. – *Energy visible in stable prongs in* (π, D.S.) *events* (*Kin. En.*+*Bind. En.*).

Energy	0÷10	10÷20	20÷30	30÷40	40÷50	50÷60	60÷80	80÷100	100÷120
No. events (*)	6	7	5	6	5	4	7	3	1
No. events with «fast» protons $T_p > 30$ MeV	—	—	—	—	—	—	(6)	(3)	(1)

(*) 2 more D.S. events not classified here because attribution of prongs to primary and secondary star is ambiguous (no «fast» protons).

As will be shown later, this large energy release in stable prongs may be attributed mainly to the interaction of Σ^+- and Σ^0-hyperons. Thus, out of 46 (π, D.S.) events, 10 may be attributed to $\Sigma^{+,0}$-absorption (Sect. 5·5, *e*). Taking the value 4 : 1 for the π^-/π^+ ratio, there should be 10 π^+, and therefore 10 Σ^--emitted or absorbed. The remaining 26, as will be shown later, may be due to the direct production of Λ^0.

5·5. *Analysis* of (π, n) *events.*

a) General characteristics. – In this class of events, in which no hyperon has been identified, the fate of the hyperons will be as follows:

1) $\Sigma^{\pm}$-hyperons are emitted but are unidentified; 80% of these would be expected to appear as (π, 1) events.

2) Λ^0 or Σ^0-hyperons are emitted and appear, in part, as (π, 0) events.

3) The hyperons are absorbed.

The main characteristics of these events are shown in Table IX and may be summarized as follows:

i) (π, 0) events: a high mean energy of the π-meson, and energy spectrum similar to that for (π, D.S.) events. A π^-/π^+ ratio of 19 : 6, not significantly different from the average ,indicating that the emission of neutral hyperons, associated with π^-, is not the only operative process.

ii) $(\pi, 1)$ events: the mean energy of π, mean energy of stable prongs and total visible energy similar to those in (π, Σ) events. The π^-/π^+ ratio, 38: 16, rather lower than the average, as would be expected if Σ^- tends to remain unrecognized more frequently than Σ^+.

iii) $(\pi, 2)$ events and $(\pi, \geqslant 3)$ events. There appears to be a decrease in the mean π-energy, and an increase in energy of stable prongs, total visible energy and π^-/π^+ ratio, with respect to $(\pi, 0)$ and $(\pi, 1)$ events. This would imply an association of large energy release mainly with negative π-mesons.

b) Estimate of number of unidentified $\Sigma^{\pm}$-hyperons. – An estimate of the number of unidentified Σ-hyperons in $(\pi, 1)$ events, can be obtained from an analysis of the distribution of the angle between the π-meson and the prong, and the π^-/π^+ ratio for different energy intervals of the associated prong. This analysis is described in Part II and leads to an estimate of 77 unidentified Σ-hyperons in $(\pi, 1)$ events, of which 43 are negative and 34 positive. Removing these events from the $(\pi, 1)$ category, would leave a sign ratio $\pi^-/\pi^+ \sim 4.5$ for $(\pi, 1)$ events, from a total number of 174 events.

From the distribution of stable prongs associated with identified (π, Σ) events, the total number of unidentified Σ-hyperons should be 1.25x the number appearing as $(\pi, 1)$ events. There will be therefore, 54 negative and 42 positive hyperons unidentified in this class. It follows that the total corrected numbers of Σ-hyperons accompanying an observed π-meson are respectively (187 ± 17) positive, and (89 ± 17) negative.

c) Absorption of Σ^--hyperons. – The distribution of prongs in (π^+, n) events is given in Table XVI. In addition to these 37 events, there

TABLE XVI. – *Prong distribution of* (π, n) *events where the sign of the* π*-meson is known.*

Sign of π	No. of (π, n) events						
	$(\pi, 0)$	$(\pi, 1)$	$(\pi, 2)$	$(\pi, 3)$	$(\pi, 3)$	$(\pi, 5)$	$(\pi, 6)$
Negative	19	38	46	20	12	4	1
Positive	6	16	9	1	3	2	0

are 9 π^+ accompanied by a hyperon, and 1 by a D.S. event. Assuming that π^+ are always produced together with a Σ^- (*i.e.* supposing the reaction $K^- + p + p \rightarrow \Sigma^0 + \pi^+ + n$ to be infrequent), an estimate of the probability of

absorption of Σ^--hyperons $p(\Sigma^-)$ is given by

$$p(\Sigma^-) = \frac{\text{number of } \pi^+ \text{ unaccompanied by a } \Sigma^-}{\text{total number of } \pi^+}.$$

It is known however, that a certain fraction of Σ^--hyperons will remain unidentified. Among the 9 which were recognized, 6 decayed in flight, and 3 came to rest and gave rise to a star with 2 or more prongs. Corresponding to these, as will be shown later (Part II), one would expect to have 9 unidentified hyperons. The value obtained for $P(\Sigma^-)$ is then,

$$p(\Sigma^-) = 1 - \frac{9+9}{47} = (62 \pm 13)\%.$$

The above method of estimating $p(\Sigma^-)$ suffers from the defect that a bias is introduced in selecting events containing a π-meson of determinable charge. Such π-mesons, if they were to be followed to rest, will be mainly of low energy. In consequence, the Σ-hyperons produced in association with them will tend to be of high energy and if, as seems plausible, the absorption probability is a function of the energy of the Σ-hyperon, this procedure will not yield a valid estimate of the average value of $p(\Sigma^-)$.

An estimate of upper and lower limits of the absorption over the energy-intervals of π and Σ, with which we are concerned, may be obtained from the estimated number of π^+ mesons and of Σ^--hyperons, associated with π's.

As shown above, the total number of Σ^--hyperons accompanied by a π-meson is estimated to be 89 ± 17 (apart the 10 (π, D.S.) events, Section 5·4). The number of π^+-mesons of energy less than 90 MeV can be deduced from the mean sign ratio, and is 151 ± 20 (uncorrected for observational loss). The number of π^+-mesons of energy greater than 90 MeV is unknown. It must lie however between 0, and the total number of π's of this energy, *i.e.* 104 (estimated from the fraction of π's > 90 MeV in the energy spectrum of π's of dip less than 20°). Considering these uncertainties, the probability of absorption of the Σ^- can be placed between the limits

$$0.41 \pm 0.11 < p(\Sigma^-) < 0.65 \pm 0.22\,,$$

the lower limit being favoured since there is evidence ([22]) that the faster π-mesons may be attributed to Λ^0 production (see later, section 5·5-*f*). Taking into account the 10 Σ^- unidentified among the (π, D.S.) events does not change appreciably the results.

([22]) Y. EISENBERG, W. KOCH, M. NIKOLIĆ, M. SCHNEEBERGER and H. WINZELER: *Nuovo Cimento*, **11**, 351 (1959).

d) Emission of Σ^0-hyperons. – An estimate of the number of Σ^0 hyperons, emitted from the nucleus, may be obtained from the number of $(\pi^-, 0)$ events compared with that of $(\pi^-, \Sigma^+, 0)$ events. Among the 10 $(\pi^-, 0)$ events in which the identified π^--meson has an energy of less than 50 MeV, one would not expect an important contribution from hyperons from the reaction $(K^-n, \Lambda^0\pi^-)$, since the chance is small that a high energy π-meson lose energy without giving rise to a visible star. Neither are the interactions $(\Sigma^+n, p\Lambda^0)$ and $(\Sigma^0p, p\Lambda^0)$ likely to give 0-prong events. There remain those events arising from the interaction $(\Sigma^0n, n\Lambda^0)$. A first-order correction for these may be obtained by analogy with Σ^- absorption.

Out of 37 π^+-mesons identified, only 6 are without associated prongs. Assuming that half the Σ^0 absorbed interact with neutrons, that the probability of absorption and prong distribution is similar to that of the Σ^-, and taking account also of the fact that about 6 Σ^- prongs would fail to be identified as such, one would expect about 3/31 or 0.10 of the Σ^0 to be absorbed in such a way as to give a 0-prong star.

Since 21 $(\pi^-, \Sigma^+, 0)$ events have an identified π^--meson of energy less than 50 MeV, and little difference is to be expected between the π-meson energy spectra of (π^-, Σ^+) and (π^-, Σ^0) or between the associated stable prong distributions, we can write:

$$\frac{\pi^-, \Sigma^0_{\text{emitted}}}{\pi^-, \Sigma^+_{\text{emitted}}} = \frac{10 \times 0.90}{21 + x} .$$

where x is the number of unidentified Σ^+-hyperons corresponding to this sample. Using corrections factors for Σ-loss from Part II, we can estimate $x=6$, so that

$$\frac{\pi^-, \Sigma^0_{\text{emitted}}}{\pi^-, \Sigma^+_{\text{emitted}}} = 0.34 ,$$

and an estimate of the absolute number of Σ^0-hyperons emitted is 64 ± 20.

e) Absorption of hyperons and fast proton emission. – An energy, visible in the star, of more than 110 MeV, implies that

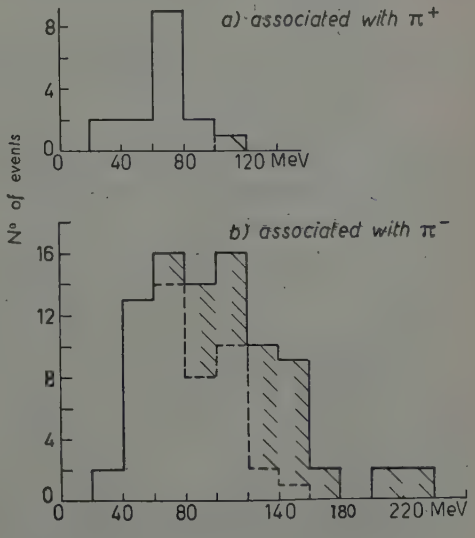

Fig. 8. – Distribution of total visible energy in $(\pi^-, \geqslant 2)$ events. The shading indicates the presence of 1 or more protons of energy greater than 30 MeV.

a Σ-hyperon has not left the nucleus. Either it has been absorbed, and a Λ^0-hyperon produced, or a Λ^0-hyperon was produced in the primary reaction.

In Fig. 8*a*,*b*) are shown the distributions in total visible energy of $(\pi, \geqslant 2)$ stars containing an identified π^- and π^+-meson respectively. There appears to be a marked difference between the two distributions, in that 31 out of 86 of the $(\pi^-, \geqslant 2)$ events show a total visible energy greater than 110 MeV, compared to 1 out of 16 of the $(\pi^+, \geqslant 2)$ events. The shading in the figure denotes the presence of one or more fast protons, of energy greater than 30 MeV. It can be seen that 26 of the 32 events with large energy release contain a fast proton. If the energy of the fast protons is subtracted from the total visible energy, the difference between the π^- and π^+ distributions is greatly reduced, and in fact is no longer significant (see Fig. 9).

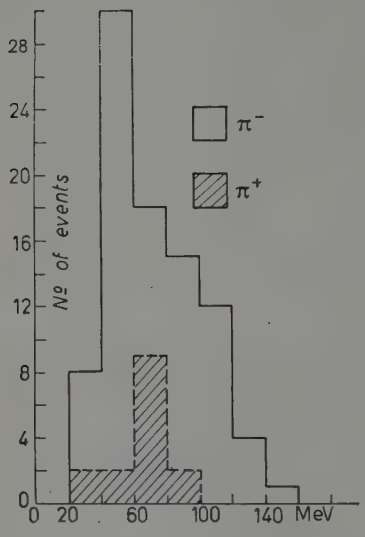

Fig. 9. – Distribution of total visible energy less energy of fast protons in $(\pi^-, \geqslant 2)$ events.

It appears, therefore, from these figures, that large energy release is associated predominantly with negative π-mesons, and that it is mainly associated with the emission of protons of energy greater than 30 MeV. Such protons may be formed in one or more of the following processes:

1) Inelastic scattering of a fast π-meson, accompanying a directly produced Λ^0.

2) The interaction of Σ^+ or Σ^0-hyperons.

3) The stimulated decay of Λ^0-hyperons.

In Table XVII is given the fraction of events giving fast protons in inelastic scattering of incident π^- and π^+-mesons at average incident energies of 80 and 120 MeV, as measured by the Bologna group (*). This is compared with the corresponding fraction of K^--interactions giving (π, n) stars, in which a fast proton is emitted together with an identified π^- or π^+-meson.

It is clear that:

i) The percentage of fast protons in K^--stars giving a π^--meson, is higher than that obtained from inelastic scattering, considering that not all

(*) Bologna Group: private communication and unpublished results.

TABLE XVII. – *Percentage of events giving a fast proton.*

	a) In inelastic scattering of π-mesons (Bologna Group results) Kin. En. of incident π-mesons				*b*) In K⁻-capture stars (present experiment)			
	80 MeV		120 MeV		all (π,n)		$(\pi,\ n>2)$	
	π^-	π^+	π^-	π^+	π^-	π^+	π^-	π^+
Emission of a proton of energy > 30 MeV	1/19 5%	2/40 5%	6/59 10%	8/42 20%	51/149 34%	3/31 10%	38/83 46%	1/14 7%
Emission of a proton of energy > 60 MeV	0/19 0	0/40 0	2/59 3.4%	1/42 2.4%	18/149 12%	0/31 0	16/8 19%	0/14 0
Emission of two protons of energy > 30 MeV	— 0	— 0	— 0	— 0	4/149 2.7%	0/31 0	4/83 4.8%	0/14 0

the π's will have been scattered. In fact, from the number of π's of energy less than 40 MeV (36%), about 50% should have undergone inelastic scattering.

ii) The ratio of the fraction of fast protons from π^- to that from π^+ is 3:1 in K^- (π, n) stars, compared with 0.7:1 for inelastic scattering.

This discrepancy becomes more marked if we consider only $(\pi, n>2)$ events, in which the number of unidentified Σ and escaping Σ is expected to be very small.

The inelastic scattering of π-mesons does not therefore seem to be an important source of high energy protons.

The interaction of Σ-hyperons would, on the other hand, be expected to show a strong correlation with negative π-mesons. The absorption processes involving Σ-hyperons are:

(1) $\Sigma^- + p \rightarrow \Lambda^0 + p$,

(2) $\Sigma^+ + n \rightarrow \Lambda^0 + p$,

(3) $\Sigma^0 + n \rightarrow \Lambda^0 + p$,

(4) $\Sigma^0 + n \rightarrow \Lambda^0 + n$.

From this, we may see that in such interactions a fast proton can only be produced through the absorption of a Σ^+ or Σ^0. However, the production of

Σ^+ or Σ^0 must take place in association with a π^--meson. Hence, in stars containing a charged π-meson and a fast proton, the π-meson will generally be negative if the fast proton is produced by Σ-absorption.

The stimulated decay of the Λ^0-hyperon will also be associated with a π^-, if its mode of production is direct (K^-n, $\pi^-\Lambda^0$). In light hyperfragments, about 50% of the non-mesonic decays give a fast proton ([23]), but the fraction of such events in nuclei as heavy as those of the emulsion is not known. Some indication may be obtained from the K^- interactions themselves:

i) Fast π-mesons, of more than 90 MeV energy, should be associated with a Λ^0 either from a trapped Σ, or directly produced. Of the 36 π-mesons of energy known to be greater than 90 MeV, none is accompanied by a fast proton.

ii) The fact that π^+-mesons are rarely associated with a fast proton, indicates that the absorption of Σ^--hyperons does not generally lead to a trapping of a Λ^0, which would then undergo stimulated decay with emission of a fast proton. The mean energy of emission of a Λ^0-hyperon produced directly in the reaction (K^-n, $\Lambda^0\pi^-$) is expected to be ~ 40 MeV, which is similar to that of the Λ^0 produced by Σ interaction. The probability of trapping should therefore be similar in both cases.

iii) In the (π, D.S.) events, supposed to be mainly due to hyperfragment emission, there cannot be a Λ^0-hyperon in the primary star. In Tables XVIII and XIX are compared the distribution of prongs and the energy visible in stable prongs, of (π, D.S.) events and of (π, n) events, the latter being corrected for unidentified $\Sigma^\pm$ and for Σ^0-emission.

TABLE XVIII. – *Stable prong distribution in* (π, n) *and* (π, D.S.) *events.*

No. of stable prongs	0	1	2	3	4	5	6
No. of (π, n) events (*)	82	165	121	52	45	21	3
%	17	34	25	11	9	4	0
No. of (π, D.S.) events	6	14	14	9	1	1	—
%	13	31	31	24	2	2	—

(*) Corrected for unidentified $\Sigma^\pm$ and for Σ^0 emission.

([23]) M. BALDO-CEOLIN, C. DILWORTH, W. F. FRY, W. D. B. GREENING, H. HUZITA, S. LIMENTANI and A. E. SICHIROLLO: *Nuovo Cimento*, **7**, 328 (1958).

The two distributions show a marked similarity. It seems reasonable to conclude that, if the stable prongs in the two classes of event are produced by similar processes it would follow from this assumption that the chief source of fast protons is most likely the interaction of Σ^+ and Σ^0-hyperons.

TABLE XIX. – *Distribution of energy visible in stable prongs in* (π, n) *and* $(\pi, \text{D.S.})$ *events* (*).

MeV	0÷10	10÷20	20÷30	30÷40	40÷50	50÷60	60÷80	80÷100	100÷140	> 140
No. of (π, n) events (**)	75	82	53	$47_{(2)}$	$59_{(11)}$	$46_{(17)}$	$56_{(37)}$	$35_{(27)}$	$18_{(13)}$	$16_{(12)}$
(%)	15.6	17.1	11.0	9.8	$10.8_{(2.7)}$	$9.6_{(3.5)}$	$11.7_{(7.5)}$	$7.3_{(5.8)}$	$3.7_{(3.1)}$	$3.3_{(2.9)}$
No. of $(\pi, \text{D.S.})$ events	6	7	5	6	5	4	$7_{(6)}$	$3_{(3)}$	$1_{(1)}$	0
(%)	14.0	16.2	11.6	14.0	11.6	9.3	$16.3_{(14)}$	$8.1_{(8)}$	$2.3_{(2)}$	0

(*) Bracketed figures are number and percentage of events containing a fast proton.
(**) Corrected for unidentified $\Sigma^{\pm}$ and for Σ^0 emission.

On this basis, it is possible to estimate the combined Σ^0 and Σ^+ absorption, assuming that the proton produced in the interaction always escapes. A rough correction can be applied, to account for the number of cases in which the proton is emitted in this interaction with less than 30 MeV energy. Fig. 10 shows the energy spectrum of protons from $(\pi, \geqslant 2)$ events above 30 MeV. A reasonable extrapolation to zero energy, taking into account the fact that a maximum in the curve is expected at (30÷40) MeV, would lead to a raising of the above figure, 34% (see Table XVII), to about 40% of the (π^-, n) events ($E_\pi < 90$ MeV), *i.e.* in absolute number, about 186 events. Adding to these the 10 $(\pi, \text{D.S.})$ events containing a fast proton, the number of (Σ^+, n) and (Σ^0, p) interactions is 196 which can be divided into 167 Σ^+_{abs} and 29 Σ^0_{abs} (Section 5·5-*d*). The corrected total number of the emitted Σ^+ and one half of the emitted Σ^0 is 219, giving an overall absorption probability of 47%. Within the uncertainties, this probability equals that of the Σ^--hyperons.

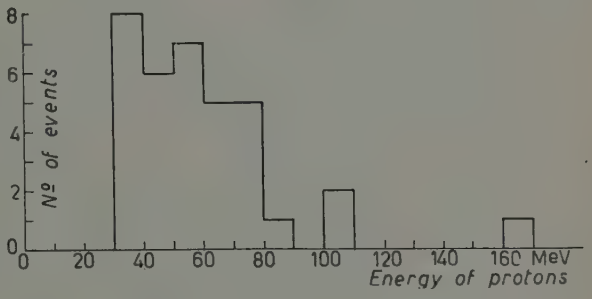

Fig. 10. – Energy distribution of protons of energy greater than 30 MeV emitted in $(\pi, \geqslant 2)$ events.

It seems reasonable therefore to write $P_{\Sigma^-} \sim P_{\Sigma^+} \sim P_{\Sigma^0} \sim 45\%$.

f) Production of Λ^0-hyperons. – In Table XX are shown the numbers of observed (π, n) and $(\pi, \text{D.S.})$ events which have been attributed to the variousprocesses so far discussed.

TABLE XX. – *Classification of* (π, n) *and* $(\pi, \text{D.S.})$ *events.*

Process	$\Sigma^{\pm}_{\text{unidentified}}$	$\Sigma^{-}_{\text{absorbed}}$	$\Sigma^{0}_{\text{emitted}}$	$\Sigma^{+,0}_{\text{absorbed}}$	Total
No. events	96 ± 18 (*)	$62(+10)$ (**) ± 20 (*)	64 ± 20 (*)	225 ± 30 (*)	457 ± 45 (*)

(*) These errors are based only on the numbers in the sample on which the classification was based, and do not take account of experimental bias or other sources of error.
(**) Σ^- unidentified (emitted and absorbed) from $(\pi, \text{D.S.})$ events.

The total number of events is 457 ± 45. The total number of $(\pi, n) + (\pi, \text{D.S.})$ events being 713, this leaves 256 ± 45 events to be explained. One other reaction to which they may be attributed is the $(K^-n, \Lambda^0\pi^-)$ reaction.

There has been some difficulty in the past in estimating the importance of this reaction in K^--stars at rest in emulsions, due to the difficulty of observing π-mesons of very high energy. The theoretical spectrum, calculated on reasonable assumptions (Fig. 11), would lead one to expect that between 90 and 95% of the π-mesons associated with Λ^0 production, have an energy greater

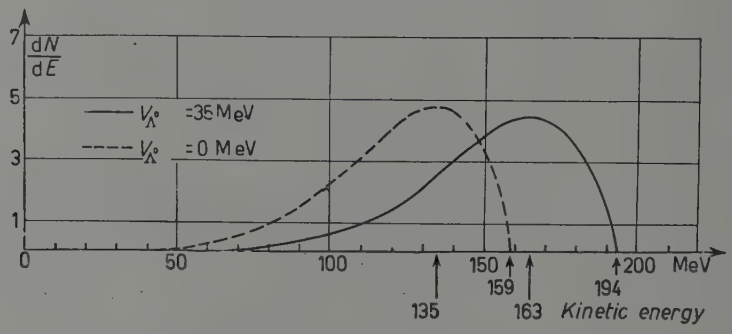

Fig. 11. – Theoretical energy distribution of π-mesons from the reaction $(K^-n, \pi^-\Lambda^0)$. V_π and V_N as in Section 5·3. *c*) and Fig. 7.

than 90 MeV, and between 50% and 85%, have an energy greater than 120 MeV. In our sample, the number of π-mesons above 90 MeV is estimated to be 104, *i.e.* about one half, of the estimated number of the $(\pi, n) + (\pi, \text{D.S.})$ events attributed to Λ^0 production. Further, there is no clear evidence for the existence of π-mesons of energy greater than 120 MeV (see Section 5·2.)

GILBERT and WHITE ([24]) have attempted to explain this absence of π-mesons of energy greater than 120 MeV by leaving aside the direct production of Λ^0, and attributing all π-mesons of energy greater than 90 MeV to interaction in which a Σ^--hyperon is produced inside the nucleus with insufficient energy to escape through the attractive well. Assuming a square well interactions of the Σ-hyperon of depth V_Σ MeV, the maximum energy of the π-meson should be $(90+V_\Sigma)$ MeV.

With the estimated value of V_Σ not greater than 15 MeV (Section 5·3-*c*), this maximum energy is not greater than 105 MeV, whereas the measured π-energies extend up to 120 MeV. In view, however, of the uncertainties in the estimate of V_Σ and the experimental spread in the π-meson energies (see Table X, appendix), this mechanism cannot be entirely ruled out on the basis of our experimental figures. Further information is however available from the Berne group ([22]) who have obtained two definite examples of π-mesons with energy greater than 120 MeV, and have followed to rest two π-mesons of energy greater than 100 MeV and found them to be negatively charged (the Gilbert and White mechanism predicts a predominance of positive π-mesons above 90 MeV).

It seems reasonable, therefore, to ascribe the fast π-mesons to the reaction $(K^-n, \Lambda^0\pi^-)$, and this assumption is also required by the preceding analysis of (π, n) and (π, D.S.) events.

The small number of these Λ^0-events containing a fast π-meson remains, however, unexplained. A large cross-section for inelastic scattering might account for it since the energy of these π-mesons is near the $(\frac{3}{2}, \frac{3}{2})$ resonance. On the other hand, as already pointed out, a preferential loss of the faster π-mesons is to be expected, so that it may be that the π-mesons of high energy have simply escaped observation (*).

6. – Conclusions.

1) A comparison of the general characteristics of K^--stars in flight at a mean energy of 40 MeV and at rest shows very little change in the percentage of unstable particles emitted, but an increase in the number of stable prongs accompanying them.

2) No evidence has been found for charge exchange effects or multinucleon processes giving rise to a π-meson. The number of events involved is small however, and such processes cannot be definitely excluded.

([24]) F. C. GILBERT and R. S. WHITE: *Phys. Rev.*, **107**, 1770 (1957).

(*) See note in proof, Sect. **3.5**.

3) From the energy spectra of the π-mesons associated with identified Σ-hyperons, the Σ nuclear potential, as defined in reference ([21]), is estimated to be not greater than 15 MeV.

4) The probability of absorption in the parent nucleus of Σ^+, Σ^- and Σ^0-hyperons produced in the K^- interaction with a single nucleon is found to be about the same, and of the order of 45%.

5) A reasonable classification among the various possible primary reactions, of K^--stars in which a π-meson is emitted is given in Table XXI. These numbers, particularly those of (π^-, Λ^0), may well have been underestimated due to scanning loss, the corrections applied being underestimated (*). The errors quoted are indicative only of the number of events on which the classification is based. The central values are subject to the large uncertainties in interpretation.

TABLE XXI. – *Classification of K^--stars in which a charged π-meson is emitted.*

Process	$\Sigma^-_{emitted}$	$\Sigma^-_{absorbed}$	$\Sigma^+_{emitted}$	$\Sigma^+_{absorbed}$	$\Sigma^0_{emitted}$	$\Sigma^0_{absorbed}$	π^-, Λ^0
Number based on π-mesons observed	89 ± 17	$62(+10)(*) \pm 20$	187 ± 17	167 ± 22	64 ± 20	58 ± 20	256 ± 45
Number corrected for observational loss of π-mesons	99	69(+11) (*)	206	183	71	64	300

(*) Σ^- unidentified (emitted and adsorbed) from (π, D.S.) events.

In Part II we will attempt to estimate the absorption of the π-mesons, the number of multinucleon events and hence to classify all the K^--interactions at rest.

* * *

We wish to thank Prof. POWELL for his interest and help in this work, also numerous colleagues for stimulating discussions, in particular Drs. CASTILLEJO, DELL'ANTONIO, DUIMIO and FERRARI, and finally Prof. PUPPI, Prof. QUARENI and the Bologna group for communicating to us and discussing their unpublished results. F.H. and M.A.S. are indebted for scholarships to the U.A.R. Ministry of Education, and to the Pakistani Ministry of Education respectively. K.N. thanks the Colombo Plan authorities for a grant.

(*) See note in proof, Sect. **3.5**.

RIASSUNTO

È stato esaminato un totale di 3480 mesoni K^-. Di essi 3035 interagiscono a riposo, 445 interagiscono in volo con un'energia media di 40 MeV. Delle interazioni in volo sono state studiate solo le caratteristiche generali. Si osserva poca differenza nel numero di particelle instabili (iperoni Σ e mesoni π) emesse nelle interazioni in volo e nelle interazioni a riposo. Le 3035 interazioni a riposo sono state studiate particolareggiatamente. In questo lavoro (Parte I) sono presentati i risultati relativi alle interazioni nelle quali sono emessi mesoni π carichi. Dallo spettro di energia dei mesoni π emessi nelle interazioni in cui le sole particelle cariche emesse sono un mesone π e un iperone Σ è stata ricavata una stima del potenziale nucleare degli iperoni Σ. Un'analisi particolareggiata della distribuzione angolare delle stelle a due rami, del rapporto dei segni dei mesoni π, della distribuzione del numero di rami delle stelle e dell'energia totale visibile ha condotto a una stima della probabilità di assorbimento degli iperoni Σ positivi e negativi nel nucleo di origine, e a una ripartizione degli eventi tra le varie reazioni primarie (*).

(*) Nella Parte II saranno presi in esame gli eventi in cui è emesso un iperone Σ, e saranno combinati i risultati dei due lavori per ottenere una stima del numero delle interazioni a più di un nucleone, e da esso il rapporto $\Sigma : \Lambda^0$ alla produzione, la probabilità di assorbimento dei mesoni π, e le intensità relative dei vari tipi di reazioni primarie.

IL NUOVO CIMENTO Vol. XIII, N. 4 16 Agosto 1959

n, p and n, np Reactions with 14 MeV Neutrons.

L. Colli

Laboratori CISE - Milano, e Istituto di Fisica dell'Università - Milano

U. Facchini

Laboratori CISE - Milano, e Istituto di Fisica dell'Università - Torino

I. Iori, M. G. Marcazzan and A. M. Sona

Laboratori CISE - Milano

(ricevuto il 4 Marzo 1959)

Summary. — Measurements of the energy spectra of protons emitted in n, p and n, np reactions with 14 MeV neutrons are described. The spectra are taken at four different angles in the case of Ni, Cu, Mo, and Ag. The results are compared with other results in the domain of the nuclear reactions at intermediate energy. The mechanisms responsible for the various reactions can be shortly indicated: 1) instantaneous effects: the forward emitted high energy particles are due to such effects. 2) non equilibrium escape is responsible for the main part of the spectra and for emission at any angle. The escape is supposed to be due to the strong interactions between few excited nucleons at the nuclear surface; 3) retarded emission, probably after stabilized equilibrium is reached, will explain the emission of protons by medium A nuclei and of neutrons when incident energy is below 18 MeV. Values of temperatures of ~ 1 MeV are found. In n, 2n and n, np reactions strong emission of protons competes in some cases with neutron emissions. The role of surface conditions in this retarded emission is enlightened.

Introduction.

A wide discussion on the nuclear reactions mechanisms at medium energies was given by Peaslee [1] in 1955.

It was shown, in that work, how a great number of experiments gave results in clear disagreement with the statistical evaporation model. In the last few years many other experimental results have followed those discussed by

[1] D. C. Peaslee: *Ann. Rev. Nucl. Sci.*, **5**, 99 (1955).

PEASLEE. A certain number of results seems partly to agree with this theory: in some cases there is agreement in the shape of the emitted particles spectrum ([2,3]); in other cases the angular distribution of a part of the emitted particles agrees with the previsions of the theory ([4-7]); in some cases a part of the spectrum of the emitted particles is attributed to an evaporation process ([8-11]); in others the value of a particular cross-section ([12,13]), or a fraction of it is explained ([14]).

When the results concerning evaporation are taken into consideration as a whole, we find a rather confused picture of the properties of evaporation itself. IGO and WEGNER ([15]) describe this situation in a diagram, in which disagreement is shown between the values of the coefficient a relative to the nuclear level density obtainable by various experiments.

Besides this, in a certain number of results, there is evidence of direct or instantaneous effects ([16]).

The aim of this work is to present a few recent results on the spectrum and the angular distribution of protons emitted in reactions produced by 14 MeV neutrons and to discuss these results in the light of the present experimental situation.

These measurements follow other ones previously published ([17-20]), giving the energy spectrum of protons emitted by Mg, Al, Si, S, Ca, Ti, Fe, Ni, Cu, Zn,

---

([2]) R. M. EISBERG, G. IGO and H. E. WEGNER: *Phys. Rev.*, **100**, 1309 (1955).

([3]) B. L. COHEN and A. G. RUBIN: to be published.

([4]) N. O. LASSEN and N. O. ROY PULSEN: *International Conference on Low Energy Nuclear Physics in Paris* (July 1958).

([5]) I. KUMABE, E. TAKEKOSHI, H. OGATA, Y. TSUNEOKA and S. OKI: *Phys. Rev.*, **106**, 155 (1957).

([6]) L. ROSEN and L. STEWART: *Phys. Rev.*, **107**, 824 (1957).

([7]) S. H. AHN and J. H. ROBERTS: *Phys. Rev.*, **108**, 110 (1957).

([8]) D. L. ALLAN: *Proc. Phys. Soc.*, A **70**, 195 (1957).

([9]) G. BROWN, G. C. MORRISON, H. MUIRHEAD and W. T. MORTON: *Phil. Mag.*, **2**, 785 (1957).

([10]) P. V. MARCH and W. T. MORTON: *Phil. Mag.*, **3**, 143 (1958).

([11]) P. V. MARCH and W. T. MORTON: *Phil. Mag.*, **3**, 577 (1958).

([12]) *Handb. d. Phys., Nuclear Reactions I*, **40**, 202 and foll.

([13]) J. BENVENISTE: *International Conference of Geneva*, P/2494 (1958).

([14]) G. BROWN and H. MUIRHEAD: *Phil. Mag.*, **2**, 473 (1957).

([15]) G. IGO and H. E. WEGNER: *Phys. Rev.*, **102**, 1364 (1956).

([16]) See for instance: C. T. DE DOMINICIS: *International Conference on Low Energy Nuclear Physics in Paris* (July 1958) and *Journ. Phys. Rad.*, **19**, 1 (1958).

([17]) C. BADONI, L. COLLI and U. FACCHINI: *Nuovo Cimento*, **4**, 1618 (1956).

([18]) L. COLLI and U. FACCHINI: *Nuovo Cimento*, **5**, 309 (1957).

([19]) L. COLLI, U. FACCHINI, I. IORI, G. MARCAZZAN, A. M. SONA and M. PIGNANELLI: *Nuovo Cimento*, **7**, 400 (1958).

([20]) L. COLLI, M. PIGNANELLI, A. RYTZ and R. ZURMÜHLE: *Nuovo Cimento*, **9**, 280 (1958).

Zr, Rh, Sn, Ta and Au in the forward angles. In Section 1 the experimental measurements on Ni, Cu, Mo, Ag are discussed; in Section 2 a comparison is made between the evaporation model and our, as well as other authors', data; finally in Section 3 some hypotheses are put forward on the mechanisms relative to these reactions.

1. – Experimental results.

1·1. *Experimental procedure and apparatus.* – The measurements consist in the detection of protons emitted by the studied elements, when bombarded with 14 MeV neutrons.

The detector consists of a coincidence and anticoincidence equipment, between three proportional counters and a scintillation counter. This instrument has been described in detail in a previous publication ([21]).

In this work we present the energy and angular distributions of the photons emitted by Ni, Cu, Ag, Mo in natural isotopic mixture. The width of the useful angle into which the emitted particles are detected is about 18°. The background is generally much smaller than the effect, being about $\frac{1}{2}$ of the effect in the case of the smallest cross-section (Ag).

One must note that, because of the scintillation detector characteristics, it is not possible to distinguish between the pulses due to protons and those due to probable deuterons emitted by the elements under study. Therefore it is possible that the spectra presented are not constituted only by protons emitted in n, p or n, np reactions, but also contain deuterons emitted in n, d reactions, which are almost always energetically possible with 14 MeV neutrons. Recently it was put into evidence ([22]) that the n, d reaction is present in amounts not much lower than those of the n, p reactions in the case of the ^{31}P, ^{32}S and ^{63}Cu nuclei at least at forward angles, and it is therefore reasonable to think that deuterons are present even for other elements.

Owing to the finite thickness of the targets, significant points for the spectra below 3 MeV protons cannot be given, as the resolution here becomes too bad, and the spectrum shape is no more meaningful.

1·2. *Copper.* – The spectra of the particles emitted by Cu taken at four different angles are shown in Fig. 1. The measurement was made using a target 18 mg/cm² thick.

The spectrum in Fig. 1 given in the centre of mass system, clearly shows two components with different behaviour: one part at high energy, with a

([21]) G. MARCAZZAN, M. PIGNANELLI and A. SONA: *Nuovo Cimento*, **10**, 155 (1958).
([22]) L. COLLI, F. CVELBAR, S. MICHELETTI and M. PIGNANELLI: to be published.

strong forward component, above 7 MeV, mainly constituted by a peak at 9 MeV and an isotropic part at low energy.

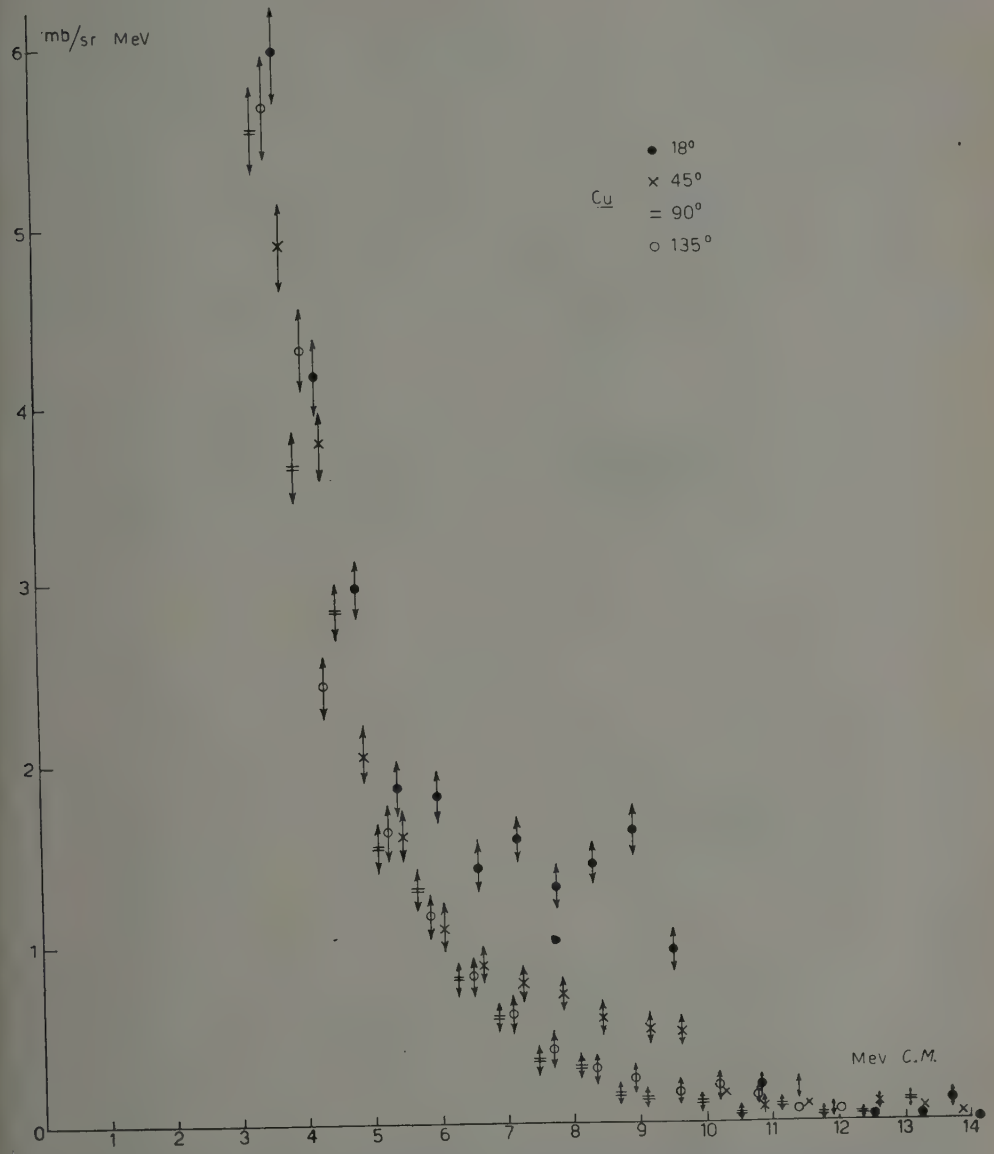

Fig. 1. – Energy and angular distribution of protons (and deuterons) emitted by Cu. Ordinate: in mb/sr·MeV; abscissa: energy of the particles in the C.M. system.

By means of absorption measurements it has been shown in the above mentioned paper ([22]) that this part of the spectrum is made up of deuterons.

Confirmation of this fact is obtained by comparing the spectrum in Fig. 1 with the spectrum obtained in similar conditions by ALLAN ([23]), using nuclear emulsions as detection technique. In fact one similar peak is observed by this author, but it corresponds to 7 MeV proton energies. If one attributes this peak to deuterons, a reasonable agreement is reached between the two measurements, considering the difference between the two techniques, one of which is based on the range measurements in nuclear emulsions, and the other on the energy measurements by means of the scintillation of CsI, which has about the same response to protons and deuterons.

The lower energy part of the spectrum agrees with the measurements made by ALLAN, if compared in the centre of mass system. Thus, it must be made up chiefly of protons which may be attributed to the n, np reaction, their energy being below the threshold of this reaction ($Q = -5.84$ MeV).

1·3. *Nickel.* – We show in Fig. 2 the nickel spectrum at four angles obtained with a statistic better than that previously published ([19]). A target of 14.4 mg/cm² thickness was used. It is interesting to observe that there is only anisotropy for the spectrum at 18°, which is by 20% more intense than the others even at low energy.

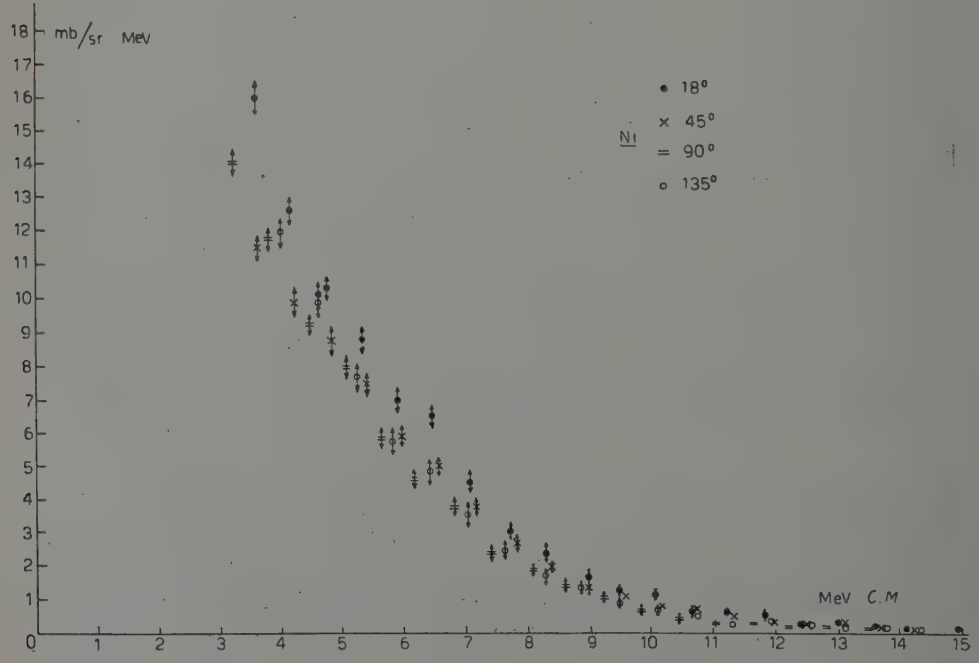

Fig. 2. – Energy and angular distribution of particles emitted by Ni.

([23]) D. L. ALLAN: *Nucl. Phys.*, **6**, 464 (1958).

At low energy ((3.5÷4.5) MeV) the angular distribution seems to show a minimum at 90° even though the difference between the curves is not completely out of statistical errors.

1'4. *Molibdenum.* – The measurement was carried out with a target of 32 mg/cm² thickness (Fig. 3).

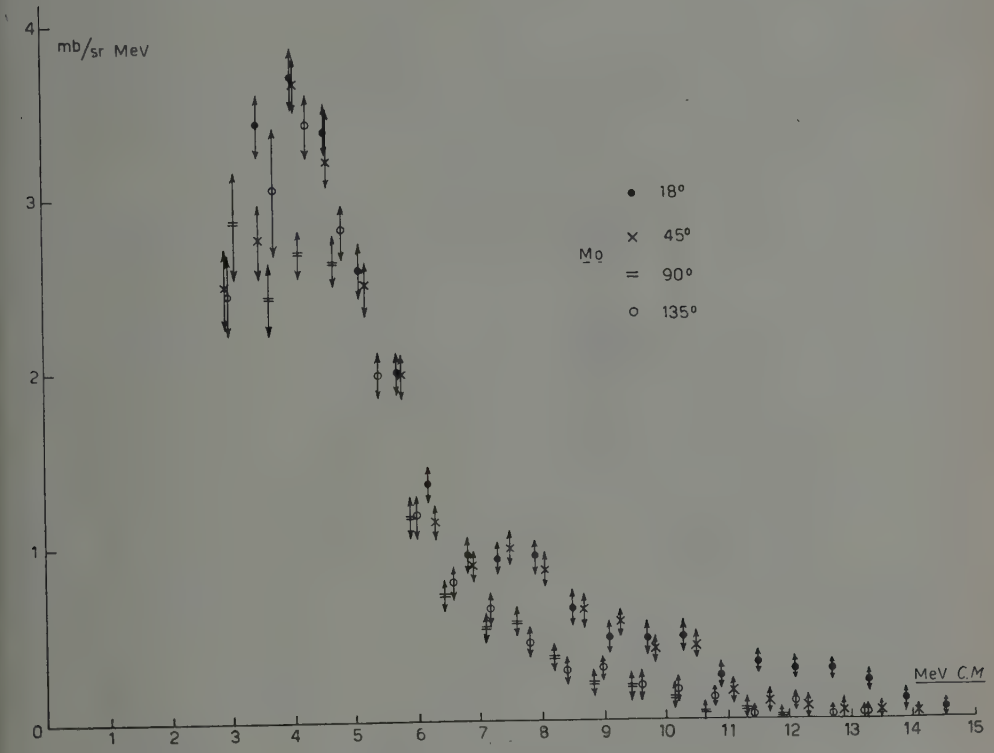

Fig. 3. – Energy and angular distribution of particles emitted by Mo.

Natural Mo contains a high number of isotopes in almost similar percentages. It is however probable that the emission of protons should be attributed mainly to the lighest isotope ^{92}Mo, which is present in a relatively high percentage and has Q values for n, p and n, np reactions lower than those of all the other isotopes.

From the angular distribution point of view the spectrum may be divided into two parts: one below 6 MeV, with angular distribution symmetric through 90° angle, where it seems to present a probable minimum, and another above 6 MeV, with an evident anisotropy and preference for forward angles. It is possible that a contribution of deuterons is present, because the maximum energy for the n, d reaction is 7,8 MeV, and this could be indicated by the

form of the spectrum. It is clear however that the part of the spectrum above 8 MeV must be completely attributed to protons, which show an angular distribution with accentuated forward anisotropy.

Here, too, the lower energy part of the spectrum can be attributed to the n, np reaction. The maximum energy of protons that come from this reaction is of 5.8 MeV. The 90° degree curve is clearly less intense than the 45° and 135° ones.

1·5. *Silver.* – Fig. 4 shows the n, p reaction spectra of silver for the different angles examined, obtained with a target 24.6 mg/cm² thick.

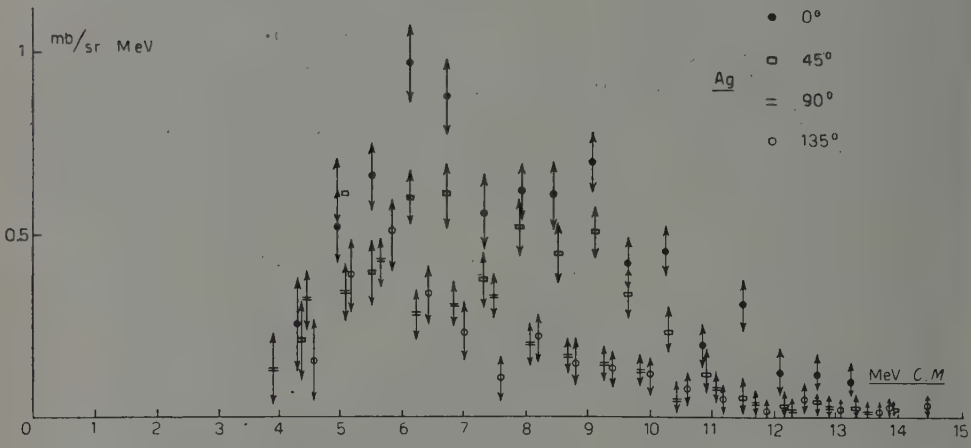

Fig. 4. – Energy and angular distribution of particles emitted by Ag.

It is interesting to observe how these spectra have a very different shape from those of Cu and Mo, even though silver is not much heavier. On these spectra there is a complete lack of the isotropic part at low energy. It is probable that a contribution of deuterons is present as the threshold for the n, d reaction is low and this reaction is energetically possible below 10.5 MeV.

1·6. *Cross-sections.* – Table I indicates the cross-section values of the (n, p+n, d) reactions together, obtained from the spectra of Fig. 1, 3, 4, 5 and the cross-sections attributed to the n, np reactions of Cu and Mo.

The calculation of the cross-sections of the n, np and (n, p+n, d) reactions is made by attributing to the n, np reaction that part of the low energy spectrum, which is below the maximum value of the proton energy possible for this reaction, and which shows a rather different shape from that above this

TABLE I. – *Cross sections* (*).

	Cu	Mo	Ag
(n, p) + (n, d): (mb)	46	31	28
(n, np): (mb)	181	112	0
	^{63}Cu	^{92}Mo	
(n, np): (mb)	250	744	

(*) Errors are of the order of ± 10%.

energy. In the table the cross-section values of the n, p reactions, when attributed to the lighest isotope in the mixture are also indicated.

2. – Comparison between the experimental results and the evaporation model.

2·1. *Foreword.* – The most general description of a nuclear reaction that one can give according to WEISSKOPF (24) consists of a first step in which the

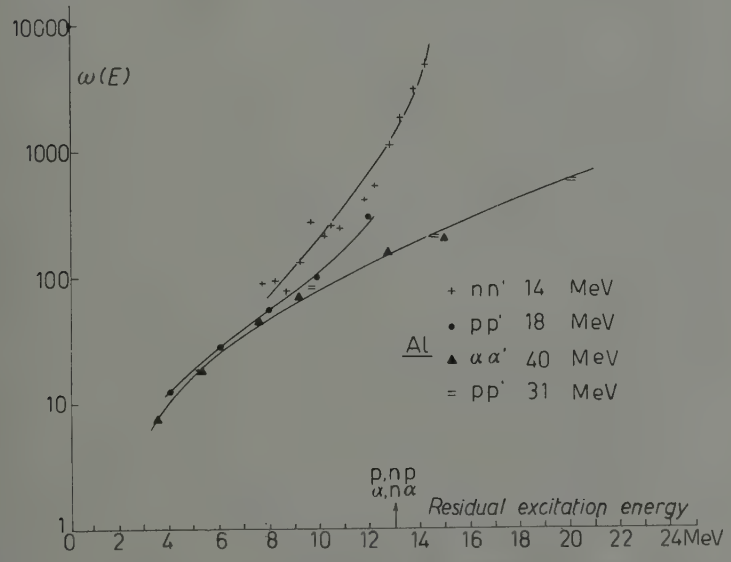

Fig. 5. – Curves of apparent $\omega(E)$ deduced from various reaction on Al plotted as functions of the excitation energy of the residual Al nucleus. Ordinate in arbitrary units: normalization among the various curves is roughly made at the lowest excitation energies. Threshold of p, np and α, nα reactions are indicated. Ref. (43,31,32,44).

(24) V. F. WEISSKOPF: *Proc. of the International Conference on Nuclear Reactions* (Amsterdam, 1956).

incident nucleon may be described as a single particle moving in a potential well, and in a subsequent absorption process, leading, at least in some cases, to the formation of a compound nucleus having the well known properties given by the statistical model: quite a long half life so that all the possible states are mixed compatibly with the initial conditions, and an emission of particles with laws independent of the formation channel of the compound nucleus itself.

It is possible to obtain other decay channels (instantaneous effects, etc.) through which the initial system decays without reaching equilibrium states. BROWN and DE DOMINICIS ([25,26]) show how the instantaneous emission can become very important with the increase of the energy of the incident particle, while the delayed emission tends to go to zero.

Moreover WEISSKOPF and FRIEDMAN ([27]) show that the equilibrium and independence properties are valid when the compound nucleus is excited in a definite state; these properties can be assumed to be valid also when many states are excited but well separated. On the contrary these properties are not to be held probable when, as it happens at intermediate energies the compound nucleus levels are dense and overlapping, their width being much bigger than their spacing. In this case it seems that the statistical equilibrium cannot be reached. Therefore at intermediate energy the independence law cannot be valid on theoretical grounds. A comparison between the experimental results and the theory has at least the meaning suggested recently by WEISSKOPF ([28]), that is to establish how much the results of the experiments diverge from the previsions of the statistical model.

2·2. *The statistical model.* – To make discussions easier we can briefly recapitulare some simple previsions of the statistical model:

1) The angular distribution of the emitted particles is isotropic in the centre of mass system, or at least symmetric with respect to the direction perpendicular to the incidence direction ([29]).

2) The statistical model assumes a particular aspect when the density of final states is quite high. The transitions to the final states are assumed as roughly equiprobable and the energy distribution of emitted particles is regulated by the law ([1,30])

$$(*) \qquad n(\varepsilon)\,\mathrm{d}\varepsilon \div \sigma(\varepsilon)\varepsilon\cdot\omega(E)\,\mathrm{d}\varepsilon\,,$$

([25]) G. E. BROWN and C. T. DE DOMINICIS: *Proc. Phys. Soc.*, A **70**, 668 (1957).
([26]) G. E. BROWN and C. T. DE DOMINICIS: *Proc. Phys. Soc.*, A **72**, 70 (1958).
([27]) F. FRIEDMAN and V. WEISSKOPF: *Niels Bohr and the development of Physics* (London, 1955).
([28]) V. F. WEISSKOPF: *Geneva Conference* (Sept. 1958), discussion in Sect. A 19.
([29]) *Handb. d. Phys.*, **40**, 212.
([30]) V. F. WEISSKOPF and D. H. EWING: *Phys. Rev.*, **57**, 472 (1940).

in which $n(\varepsilon)\,\mathrm{d}\varepsilon$ represents the number of particles emitted in the energy interval $\mathrm{d}\varepsilon$; $E = \varepsilon_{\max} - \varepsilon$ is the energy of the residual nucleus, ε is the energy of the outgoing particle, and $\varepsilon_{\max}$ the maximum energy of the outgoing particle; $\sigma(\varepsilon)$ represents the cross-section of the inverse reaction and $\omega(E)$ the density of levels of the residual nucleus excited to the energy E.

This formula represents the well known evaporation emission.

3) When many final nuclei are involved the equiprobability hypothesis permits to calculate the values of the cross-sections for competing reactions ([29]). The ratio between the exit probabilities of protons or α-particles with respect to neutrons, is chiefly determined by the transparence of the Coulomb barrier; consequently, for particles emitted with low energy, the escape probability of neutrons is generally assumed to be much greater than the others. A particularly simple formula can be deduced to represent the cross-sections for n, 2n, α, 2n, etc., type reactions.

2·3. *Angular distributions.* – The examination of the angular distributions of emitted particles has been made for a certain number of reactions and it widely shows the presence of components having a greater intensity for forward angles ([6,7,10,11,23,31-35]). While for a group of cases it is observed a practically complete isotropy (see Fig. 2 and ([4,10,11])) for nuclei with Z around 30.

The forward components are generally interpreted as an emission due to an instantaneous effect ([16]).

It is interesting to note that from all these results, the forward asymmetry appears much greater with the greater energy of the incident and the outgoing particle (Fig. 1, 3, 4). At the lowest emission energies, when reactions corresponding to the exit of more particles (n, np, n, 2n, p, np, etc.) are generally present, isotropic or at least symmetric angular distributions are often observed (Fig. 1 and 3) ([5-7,10,11]).

In the case of heavy nuclei, and in the case of proton emission, the isotropic part at low energy is lacking because of the Coulomb barrier, and we have only the higher energy part emitted chiefly in forward direction (Fig. 4).

2·4. *The shape of the spectrum.* – A comparison between the spectra of the particles emitted in various reactions and the evaporation law is reasonable only for that part of the results which present symmetrical angular distribution.

For this purpose we may consider in our comparison the particles emitted

---

([31]) P. C. GUGELOT: *Phys. Rev.*, **93**, 425 (1954).
([32]) G. IGO: *Phys. Rev.*, **106**, 256 (1957).
([33]) R. M. EISBERG and G. IGO: *Phys. Rev.*, **93**, 1039 (1954).
([34]) B. L. COHEN: *Phys. Rev.*, **105**, 1549 (1957).
([35]) B. L. COHEN: *Phys. Rev.*, in print.

backwards. As mentioned above, the low energy part of the spectrum generally corresponds to the emission of more particles and in such a case the shape of the spectrum is more difficult to interpret.

Therefore considering that part of the spectrum in which certainly only one particle is emitted we may compare the value of $\omega(E)$ of formula (*) obtained by different reactions on a certain nucleus.

Where charged particles are emitted, to obtain the value of $\omega(E)$ from experimental results, it is necessary to know the transparence of the Coulomb barrier $\varepsilon \cdot \sigma(\varepsilon)$.

Our knowledge on the Coulomb barrier is still not very precise: in fact the introduction of the nuclear potential with round edged surface has brought a changement on the previous ideas on the Coulomb barrier. To a barrier corresponding to a nuclear radius $1.5\, A^{\frac{1}{3}} \cdot 10^{-13}$ cm, and a sharp surface it is better to substitute a barrier corresponding to a smaller radius, and a round edged surface. Evidently the two effects are partially compensating in determining the transparence of the barrier but the height of the barrier would become lower ([36-39]).

On the other hand some difficulties seem to arise in the interpretation of the charged particles emitted at low energy inasmuch as the barriers of excited nuclei valid for particle emission could be different from those of stationary nuclei ([40-42]).

Apart from these difficulties we have gathered a certain amount of nn′ ([43]), pp′ ([31,3,44]) and $\alpha\alpha'$ ([4,32]) reactions and from the spectra emitted backwards we have deduced the values of $\omega(E)$ for a few residual nuclei. These values are shown in Fig. 5, 6 and 7. The calculation has been made using the values of the Coulomb transparence, given by FESHBACH, SHAPIRO and WEISSKOPF ([45]). The errors introduced considering these values of the Coulomb barrier is certainly small inasmuch as the correction itself introduced in the barrier is small, because a part of the spectra shown in Fig. 5 and subsequent figures brings about the exit of charged particles having energy above the height of the barrier in which therefore the transparence is ≈ 1;

([31]) J. S. LEVINGER: *Int. Conf. on Low Energy Nuclear Physics* (Paris, July 1958).
([37]) J. M. C. SCOTT: *Phil. Mag.*, **45**, 441 (1954).
([38]) J. A. EVANS: *Proc. Phys. Soc.*, **73**, 33 (1959).
([39]) K. KIKUCHI: *Progr. Theor. Phys.*, **17**, 643 (1957).
([40]) J. NEMETH: *Nucl. Phys.*, **6**, 686 (1958).
([41]) A. M. LANE: *Discussion at Int. Conf. on Low Energy Nuclear Physics* (Paris, July 1958).
([42]) B. L. COHEN: *Int. Conf. on Low Energy Nuclear Physics* (Paris, July 1958).
([43]) E. R. GRAVES and L. ROSEN: *Phys. Rev.*, **89**, 343 (1953).
([44]) R. BRITTEN: *Phys. Rev.*, **88**, 283 (1952).
([45]) H. FESHBACH, M. M. SHAPIRO and V. F. WEISSKOPF: NYO-3077 (1954).

furthermore the parts of the spectrum at low energy where the corrections of the barrier could notably change the form of the curve are not considered because they correspond to an emission of more particles.

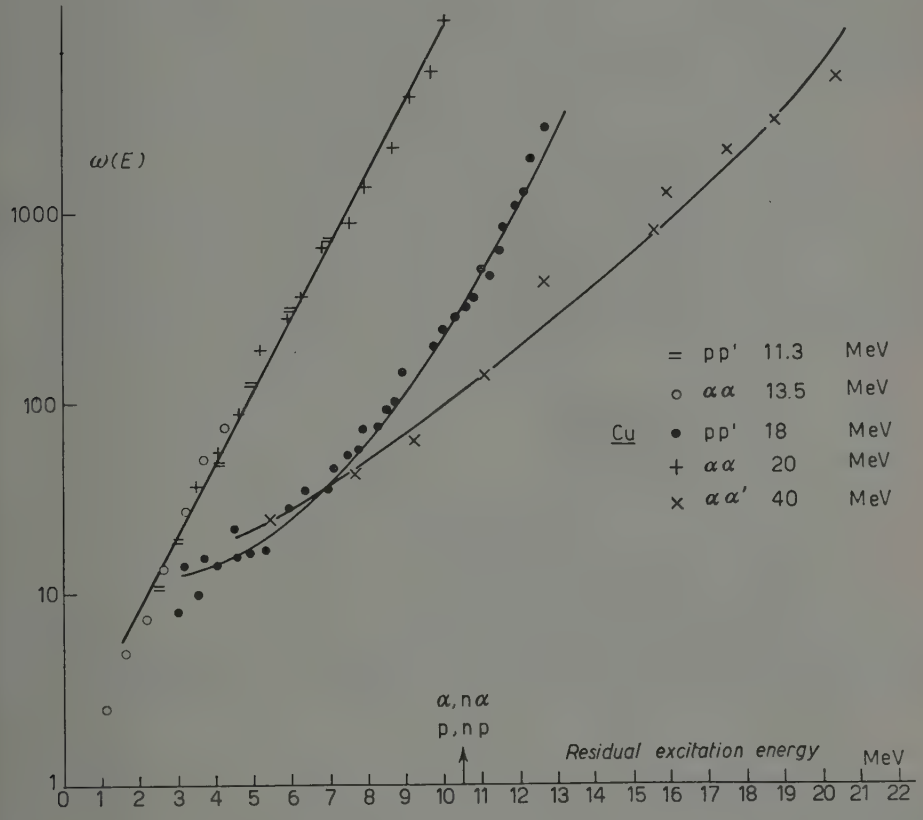

Fig. 6. – Curves of apparent $\omega(E)$ deduced from various reactions on Cu and plotted as function of the excitation energy of the residual Cu nucleus. Ordinate in arbitrary units: normalization among the various curves is roughly made at the lowest excitation energies. Threshold of p, np and α, nα reactions are indicated. Ref. [3,4,31,32].

We must recall that a previous comparison between backward emission spectra of Ag (p, p′) at 16 and 18 MeV has been carried out by GUGELOT [31] as also a comparison between forward spectra in n, p reactions at 14 MeV and (p, p′) at 18 MeV has been carried out by COLLI, FACCHINI and MICHELETTI [46] and finally a new comparison of forward n, p spectra of Al and Ni at two energies 14 and 17 MeV has been carried out by COLLI, PIGNANELLI

[46] L. COLLI, U. FACCHINI and S. MICHELETTI: *Nuovo Cimento*, **5**, 502 (1957).

RYTZ and ZURMÜHLE ([20]). The results of the Fig. 5, 6, 7 give the above mentioned comparisons for a larger energy range and for backward angles.

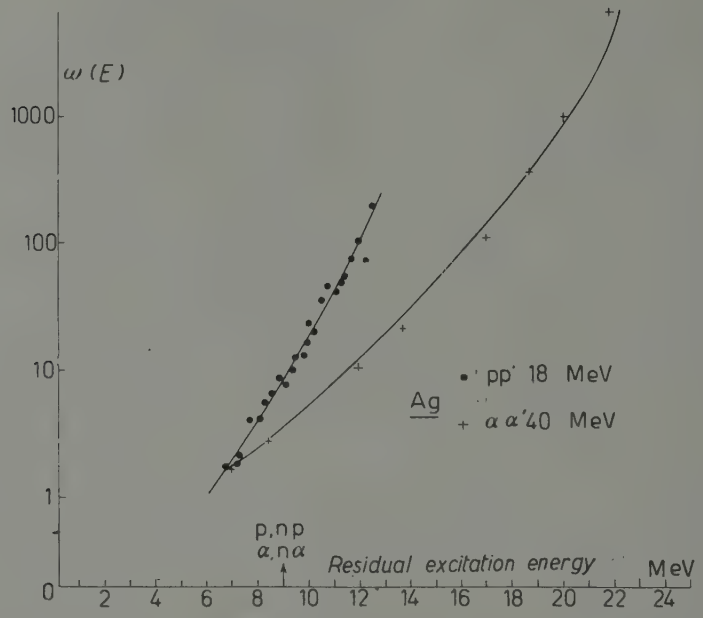

Fig. 7. – Curves of apparent $\omega(E)$ deduced from various reaction on Ag and plotted as function of the excitation energy of the residual Ag nucleus. Ordinate in arbitrary units: normalization among the various curves is roughly made at the lowest excitation energies. Threshold of p, np and α, nα reactions are indicated. Ref. ([31,32]).

The curves represented can not evidently correspond all to the level density as they are different each other.

The figures show a number of curves of various slopes.

If we consider the steepest curve, particularly in the case of Cu, we note that a certain number of results give the same curve, which can then correspond to the level density of the residual nucleus, and can be represented by an exponential formula:

$$\omega(E) \simeq \exp[E/\theta] \quad \text{with} \quad \theta \simeq 1 \text{ MeV} .$$

A careful discussion on the comparison between the curves $\omega(E)$ obtained by the reactions $\alpha\alpha'$ at 13.5 and 20 MeV and the above exponential law was given by LASSEN *et al.* ([4]). The same result was found by other authors, who given better agreement of the experimental results for $\omega(E)$ with the formula $\exp[E/\theta]$ than with a formula that gives a parabolic dependence of

the log $\omega(E)$ in function of E, as should be the case where the excited nucleus could be described as Fermi gas.

Studying the anelastic scattering of the protons on the Cu from 11.5 to 23 MeV, COHEN and RUBIN [3] found a similar result to that shown in Fig. 6 The curves $\omega(E)$ obtained from the measurements made at lower energies the one at 11.5 MeV reported in Fig. 6, were rather similar among themselves and to those discussed here, while the curves corresponding to higher energies than 15 MeV have a minor slope.

If we now consider the curves $\omega(E)$ that are obtained from reactions n, p for medium weight nuclei (Fe, Ni, Cu), it will be seen that the curves obtained obey the same exponential law $\exp[E/\theta]$ with temperature of the order of 1 MeV, as has been already shown by ALLAN [23,47] and by MARCH and coll. [10,11].

The present results give a similar behaviour for Ni, Cu and Mo (Fig. 8 and 9).

The values of θ obtained from all these measurements are collected in Table VI.

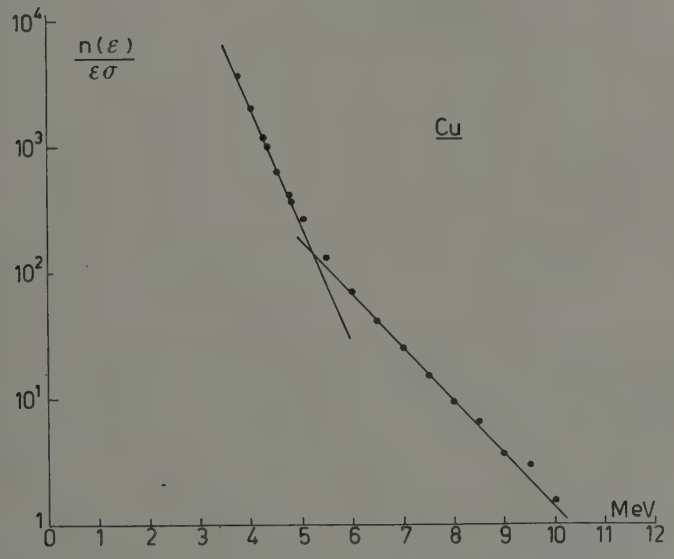

Fig. 8. – Backward spectrum of Fig. 1 (Cu) plotted as $n(\varepsilon)/\sigma\varepsilon$. Values of θ in Table IV.

Even the $\omega(E)$ deduced from the measurements of n, n′ show agreement with the exponential law and with a value of $\theta \simeq 1$ MeV (see 2·7).

We have on the whole, therefore, a good evidence that these curves of greater slope represent the level density of the residual nucleus of the reaction,

---

[47] D. L. ALLAN: Private Communication on ^{54}Fe (n, p).

even if this density does not correspond to the shape foreseen by the Fermi gas model.

In contrast with the Fermi gas model θ is independent, in this field of the excitation energy, E and almost independent of A. A notable confirmation

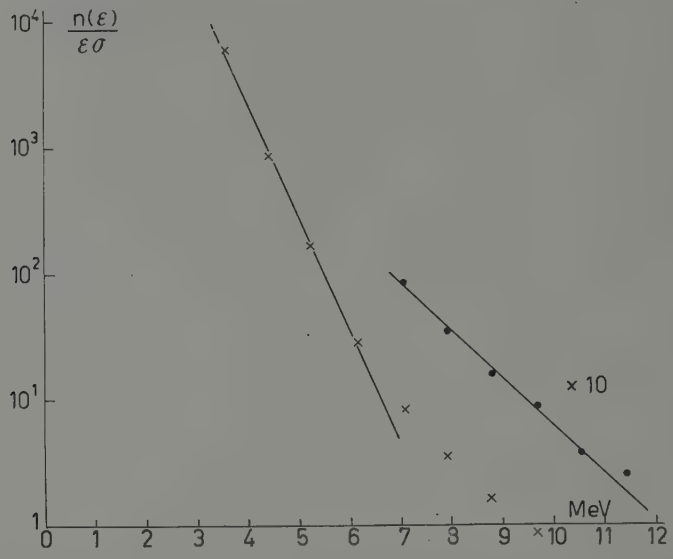

Fig. 9. – Backward spectrum of Fig. 3 (Mo) plotted as $n(\varepsilon)/\sigma\varepsilon$. Values of θ in Table IV.

of these conclusions has been found in a recent work by ERICSON [48] which shows the validity of the laws discussed, by studying the level densities obtained directly from the measurements of individual levels in reactions d, p and pp′ made with a very good energy resolution [49].

While there is good evidence, as has been discussed here, that for a certain number of reactions, and below a certain energy, an emission of the evaporative type is obtained, the curves of Figs. 5, 6 and 7 corresponding to incident energies above 18 MeV show that a process of a different type predominates here.

It can be said that in these curves the level density seems to be multiplied by a factor depending on the energy of the outgoing and ingoing particles. The transitions to the final levels are not therefore equally probable as the evaporation model would like them to be.

---

[48] T. ERICSON: Private Communication by A. M. LANE.

[49] See the papers of the ONR group at MIT in 1957-1958.

The evidence of the non validity of the evaporation model refers to the backward part of the spectra. Since the comparison is made depending on the residual energy between 0 and a value E of $(10 \div 15)$ MeV, we may observe that the part of the spectrum represented in the figures corresponds to particles emitted with the higher emission energies comprised between ε_{max} and $\varepsilon_{max} - E$. From the comparison we can conclude the following: the components at backward angles and emission energies up to $(10 \div 15)$ MeV below maximum are not emitted in evaporative mechanisms for incident energies greater than 18 MeV.

At the higher excitation energies in the α, α' curves multiple reactions are probably present. It has to be remarked that the steepness of those curves is not changed at the corresponding threshold energy and remains much smaller than the steepness of the other curves.

2·5. *Cross-sections.* – We recall that for n, p and n, α reactions, considerable discrepancies between the experimental cross-section and that foreseen by the evaporation model were already noted in PAUL and CLARKE's first work ([50-52]). The proton emission for heavy nuclei resulted greater than foreseen according to the evaporation model. The presence of direct effects in n, p reactions at 14 MeV is evident from the study of angular distributions. These effects are particularly intense in light nuclei ([22]) with $Z < 20$ and in heavy nuclei (see Fig. 4).

In the middle nuclei region (Z around 30), as we have discussed, the evaporation model seem to be satisfactory and it will be interesting to compare the n, p cross-section with this model.

Another question to be cleared are the cross-sections of reactions of the type (x, 2n). A certain number of results relative to the cross-sections of the x, 2n type reactions, are taken as proofs of the evaporation model ([53]).

In fact the following should be noted: according to this theory, the shape of the spectrum of the neutrons emitted in the x, n type reactions, as a first approximation is a $\varepsilon \exp[-\varepsilon/\theta]$ type maxwellian form. If the emitted neutron energy is lower than a certain value ε_0 the excited residual nucleus has enough energy to emit a second neutron or a proton.

The hypothesis is then made that the second neutron emission is the chief process, and that the proton emission is unfavoured by the presence of the Coulomb barrier. In such a hypothesis the ratio between the cross-sections

---

([50]) E. B. PAUL and R. L. CLARKE: *Can. Journ. Phys.*, **31**, 267 (1953).
([51]) *Handb. d. Phys.*, Nuclear Reactions I, **40**, 251.
([52]) P. C. GUGELOT in *Nuclear Reactions*, (Amsterdam, 1959).
([53]) *Handb. d. Phys.* Nuclear Reactions I, **40**, 218 and 255.

$\sigma(x, 2n)$ and $\sigma(x, n)$ is simply given by the area of the first neutron spectrum for energies lower than ε_0, which comprises all the cases in which the emission of the second neutron is allowed, divided by the area of the same spectrum for the energies higher than ε_0. In this manner the n, np, n, nα reactions, etc., are often left out. The control of this model, and of the other hypothesis has been made by a certain number of authors measuring the ratio (x, 2n)/(x, n) and trying to find which temperature value should be attributed to the emission spectrum to get a good agreement between the theoretical and the experimental results ([12]).

The values obtained in many cases are of the order of 2 MeV. Actually, successive measurements of the emission spectrum of the first neutron gave a θ value different from this and of the order of 1 MeV ([43]).

The only measurement of the cross-section is therefore not very significant. A more precise discussion could be held only when the spectra, the angular distribution and the various cross-sections will be known as in the case of some 14 MeV neutron reaction.

2·6. *Cross-sections at* 14 MeV. – At present for some nuclei the cross-sections of the most important reactions are known. Table II gathers together all the known values for ^{27}Al, ^{54}Fe, ^{56}Fe, ^{58}Ni, ^{60}Ni, ^{63}Cu, ^{65}Cu, ^{90}Zr, ^{92}Mo. Some n, p reactions measurements are made by activation, others directly on emitted protons. In these measurements indicated with (*) n, p and n, d reactions are included.

The n, np reactions are obtained by direct measurement of the emitted protons: from these measurements one obtains $\sigma(n, p)+\sigma(n, d)+\sigma(n, np)$; the division into $\sigma(n, np)$ and $\sigma(n, p)+\sigma(n, d)$ is not very sure but represents a reasonable compromise.

Because one can deduce from the recent works available ([5,54-56]) that the (n, α), (n, nα) and (n, γ) reactions for medium nuclei are not very important, it is possible to calculate from the values of Table I, the cross-sections for the anelastic neutron reemissions (n, n′) given in the 8th column of Table II.

The 9th column gives the cross-sections σ_I of reactions in which at least one neutron is emitted. It can be seen from the 9th column that the neutron reemission is the most probable process.

([54]) H. G. Blosser, C. D. Goodman and T. H. Handley: *Phys. Rev.*, **110**, 521 (1958).

([55]) J. L. Perkin, L. P. O'Connor and E. F. Coleman: *Proc. Phys. Soc.*, **72**, 505 (1958).

([56]) R. F. Coleman, B. E. Hawker, L. P. O'Connor and J. L. Perkin: *Proc. Phys. Soc.*, **73**, 215 (1959).

Nucleus	σ_{in}	σ(n, p)	σ(n, α)	σ(n, γ)	σ(n, 2n)	σ(n, np)	(1) σ(nn′)	(2) σ_I	σ_I/σ_{in}
^{27}Al	910±50 [57]	52± 9 [52]	80±20 [51]	0.5±0.1 [55]	0.00±20 [69]	70 [8]	790±30 [69]		
	1 000±10 [69]	79± 6 [60]	135± 9 [60]			85±35 [9]			
	1 020±20 [58]	70 [8] (*)	120±14 [61]						
	970±20 [59]	55±10 [9] (*)	116± 8 [62]						
		87± 7 [61]	82±17 [5]						
aver.	986±10	68± 6	107±10	0.5±0.1	0.00±20	78	732	811	0.82
^{54}Fe	1 380±30 [57]	460 [8] (*)			10± 4 [8]	220 [8]			
	1 270±40 [69]	376 [10] (*)				224 [10]			
	1 380±20 [58]								
	1 360±30 [59]								
aver.	1347±20	418			10± 4	222	697	929	0.69
^{56}Fe	1 380±30 [57]	97±12 [52]				0 [8]			
	1 270±40 [69]	124±12 [60]			470± 40 [13] (*,*)	0 [10]			
	1 380±20 [58]	190 [8] (*)							
	1 360±30 [59]	95 [10] (*)							
		144±19 [61]							
		120±30 [9]							
aver.	1 347±20	116±10			485± 30	0	746	1 231	0.91

TABLE II (*continued*).

Nucleus	σ_{in}	σ(n, p)	σ(n, α)	σ(n, γ)	σ(n, 2n)	σ(n, np)	(1) σ(nn′)	(2) σ_I	σ_I/σ_{in}
^{58}Ni	1450±50 ([57])	310 ([8]) (*)			41±12 ([52])	220 ([8])			
	1380±30 ([59])				21± 2 ([67])				
aver.	1405±30	310			31± 5	220	844	1095	0.7
^{60}Ni	1450±50 ([57])	240 ([8]) (*)			200± 20 ([13]) (**)	60 ([8])			
	1380±30 ([59])	155 ([11]) (*)				68 ([11])			
aver.	1405±30	197			600±100	64	544	1208	0.85
^{63}Cu	1440±40 ([57])	120 ([8]) (*)		2.56±0.4 ([55])	482± 70 ([52])	180 ([8])			
	1420±40 ([69])	∼ 57 pv (*)			510± 36 ([60])	250 pv			
	1480±20 ([58])				556± 28 ([61])				
	1490±20 ([59])								
aver.	1466±20	∼ 57		2.56	522± 20	250	634	1406	0.96
^{65}Cu	1440±40 ([57])	19±4 ([60])		6.3±2 ([55])	1085±170 ([52])	<40 ([8])			
	1420±40 ([69])	<40 ([8]) (*)			970± 70 ([60])				
	1480±20 ([58])								
	1490±20 ([59])				760± 60 ([13]) (**)				
aver.	1466±20	19±4		6.3±2	1116±100	40	316	1440	0.98
^{90}Zr	1720±30 ([59])	30÷50 ([68]) (**)	3.0±0.2 ([64])		590± 60 ([66])	55 ([63]) (**)			
			3.3±0.6 ([65])		630± 30 ([67])				
					1250± 90 ([13]) (**)				

2321									
						230 ± 85 ([68])	112 pv (**)		
						132 ± 20 ([61])			
aver.	1720 ± 30 (**)					1590 ± 120 ([13]) (**)			
						164	744 (**)	606	1514	0.87

(*) Values accoresponding to $\sigma(n, p) + \sigma(n, d)$.

(**) Values obtained by attributing all the observed cross sections to the lighter isotope.

(**) Values referring to the natural isotopic mixture: the particular isotope cross section is evaluated with suitable hyphoteses on the contributes of the various isotopes.

(**) The σ_{in} of Mo has not been measured: the quoted value refers to Zr.

pv: present value.

(1) $$\sigma_{nn'} = \sigma_{in} - [\sigma(n, p) + \sigma(n, d) + \sigma(n, \alpha) + \sigma(n, \gamma) + \sigma(n, 2n) + \sigma(n, np)] ,$$

(2) $$\sigma_{I} = \sigma_{in} - [\sigma(n, p) + \sigma(n, d) + \sigma(n, \alpha) + \sigma(n, \gamma)] .$$

Reactions n, nα are disregarded and reactions n,d, nα, nγ are disregarded when not known.

([57]) T. W. BONNER, O. LONSJO and H. L. TAYLOR: *Phys. Rev.*, **100**, 174 (1955).

([58]) N. N. FLEROV and V. N. TALYZIN: *Atomic Energy SSSR*, **1**, 617 (1956).

([59]) M. H. MAC GREGOR, W. P. BALL and R. BOOTH: *Phys. Rev.*, **108**, 726 (1957).

([60]) S. G. FORBES: *Phys. Rev.*, **88**, 1309 (1952).

([61]) S. YASUMI: *Journ. Phys. Soc. Japan*, **12**, 443 (1957).

([62]) J. A. GRUNDL, R. L. HENKEL and B. L. PERKINS: *Phys. Rev.*, **109**, 425 (1958).

([63]) Preliminary values communicate dby M. G. MARCAZZAN and A. M. SONA.

([64]) J. E. BRODLEY, M. E. BUNKER, D. R. F. COCHRAN, R. L. HENKEL, J. P. MIZEand J. W. STARSEN: *Phys. Rev.*, **99**, 330 (1955).

([65]) H. G. BLOSSER, C. D. G. GOODMAN, T. H. HANDLEY and M. L. RANDOLPH: *Phys. Rev.*, **100**, 429 (1955).

([66]) C. H. REED: to be published, quoted in F. L. RIBE: *Fast neutron Phys.*, ch. V.

([67]) B. P. BAYHURST and R. J. PRESTWOOD, quoted in F. L. RIBE: *Fast neutronPhys.*, ch. V.

([68]) J. E. BROLLEY, J. L. FOWLER and L. K. SCHLACKS: *Phys. Rev.*, **88**, 618 (1952).

([69]) E. R. GRAVES and R. W. DAVIS: *Phys. Rev.*, **97**, 1205 (1955).

2·7. *Relative width of the outgoing neutron — n, 2n reactions.* – The most recent discussion on n, 2n reactions has been made by BENVENISTE and his collaborators ([13]), and it can be resumed as follows. For heavy nuclei ($>$ Ag) the total cross section of inelastic reaction is almost the same as σ(n, 2n). In these conditions the emission spectrum temperature of the first neutron deduced by the value of the (n, 2n) cross-section must be less than or equal to 1 MeV. This value agrees with the direct measurements of the spectra of the emitted neutrons ([6,7]) and it seems that the evaporation model is confirmed.

It should be remembered however that some other authors who measured (n, 2n) by means of activation of separate isotopes, obtained results in disagreement with BENVENISTE ([63,66,67]).

It could be very interesting to clarify this point with new measurements on separate isotopes.

For light nuclei, the situation is similar to the one indicated in 2·5. The (n, 2n) cross-sections are fitted with $\theta \sim 2$ MeV while the experimental results on the spectrum shape give $\theta \sim 1$ MeV. This means that the emission of the second neutron from the nucleus excited at sufficient energy to emit the neutron, is not the most important process.

The following calculation of the relative width Γ_n/Γ of the neutron emission can be made: the spectrum of the first outgoing neutron averaged over the angle of emission can be known with sufficient approximation. For example it is known directly in the case of Al (n, n′) ([43]) and corresponds roughly to a maxwellian curve with $\theta \simeq 1$ MeV, with an abundance of neutrons at energies above (4÷5) MeV and probably with anisotropic components.

In the case of Fe, BENVENISTE gives a comprehensive spectrum of nn′ and n, 2n reactions; knowing the values of the n, 2n cross-section, one can remove the contribution of the second neutron from this spectrum, and get the required spectrum. It is necessary for this purpose to assume a certain spectral distribution for the second neutron.

It can be noted how in the case of proton emissions from Ni and Cu in the backward direction, taking into account the $n(\varepsilon)/\sigma \cdot \varepsilon$ curves besides the component of protons of $\theta \sim 1$ MeV temperature a lower energy component corresponding to $\theta \sim 0.45$ MeV is observed ([11,23]); this second component is interpreted as corresponding to protons emitted in n, np reactions, that is as a second particle. Similar behaviour is to be noted from the results of Fig. 1 and is reported in Fig. 8.

The forward components of the various spectra are of no great importance in the evaluation of the average spectrum.

Returning to the Benveniste spectrum and subtracting the contribution due to the second neutron from the neutron spectrum emitted from Fe, and assuming for it a temperature of 0.45 MeV, the emission spectrum of the first

neutron is obtained in Table III: it corresponds roughly to a temperature of 1 MeV with an excess of higher energy particles.

This spectrum is shown in Fig. 10.

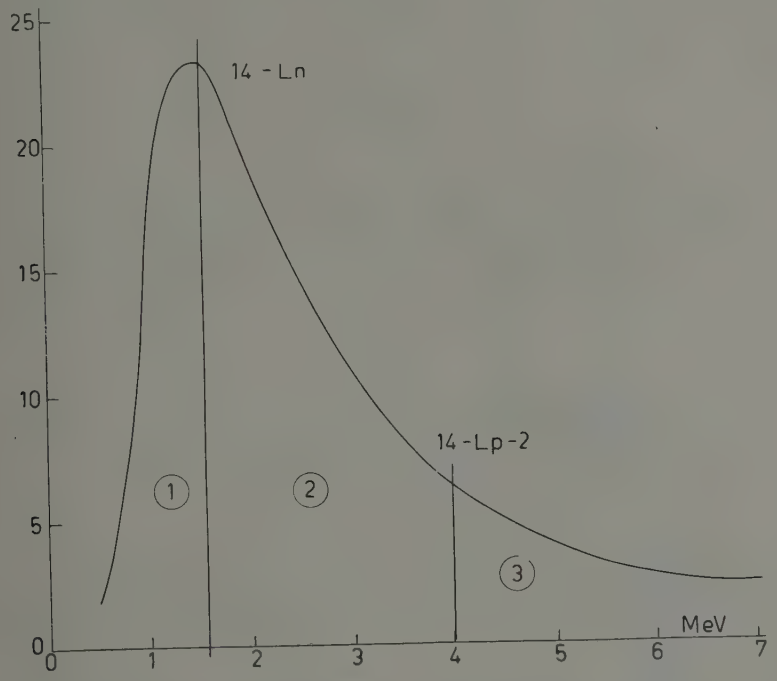

Fig. 10. – Energy spectrum of the first neutron emitted deduced from Table III. Ordinate: relative units. The values of $\varepsilon_1 - L_n$ and $\varepsilon_1 - L_p - 2$ are indicated as an example and determine the regions (1) (2) (3). This spectrum refers to nuclei from Al to Mo.

For heavier elements, for instance Zr, SE HEE AHN and ROBERTS [7] agree with a maxwellian curve with $\theta \sim 1$ MeV for the first neutron emitted and $\theta \sim 0.57$ MeV for the second. A similar behaviour shows Mo in n, p and n, np reactions (Fig. 9).

The values corresponding to all the discussed cases are shown in Table IV.

From here one can proceed as follows: after the exit of the 1st neutron from the nucleus A, which happens with a cross-section given in Table II, we shall have three atlernatives: if the energy of the 1st neutron is $> \varepsilon_1 - L_p - 2$ MeV, where ε_1 is the incident energy, that is 14 MeV, L_p represents the binding energy of the proton in the nucleus A, the only subsequent process possible is the γ-ray emission (*). If the energy is between $\varepsilon_1 - L_n$ and $\varepsilon_1 -$

(*) No proton is emitted with energies lower than 2 MeV.

TABLE III. – *Emission spectrum of first neutron.*

MeV	$n(\varepsilon)$ (relative units)	f (*)
0.5	24	0
1	186	0.15
1.5	233	0.26
2	192	0.43
2.5	148	0.57
3	109	0.68
3.5	80	0.76
4	58	0.82
4.5	51	0.86
5	36	0.90
5.5	33	0.93
6	25	0.95
6.5	25	0.98
7	22	0.99

(*) f represents the fraction of neutrons with energy $< \varepsilon$.

$- L_p - 2$ MeV, L_n being the binding energy of the neutron in the nucleus A, a proton or a γ-ray can be emitted. If the energy is less than $\varepsilon_1 - L_n$ the proton, the γ-ray and a second neutron can be emitted. In Fig. 10 the three

TABLE IV. – *Emission temperatures θ for neutrons and protons in* 14 MeV *reactions.*

Nucleus	Reactions	θ (apparent) (MeV)	θ_1 I particle (MeV)	θ_2 II particle	Authors
Al	nn′	—	1.01±0.1	—	(43)
Fe	nn′+ n, 2n	0.76±0.08	—	—	(43)
	nn′+ n, 2n	—	1.2	0.5	(*)
^{54}Fe	np + nnp	—	1	—	(47)
^{56}Fe	np	—	1.2	—	(10)
^{60}Ni	np + nnp	—	1	0.45	(11)
Ni	np + npn	—	1.3	0.6	(***)
Cu	nn′+ n, 2n	0.77±0.08	—	—	(43)
Cu	np + nnp	—	1	0.5	(**)
Cu	np + nnp	—	1	0.4	(23)
Zr	nn′+ n, 2n	0.74±0.09	0.99±0.12	0.57±0.07	(7)
Mo	np + nnp	—	1.1	0.5	(**)

(*) Value obtained from the results of BENVENISTE (18) *et al.*
(**) Values from Fig. 8 and 9.
(***) Values from backward spectra of Fig. 2.

cases correspond to the regions indicated. In the third case the statistical theory foresees that the neutron emission is the most important one. Indicating with Γ_n the average neutron width of a nucleus A, excited at an energy corresponding to a first neutron emitted in the area (1) of Fig. 10, Γ being its average total width, one gets

$$\frac{\Gamma_n}{\Gamma} = \frac{\sigma_{(n,2n)}}{\sigma_I \cdot f_n};$$

f_n is the fraction of primary neutrons corresponding to area (1) emitted with energy $< \varepsilon_1 - L_n$.

The values of f_n are given in Table III. In Table V, are shown the values of $\varepsilon_1 - L_n$ and that of Γ_n/Γ.

TABLE V. – *Relative width of neutron emission.*

Nucleus	$\varepsilon_1 - L_n$ (MeV)	f_n	$\sigma_{n,2n}/f_n\sigma_I = \Gamma_n/\Gamma$
^{27}Al	0.94	0.13	0
^{56}Fe	2.83	0.63	0.62
^{58}Ni	2.2	0.47	0.06
^{60}Ni	2.6	0.58	0.85
^{63}Cu	3.44	0.75	0.50
^{65}Cu	4.2	0.84	0.92
^{90}Zr	1.64	0.32	1.1
^{92}Mo	1.65	0.32	0.34

It could be noted how, for some nuclei the width of the outgoing neutron is rather small in respect to the other possible processes, which is in contrast with the evaporation model.

For the nuclei ^{27}Al, ^{54}Fe, ^{58}Ni, ^{92}Mo in which the σ(n, 2n) is very small, a similar calculation can be made with respect to the outgoing protons: in fact indicating with Γ_p and Γ the average width of proton emission and the total width of suitably excited nuclei A (that is after the reemission of a first neutron with energy less than $\varepsilon_1 - L_p - 2$ one gets:

$$\frac{\Gamma_p}{\Gamma} = \frac{\sigma_{n,np}}{\sigma_I \cdot f_p},$$

f_p represents the fraction of primary neutrons emitted with energy lower than $\varepsilon_1 - L_p - 2$ MeV.

It is interesting to observe from the Γ_p/Γ values given in Table VI, how the proton emission is relatively more important for heavy nuclei, such as ^{58}Ni and ^{92}Mo, notwidthstanding the stronger Coulomb barrier than for a light nucleus like ^{27}Al. Because of the small transparence of the barrier, it must be concluded that the proton had to present itself at the nuclear surface a number of times.

TABLE VI. – *Relative width of proton emission.*

Nucleus	$\varepsilon_1 - L_p - 2$ (MeV)	f_p	$\sigma_{npp}/f_p\sigma_I = \Gamma_p/\Gamma$
^{27}Al	3.8	0.80	0.12
^{54}Fe	3.1	0.69	0.35
^{58}Ni	4.2	0.84	0.24
^{92}Mo	4	0.82	0.60

2·8. *Comparison between Γ_p and Γ_n.* – As is shown in Table VI, some nuclei have high n, np cross-sections, others have small ones.

ALLAN [8], the first author to observe this fact, justified it by assuming that the protons are produced from nuclei, excited in the area (2) of Fig. 10, that is after the reemission of a first neutron of energy between $\varepsilon_1 - L_n$ and $\varepsilon_1 - L_p - 2$ MeV. The changes of the L_p and L_n values from one nucleus to another, should explain the high variations of the n, np cross-sections.

A thorough examination permits us to conclude that where the n, np reactions are more probable not all the protons must be produced in area (2); a large part of them must be produced in area (1), that is they must be in direct competition with the neutron emissions. This fact follows from that derived in 2·7. The neutron emissions in area (1), that is the n, 2n reactions, are not the major process for those nuclei in which the n, np reactions, are intense. σ_1 excited nuclei being in area (1) ($\sigma_1 = f_n\sigma_I$) a part $\sigma_1 - \sigma_{n,2n}$ does not disintegrate by emission of the second neutron. It is reasonable to suppose that these nuclei can emit γ-rays or protons with a repartition law similar to that of the nuclei excited in area (2). The excited nuclei in area (2) are $\sigma_2 = \sigma_I (f_p - f_n)$. We indicate with $(\Gamma_p)_1$, $(\Gamma_\gamma)_1$ and $(\Gamma_n)_1$ the various average emission widths of excited nuclei in area (1), with $(\Gamma_p)_2$ and $(\Gamma_\gamma)_2$ the corresponding widths of excited nuclei in area (2). On this hypothesis we get the following:

$$\frac{(\Gamma_p)_1}{(\Gamma_p)_1 + (\Gamma_\gamma)_1} \simeq \frac{(\Gamma_p)_2}{(\Gamma_p)_2 + (\Gamma_\gamma)_2}.$$

We indicate by f^* and $(1-f^*)$ the fraction of protons produced by nuclei excited

in area (1) and respectively in area (2). One gets:

$$\frac{f^*\sigma_{n,np}}{\sigma_1 - \sigma_{n,2n}} \simeq \frac{(1-f^*)\sigma_{n,np}}{\sigma_2},$$

and therefore

$$(**) \qquad f^* \simeq \frac{\sigma_1 - \sigma_{n,2n}}{\sigma_1 - \sigma_{n,2n} + \sigma_2}.$$

Commenting on this procedure we observe that the hypothesis $f^* = 0$ by which the protons are emitted only in area (2) would have meaning only if $\sigma_1 \simeq \sigma_{n,2n}$ as happens for ^{60}Ni, ^{56}Fe, ^{65}Cu, ^{90}Zr. If we consider nuclei as ^{58}Ni or ^{92}Mo this hypothesis would bring one to suppose that the major part of the nuclei corresponding to area (1), could decay only by γ emission, while those in area (2), could decay only by proton emission.

The relative number of protons $f^* \cdot \sigma_{n,np}$ obtained using formula (**) are given in Table VII, the average relative emission width of neutrons and of protons in area (1), where both processes are in competition is given by

$$\frac{(\Gamma_p)_1}{(\Gamma_n)_1} = \frac{f^*\sigma_{n,np}}{\sigma_{n,2n}}.$$

TABLE VII. – *Ratio between the emission widths of protons and neutrons when the emissions are in competition.*

Nucleus	Maximum energy of the II neutron $\sim 14 - L_n - 1$ (MeV)	Average energy of the II neutron (MeV)	Average energy of the proton (MeV)	$\sigma_{n,2n}$ (mb)	$f^* \cdot \sigma_{nnp}$ (mb)	$\Gamma_p/\Gamma_n = f^* \cdot \sigma_{nnp}/\sigma_{n,2n}$
^{56}Fe	~ 1.83	~ 0.4	~ 2.5	485	0	0
^{58}Ni	~ 1.2	~ 0.4	~ 2.5	31	118	3.8
^{60}Ni	~ 1.6	~ 0.4	~ 2.5	600	64	0.1
^{63}Cu	~ 2.44	~ 0.4	~ 2.5	522	160	0.31
^{65}Cu	~ 3.2	~ 0.4	~ 2.5	1116	0	0
^{90}Zr	~ 0.64	~ 0.4	~ 3.5	616	0	0
^{92}Mo	~ 0.65	~ 0.4	~ 3.5	164	215	1.3

The values thus obtained are given in column 7 of Table VII. It is interesting to note that for some nuclei such as ^{58}Ni and ^{92}Mo, the proton emission is not at all unfavourable with respect to that of neutrons, even though the barriers are strong.

In agreement with this facts is the behaviour of p, 2p reactions with 21.5 MeV protons, which in some cases prevail on p, pn or p, 2n reac-

tions. Even here in the case of ^{54}Fe and ^{58}Ni one obtains a strong emission of a second proton, while this emission does not happen for ^{63}Cu ([12]). From this viewpoint the situation with 21.5 MeV protons is rather similar to that for 14 MeV neutrons.

For other nuclei such as ^{56}Fe, ^{60}Ni, ^{65}Cu, ^{90}Zr, the neutron emission is the only important one, as we have already seen.

3. – Discussion of the emission mechanisms.

3·1. *Instantaneous effects.* – The high energy part of the spectra shows a high degree of anisotropy and evidently indicates the presence of instantaneous effects (Fig. 3, 4, 5).

General theories of such effects have been developed by many authors ([16]); the necessary calculations to apply these theories in specific reactions are however very complicated, and have so far been made only in a few cases ([70,71]).

Three types of instantaneous effects have been shown in the case of an incident nucleon:

1) Pick up reactions (n, d and p, d) in which the incident nucleon brings another nucleon with it, binding it to form a deuteron ([72]).
2) Direct excitation of collective motions ([35,71,76]).
3) Direct effect in which only collisions with single nucleons of the bombarded nucleus intervene ([14,74-77]).

Referring to the results shown in Section **1**, we must remember how in the case of Cu there is evidence of pick up reactions, while the n, p spectra of Mo and Ag above the deuteron threshold, strongly anisotropic, are to be attributed to direct collisions, in which a single proton intervenes.

It is interesting to consider the situation from the optical model point of view: there is a close connection between the imaginary potential and the possibility of having instantaneous effects. As is well known the imaginary part of the optical nuclear potential corresponds to the absorption of the incident

---

([70]) C. A. LEVINSON and M. K. BANERJEE: *Ann. Phys.*, **2**, 471, 499 (1957) and **3**, 67 (1958).

([71]) J. SAWICKI: NYO-8084 (1958).

([72]) *Handb. d. Phys.*, Nuclear Reactions I, **40**, 143.

([73]) A. M. LANE: *Discussion at International Conf. on Low Energy Nuclear Physics* (Paris, July 1958).

([74]) N. AUSTERN, S. T. BUTLER and H. MCMANUS: *Phys. Rev.*, **92**, 350 (1953).

([75]) S. HAYAKAWA, M. KAWAI and K. KIKUCHI: *Progr. Theor. Phys.*, **13**, 415 (1955).

([76]) L. B. B. ELTON and L. C. GOMES: *Phys. Rev.*, **105**, 1027 (1957).

([77]) S. T. BUTLER: *Phys. Rev.*, **106**, 272 (1956).

nucleon: in particular it is responsible for the first act of absorption and is therefore connected to the instantaneous effect which represents the first act of the emission.

Recent opinions tend to establish the absorption on the nuclear surface ([78,79]). In the case of direct interaction with single nucleons the localization can mean that the interaction takes place with the outer nucleons which are less bound; direct evidence in which the protons emitted in n, p reactions on light nuclei are the outermost ones has been obtained in a few cases, recently by COLLI and collaborators ([22]).

In this order of ideas may find place the observation of LEVKOWSKJI ([80]) for whom σ(n, p) for a certain group of isotopes is smaller for the heaviest isotopes.

3·2. *Non equilibrium escape.* – Another discussion may be held for the backward emitted spectra considered in Section 2 at energies $\gtrsim$ 18 MeV. As we have seen these spectra show that the probability of the emission is not simply proportional to the density of final states notwithstanding the fact that the final states in nuclei as Cu and Ag are very dense.

A deeper analysis of Fig. 5, 6, 7 indicates that the emission is a not equilibrium one.

In fact one can note from these spectra that the curves of Fig. 5, 6, 7 are less steep for higher incident energies. This fact means that the emission of energetic nucleons corresponding to a given residual energy, is much more favoured when the incident energy is greater. To give more evidence to this statement we have collected in Fig. 11 the spectra of Fig. 6 relative to Cu with the addition of spectra of other reactions on nuclei not much different from Cu. The curves are roughly normalized at the highest excitation energy of the residual nucleus.

It is sufficiently established from this figure that the change in steepness in the various curves is connected with the incident energy. Similar results are obtained in all the considered cases. This would show that the particle escape takes place before the mixing of energy is completed and the equilibrium is reached.

This escape however is not to be attributed necessarily to a pure istantaneous effect or to an usual nuclear cascade.

One can consider an emission based on fast energy exchange among few nucleons excited above the top of the nuclear distribution: the collisions be-

([78]) K. A. BRUECKNER: *Phys. Rev.*, **103**, 172 (1956).
([79]) F. BJORKLUND and S. FERNBACH: *Geneva Conf.*, P/649 (Sept. 1958).
([80]) V. N. LEVKOVSKJI: *Sov. Phys. Journ. Exp. Phys. Theor.*, **6**, 1174 (1958).

tween one excited nucleon and the core nucleons are much less probable than the collisions between two excited nucleons, and rapid escape of one of them is made possible when the excitation energy is sufficiently high.

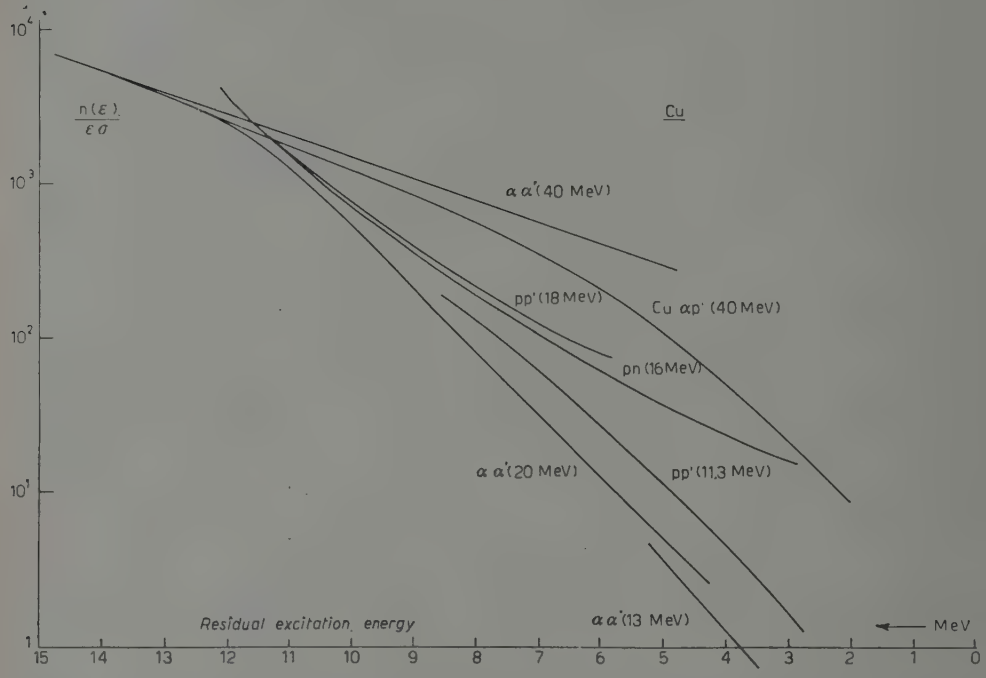

Fig. 11. – The same curves of Fig. 6 compared with other spectra obtained from α, p and p, n reactions on Cu. Normalization is made at the highest excitation energies. References as in Fig. 6 plus ([2,81]).

Such a process could be held responsible for a type of spectrum of fast particles, similar in light and heavy nuclei: in fact only a few nucleons intervene in the reaction. A remarkable fact from this point of view is the similar behaviour of the $n(\varepsilon)/\sigma\varepsilon$ curves for various nuclei, for a given incident energy indipendently of the mass number A (*).

This fact is concluded from the curves on pp′ reactions at 18 MeV by GUGELOT ([31]).

([81]) P. C. GUGELOT: *Phys. Rev.*, **81**, 51 (1951).

(*) We recall that we are considering the backward angles. In fact in the forward direction different behaviours for various nuclei and the appearance of well defined excited states of residual nuclei has been evidenced recently in n, p reactions ([22]).

3·3. *Equilibrium emission* – As we have seen in the case of medium weight nuclei and with energies of about 14 MeV, the spectrum of the emitted particles shows an equilibrium emission and this is demonstrated pretty well by comparing the various results. The fact observed by many authors that the curve of the level density has the shape of $\exp[E/\theta]$, where θ is constant with respect to the variations of E, is interpreted as due to a process of partial melting of the nucleus, hence at constant temperature, that takes place in the nucleus, and therefore the description of the excited nucleus with Fermi gas model is no longer valid ([82]). In this type of partial melting the interactions between the nucleons at the surface take on a particular, still ununderstood, importance.

The fact that the temperature θ depends very little even on A, can give the same indication: only a limited number of nucleons, probably at the surface, take part in the reactions, and therefore the process is not strongly depending on A.

A further discussion can be done for n, np and n, 2n reactions. As we have already mentioned the values of Tables V and VII contraddict hypotheses 3) and 4) of Section 2, and show that the matrix elements for the various possible transitions are not equiprobable. However due to the low energy at disposal for the residual nuclei the density of final states is not so high to justify the use of hypotheses 3) and 4) and at least spin selection rules and centrifugal barriers must be considered. It is also interesting to note from Table VII how the passing from one nucleus with weak neutron (or proton) emission, to a nucleus with strong neutron (or proton) emission, seems to be bound to the joining of two neutrons (or protons) to the first nucleus. The couples ^{63}Cu, ^{65}Cu and ^{58}Ni, ^{60}Ni must be considered for the effect on neutrons, and the couple ^{90}Zr, ^{92}Mo for the effect on protons: the properties of the emission of these reactions seem to depend largely on the conditions on the nuclear surface. In fact due to the low excitation of the compound nucleus only the less bound neutrons or protons can be emitted, the rest of the nucleus remaining not excited or excited in the low energy collective states.

3·4. *Conclusions.* – This discussion is qualitative, and if valid is to be referred to the particular cases discussed. However the following can be safely stated:

1) A part of the reactions take place through instantaneous effects.

2) The emission of evaporated neutrons dominate in heavy nuclei.

([82]) L. E. TRAINOR, W. R. DIXON: *Can. Journ. of Phys.*, **34**, 229 (1956).

3) In medium nuclei proton evaporation plays an important role below 18 MeV incident energy.

4) Not equilibrium escape even in backward angles is present in reactions at higher incident energies.

5) All the types of mechanisms discussed seem to be connected with the nuclear surface.

RIASSUNTO

Vengono descritte misure dello spettro energetico di protoni emessi in relazioni n,p ed n, np prodotte da neutroni di 14 MeV per Ni, Cu, Mo ed Ag. Lo spettro è misurato a quattro angoli per ciascuno di questi casi. I risultati ottenuti vengono confrontati con altri risultati noti di spettri di particelle emesse in reazioni nucleari alle medie energie. I meccanismi che intervengono in queste reazioni possono così riassumersi: 1) effetti istantanei responsabili dell'emissione delle particelle a più alta energia ed emesse soprattutto ad angoli in avanti. 2) fuga di non equilibrio relativa alle particelle delle parti medie dello spettro ed emesse a tutti gli angoli. Viene discussa la possibilità di tali processi di fuga in connessione con le interazioni fra nucleoni eccitati alla superficie del nucleo. 3) emissione ritardata, probabilmente successiva ad un equilibrio statistico, responsabile della emissione di protoni in nuclei medi e di neutroni per energie incidenti non superiori a 18 MeV. Temperature di ~ 1 MeV vengono confermate. In reazioni n, np od n, 2n vengono osservate in alcuni casi probabilità di emissione maggiori per protoni che per neutroni. Una discussione di queste emissioni porta a fare l'ipotesi che gli elementi di matrice delle varie reazioni risentano fortemente delle condizioni della superficie nucleare.

IL NUOVO CIMENTO Vol. XIII, N. 4 16 Agosto 1959

Theoretical Study of the Cosmic Ray Equator.

P. J. Kellogg and M. Schwartz (*)

University of Minnesota - Minneapolis, Minn.

(ricevuto il 27 Aprile 1959)

Summary. — Calculations of cut-off rigidities for cosmic ray particles in the earth's magnetic field have been carried out, using an approximation to the earth's field which includes all moments up to and including the octupole moments. The results show that deviations of the cosmic ray intensity from that calculated on the dipole approximation may be ascribed to the higher moments of the earth's field.

1. – Introduction.

A number of experiments in the past few years have shown that the cosmic ray intensity deviates from that which would be expected if the earth's magnetic field were exactly that of a dipole. Simpson [1] has suggested that the deviations are produced by extraterrestrial currents. Rothwell and Quenby [2] however, have pointed out that the cosmic ray equator coincides rather closely with the magnetic dip equator and argue that the coincidence of cosmic ray intensity and a feature of the earth's field suggest that the deviations of the earth's field from that of a dipole are responsible for the deviations of cosmic ray intensity. In order to settle this question, calculations of the cosmic ray intensity using a more accurate approximation to the earth's field are necessary and the purpose of this paper is to report such calculations. Calculations using a different sort of approximation have been carried out by Quenby and Webber [3].

(*) This work was supported by the U.S. National Committee for the IGY and the University of Minnesota Graduate School.

(1) L. Katz, P. Meyer and J. A. Simpson: *Suppl. Nuovo Cimento*, **8**, 277 (1958).

(2) P. Rothwell and J. Quenby: *Suppl. Nuovo Cimento*, **8**, 249 (1958).

(3) J. Quenby and W. Webber: *Phil. Mag.*, **4**, 90 (1959).

2. – Description of catculation.

We have approximated the earth's field by the sum of its dipole, quadrupole, and octupole moments using the coefficients calculated for epoch 1955 by FINCH and LEATON (4). The sum of these terms is still not a very good approximation to the earth's actual field. Fig. 1 shows comparison of the measured total field on the geographic equator together with the total field calculated on the present approximation. It will be seen that the error in the approximation amounts to nearly 15% in the region 0 to 20 degrees east.

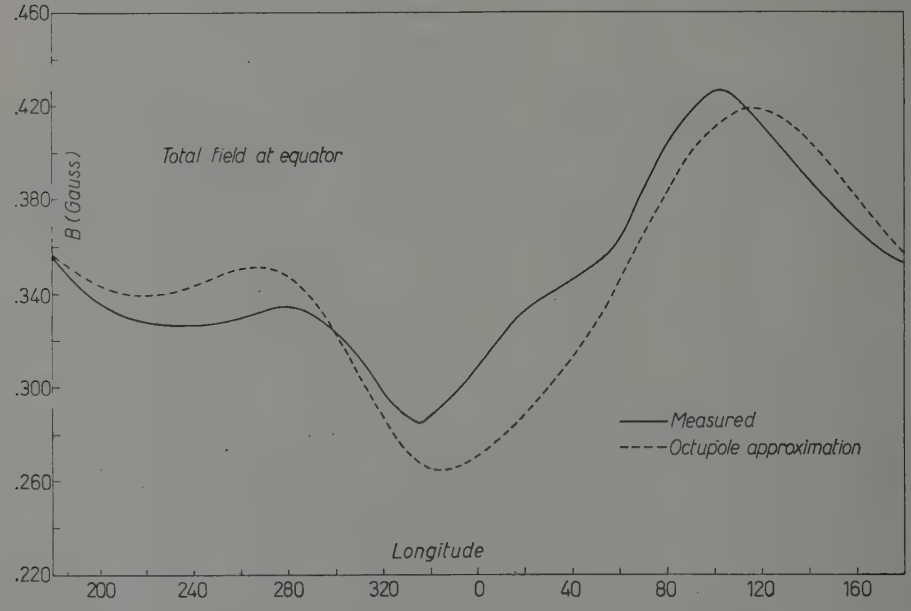

Fig. 1. – Measured total magnetic field at the equator and present approximation.

Experimentally the position of the cosmic ray equator is measured by measuring the cosmic ray intensity along a roughly north-south line. The minimum of the intensity determines the cosmic ray equator. The cosmic rays which contribute to the measured intensity come, of course, from all directions in the sky. Theoretically, one may define the cosmic ray « equator » for a given direction of incidence by calculating cut-off rigidities at each longitude as a function of latitude. For each longitude one determines a maximum

(4) FINCH and LEATON: *Month. Not. Roy. Astron. Soc., Geophys. Suppl.*, **7**, 314 (1954). We used their solution 2.

cut-off rigidity. One then uses the isotropy of cosmic rays and Liouville's theorem to call the locus of the above maximum cut-off rigidities the cosmic ray « equator » for the given direction of incidence.

For a magnetic dipole field, the theoretical equator coincides with the dipole equator for all directions of incidence. For a non-dipole field, the theoretical equator will not necessarily be the same for all directions of incidence. In the present work, we have determined the theoretical equator for the vertical direction.

Since cylindrical symmetry is lost when one adds the quadrupole and octupole fields to the dipole field, one must pay particular attention to the sign of the charge associated with the orbits used for calculating cut-off rigidities. For cosmic rays, one is interested in positive particle orbits incident on the earth, but for convenience we integrated negative particle orbits starting out from the earth.

As a matter of convenience, both in interpretation of results and in use of the moments calculated by FINCH and LEATON ([3]), all of the calculations were carried out using geographic co-ordinates and unless otherwise noted for the rest of this paper we will discuss only the ordinary geographic latitudes and longitudes.

The cut-off rigidities which we calculate correspond to main cone cut-offs (in the sense of LEMAITRE and VALLARTA ([5])). The justification for this is as follows. The overall predominance of the dipole component of the earth's field allows us to talk about a cut-off analogous to a Störmer cut-off at any point on the earth. One is then led to expect that if one calculates orbits starting at a fixed point and in a fixed direction, then by varying the rigidity from higher to lower values, one can find a transition from orbits which go directly to infinity without looping back toward the earth and those which do not. The existence of such a transition has been verified by our computations. The orbits corresponding to rigidities less than the transition rigidity are of the penumbral type encountered in the dipole theory ([6]). The predominance of the dipole component also leads one to expect that for sufficiently low latitudes, the penumbra will be black (*i.e.*, the returning orbits penetrate the earth). This is also verified by our calculations. Thus for the latitude regions which we investigate, the main cone cut-off indeed corresponds to the minimum allowed rigidity.

To begin the computation, initial geographic co-ordinates and reasonable values of rigidity and rigidity increment are fed into the machine. The ma-

---

([5]) G. LEMAITRE and M. S. VALLARTA: *Phys. Rev.*, **50**, 493 (1936).

([6]) R. A. HUTNER: *Phys. Rev.*, **55**, 15 (1939); M. SCHWARTZ: *Suppl. Nuovo Cimento*, **11**, 27 (1959).

chine integrates the equations:

$$(1)\qquad \begin{cases} \dfrac{d\boldsymbol{x}}{ds} = \boldsymbol{v}\,, & a = \text{rigidity} = \dfrac{pc}{Ze}\,, \\ \dfrac{d\boldsymbol{v}}{ds} = \dfrac{1}{a}(\boldsymbol{v}\times\boldsymbol{B})\,, & \boldsymbol{v}\cdot\boldsymbol{v} = 1\,, \end{cases}$$

and determines whether the orbit of the particles reaches infinity, or intersects the earth. Supposing that the orbit intersected the earth, the rigidity is increased by the rigidity increment and a new orbit is computed. When an orbit is found which reaches infinity the increment is halved and the new increment subtracted from the rigidity. This procedure, similar to the procedure used in proving a Weierstrass theorem on limits, is continued until the desired accuracy is attained. If all rigidities less than a certain limit are forbidden and all rigidities greater than a certain limit allowed, this procedure will converge on that limit. If, however, there are allowed and forbidden rigidity bands the procedure may converge on the upper edge of any of the bands. At a number of points near the equator a survey was made of the rigidity region near the critical rigidity and no such penumbral bands were

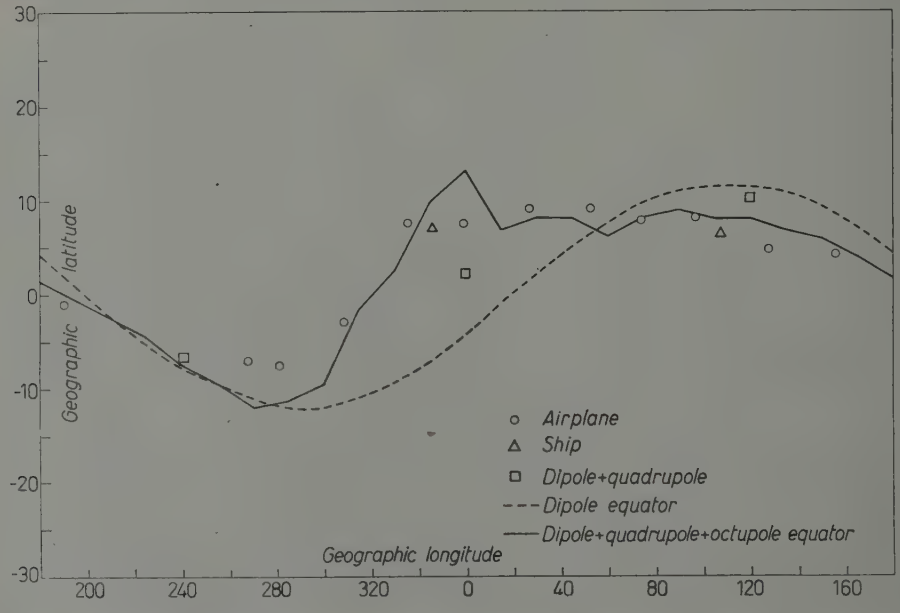

Fig. 2. – Computed cosmic ray equator compared with measured position. The squares give results of computations without octupole moments.

found in the vertical direction. There is a unique cut-off rigidity, therefore, and our procedure computes it. Normally the cut-off rigidity was computed

to an accuracy of $\frac{1}{4}$ %. This accuracy is higher than is physically meaningful, but is necessary to avoid error in computing the position of the rigidity maximum.

Cut-off rigidities were computed at intervals of 5° of longitude for a fixed latitude. A parabola was fitted through the three highest points and used to find the position of the maximum. When the error in the rigidities is about $\frac{1}{4}$ % the error in the position of the maximum will not exceed about 1°. The cosmic ray equator thus computed is plotted in Fig. 2, together with a number of measurements ([1,2,7]). The computed vertical cut-off rigidity at the computed cosmic ray equator is shown as a function of longitude in Fig. 3.

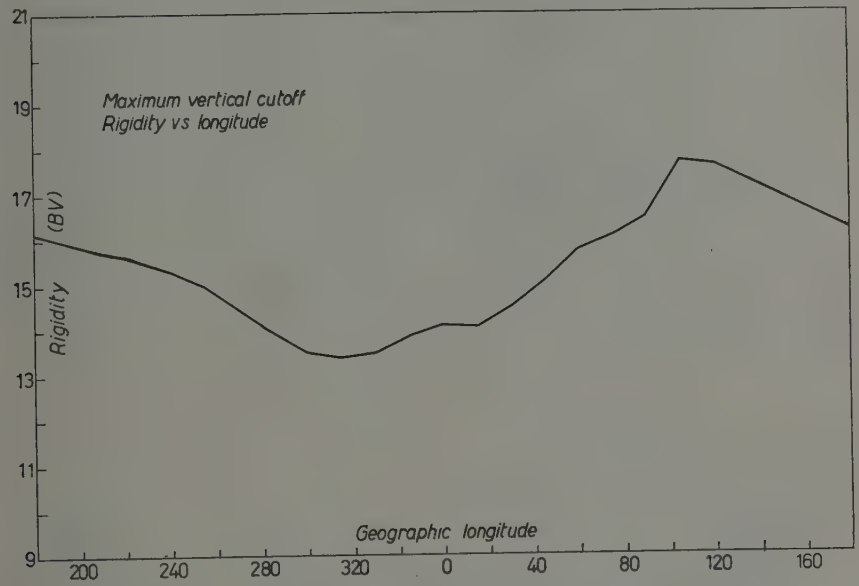

Fig. 3. – Calculated cut-off rigidity at the theoretical equator.

The points circumscribed by squares in Fig. 2 refer to cosmic ray equator points determined by dropping the octupole terms from our magnetic field approximation. As can be seen, except for the region of 0° longitude, the major part of the shift is due to the octupole moment. This is in agreement with an approximate calculation by SCHWARTZ ([8]), which showed that, except near 0° longitude, the quadrupole terms do not produce an appreciable equator shift.

([7]) N. A. POMERANTZ, A. E. SANDSTRÖM and D. C. ROSE: *Suppl. Nuovo Cimento*, **8**, 257 (1958).

([8]) M. SCHWARTZ: *Bull. Amer. Phys. Soc.*, **3**, 221 (1958). The check at 0° longitude was done after the publication of the abstract.

3. – Discussion of results.

It is evident from Fig. 2 that except for the longitude regions, 240° to 300° and 340° to 5°, the experimentally determined cosmic ray equator is essentially in agreement with our calculation. However, one may ask whether or not there is a sizeable latitude variation of the cosmic ray equators corresponding to directions of incidence other than vertical. From continuity considerations one may expect that for directions sufficiently close to the vertical, there will be no significant latitude variation. As a check on this, supplementary calculations for a direction of incidence 5° west (of vertical) were made. Around (285÷300)° longitude, the latitude shift was of the order of a degree, but in most other places it was of the order 0.1° or less. The neutron monitors at airplane altitudes have an effective angular aperture of about (20÷30)° with the maximum coming around 6° west. The distribution is sufficiently narrow around the maximum so that (considering also our 5° west results) one should not expect that the effect of the rest of the sky will introduce an error of more than about 2° on the average in our equator determination. Support is lent to this conclusion by the fact that the shipboard data and the airplane data appear to fall on the same curve as one sees from our Fig. 2, while their effective angular apertures are different by a factor of 2.

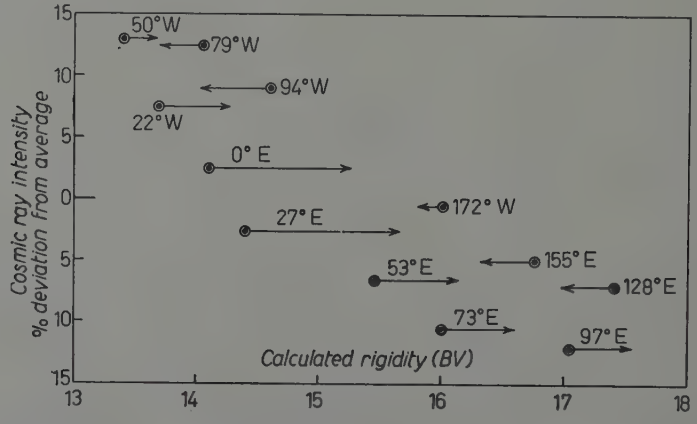

Fig. 4. – Comparison of measured cosmic ray intensity and calculated cut-off rigidity.

In order further to compare the results of experiments with our calculations, we have plotted, in Fig. 4, our calculated cut-off rigidity versus the cosmic ray intensity at airplane altitudes measured by SIMPSON [1]. Since there is no penumbra near the equator, these points should all fall on a single

curve. In fact, there is considerable scatter and we now discuss the possible reasons for this scatter.

The lack of agreement between our calculated cut-off rigidities and Simpson's measured intensities demonstrated in Fig. 4 could be due to two causes; either 1) because we have not used a sufficiently good approximation to the earth's field, or because 2) we have neglected the effect of particles arriving from other directions than the vertical.

The results of the calculations at 5° west of vertical indicate that the effects of directions other than the vertical are smaller than the errors due to the field. Furthermore, the effect of the whole sky is probably smaller than the experimental errors in determination of the position of the equator.

On the other hand, there is definite evidence that errors in our approximation for the earth's magnetic field are responsible for the discrepancies shown in Fig. 4. In Fig. 4 an arrow is attached to each of the points whose length is proportional to the difference between our approximation to the earth's magnetic field and the measured value. These differences actually apply to the geographical equator, but this is accurate enough for our present argument. In other words, the length and direction of the arrows represents the change in cut-off rigidity we would expect if the earth's surface field is the controlling factor, as suggested by ROTHWELL [9].

For a dipole field the vertical cut-off rigidity at the equator is given by

$$\frac{pc}{Z} = \frac{\varepsilon/\mu}{4R_E^2} = 48 B_{eq} \text{ (GeV)},$$

where B_{eq} is the surface field at the equator. Hence we should expect $\Delta R = 48\,\Delta B$. We have actually used $\Delta R = 30\,\Delta B$ but $48\,\Delta B$ would also be of the right order of magnitude. We see that all of the points move in such a way as to fall more nearly on a curve. We feel that this is convincing evidence that the discrepancies represented by Fig. 4 are due to errors in our approximation to the earth's field.

The errors in our approximation to the earth's field are also undoubtedly sufficient to account for the difference between the computed and observed positions of the cosmic ray equator. We have shown in Fig. 2 the position of the cosmic ray equator at 1, 120° and 240° longitude computed with the dipole and quadrupole moments alone. The contribution to the earth's field due to moments higher than the octupole moment is roughly the same size as the contribution of the octupole moments and therefore may be expected to have a similar effect.

---

[9] P. ROTHWELL: *Phil. Mag.*, **3**, 961 (1958).

4. – Summary.

We have shown conclusively that the non-dipole terms in the earth's field are sufficiently large to account for the deviation of the cosmic ray equator from the dipole equator. We have shown that very probably the remaining discrepancy between our calculations and measurements are due to the remaining deviations of the earth's field from our approximation to it. It is therefore not necessary to postulate extraterrestrial currents in order to account for the observations of cosmic ray intensity at low latitudes.

* * *

The authors are greatly indebted to Mr. ROBERT TENNISON, who programmed this problem for the computer.

RIASSUNTO (*)

Si sono eseguiti calcoli delle rigidità di taglio per particelle di raggi cosmici nel campo magnetico terrestre usando per il campo terrestre un'approssimazione comprendente tutti i momenti fino a quelli di ottupolo. I risultati dimostrano che le deviazioni dell'intensità da quella calcolata con l'approssimazione di dipolo possono attribuirsi ai momenti superiori del campo terrestre.

(*) *Traduzione a cura della Redazione.*

IL NUOVO CIMENTO Vol. XIII, N. 4 16 Agosto 1959

A Multi-Purpose 2π Counter.

D. Prosperi and S. Sciuti

Laboratorio Fisico Divisione Geomineraria del CNRN
Istituto Nazionale di Fisica Nucleare - Sezione di Roma

(ricevuto il 4 Maggio 1959)

Summary. — A gas counter with a spherical symmetry is described. This detector can work in a very satisfactory manner, either as a flow counter or a ionization chamber reaching, in the latter case, a good α pulse-height resolution, even with large emitting sources. Calculations are made in order to find the dependence of the pulse shape on the direction of emission of an α-particle by a point source in the chamber (finite track). A good agreement is found between these calculations and the experimental tests performed, which show that this dependence can be employed in high efficiency measurements of angular α-γ correlations.

Introduction.

The advantages offered by scintillation counters have induced most researchers to forego almost entirely ionization counters, particularly when high counting rates or fast coincidences are required.

Nevertheless, in experiments for which the high velocity of the detector if not the determining factor, ionization chambers and proportional counters can still be of valid use. Gas-type counters are still particularly useful, at least as regards α-particles, both for performing absolute measurements and for some spectroscopic researches (α-γ coincidences, etc.). We have therefore felt it would be worth-while to design and construct a spherically-symmetrical gas-type detector of rapid use endowed with very flexible features and capable of operating either as a flow counter or an ionization chamber. In the latter case it may also function as a directional detector, permitting measurement of the angular distribution of α-particles emitted by a point source.

1. – Limits of operation.

1·1. *Details of construction.* – A schematic drawing of the detector is shown in Fig. 1. The external electrode is a copper sphere (diameter: 200 mm, thickness: 1 mm). The collecting electrode, shown in the drawing as a little sphere (1 cm in diameter), may be easily substituted by others of different features.

The spherical symmetry of the chamber has been partially altered by substituting (Fig. 1) a spherical bowl with a plane disc working as sample holder; this latter is easily removable.

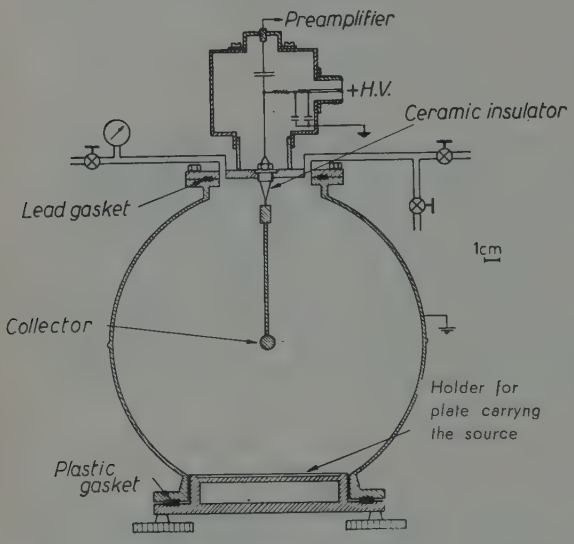

Fig. 1. – 2π spherical counter; $a = 0.5$ cm; $b = 8.5$ cm.

In order to study the possible uses of the detector, we have made various measurements, changing the type of gas mixture as well as the form of the collecting electrode. The results are summarized further below.

1·2. *Flow counter.* – As was expected, the detector is easily adapted to operate in the multiplication region. In fact, excellent results were obtained for detecting β and α-particles by using a mixture of 90% argon and 10% C_4H_{10} at atmospheric pressure, with either point or loop-shaped collectors.

1·3. *Ionization chamber.* – The collecting electrode is normally maintained at a voltage of about 2 000 V in order to avoid ion recombination in argon or in other gases usually employed. Its capacity to ground, when connected to the pre-amplifier, is of 20 pF.

Operation is satisfactory even in the case of extended α sources. This was verified by measuring, by means of a 100 channel pulse height analyser, the percentage width at half height of the α-line of ^{210}Po (5.3 MeV) using both point and extended sources. The results obtained for pure argon are shown in Table I.

In closing this paragraph we may say that the detector permits absolute

measurements of β- and α-activities and may also be used for differential analyses of complex α spectra when the resolutions appearing in Table I are sufficient.

TABLE I.

Area of the source (cm^2)	Position of the source	Percentage full width at half-height
point source	at the center	2.3
point source	9 cm from center	2.3
0.4	at the center	2.5
4.3	at the center	5.0

2. – Dependence of the pulse shape on the angular distribution of the ionization.

2·1. – As is known, ROSSI and collaborators [1] were the first to observe that the shape of a pulse in a cylindrical chamber could supply information as to the type of the ionizing event which had produced it.

Recently, CERNIGOI *et al.* [2], have achieved some calculations showing how it is possible to recognize, from the shape of the pulses in a cylindrical chamber, one of the following events:

a) ionization confined to an infinitely small volume;

b) uniform ionization along a straight line with various orientations;

c) ionization uniformly distributed throughout the volume of the chamber.

The calculations are in agreement with experimental data. These investigators, however, have not considered the case of a particle which is produced in the chamber and whose trajectory ends in the chamber itself (finite track).

The calculation in respect of this case is of particular interest for determining whether the shape of the pulses can be put in a simple correlation with the direction of emission of the ionizing particles. In case this is true, a ionization chamber of non-planar geometry could be a simple, high resolving power instrument for the study of α-γ angular correlations.

Since our chamber appears to possess the most promising features for this kind of studies, we have carried out similar calculations, for the spherically-symmetrical chamber.

---

(1) H. S. BRIDGE, W. E. HAZEN, B. ROSSI and R. W. WILLIAMS: *Phys. Rev.*, **74**, 1083 (1948).

(2) C. CERNIGOI, G. PAULI and C. POIANI: *Nucl. Instr.*, **2**, 261 (1958).

2·2. *Calculation of the pulse-shape.* – Going now to Fig. 2, let r_E be the length of the « instantaneous » track of an α-particle of energy E which terminates its trajectory at a point of radial co-ordinate r_{02}. Let r_{00} be the shortest distance of this track from the center O.

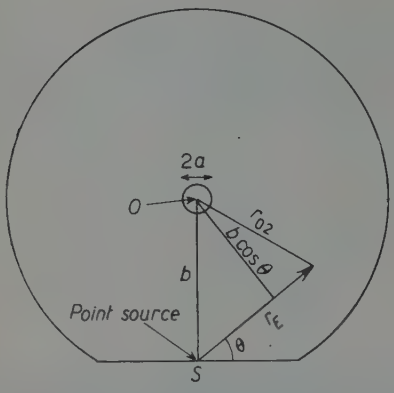

Fig. 2. – Representation of the chamber, for use in the calculation of pulse-shape.

The calculation of the profile of voltage pulses at the collector will be carried out under the following assumptions:

a) The time constant RC of the amplifier fulfils the following conditions valid for a « fast » chamber:

$$t^- \ll RC \ll t^+ ,$$

where t^- and t^+ are the longest electron collection time and the shortest ion collection time respectively.

In consequence of this choice, one may assume that during the whole electron collection time, the anode can be considered insulated and that the ions still remain in their initial position.

b) We neglect the fact that the chamber does not have exactly a spherical symmetry; the calculations have therefore been made by giving the radius of the external sphere a value b equal to the distance between the center O and the surface of the emitting electrode. This assumption does not affect the qualitative behaviour of the pulse-shape.

c) In order to simplify the exposition we shall write the expressions for the voltage pulses $\Delta V(t)$ at the collector separately in the three following cases in which it is always assumed that $r_E < b$:

(1) $$b \geqslant r_{02} \quad \begin{cases} r_E \leqslant b \sin\theta & \text{for which} \quad r_{00} = r_{02} \\ r_E \geqslant b \sin\theta & \text{for which} \quad r_{00} \leqslant r_{02} \end{cases}$$ (2)

(3) $$b \leqslant r_{02} ; \qquad r_E > b \sin\theta \quad \text{for which} \quad r_{00} < r_{02} .$$

d) To calculate the drift velocity of the electrons we use the well-known semi-empirical formula:

$$v^- = \mu^- \left(\frac{\mathcal{E}}{p}\right)^{\frac{1}{2}} ; \qquad \begin{aligned} \mathcal{E} &= \text{electric field strength}, \\ p &= \text{pressure}, \\ \mu^- &= \text{electron mobility}. \end{aligned}$$

The voltage pulse at the collector, observed at any time t, is in any case given by:

$$\Delta V(t) = \int_{b}^{r_{02}(E,\theta)} \Delta v(r_0, t) n(r_0)\, \mathrm{d}r_0 ,$$

where $\Delta v(r_0, t)$ is the voltage at the time t due to a single pair of ions generated at r_0, $n(r_0)$ is the ionization density, and E is the energy of the α-particle emitted at an angle θ (see Fig. 2). Applying known formulas [3] to the case of spherical symmetry, we find that the voltage pulse $\Delta V(t)$ at each instant prior to the collection of the first electron is given by:

$$\Delta V(t) = -\frac{e}{C}\frac{y}{y-1} a \int_{b}^{r_{02}(E,\theta)} r_0^{-1} \left[\left(1 - \frac{t}{t_0}\right)^{-\frac{1}{2}} - 1 \right] n(r_0)\, \mathrm{d}r_0 , \tag{4}$$

where:

C = capacity of the chamber,

$y = b/a$;

$t_0 = \dfrac{r_0^2}{2\mu^-[yaV/(y-1)p]^{\frac{1}{2}}}$,

V = voltage between the electrodes.

The first electron to be collected will be the one which was initially at the point of radial co-ordinate r_{00}, and the corresponding collection time t_m is given by:

$$t_m = -\int_{r_{00}}^{a} \frac{\mathrm{d}r_0}{v^-} = \frac{t_0}{r_{00}^2}(r_{00}^2 - a^2) . \tag{5}$$

The voltage pulse at any time between t_m and the time t_M at which the last electron is collected, is expressed by one of three relations, depending on whether (1), (2) or (3) is satisfied. In fact, indicating by $r_{01}(t)$ the co-ordinate relative to the last electron which can be collected up to the time t (*), we find in the three cases:

---

[3] (*i.e.*), J. SHARPE: *Nuclear Radiation Detectors* (London, 1955), p. 135.

(*) The value of r_{01} is determined from an expression similar to (5):

$$t = \frac{t_0}{r_{01}^2}(r_{01}^2 - a^2) .$$

case (1):

$$\Delta V(t) = -\frac{e}{C}\frac{y}{y-1}\left\{a\int_{b}^{r_{01}(t)} r_0^{-1}\left(1-\frac{t}{t_0}\right)^{-\frac{1}{2}} n(r_0)\,\mathrm{d}r_0 + \right. \tag{6}$$

$$\left. + \int_{r_{01}(t)}^{r_{02}E_1(\theta)} n(r_0)\,\mathrm{d}r_0 - a\int_{b}^{r_{02}(E,\theta)} r_0^{-1} n(r_0)\,\mathrm{d}r_0\right\},$$

case (2):

$$\Delta V(t) = -\frac{e}{C}\frac{y}{y-1}\left\{a\int_{b}^{r_{02}(E,\theta)} r_0^{-1}\left(1-\frac{t}{t_0}\right)^{-\frac{1}{2}} n(r_0)\,\mathrm{d}r_0 - \right. \tag{7}$$

$$\left. - 2a\int_{r_{01}(t)}^{r_{00}(E,\theta)} r_0^{-1}\left(1-\frac{t}{t_0}\right)^{-\frac{1}{2}} n(r_0)\,\mathrm{d}r_0 + A + 2\int_{r_{01}(t)}^{r_{00}(E,\theta)} n(r_0)\,\mathrm{d}r_0 - a\int_{b}^{r_{02}(E\,\theta)} r_0^{-1} n(r_0)\,\mathrm{d}r_0\right\},$$

where the term A is zero for $r_{01}(t) \leqslant r_{02}$ and assumes for $r_{01} > r_{02}$ the value:

$$A = \int_{r_{02}(t)}^{r_{02}(E,\theta)}\left[a r_0^{-1}\left(1-\frac{t}{t_0}\right)^{-\frac{1}{2}} - 1\right] n(r_0)\,\mathrm{d}r_0\,,$$

case (3):

$$\Delta V(t) = -\frac{e}{C}\frac{y}{y-1}\left\{a\int_{b}^{r_{02}(E,\theta)} r_0^{-1}\left(1-\frac{t}{t_0}\right)^{-\frac{1}{2}} n(r_0)\,\mathrm{d}r_0 - 2a\int_{r_0(t)}^{r_{00}(E,\theta)} r_0^{-1}\left(1-\frac{t}{t_0}\right)^{\frac{1}{2}} n(r_0)\,\mathrm{d}r_0 + \right. \tag{8}$$

$$\left. + B + 2\int_{r_0(t)}^{r_{00}(E,\theta)} n(r_0\,\mathrm{d}r_0 - a\int_{b}^{r_{02}(E,\theta)} r_0^{-1} n(r_0)\,\mathrm{d}r_0\right\},$$

where the term B is zero for $r_{01} \leqslant b$ and assumes for $r_{01} > b$ the value:

$$B = \int_{r_{01}(t)}^{b}\left[a r_0^{-1}\left(1-\frac{t}{t_0}\right)^{-\frac{1}{2}} - 1\right] n(r_0)\,\mathrm{d}r_0\,.$$

The maximum voltage pulse (for $t = t_M$) is given, in all cases, by:

$$\Delta V(t) = -\frac{e}{C}\frac{y}{y-1}\int_{b}^{r_{02}(E,\theta)}\left(1-\frac{a}{r_0}\right) n(r_0)\,\mathrm{d}r_0 = -\frac{e}{C}\frac{y}{y-1} N\left[1-\frac{a}{N}\int_{b}^{r_{02}(E,\theta)} r_0^{-1} n(r_0)\,\mathrm{d}r_0\right], \tag{9}$$

where N is the total number of ion pairs produced.

In order to calculate (6), (7), (8) and (9), we should express $n(r_0)$ as function of the specific ionization along the track $n(r_\varepsilon)$:

$$n(r_0) = n(r_\varepsilon)\left|\frac{\mathrm{d}r_\varepsilon}{\mathrm{d}r_0}\right| = n(r_\varepsilon)\frac{r_0}{(r_0^2 - b^2\cos^2\theta)^{\frac{1}{2}}}. \tag{10}$$

We have integrated numerically the above-mentioned equations giving to p, V, C and E the values used in our measurements. The specific ionization of argon was obtained by multiplying, by a suitable normalization factor, the similar experimental curve for air given by STETTER [4].

We have calculated the pulse-shape for the angles $\theta = 90°$, $45°$ and $0°$. For the first two angles, equations (4), (6) and (9) should be used, while for $\theta = 0°$ equations (4), (8) and (9) are valid. The results of these calculations, set in a manner independent of the mobility of the particular mixture of argon employed (*), are shown in Fig. 3. In this figure is drawn for comparison the pulse-shape due to ionization confined to an infinitesimal volume.

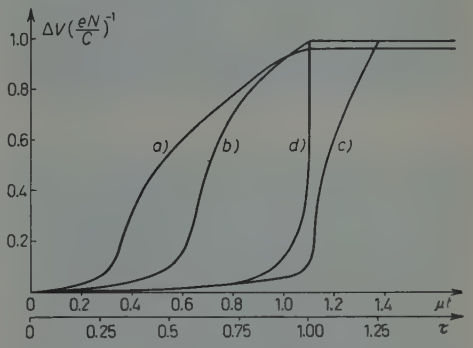

Fig. 3. – Pulse-shape distribution curves for different angles of emission. *a*) $\theta = 90°$; *b*) $\theta = 45°$; *c*) $\theta = 0°$; *d*) pulse-shape due to ionization confined to an infinitesimal volume.

All tracks whose end points lie at a distance less than b from the center O originate pulses reaching their maximum for $\mu^- t = \mu^- T \simeq 1.1\ \mathrm{cm}^{\frac{3}{2}}\ \mathrm{V}^{\frac{1}{2}}\ \mathrm{atm}^{-\frac{1}{2}}$. In our case this condition is fulfilled for $\theta \geqslant 14°$. For $\theta < 14°$ the collection time increases as θ decreases.

For $\theta = 0°$, collection is complete when $\mu^- t \simeq 1.4\ \mathrm{cm}^{\frac{3}{2}}\ \mathrm{V}^{\frac{1}{2}}\ \mathrm{atm}^{-\frac{1}{2}}$. It is also convenient to introduce a parameter $\tau = t/T$ (Fig. 3).

2·3. *Comparison with experimental data.* – The calculated pulse-shape was in very good agreement with the experimental behaviour attained with our chamber. Figures 4 were obtained by photographing the trace of a Tektronix 545 oscilloscope by means of a conventional electronic circuit.

---

(4) G. STETTER: *Zeits. Phys.*, **120**, 644 (1942).

(*) The range values of α-particles in common admixtures of argon and gases as CO_2 or N_2 are assumed here to be equal between them.

During the experiments the chamber was operated in the same conditions for which the calculations were made, that is:

Gas: Mixture of 95% A + 5% CO_2 at atmospheric pressure.

Voltage between the electrodes: 2 000 V.

Source: thin layer of ^{210}Po on nickel.

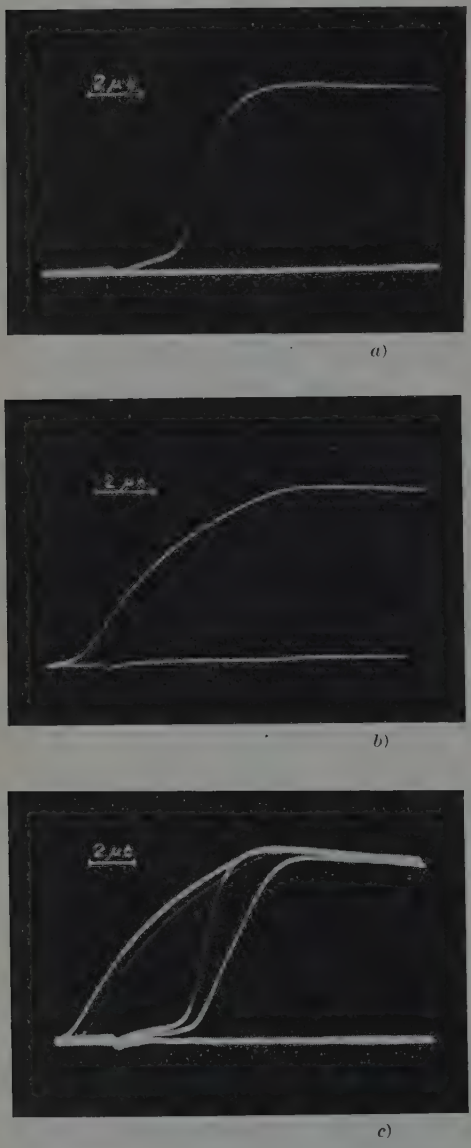

Fig. 4. – Oscilloscope records of pulses obtained by using a gas mixture of 95% A + 5%CO_2.

Comparison between the experimental and the calculated data shows that in the case of a spherical chamber, the pulse-shape is strongly dependent on the angle of emission of the particle.

Fig. 5 shows qualitatively the behaviour of the pulses observed experimentally for $\theta = 90°$ and $\theta = 0°$. In order to fix θ, plastic collimators were employed to delimit a small solid angle around the desired direction.

2·4. *Conclusions.* – The study of α-γ angular correlations is of considerable interest in work on heavy elements nuclear spectra because it provides information on spins and parities of nuclear excited levels. The experimental achievement exhibits, however, some difficulties due chiefly to the very short range of α-particles in matter.

As VALLADAS *et al.* [5] pointed out, such difficulties can be eliminated if the detection and the measurement of the angular distribution of α-particles is done by means of a plane ion chamber. The use of such

[5] G. VALLADAS, J. TEILLAC, P. FALK-VAIRANT and P. BENOIST: *Journ. Phys. Rad.*, **16**, 125 (1955).

an instrument must, however, be limited to those sources which contain only the α emitter under consideration, while with our ion chamber it is also possible—by keeping all the advantages offered by Valladas' technique—to extend the study of the angular correlation to sources containing several α emitters. In fact, in a non planar geometry the α-particles' direction of emission does not appreciably affect the pulse height distribution which depends only on the α energy. Therefore one can select a given transition by amplitude discrimination and study by means of a pulse-shape analysis the angular distribution of the α-particles characterizing the transition itself.

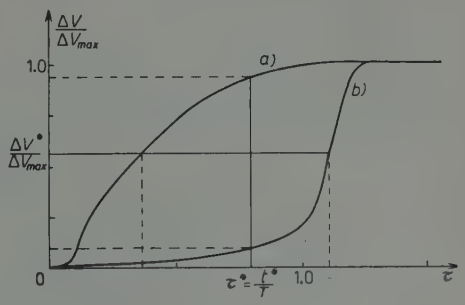

Fig. 5. – Typical behaviour of observed pulse-shapes. *a*) $\theta = 90°$; *b*) $\theta = 0°$.

From the foregoing paragraph it appears possible to analyse the angular distribution of the traces of an α-line in the following two manners (see Fig. 5):

I) By studying the distribution of the amplitudes reached by the pulses at a prefixed time t^*.

II) By studying the distribution of time intervals required by the pulses to rise from $\Delta V = 0$ to a prefixed valued ΔV^*.

In the study of α-γ angular correlations, the « time zero » and the direction of reference can be established by detecting the γ with a scintillator.

RIASSUNTO

Viene descritto un contatore a gas dotato di simmetria sferica capace di lavorare in maniera soddisfacente sia come contatore a flusso sia come camera a ionizzazione. In quest'ultimo caso permette di analizzare spettri α con un buon potere risolutivo anche se si impiegano sorgenti estese. Sono stati fatti dei calcoli per studiare la dipendenza della forma degli impulsi dalla direzione di emissione delle particelle da parte di una sorgente puntiforme (traccia finita). È stato trovato un buon accordo tra questi calcoli e l'esperienza. Si mostra che tale dipendenza può essere utilmente impiegata per lo studio di correlazioni angolari α-γ.

2319

IL NUOVO CIMENTO Vol. XIII, N. 4 16 Agosto 1959

Structure Singularities of Electromagnetic Form Factors (*).

R. Oehme

Enrico Fermi Institute for Nuclear Studies
Department of Physics, the University of Chicago - Chicago, Ill.

(ricevuto il 5 Maggio 1959)

Summary. — In local field theories the form factors of particles can have singularities which are characteristic for the structure of these particles as composite systems. These « structure singularities » are studied with the help of examples from perturbation theory. Their mathematical properties are described for real and complex values of the mass variable, and their physical implications are discussed.

1. – Introduction.

In the present note we shall discuss some gross features of the electromagnetic structure of strongly interacting particles. We assume that these particles are described within the general framework of local relativistic field theory. Their structure is then characterized by form factors which are special cases of the general vertex function.

The analytic properties of the vertex function have been discussed from various points of view. To a certain extent they are consequences of the fundamental notions of field theory, which include Lorentz invariance, microscopic causality and the spectral conditions ([1-4]). It is an important problem to understand the significance of the remaining singularities in terms of phy-

(*) Work supported in part by the U.S. Atomic Energy Commission.

(1) H. Bremermann, R. Oehme and J. G. Taylor: *Phys. Rev.*, **109**, 2178 (1958); R. Oehme and J. G. Taylor: *Phys. Rev.*, **113**, 371 (1959).

(2) R. Oehme: *Phys. Rev.*, **111**, 1430 (1958).

(3) R. Jost: *Helv. Phys. Acta*, **31**, 263 (1958).

(4) G. Källén and A. S. Wightman: *Kgl. Dan. Videnskab. Selskab, Mat.-Fys. Medd.* (in print).

sical concepts. There are two types of singularities which can be interpreted. These are also present in examples taken from perturbation theory [2,5,6]. The first and most familiar of these are the branch lines corresponding to absorptive processes. In the complex plane of the momentum transfer variable, they are always on the real axis and independent of the mass variable of the particle, depending only upon the spectral conditions. The second kind of singularities depends sensitively upon the mass variable and also upon the spectral conditions. It is connected with what one might call the *composite structure* of the particle.

A given particle involved in the strong interactions may in principle be considered as a bound state of two or more particles. Whether or not such a composite picture is sensible depends to a large extent upon the magnitude of the binding energy in comparison with the masses of the particles involved. If the binding is too strong, the constituents lose their individuality, and a composite picture has little content. On the other hand, for a loosely bound system the composite structure may be the dominant feature at low energies.

Properties of particles like those described above are reflected in the position of the structure singularities of their form factors. For tightly bound systems these singularities are in the unphysical sheet of the Riemann surface corresponding to the momentum transfer variable, whereas for loosely bound systems they appear on the positive real axis in the physical sheet and may determine then the slope of the charge and/or magnetic moment distributions of the particle in question.

In the present paper we study the structure singularities on the basis of examples from perturbation theory. The intrinsic difference between absorptive singularities and structure singularities becomes most apparent if the form factors are considered as functions of at least two complex variables. Therefore, we discuss the examples not only for real, but also for complex values of the mass variable. The latter case may also be of interest for the description of unstable particles within the framework of relativistic field theories.

2. – The examples.

Let us consider the function $V(z_1 z_2 z_3, m_1 m_2 m_3)$ which corresponds to the Feynman diagram in Fig. 1 for the case of a scalar theory with scalar couplings. The variables z_1, z_2 and z_3 are the three inner products which can be formed from the two independent vectors k and p, namely, $z_1 = k^2$, $z_2 = p^2$ and

---

(5) Y. NAMBU: *Nuovo Cimento*, **9**, 610 (1958).

(6) R. KARPLUS, C. M. SOMMERFIELD and E. H. WICHMANN: *Phys. Rev.*, **411**, 1187 (1958).

$z_3 = (k-p)^2$. Since we are mainly interested in form factors, we can omit unessential complications and consider the special case $z_1 = z_2 = z$, $m_1 = m_2 = m$. Then we write

$$f(z, z_3) = V(zzz_3, mmm_3)$$

and obtain, disregarding constant factors,

$$(1) \qquad f(z, z_3) = \int_0^1 \int_0^1 \int_0^1 \frac{\mathrm{d}\alpha\, \mathrm{d}\beta\, \mathrm{d}\gamma\, \delta(1-\alpha-\beta-\gamma)}{(\alpha+\beta)m^2 + \gamma m_3^2 - (\alpha+\beta)\gamma z - \alpha\beta z_3} .$$

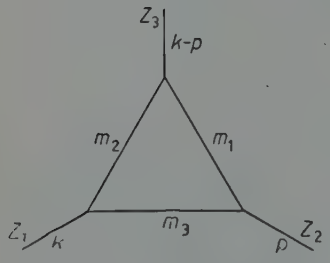

Fig. 1. – A Feynman graph for the vertex function.

Although the integrations in Eq. (1) lead to finite expressions, it is convenient to use instead of $f(z, z_3)$ the function [2,4]

$$(2) \qquad F(z, z_3) = \left(\frac{\partial}{\partial m^2} + \frac{\partial}{\partial m_3^2}\right) f(z, z_3) .$$

This function has a representation corresponding to Eq. (1) but with the denominator taken to the second power. We shall discuss later some of the differences between both functions. In an earlier paper [2] we have obtained an explicit expression for $F(z, z_3)$; it may be written in the form

$$(3) \qquad F(z, z_3) = \frac{1}{m_3^2 z_3 + [z-(m+m_3)^2][z-(m-m_3)^2]} \cdot$$

$$\cdot \left\{ \frac{2(z+m_3^2-m^2)}{\{[z-(m+m_3)^2][z-(m-m_3)^2]\}^{\frac{1}{2}}} \cdot \right.$$

$$\cdot \lg \frac{1}{2mm_3} [m_3^2 + m^2 - z + \{[z-(m+m_3)^2][z-(m-m_3)^2]\}^{\frac{1}{2}}] -$$

$$\left. - \frac{z_3 - 2(z+m^2-m_3^2)}{\{z_3(z_3-4m^2)\}^{\frac{1}{2}}} \lg \frac{1}{2m^2} [2m^2 - z_3 + \{z_3(z_3-4m^2)\}^{\frac{1}{2}}] \right\} .$$

The vertex function $F(z, z_3)$ has two distinct types of singularities. First there are the branch lines $x_3 \geqslant 4m^2$, $y_3 = 0$ and $x \geqslant (m+m_3)^2$, $y = 0$, which we have named « static cuts » in Ref. [2], because their position depends only upon a single variable of the vertex function. The second kind of singularities are « dynamic », they are characterized by the vanishing of the denominator in Eq. (3):

$$(4) \qquad m_3^2 z_3 + [z-(m+m_3)^2][z-(m-m_3)^2] = 0 .$$

Since we are mainly interested in the momentum transfer variable z_3, we may consider the singularity (4) as a pole of the many-valued function $F(z, z_3)$. The position as well as the residuum of this pole are functions of the mass variable z.

Let us consider the relation

$$z_3 = g(z) = -\frac{1}{m_3^2}[z - (m + m_3)^2][z - (m - m_2)^2] \tag{5}$$

as a complex mapping of the z-plane onto two separate sheets of the z_3-plane. Then the line $\mathcal{L}$ in the z-plane

$$\mathcal{L}: \quad x = m^2 + m_3^2, \qquad -\infty < y < +\infty \tag{6}$$

goes into the cut $x_3 \geqslant 4m^2$, $y_3 = 0$. The points $x > m^2 + m_3^2$, $y > 0$ ($y < 0$) are mapped into the *lower* (*upper*) half of the first sheet and the points $x < m^2 + m_3^2$, $y > 0$ ($y < 0$) into the *lower* (*upper*) half of the second sheet. Furthermore we note that for $z_3 = g(z)$ the sum of the two log-terms in Eq. (3) becomes

$$\frac{2\pi i(z + m_3^2 - m^2)}{\{[z - (m + m_3)^2][z - (m - m_3)^2]\}^{\frac{1}{2}}}\, n, \qquad n = 0, \pm 1, \pm 2, \text{ etc.} \tag{7}$$

where n is fixed by the choice of the branches of the logarithms. Now the physical branch of the function $F(z, z_3)$ is determined by Eq. (2) and the representation (1), which shows that $F(z, z_3)$ certainly cannot have a singularity for z and z_3 both real and negative. Hence we must have $n = 0$ for real negative values of z, and this implies $n = 0$ for all $z = x + iy$ with $x < m^2 + m_3^2$. Let us continue our function $F(z, z_3)$ in z from the region $x < m^2 + m_3^2$ into $x > m^2 + m_3^2$. As we cross the line $\mathcal{L}$ the point $z_3 = g(z)$ moves across the cut $x_3 \geqslant 4m^2$, $y_3 = 0$, which is the branch line of the first logarithm in Eq. (3). This logarithm consequently makes a jump and we get $n = 1$ in Eq. (7); the pole (4) moves into the physical sheet of the z_3-plane. As a special case we may take $y = 0$ and vary x from $(m - m_3)^2$ over $m^2 + m_3^2$ to $(m + m_3)^2$. Then the pole $x_3 = g(x)$ moves from $x_3 = 0$ in the *unphysical* sheet up to $x_3 = 4m^2$, where it comes out of the branch point into the *physical* sheet and then moves down the real axis toward $x_3 = 0$.

It is instructive to write down the explicit dispersion formulae for $F(z, z_3)$ as a function of the momentum transfer variable z_3. We have seen that $F(z, z_3)$ is an analytic function in the z_3-plane except for the static cut $x_3 \geqslant 4m^2$, $y_3 = 0$, provided we take z to the left of the line $\mathcal{L}$. The discon-

tinuity across the cut is given by

$$(8)\qquad A(z,\sigma^2)=\lim_{\varepsilon\to 0+}\frac{1}{2\pi i}\{F(z,\sigma^2+i\varepsilon)-F(z,\sigma^2-i\varepsilon)\}=$$

$$=\frac{\theta(\sigma^2-4m^2)}{m_3^2\sigma^2+[z-(m+m_3)^2][z-(m-m_3)^2]}\,\frac{2(z-m_3^2+m^2)-\sigma^2}{\{\sigma^2(\sigma^2-4m^2)\}^{\frac{1}{2}}}\,.$$

The Function $F(z,z_3)$ vanishes like $1/z_3$ for $z_3\to\infty$, and hence it may be represented in the form

$$(9)\qquad F(z,z_3)=\int_{4m^2}^{\infty}\mathrm{d}\sigma^2\,\frac{A(z,\sigma^2)}{\sigma^2-z_3}$$

for $z=x+iy$ with $x<m^2+m_3^2$.

For fixed values of $\sigma\geqslant 2m$ the « absorptive part » $A(z,\sigma^2)$ is an analytic function of z which is regular in the complex z-plane except for the two complex conjugate poles at

$$(10)\qquad z=m^2+m_3^2\pm im_3\{\sigma^2-4m^2\}^{\frac{1}{2}}\,.$$

As σ varies in the range $4m^2\leqslant\sigma<\infty$, the poles (10) move over all of the line $x=m^2+m_3^2$, $-\infty<y<+\infty$. Since the dispersion integral in Eq. (9) involves $A(z,\sigma^2)$ for all $\sigma\geqslant 2m$, we cannot continue the function $F(z,z_3)$ from $x<m^2+m_3^2$ to $x>m^2+m_3^2$ using only the dispersion formula without performing the σ-integration explicitly, Of course, this is what we expect because for $x>m^2+m_3^2$ the function $F(z,z_3)$ has an additional pole in the physical sheet of the z_3-plane at $z_3=g(z)$. We have the representation

$$(11)\qquad F(z,z_3)=\frac{2\pi i(z+m_3^2-m^2)}{\{[z-(m+m_3)^2][z-(m-m_3)^2]\}^{\frac{1}{2}}}\,\frac{1}{m_3^2[z_3-g(z)]}+$$

$$+\int_{4m^2}^{\infty}\mathrm{d}\sigma^2\,\frac{A(z,\sigma^2)}{\sigma^2-z_3}\,,\qquad \text{for } z=x+iy \text{ with } x>m^2+m_3^2,$$

where $A(z,\sigma^2)$ is given in Eq. (8) and $g(z)$ in Eq. (5). The static cut in the z-plane: $x\geqslant(m+m_3)^2$, $y=0$, appears in Eq. (11) only in the residuum of the pole at $z_3=g(z)$.

We would like to add a few remarks about the function $f(z,z_3)$,which has been defined in Eq. (1) and which is the actual vertex-function corresponding to Fig. 1. Clearly, the function $f(z,z_3)$ has singularities at the same points as $F(z,z_3)$, but the character of these singularities may be different. Instead of the pole, we have now a branch point at $z_3=g(z)$, but as a function of z

it behaves in exactly the same way as the corresponding pole of F. Let us take $x < m^2 + m_3^2$ and compute the « absorptive part » of $f(z, z_3)$:

$$a(z, \sigma^2) = \lim_{\varepsilon \to 1} \frac{1}{2\pi i} \{f(z, \sigma^2 + i\varepsilon) - f(z, \sigma^2 - i\varepsilon)\}. \tag{12}$$

Using Eq. (1) we find for $\sigma \geqslant 2m$ an expression of the form

$$a(z, \sigma^2) = \frac{1}{\{\sigma^2(\sigma^2 - 4z)\}^{\frac{1}{2}}} \lg \frac{\sigma^2 - 2(z - m_3^2 + m^2) + \{(\sigma^2 - 4m^2)(\sigma^2 - 4z)\}^{\frac{1}{2}}}{\sigma^2 - 2(z - m_3^2 + m^2) - \{(\sigma^2 - 4m^2)(\sigma^2 - 4z)\}^{\frac{1}{2}}}.$$

One easily checks that differentiation with respect to the masses yields

$$A(z, \sigma^2) = \left(\frac{\partial}{\partial m^2} + \frac{\partial}{\partial m_3^2}\right) a(z, \sigma^2).$$

The function $a(z, \sigma^2)$ has logarithmic branch points at

$$z = m^2 + m_3^2 \pm i m_3 \{\sigma^2 - 4m^2\}^{\frac{1}{2}},$$

which are connected by an appropriately placed cut. It follows from Eqs. (12), and (1) that $a(z, \sigma^2)$ must be real for real z, and this leads to the choice of the principal branch for the logarithm in Eq. (13). If we then continue $a(z, \sigma^2)$ from $x < m^2 + m_3^2$ to the right of the line $\mathcal{L}$, we encounter the branch line

$$\begin{cases} y = \left\{(x - m^2 + m_3^2)\left(\dfrac{\sigma^2}{2} - x + m_3^2 - m^2\right)\right\}^{\frac{1}{2}}, \\ m^2 + m_3^2 \leqslant x \leqslant \dfrac{\sigma^2}{2} + m_3^2 - m^2 \end{cases} \tag{14}$$

which lies on a circle with radius $((\sigma^2/4) + m_3^2 - m^2)$ around the point $z = \sigma^2/4$ and connects the two branch points mentioned above (see Fig. 2). Approaching this cut from both sides along the real axis we find

$$\lim_{\varepsilon \to 0_+} a\left(\frac{\sigma^2}{2} + m_3^2 - m^2 \pm \varepsilon, \sigma^2\right) = \frac{\mp \pi}{\{\sigma^2(\sigma^2 + 4m_3^2 - 4m^2)\}^{\frac{1}{2}}}. \tag{15}$$

Note also that $a(z, \sigma^2)$ vanishes for $\sigma^2 = 4m^2$.

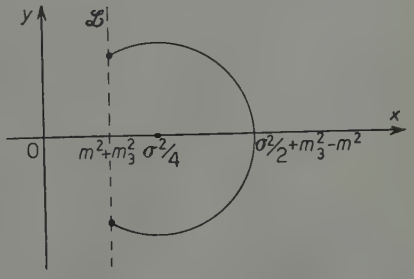

Fig. 2. – Complex z-plane corresponding to the mass variable. The two complex conjugate branch points on the line $\mathcal{L}$ are connected by a circular branch line.

For $x < m^2 + m_3^2$ we have again the usual dispersion formula

$$f(z, z_3) = \int_{4m^2}^{\infty} \mathrm{d}\sigma^2 \frac{a(z, \sigma^2)}{\sigma^2 - z_3}, \tag{16}$$

because the dynamic singularities are in the unphysical sheet of the z_3-plane. But for $x > m^2 + m_3^2$ the branch point $z_3 = g(z)$ and the corresponding branch cut appear in the physical sheet. If we take $z = x$ real and $x > m^2 + m_3^2$, we obtain a dispersion relation which may be written in the form

$$f(x, z_3) = \int_{g(x)}^{2(x - m_3^2 + m^2)} \mathrm{d}\sigma^2 \frac{2\pi}{\{(4x - \sigma^2)\sigma^2\}^{\frac{1}{2}}} \frac{1}{\sigma^2 - z_3} + \int_{4m^2}^{\infty} \mathrm{d}\sigma^2 \frac{a(x, \sigma^2)}{\sigma^2 - z_3}, \tag{17}$$

where $a(x, \sigma^2)$ is the « absorptive part » as we have defined it above, using the principal branch of the logarithm in Eq. (13). In the region $4m^2 \leqslant \sigma^2 \leqslant 2(x - m_3^2 + m^2)$ we could, of course, take the two terms

$$a(x, \sigma^2) + \frac{2\pi i}{\{\sigma^2(\sigma^2 - 4x)\}^{\frac{1}{2}}} = \bar{a}(x, \sigma^2), \tag{18}$$

together, which just amounts to the choice of another branch of the logarithm obtained by continuation through the circular branch line in Fig. 2. One easily shows that Eq. (17) reduces to the formula (11) for $F(x, z_3)$ if the differential operation (2) is applied.

3. – Physical interpretation.

For the discussion of the electromagnetic structure of particles, it is sometimes convenient to go into configuration space. We may introduce a three-dimensional Fourier transform of $f(x, x_3)$ by writing

$$\tilde{f}(x, r) = \frac{1}{(2\pi)^3} \int \mathrm{d}^3 q \exp\left[i \boldsymbol{q} \cdot \boldsymbol{r}\right] f(x, q^2). \tag{19}$$

The spatial distribution $\tilde{f}(x, r)$ allows us to speak about particle structure in an intuitive, non-relativistic way, which is, however, somewhat imprecise.

The physical significance of the *static* branch points is well known; they correspond to the thresholds for the creation of real particles. Let, for instance, $q = k - p$, with $q^2 = \sigma^2 = z_3$, describe the four-momentum of the virtual photon. If $\sigma \geqslant 2m$, then the photon can create a pair of particles with

mass m which interact strongly with the particle under consideration (mass $x^{\frac{1}{2}}$). The longest « range » of the structure connected with these absorptive singularities is determined by the branch point $z_3 = (2m)^2$. This range is independent of the mass $x^{\frac{1}{2}}$ as well as of the detailed interaction of our particle with the m-particles. For $x < m^2 + m_3^2$ we may take the transform (19) of Eq. (16) and write

$$\tilde{f}(x, r) = \frac{1}{2\pi} \int_{4m^2}^{\infty} \mathrm{d}\sigma^2 \, a(x, \sigma^2) \frac{\exp[-\sigma r]}{r} . \tag{20}$$

Note that the picture of a distribution with a « longest range » etc., is of course only reasonable if the weight function $a(x, \sigma^2)$ is positive, at least for small values of σ. The function $a(x, \sigma^2)$ depends upon the details of the strong interaction with the m-particle field.

We consider now the possible physical meaning of the dynamic singularities, which appear on the physical sheet of the z_3-plane if $x > m^2 + m_3^2$. For real masses (stable particles) these singularities are on the real axis and below the onset of the related static cut. Then Eq. (20) must be supplemented by the additional integral

$$+ \int_{g(x)}^{2(x - m_3^2 + m^2)} \mathrm{d}\sigma^2 \, \frac{1}{\{(4x - \sigma^2)\sigma^2\}^{\frac{1}{2}}} \frac{\exp[-\sigma r]}{r} . \tag{21}$$

Let us consider the particle in question as composite, being a bound state of two particles with masses m and m_3 respectively. We write

$$x^{\frac{1}{2}} = m + m_3 - B ,$$

where B is the binding energy. The condition for the appearance of « long range » contributions like the term (21) is then

$$B < m + m_3 - \{m^2 + m_3^2\}^{\frac{1}{2}} . \tag{22}$$

The longest range is given by $r_0(B) = 1/g(x)$, which is the larger the smaller B. In the limiting case where $B \ll m, m_3$ we obtain from Eq. (5)

$$g(x) = \frac{8 m m_3 (m + m_3)}{m_3^2} B + 0(B^2) . \tag{23}$$

The corresponding length $r_0(B)$ is just the range of the probability distribution of the m-particle, which one obtains from the non-relativistic Schrödinger wave function describing the bound system of an m and m_3-particle ([5]).

All these considerations make it plausible that the dynamic singularities appearing for real $z = x > m^2 + m_3^2$ should be interpreted as structure effects due to the composite nature of the particle. Because of the quantum mechanical tunnel effect, the probability distribution of the m-particle with respect to the center of mass of the bound system may be spread out well beyond the range of the binding forces. In our example we compare the range of this structure not necessarily with the range of the forces, but rather with the extent of the usual « m-particle » cloud, which is related to the static cut $x_3 \geqslant 4m^2$, $y_3 = 0$. Clearly the composite structure effects must decrease with increasing binding energy. If B passes the limit given in Eq. (22) and becomes larger than $m + m_3 - \{m^2 + m_3^2\}^{\frac{1}{2}}$, then the explicit long-range contribution (21) to $\tilde{f}(x, r)$ disappears. We have seen in Section 2 that in this case the singularity $z_3 = g(x)$ moves into the unphysical sheet. Here it may still influence the distribution $\tilde{f}(x, r)$ indirectly via the weight function $a(x, \sigma^2)$, especially for small values of σ^2.

So far we have considered the dynamic singularities of form factors occurring in the contribution from a given basic vertex diagram. There may, of course, be other possible intermediate states, and corresponding diagrams, which lead to composite structure effects for a given particle. Sometimes the dynamic singularities associated with such structure effects are superimposed upon the static cuts which are related to clouds of particles with lower mass. In the following we shall consider briefly a few well known examples of physical particles.

The *deuteron* interacts strongly with the pion field ($\mathrm{d} \leftrightarrow \pi + 2\mathrm{n}$), and this interaction gives rise to an electromagnetic structure with a maximal range $r_0 = (2m_\pi)^{-1}$. A graph corresponding to Fig. 1 with $m = m_\pi$ and $m_3 = 2M$ (two nucleon lines: $m_\mathrm{n} = m_\mathrm{p} = M$) would, for instance, lead to a static cut $y_3 = 0$, $x_3 \geqslant 4m_\pi$, which is due to the possibility of an absorptive process. The dynamic singularity of this contribution is in the *un*physical sheet slightly below the threshold $4m_\pi^2$, namely at $z_3 = g(m_\mathrm{d}^2) \sim 4m_\pi^2(1 - m_\pi^2/16M^2)$.

On the other hand the deuteron may be considered as a bound state of a neutron and a proton. Since it is a weakly bound system, the probability distribution of the nucleons is spread out beyond the pion cloud mentioned above. The dynamic singularities connected with this composite structure are found f.i. in the contribution from the diagram given in Fig. 1 with $m = m_3 = M$, which gives $r_0(B) \sim (16MB)^{-\frac{1}{2}} > (2m_\pi)^{-1}$ (7). The same graph

(7) The pion cloud of the nucleon must be folded into this long-range distribution; it changes the distribution, but does not affect the slope. One can easily draw corresponding Feynman diagrams, which then can be reduced, for the purpose of their analytic structure, to simpler graphs similar to that given in Fig. 1. See ref. (5), Y. Nambu: *Nuovo Cimento*, **6**, 1064 (1957) and K. Symanzik: *Prog. Theor. Phys.*, **20**, 690 (1958).

also leads to a static cut $x_3 \geqslant 4M^2$, $y_3 = 0$ due to the creation of a nucleon-antinucleon pair in the intermediate state. The structure associated with this « pair cloud » has maximal range $r_0'' = (2M)^{-1}$.

The deuteron form factor has other dynamic singularities which are in the physical sheet of the z_3-plane. These are, for instance, due to the probability distribution of the proton in a deuteron considered as a bound state consisting of two nucleons and a limited number of pions. Such configurations lead to branch points below $x_3 = 4M^2$, but always above $x_3 = 4m_\pi^2$. There are other intermediate states with total mass $\sigma > 2m$, which give rise to dynamic singularities below their static branch points. We shall not discuss the position of these singularities in detail. We only want to point out that, for restricted values of $x_3 (x_3 \leqslant 2\sqrt{3}M)$, the discontinuity of the deuteron form factor across the real axis is by no means determined solely by the absorptive processes which are possible at the given energy $\sigma = \{x_3\}^{\frac{1}{2}}$. Especially for small energies ($\sigma < 2m_\pi$) the composite structure effects associated with the dynamic singularities are dominant for the description of the deuteron.

Like the deuteron, we may try to describe heavier nuclei within the framework of a relativistic field theory. A discussion of the corresponding electromagnetic form factors will show that the composite structure of these particles leads to specific dynamic singularities on the real x_3-axis. We feel that the existence of such structure singularities indicates that the general framework of causal, relativistic field theories may be rich enough to account for the composite structure of such particles, at least in principle.

One may ask about the importance of dynamic singularities for the form factors of those strongly interacting particles which are usually described by quantized fields. According to the condition (22), explicit composite structure effects will only appear if the particle in question can be considered as a bound state of two (or more) particles such that the binding energy is not too large. One finds that the following particles have no composite structure (*i.e.* the dynamic singularities are in the *un*physical sheet of the z_3-plane): the pion, because it is the lightest particle involved in strong interactions, the K-meson because it is the lightest particle with non-zero strangeness, and the nucleon as a consequence of the conservation of nucleon number. For the π-meson it can be proven rigorously ([2]), using Lorentz invariance, causality and spectrum, that the form factor has only singularities due to absorptive processes. The same is true for the K-meson form factor ([2]), provided one assumes that the relative parity of charged and neutral K-particles is even. In the case of the nucleon, we know that the general notions mentioned above are *not* sufficient to prove the absence of all but the absorptive singularities ([2,3]).

The form factors of all three hyperons have some composite structure singularities; but only in the case of the Σ-particle do they appear slightly below the onset of the static cut connected with the pion cloud. We may consider

the Σ as a bound state of a Λ and a pion. The binding energy of this system is small enough to satisfy the inequality (22), where $m = m_\pi$ and $m_3 = m_\Lambda$ ([5,6]). The maximal range $r_0(B) = \{g(m_\Sigma)\}^{-\frac{1}{2}}$ for the probability distribution of the pion in the bound Λ-π system is of the order $(0.9 \cdot 2m_\pi)^{-1}$. We note that there are other structure singularities around $x_3 = 4m_\pi^2$ which are possible because the Σ may be considered as a bound system of a Λ and two pions. However with more than two pions the binding energy becomes too large, and the corresponding dynamic singularities are in the unphysical sheet. The existence of all these structure singularities below and around $z_3 = 4m_\pi^2$ does not necessarily mean that the composite structure effects due to $\Sigma \leftrightarrow \Lambda + \pi$ are more important for the charge or moment distribution of the Σ than the pion cloud (static cut). Note that the interaction $\Sigma \leftrightarrow \Sigma + \pi$ also contributes to this cloud, but it does not give rise to structure singularities.

The Λ and Σ hyperons, as well as the Ξ, have other structure singularities due to their interaction with K-mesons. If we consider Λ and Σ as bound states of a K-meson and a nucleon and Ξ as a bound (KΛ) or (KΣ) system, we find that in all these cases the binding energies satisfy Eq. (22) with $m = m_K$, $m_3 = M$ and $m_3 = m_\Lambda$, m_Σ respectively. We obtain structure singularities slightly below $x_3 = 4m_K^2$, which is the onset of the static K-meson cut. Of course, these dynamic singularities are superimposed upon the pion cuts and their effect on the distributions should be masked by the pion cloud.

4. – Concluding remarks.

Recently it has been shown that it is possible to define a local field operator for a « composite » particle in terms of the field operators describing the constituents ([8]). Using these operators, one can construct an expression for the S-matrix in exactly the same way as in the case of « elementary » particles only. Here the question arises, how the composite structure of a weakly bound system could manifest itself in this formalism. As we have seen in Sections 2 and 3, such structure effects are implicitly contained in the formalism, even if the composite particle is simply described by a separate field. These effects appear in connection with the spectral conditions and give rise to the dynamic singularities. Of course, we have studied here only the vertex function, but scattering amplitudes and other Green's functions have related properties.

In the present paper we have considered only those singularities of the vertex function which are present in a weak coupling perturbation theory.

([8]) W. Zimmermann: *Nuovo Cimento*, **10**, 597 (1958); R. Haag: *Phys. Rev.*, **112** 669 (1958); K. Nishijima: *Phys. Rev.*, **111**, 995 (1958). These papers contain further references.

It is not impossible that the general form factors have additional singularities ([2-4]). These may be connected with other physical properties of strongly interacting particles which are not contained in a perturbation approach; one might for instance think of excited states or resonances. The important question is whether or not any of these singularities can appear in the physical sheet of the z_3-plane. From Lorentz invariance, causality and spectrum we know that they are certainly restricted to a finite domain around the low energy end of the static cuts ([9]). The implications of the unitarity condition are not known at present.

Finally we would like to make a remark concerning the condition

$$B < m + m_3 - (m^2 + m_3^2)^{\frac{1}{2}}$$

for the appearance of dynamic singularities in the physical sheet of the z_3-plane. This condition may not be an unreasonable criterion if one wants to insist on a distinction between « composite » and « elementary » particles. Mathematically there appears to be a qualitative difference, but it may be of no practical importance.

* * *

The author would like to thank Professor C. Goebel for interesting conversations.

([9]) The exact shape of this region where singularities are allowed is not known at present. It depends upon the mass variable and the special conditions. See ref. ([2,3]) and R. Oehme: *Proceedings of the* 1958 *Annual International Conference on High Energy Physics at CERN*, edited by B. Ferretti (CERN, Geneva 1958).

RIASSUNTO (*)

Nelle teorie di campo locali i fattori di forma delle particelle possono presentare singolarità caratteristiche della struttura di tali particelle come sistemi composti. Si studiano queste « singolarità di struttura » con l'ausilio di esempi presi dalla teoria delle perturbazioni. Si descrivono le loro proprietà matematiche per valori reali e complessi della variabile di massa e se ne discute il significato fisico.

(*) *Traduzione a cura della Redazione.*

IL NUOVO CIMENTO Vol. XIII, N. 4 16 Agosto 1959

Electron-Positron Elastic Scattering from Extended Nuclei.

P. Budini and G. Furlan

Istituto di Fisica dell'Università - Trieste
Istituto Nazionale di Fisica Nucleare - Sottosezione di Trieste

(ricevuto il 9 Maggio 1959)

Summary. — Second order Born approximation of electron-positron elastic potential scattering from extended nuclei is calculated, and a general formula is given for any charge distribution. The dependence of $(\sigma_- - \sigma_+)/\sigma_-$ from particular charge distributions is analysed and discussed.

Introduction.

Precise information about the electric charge distribution of nuclei and nucleons may constitute an important test for the theories of nuclear forces, nuclear constitution and even for some aspects of the theory of elementary particles.

Extensive experimental work on this subject has been initiated by Hofstadter (1) through the elastic scattering of electrons by nuclei. In these experiments the electron is used as a test body to explore the charge distribution of the nucleus.

The electromagnetic nuclear sizes thus found are generally smaller than those provided by methods which depend on nuclear interactions rather than on electron scattering. The interpretation of this and other results of the Hofstadter experiment is not yet clear and still open to discussion, and further analysis of the nuclear charge distribution is certainly desirable.

It is thought that using the positron in place of the electron one could obtain further information about the charge distribution. In fact it is already

(1) R. Hofstadter: *Rev. Mod. Phys.*, **28** (3), 214 (1956).

known on classical grounds that the electron and positron with fixed initial energy and angular momentum describe different orbits when scattered by a positive central source and that these orbits, in the limit of a point source, are two hyperbolae with fixed asymptote having the scattering center as internal and external focus respectively. Thus for fixed conditions at infinity the electron will explore preferably the internal part while the positron the external part of an extended source.

In the present work we will calculate the dependence of $(\sigma_- - \sigma_+)/\sigma_-$ from the scattering angle for given values of the electron-positron energy for different forms of the charge distribution. The nucleus will be thought of as a fixed extended charge with no magnetic moment. The scattering will be a purely potential scattering with no dispersive contribution.

1. – The cross-sections.

The different behaviour of electrons and positrons in scattering by point nuclei has been studied by McKinley-Feshbach [2] and by Dalitz [3] their result is expressed by the differential cross-section:

$$\sigma_\pm = \sigma_R(1-\beta^2)\left\{1-\beta^2\sin^2\frac{\theta}{2} \mp \alpha\beta Z\pi \sin\frac{\theta}{2}\left(1-\sin\frac{\theta}{2}\right)\right\}, \tag{1}$$

where σ_R is the Rutherford cross-section and the other symbols have the conventional meaning. According to this formula (valid for $\alpha Z \leqslant 0.2$) we find $\sigma_- - \sigma_+ \geqslant 0$ for all angles and energies (due to the fact that the positron remains farther than the electron from the scattering center).

Deviations from this formula have been revealed for the first time by Miller and Robinson [4] who have shown experimentally that at high energy if one increases the scattering angle θ, then $\sigma_- - \sigma_+$ becomes negative: they ascribe this effect to the extended charge distribution of the nucleus (at large θ the electron penetrates the charge distribution and is scattered less than the positron which does not).

In our calculations in order to take into account the finite dimensions of the source we will introduce a form factor, representing the charge distribution of the nucleus, in the expression of the S-matrix. We will consider for simplicity a fixed nucleus of charge Ze with no magnetic moment. For the matrix element for elastic scattering of an electron-positron in second Born approxi-

(2) W. A. McKinley and H. Feshbach: *Phys. Rev.*, **74**, 1759 (1948).
(3) R. H. Dalitz: *Proc. Roy. Soc.*, A **206**, 509 (1951).
(4) R. C. Miller and C. S. Robinson: *Ann. Phys.*, **2**, 129 (1957).

mation we obtain, in Dalitz notations:

$$(2)\qquad M=-8\pi^2 iZe^2\left\{\gamma^0\left[\frac{F(|\boldsymbol{p}_2-\boldsymbol{p}_1|)}{\lambda^2+|\boldsymbol{p}_2-\boldsymbol{p}_1|^2}-\frac{Ze^2}{2\pi^2}m\gamma(I+J)\right]-\frac{Ze^2}{2\pi^2}m(I-J)\right\},$$

where $\boldsymbol{p}_1$ and $\boldsymbol{p}_2$ are the electron momenta before and after scattering, F is the Fourier transform of the charge density of the nucleus, λ is a shielding parameter introduced for reasons of convergence to be afterwards put to zero, $\gamma=1/\sqrt{1-\beta^2}$ and

$$(3)\qquad \begin{cases} I=\int \dfrac{F(|\boldsymbol{p}_2-\boldsymbol{q}|)F(|\boldsymbol{q}-\boldsymbol{p}_1|)\,\mathrm{d}^3q}{(\lambda^2+|\boldsymbol{p}_2-\boldsymbol{q}|^2)(\lambda^2+|\boldsymbol{q}-\boldsymbol{p}_1|^2)(\boldsymbol{p}^2-\boldsymbol{q}^2+i\varepsilon)}\,, \\ \left(\dfrac{\boldsymbol{p}_1+\boldsymbol{p}_2}{2}\right)_r J=\int \dfrac{q_r F(|\boldsymbol{p}_2-\boldsymbol{q}|)\,F(|\boldsymbol{q}-\boldsymbol{p}_1|)\,\mathrm{d}^3q}{(\lambda^2+|\boldsymbol{p}_2-\boldsymbol{q}|^2)(\lambda^2+|\boldsymbol{q}-\boldsymbol{p}_1|^2)(\boldsymbol{p}^2-\boldsymbol{q}^2+i\varepsilon)}\,. \end{cases}$$

Summing over the spins and taking the limit for $\lambda\to 0$ we obtain finally the cross-section for elastic scattering:

$$(4)\qquad \sigma_{\mp}=2Z^2e^4\left\{2m^2\gamma^2(1-\beta^2\sin^2\theta/2)\left[\frac{F^2(|\boldsymbol{p}_2-\boldsymbol{p}_1|)}{16p^4\sin^4\theta/2}\mp\frac{Ze^2}{\pi^2}m\gamma\cdot\right.\right.$$
$$\left.\left.\cdot\frac{F(|\boldsymbol{p}_2-\boldsymbol{p}_1|)}{4p^2\sin^2\theta/2}\,\mathrm{Re}\,(I+J)\right]\mp 2\gamma m^3\frac{Ze^2}{\pi^2}\frac{F(|\boldsymbol{p}_2-\boldsymbol{p}_1|)}{4p^2\sin^2\theta/2}\,\mathrm{Re}\,(I-J)\right\}.$$

Obviously the terms depending on Z^3 represent the contribution from the second approximation. The validity of calculations is limited to the case in which these terms are small, compared to those which multiply Z^2. Quantitatively this means

$$(4')\qquad \frac{F(|\boldsymbol{p}_2-\boldsymbol{p}_1|)}{4p^2\sin^2\theta/2}\gg\left|\frac{Ze^2}{\pi^2}\left\{p^2\,\mathrm{Re}\,(I+J)+\frac{m^2}{1-\beta^2\sin^2\theta/2}\,\mathrm{Re}\,(I-J)\right\}\right|,$$

which depends on θ, E, Z and the form of F (*).

(*) It may happen that for large values of θ, that is large momentum trasfer, $F(|\boldsymbol{p}_2-\boldsymbol{p}_1|)$ becomes very small, smaller than the correspondent reduction of the form factors in $(I+J)$ and $(I-J)$. In this case the condition (4') is no more satisfied. This effect is specially important for rapidly convergent form factors (see for example the curve for extended exponential in Fig. 2). For these cases the relative contribution of the second Born approximation at large angles could be relevant even for low Z and certainly larger than $2\pi Z/137$ as expected from a simple inspection of the cross-sections valid for point nuclei.

2. – Yukawa distribution.

For a point source ($F=1$) the integrals in (3) can be evaluated by use of the Feynman identity and complex integration and one obtains the cross-section (1).

For an extended source one has to choose explicitly form factor F in order to calculate the integrals (3).

The simplest expression for F, which will also constitute the basis for the general case, is that corresponding to the Yukawa distribution:

$$\varrho(r) = \frac{a^2}{4\pi}\frac{\exp[-ar]}{r}, \qquad F(q) = \frac{a^2}{a^2+q^2}. \tag{5}$$

Introducing the symbol:

$$I_{\alpha\beta} = \int \frac{\mathrm{d}^3 q}{(\lambda^2+\alpha^2+|\boldsymbol{p}_2-\boldsymbol{q}|^2)(\lambda^2+\beta^2+|\boldsymbol{q}-\boldsymbol{p}_1|^2)(\boldsymbol{p}^2-\boldsymbol{q}^2+i\varepsilon)}, \tag{6}$$

we can write for the Yukawa case

$$I = I_{\alpha\alpha} + I_{00} - 2I_{\alpha 0} \tag{7}$$

and an analogous expression is obtained for J. The integrals in (7) are evaluated in the Appendix.

Finally the cross-section for the Yukawa distribution is of the type (4) where one must substitute

$$\left\{\begin{aligned}
&F(|\boldsymbol{p}_2-\boldsymbol{p}_1|) = \frac{a^2}{a^2+4p^2\sin^2\theta/2}, \\
&\mathrm{Re}\,(I) = -\frac{\pi^2}{p\sin\theta/2\sqrt{a^2(a^2+4p^2)+4p^4\sin^2\theta/2}}\cdot \\
&\qquad\cdot \operatorname{arctg}\frac{ap\sin\theta/2}{\sqrt{a^2(a^2+4p^2)+4p^4\sin^2\theta/2}} + \\
&\qquad + \frac{\pi^2}{p(a^2+4p^2\sin^2\theta/2)}\operatorname{arctg}\left(\frac{a}{2p}\right) = \xi+\eta, \\
&\mathrm{Re}\,(J) = \frac{2p^2+a^2}{2p^2\cos^2\theta/2}\xi+\eta-\frac{\pi^2}{2p^3\sin\theta/2\cos^2\theta/2}\operatorname{arctg}\frac{p\sin\theta/2}{a} + \\
&\quad + \frac{\pi^2}{p^3\sin\theta/2\cos^2\theta/2}\operatorname{arctg}\left(\frac{2p\sin\theta/2}{a}\right) + \frac{\pi^2}{2p^3\cos^2\theta/2}\operatorname{arctg}\left(\frac{a}{2p}\right) - \\
&\qquad - \frac{\pi^3}{4p^3\sin\theta/2\cos^2\theta/2}.
\end{aligned}\right. \tag{8}$$

It can be easily verified that for $a \to \infty$ the cross-section (4) coincides with (1).

The value of Re $(I+J)$ and Re $(I-J)$ for different a/p have been tabulated in Table I.

TABLE I.

Re $(I+J)$

$\sin\theta/2$ \ a/p	2	1	0.55	0.1
0.1	— 61.57594	— 48.59569	— 28.96803	7.80210
0.2	— 23.82441	— 12.57714	— 0.87310	1.09182
0.3	— 11.78915	— 2.97401	2.63152	0.25976
0.4	— 6.24270	0.208621	2.38765	0.08795
0.5	— 3.28408	1.22656	1.71245	0.03721
0.6	— 1.59669	1.41552	1.16831	0.01827
0.7	— 0.60582	1.32488	0.79487	0.00997
0.8	0.12033	1.12717	0.54797	0.00586
0.9	0.55752	0.97184	0.38485	0.00366

Re $(I-J)$

$\sin\theta/2$ \ a/p	2	1	0.55	0.1
0.1	68.10291	62.28423	51.81466	7.01063
0.2	30.05232	24.56844	16.37251	0.65148
0.3	17.68521	12.79123	6.86157	0.14089
0.4	11.72339	7.47944	3.30732	0.04616
0.5	8.30088	4.67562	1.75520	0.01921
0.6	6.13231	3.06777	1.00297	0.00935
0.7	4.66763	2.08368	0.60824	0.00507
0.8	3.52189	1.46703	0.38736	0.00298
0.9	2.66659	1.02873	0.25701	0.00189

As an example $(\sigma_- - \sigma_+)/\sigma_-$ as a function of θ for various values of p and for $Z=12$ $(\langle r^2\rangle^{\frac{1}{2}} = 1.20A^{\frac{1}{3}}F = \sqrt{6}/a)$ is given in Fig. 1.

It is seen that at low energies and scattering angles the cross-section for an extended distribution becomes identical with that for a point source while on increasing the energy and the angle, the quantity $(\sigma_- - \sigma_+)/\sigma_-$ exhibits a change of sign which is due to a deeper penetration of the electron than the positron in the charge distribution. When both penetrate deeply into the charge, the difference of behaviour will obviously diminish and this is repre-

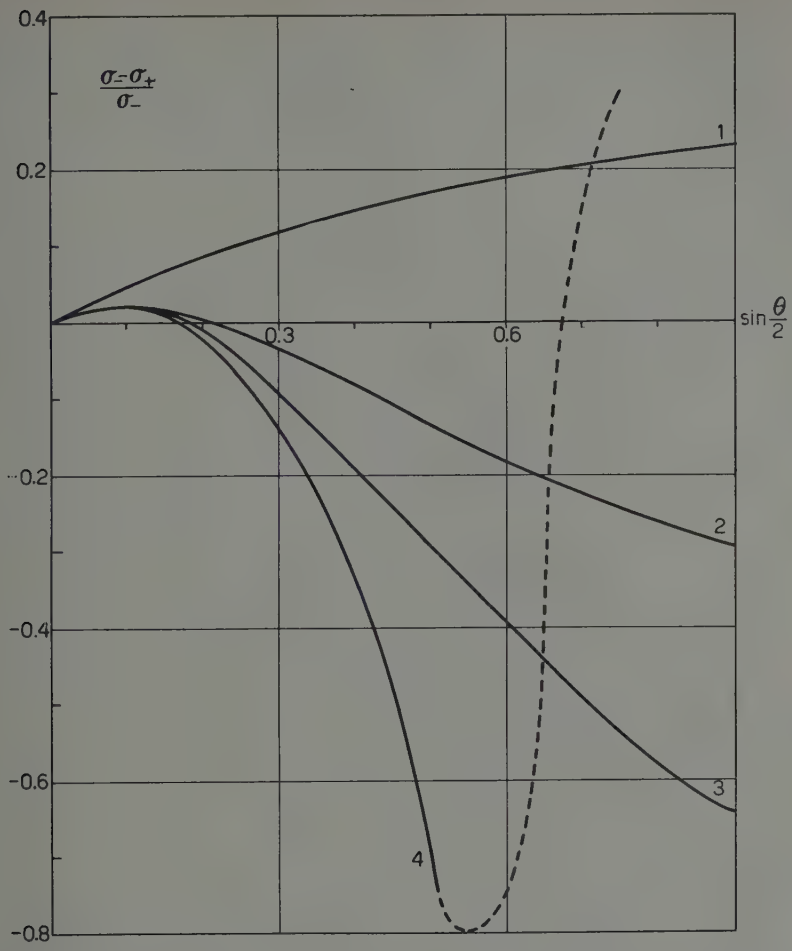

Fig. 1. – $(\sigma_- - \sigma_+)/\sigma_-$ as function of the scattering angle θ for $Z=12$ and a Yukawa charge distribution. Curve 1, 2, 3, 4, 5 correspond to $E=0$ (limiting value) $E=70$ MeV, 140 MeV, 441 MeV, 1.4 GeV.

sented by an increase of $(\sigma_- - \sigma_+)/\sigma_-$ with energy at a given scattering angle (see Fig. 1). It is to be expected that this behaviour depends strongly on the particular charge distribution chosen.

3. – General case.

A discussion on the dependence of $(\sigma_- - \sigma_+)/\sigma_-$ on the particular charge distribution, involves the evaluation of I and J with different form factors. For the general case one can proceed as follows: — let $\varphi(+)$ be the Laplace

transform of the function $r\varrho(r)$

$$r\varrho(r) = \int_0^\infty \varphi(t) \exp[-tr]\,\mathrm{d}t\,, \tag{9}$$

and

$$\varphi(t) = \frac{1}{2\pi i} \int_{c-i\infty}^{c+i\infty} r\varrho(r) \exp[tr]\,\mathrm{d}r\,.$$

From its definition

$$F(q) = \frac{4\pi}{q}\int_0^\infty r\varrho(r) \sin(qr)\,\mathrm{d}r = \frac{4\pi}{q}\int_0^\infty \varphi(t)\,\mathrm{d}t \int_0^\infty \mathrm{d}r \exp[-tr] \sin(qr) =$$

$$= 4\pi \int_0^\infty \frac{\varphi(t)\,\mathrm{d}t}{t^2+q^2} = \int_0^\infty \psi(t) F_y(q)\,\mathrm{d}t\,,$$

where

$$\psi(t) = \frac{4\pi}{t^2}\,\varphi(t)\,.$$

Since $\lim_{q\to 0} F(q) = 1$ it follows

$$\int_0^\infty \psi(t)\,\mathrm{d}t = 1\,.$$

Therefore

$$I = \int \frac{F(|\boldsymbol{p}_2 - \boldsymbol{q}|)F(|\boldsymbol{q} - \boldsymbol{p}_1|)\,\mathrm{d}^3q}{(\lambda^2 + |\boldsymbol{q} - \boldsymbol{p}_1|^2)(\lambda^2 + |\boldsymbol{p}_2 - \boldsymbol{q}|^2)(\boldsymbol{p}^2 - \boldsymbol{q}^2 + i\varepsilon)} = \int_0^\infty\int_0^\infty \mathrm{d}t\,\mathrm{d}t' \psi(t)\psi(t') I_y(t,t')\,. \tag{10}$$

Analogously for J.

The knowledge of I and J, which was previously determined, allows us to write down the desired integral starting from any $\varrho(r)$ and making use of its Laplace transform.

4. – Exponential and extended exponential case.

Let us assume that the charge distribution be

$$\varrho_E(r) = \frac{a^3}{8\pi} \exp[-ar]\,, \qquad F_E(q) = \frac{a^4}{(a^2+q^2)^2}\,. \tag{11}$$

Taking into account that

$$r \exp[-ar] = \int_0^\infty \delta'(t-a) \exp[-tr]\,\mathrm{d}t\,,$$

we have

$$r\varrho_E(r) = \frac{a^3}{8\pi} r \exp[-ar] = \frac{a^3}{8\pi} \int_0^\infty \delta'(t-a) \exp[-tr]\,\mathrm{d}t\,,$$

and

$$\varphi_E(t) = \frac{a^3}{8\pi}\,\delta'(t-a)\,.$$

(12) $$\psi_E(t) = \frac{a^3}{2t^2}\,\delta'(t-a)\,.$$

According to (10)

$$I_E = \frac{a^6}{4} \int_0^\infty\!\!\int \frac{\delta'(t-a)\,\delta'(t'-a)}{t^2 t'^2}\, I_y(t, t')\,\mathrm{d}t\,\mathrm{d}t'\,.$$

Performing the operations, I_E ultimately reads

(13) $$I_E = I_y - a^2 \frac{\partial I_y}{\partial a^2} + a^4 \left| \frac{\partial^2 I_y(t, t')}{\partial t^2\,\partial t'^2} \right|_{\substack{t=a \\ t'=a}},$$

and

(13′) $$J_E = J_y - a^2 \frac{\partial J_y}{\partial a^2} + a^4 \left| \frac{\partial^2 J_y(t, t')}{\partial t^2\,\partial t'^2} \right|_{\substack{t=a \\ t'=a}}.$$

Taking now

$$\varrho_{EE}(r) = \frac{a^3}{32\pi}(1 + ar) \exp[-ar]\,, \qquad F_{EE}(q) = \frac{a^6}{(a^2+q^2)^3}\,,$$

we have

(14) $$\psi_{EE}(t) = \frac{a^3}{8}\left\{\frac{\delta'(t-a)}{t^2} + a\,\frac{\delta''(t-a)}{t^2}\right\}.$$

The integrals read

(15) $$I_{EE} = I_y - a^2 \frac{\partial I_y}{\partial a^2} + \frac{a^4}{2} \frac{\partial^2 I_y}{\partial a^2\,\partial a^2} - \frac{a^6}{2} \left| \frac{\partial^3 I_y(t, t')}{\partial t^2\,\partial t^2\,\partial t'^2} + \right.$$
$$\left. + \frac{\partial^3 I_y(t, t')}{\partial t^2\,\partial t'^2\,\partial t'^2} \right|_{\substack{t=a \\ t'=a}} + \frac{a^8}{4} \left| \frac{\partial^4 I_y(t, t')}{\partial t^2\,\partial t^2\,\partial t'^2\,\partial t'^2} \right|_{\substack{t=a \\ t'=a}}.$$

Analogously for J_{EE}.

The calculation of the mixed derivatives is elementary but lengthy (they have to be calculated for each particular case considered), and it can be shown that they give relevant contribution for large θ only. In Fig. 2 we have compared the behaviour of $(\sigma_- - \sigma_+)/\sigma_-$ for $Z = 12$, $E = 254$ MeV for a point nu-

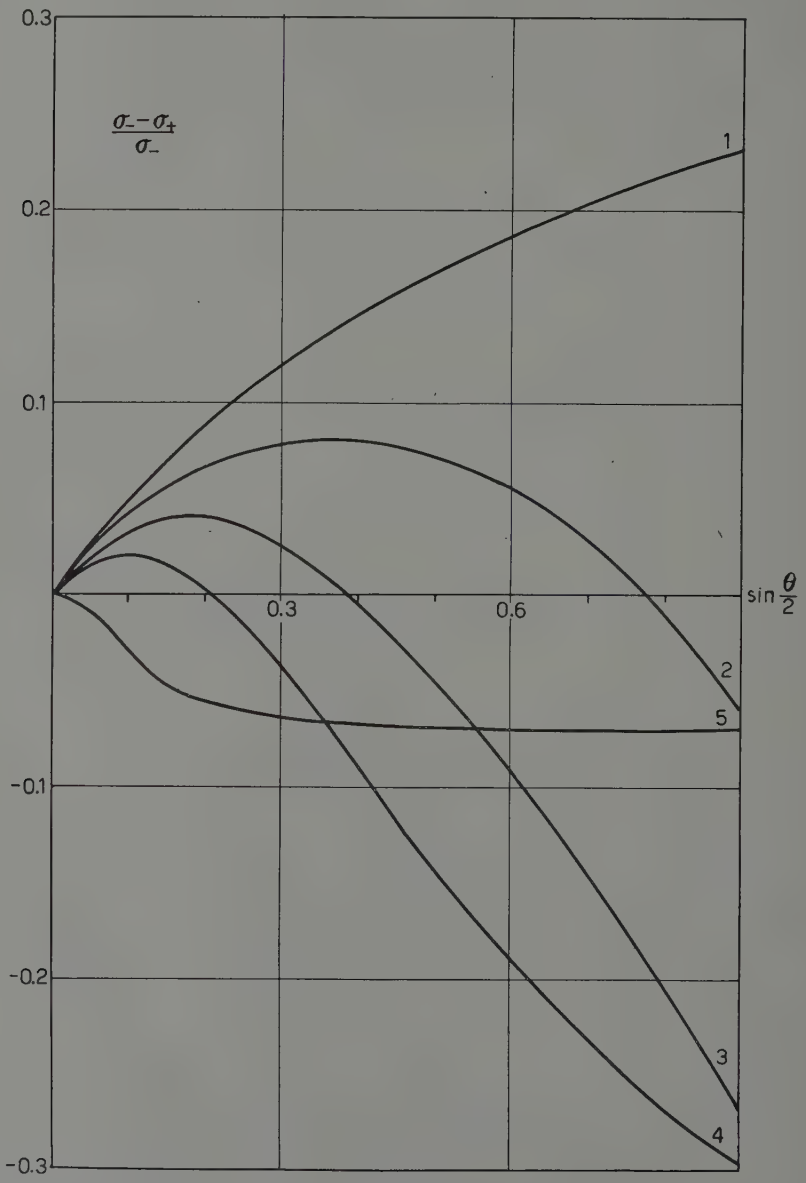

Fig. 2. – $(\sigma_- - \sigma_+)/\sigma_-$ as a function of the scattering angle θ for $z = 12$ and $E = 254$ MeV. Curves 1, 2, 3, 4 correspond to a point nucleus, a Yukawa charge distribution, an exponential charge distribution, an extended exponential charge distribution.

cleus and a Yukawa ($\langle r^2\rangle^{\frac{1}{2}} = \sqrt{6}/a$) exponential ($\langle r^2\rangle^{\frac{1}{2}} = \sqrt{12}/a$), extended exponential ($\langle r^2\rangle^{\frac{1}{2}} = \sqrt{18}/a$) distribution.

The contribution of the mixed derivatives have been taken into account approximately for the exponential distribution and has been neglected for the extended exponential, so the curve for the last case is only indicative (*).

It is seen that the behaviour of $(\sigma_- - \sigma_+)/\sigma_+$ depends strongly on the particular form of the charge distribution and this dependence is sensitive to the value of the electron-positron energy. For example we find that the exponential curve for $E = 359$ MeV presents a minimum value $\simeq -0.4$ at $\sin\theta/2 \sim 0.5$ and becomes again zero at $\sin\theta/2 \sim 0.65$.

5. – Conclusion.

Second order Born approximation of elastic potential scattering of high energy electrons from extended nuclei indicate that $(\sigma_- - \sigma_+)/\sigma_-$ should be rather sensitive to the particular form of the charge distribution. This effect should be present also for heavy ($Z > 12$) nuclei where the Born approximation is no more valid.

If this behaviour might constitute a basis for further more detailed analysis of the nuclear charge distribution, depends on the experimental possibilities.

One point which could be clarified by such methods is the contribution of the dispersive scattering to elastic scattering. In fact being $\sigma_- - \sigma_+$ dependent only on second and higher order contributions it should be particularly sensible to dispersion effects ([5]). It is reasonable to expect that at high energy and angles these contributions become important. If so one should observe incompatibility between charge distributions determined separately from σ_- and from $\sigma_- - \sigma_+$ taking into account Coulomb scattering only.

Comparison of σ_- and σ_+ should also allow analysis of the magnetic moment distribution in the nucleus. This will be discussed in a subsequent work.

(*) For $\sin\theta/2 > 0.55$, $(\sigma_- - \sigma_+)/\sigma_-$ increases rapidly indicating that the effect discussed in the note of p. 792 is present.

([5]) L. I. Schiff: *Phys. Rev.*, **98**, 756 (1955); H. S. Valk and B. J. Malenka: *Phys. Rev.*, **104**, 800 (1956).

Appendix

Evaluation of the integrals.

The integrals needed in (7) are

$$I = \int \frac{F(|\boldsymbol{p}_2 - \boldsymbol{q}|)F(|\boldsymbol{q} - \boldsymbol{p}_1|)\,\mathrm{d}^3q}{(\lambda^2 + |\boldsymbol{p}_2 - \boldsymbol{q}|^2)(\lambda^2 + |\boldsymbol{q} - \boldsymbol{p}_1|^2)(\boldsymbol{p}^2 - \boldsymbol{q}^2 + i\varepsilon)},$$

$$\left(\frac{\boldsymbol{p}_1 + \boldsymbol{p}_2}{2}\right)_r J = \int \frac{q_r F(|\boldsymbol{p}_2 - \boldsymbol{q}|)F(|\boldsymbol{q} - \boldsymbol{p}_1|)\,\mathrm{d}^3q}{(\lambda^2 + |\boldsymbol{p}_2 - \boldsymbol{q}|^2)(\lambda^2 + |\boldsymbol{q} - \boldsymbol{p}_1|^2)(\boldsymbol{p}^2 - \boldsymbol{q}^2 + i\varepsilon)}.$$

Placing

$$F(q) = 1 - \frac{q^2}{q^2 + a^2} = \lim_{\lambda \to 0}\left(1 - \frac{q^2 + \lambda^2}{q^2 + \lambda^2 + a^2}\right),$$

the result is

$$I = I_{00} + I_{aa} - 2I_{a0},$$

$$J = J_{00} + J_{aa} - 2J_{a0},$$

because, as it can be at once seen $I_{a0} = I_{0a}$.

I_{00} has been evaluated in the case of a point charge by Dalitz and I_{aa} itself can be led to that case. By means of Feynmann identity I_{a0} can be transformed in the following way:

$$I_{a0} = \int_{-1}^{1} \frac{\mathrm{d}z}{2} \int \frac{\mathrm{d}^3q}{(\Lambda^2 + |\boldsymbol{q} - \boldsymbol{P}|^2)^2(\boldsymbol{p}^2 - \boldsymbol{q}^2 + i\varepsilon)},$$

where

$$\Lambda^2 = \lambda^2 + \frac{a^2}{2}(1 + z) + p^2 \sin^2(\theta/2)(1 - z^2),$$

$$\boldsymbol{P} = \tfrac{1}{2}\{\boldsymbol{p}_1(1 + z) + \boldsymbol{p}_2(1 - z)\}.$$

The integral in d^3q can be calculated and its value is

$$\frac{\pi^2}{\Lambda(\boldsymbol{p}^2 - \boldsymbol{P}^2 - \Lambda^2 + 2ip\Lambda)}.$$

Proceeding similarly

$$J_{a0} = \frac{\pi^2}{2}\int_{-1}^{1} \frac{\mathrm{d}z}{\Lambda(\boldsymbol{p}^2 - \boldsymbol{P}^2 - \Lambda^2 + 2ip\Lambda)} - \frac{\pi^2 i}{4}\int_{-1}^{1} \frac{\mathrm{d}z}{P^3} \ln\frac{p - P + i\Lambda}{p + P + i\Lambda} -$$

$$- \pi^2 i \int_{-1}^{1} \frac{(p + i\Lambda)\,\mathrm{d}z}{\boldsymbol{P}^2(\boldsymbol{p}^2 - \boldsymbol{P}^2 - \Lambda^2 + 2ip\Lambda)}.$$

With convenient substitutions all these integrals can be rationalized and could be calculated by elementary means in the real field. However the complexity of the functions to be integrated, which makes the evaluation practically impossible, is a good reason to abandon this procedure. We have thus used the following theorem, to be found in BEHNKE and SOMMER (6).

Let there be the real integral

$$\int_a^b R(x)\,\mathrm{d}x\,,$$

where $R(z)$ is olomorphic in the $a \mapsto b$ interval. It follows that

$$\int_a^b R(x)\,\mathrm{d}x = \sum \mathrm{Res}\left[R(z)\ln\frac{z-b}{z-a}\right],$$

where the sum includes the residui of all the poles of the complex plane.

Proceeding in such a way, one obtains, once the limit $\lambda \to 0$ has been taken, the integrals reported in formula (8) (*).

---

(6) BEHNKE - SOMMER: *Theorie der analitischen Funktionen einer komplexen Veränderlichen.* (p. 198).

(*) To these integrals one should sum an expression R which we have omitted for lack of space, since its numerical evaluation for all cases considered gives

$$R/J < 10^{-3}\,.$$

RIASSUNTO

Viene calcolata in seconda approssimazione di Born la sezione d'urto per lo scattering elastico, e di potenziale, di elettroni positivi e negativi da parte di nuclei a dimensione finita; si ottiene un'espressione generale valida per ogni distribuzione di carica. Viene inoltre esaminata e discussa la dipendenza di $(\sigma_- - \sigma_+)/\sigma_-$ da differenti distribuzioni di carica.

IL NUOVO CIMENTO Vol. XIII, N. 4 16 Agosto 1959

Teoria non locale dell'effetto Compton.

A. M. Longoni

Istituto di Fisica dell'Università - Torino

(ricevuto il 9 Maggio 1959)

Riassunto. — Ci si propone di applicare al caso dell'effetto Compton la teoria non locale proposta da G. Wataghin e di studiare il comportamento asintotico della sezione d'urto differenziale secondo tale teoria.

Ci proponiamo di studiare il comportamento asintotico, per elevate energie della sezione d'urto differenziale per l'effetto Compton facendo uso dei fattori di taglio relativistici, nello spazio dei momenti, proposti da G. Wataghin.

È ben noto che il metodo di taglio viene adoperato in molti problemi; ad esempio, nel problema dell'urto elastico elettrone-protone che ha condotto Hofstadter a mostrare che la carica dell'elettrone non è puntiforme, o che l'interazione non è locale; o anche in problemi di « energia propria » delle particelle.

Molti autori utilizzano il taglio soltanto negli stati virtuali intermedi; nel presente studio si mostra l'importanza dell'applicazione del taglio relativistico agli stati corrispondenti ad ogni linea interna ed esterna dei diagrammi di Feynman che rappresentano il processo. Tale applicazione è postulata nella teoria non locale di G. Wataghin [1].

Nel caso della diffusione elastica elettrone-fotone, in cui un elettrone d'impulso p, e un fotone d'impulso k, e polarizzazione e, (ove p, k, e sono dei tetravettori) vengono diffusi in un elettrone d'impulso p' e in un fotone d'impulso k' e polarizzazione e'; qualora ci si limiti a considerare un'approssimazione del

(1) G. Wataghin: *Nuovo Cimento*, **5**, 689 (1957); **9**, 519 (1958); *On the multiple production of mesons and a non local theory of fields* (in corso di pubblicazione).

second'ordine, al processo si associano i due noti diagrammi di Feynman (altri due si ottengono invertendo l'ordine temporale dei vertici):

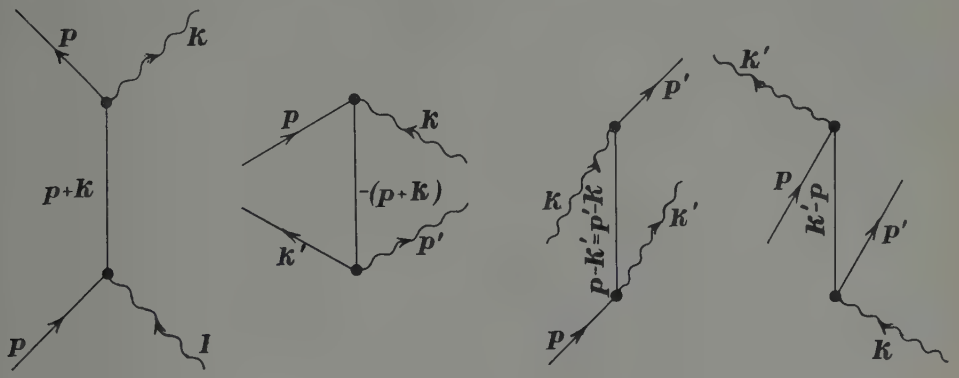

Ia Ib IIa IIb

Precisiamo ora che il calcolo sarà fatto nel sistema CM delle particelle collidenti, poichè tale scelta non soltanto semplifica i calcoli, ma sottolinea la fondamentale importanza della separazione dello spazio e del tempo nel sistema CM che è definito dalle seguenti relazioni:

$$\boldsymbol{p} + \boldsymbol{k} = 0 = \boldsymbol{p}' + \boldsymbol{k}' ,$$

donde

$$|\boldsymbol{p}| = |\boldsymbol{k}| = |\boldsymbol{k}'| = k_0 = k_0' = \omega .$$

In vista del calcolo che seguirà è opportuno richiamare l'espressione della sezione d'urto differenziale nel sistema CM, essa è fornità da (2):

$$(1) \qquad \frac{\mathrm{d}\sigma}{\mathrm{d}\Omega} = \frac{1}{2\varepsilon^2}\left(\frac{e^2}{4\pi}\right)^2 \frac{X_{\mathrm{CM}}}{(1+\beta)^2} = \frac{r_0^2 m_e^2}{2\varepsilon^2(1+\beta)^2} X_{\mathrm{CM}} ,$$

dove ε rappresenta l'energia dell'elettrone incidente e X_{CM} non è altro che la somma sugli spins del modulo a quadrato dell'elemento di matrice della transizione, cioè:

$$(2) \qquad X_{\mathrm{CM}} = \left\{ m^2 \sum_{\text{spins}} \left| \bar{u}(\boldsymbol{p}') \left[\mathrm{e}' \frac{i(p'+k')-m}{(p'+k')^2} \mathrm{e} + \mathrm{e} \frac{i(p-k')-m}{(p-k')^2+m^2} \mathrm{e}' \right] u(\boldsymbol{p}) \right|^2 \right\}_{\mathrm{CM}} ,$$

(dove indicando con a un qualsiasi tetravettore, con a s'intende il prodotto scalare $\gamma_\mu a^\mu$).

---

(2) J. M. Jauch and E. Rohrlich: *The theory of photons and electrons.*

Effettuata la somma sugli spin si ottiene:

$$X_{\text{CM}} = \frac{m^2}{K^2} A_{\text{CM}} + \frac{m^2}{K'^2} B_{\text{CM}} - \frac{m^2}{KK'} (C_{\text{CM}} + D_{\text{CM}}) , \tag{3}$$

dove (essendo θ l'angolo di diffusione):

$$\begin{cases} K = -p\cdot k = -p'\cdot k' = \omega(p_0 + \sqrt{p_0^2 - m^2}); \\ K' = -p'\cdot k = -p\cdot k' = \omega(p_0 + \sqrt{p_0^2 - m^2}\cos\theta) , \\ \\ \dfrac{m^2}{K^2} A_{\text{CM}} = \dfrac{1}{2}\dfrac{K'}{K}; \\ \dfrac{m^2}{K'^2} B_{\text{CM}} = \dfrac{1}{2}\dfrac{K}{K'} - 2\dfrac{(e'p)(ep')(ee')}{K'} - \dfrac{(pe')^2}{K'} + \dfrac{2(ep')^2(pe')^2}{K'^2} , \\ \\ \dfrac{m^2}{KK'} (D_{\text{CM}} + C_{\text{CM}}) = 2\dfrac{(pe')(ep')(ee')}{K'} - 2(ee')^2 + 1 - \dfrac{(pe')^2}{K'} + 2\dfrac{(ep')^2(pe')^2}{K'^2} . \end{cases} \tag{4}$$

Sommando sulle polarizzazioni si ottiene:

$$\sum_{\text{pol.}} X_{\text{CM}} = \overline{X}_{\text{CM}} = \frac{1}{2}\frac{m^2}{K^2}\sum_{\text{pol.}} A_{\text{CM}} + \frac{1}{2}\frac{m^2}{K'^2}\sum_{\text{pol.}} B_{\text{CM}} - \frac{1}{2}\frac{m^2}{KK'}\sum_{\text{pol.}} (C_{\text{CM}} + D_{\text{CM}}) , \tag{5}$$

dove

$$\begin{cases} \dfrac{1}{2} m^2 \sum_{\text{pol.}} A_{\text{CM}} = \dfrac{K'}{K} , \\ \\ \dfrac{1}{2} m^2 \sum_{\text{pol.}} B_{\text{CM}} = \dfrac{2K}{K'} + \dfrac{m^4}{K'^2} - 1 + \dfrac{m^2}{K'} , \\ \\ \dfrac{1}{2}\dfrac{m^2}{KK'} \sum_{\text{pol.}} (C_{\text{CM}} + D_{\text{CM}}) = 1 - \dfrac{K}{K'} . \end{cases} \tag{6}$$

Nella sezione d'urto, data dalla (2), quando non interessano le polarizzazioni, al posto della (3) si sostituisce la (5) ottenendo:

$$\frac{\mathrm{d}\sigma}{\mathrm{d}\Omega} = \frac{r_0^2 m^2}{2\varepsilon^2(1+\beta)^2}\left(\frac{K'}{K} + 3\frac{K}{K'} + \frac{m^4}{K'^2} + 2\frac{m^2}{K'} - 2\right) . \tag{7}$$

Facendo tendere a zero l'angolo di diffusione θ, si verifica immediatamente che (considerando valori di $\varepsilon = p_0 \gg m_e$ e trascurando i termini del tipo m_e/p_0; per cui $\varepsilon = p_0 \simeq k_0 = \omega$):

$$\frac{K}{K'} \to 1 , \qquad (X_{\text{CM}})_{\theta=0} \sim 2 , \qquad \left(\frac{\mathrm{d}\sigma}{\mathrm{d}\Omega}\right)_{\theta=0} \simeq \frac{r_0^2 m_e^2}{\omega^2(1+\beta)^2} . \tag{8}$$

Di qui si vede che la sezione d'urto tende a zero come ω^{-2} per $\omega \to \infty$.

Questi sono i risultati che si ottengono con la teoria locale; supponiamo ora che l'interazione non sia puntiforme e che di conseguenza gli elementi di matrice S nello spazio degli impulsi siano tagliati da opportuni fattori di forma.

Consideriamo la formulazione non locale di G. WATAGHIN (3), il quale dà delle regole per l'introduzione dei fattori di taglio relativistici dipendenti da invarianti spaziali I_s e da invarianti temporali I_t che mettono in evidenza la funzione del sistema baricentrico.

Indicando con $P_\mu = \sum p_\mu^{(i)}$ $(\mu = 0, 1, 2, 3)$ il tetravettore energia-impulso delle particelle incidenti e con $u_\mu = (1/m)P_\mu$ il tetravettore velocità del baricentro delle particelle incidenti (nel sistema baricentrico le componenti u_μ sono (1, 0, 0, 0) e prendendo il prodotto scalare $k_\mu u^\nu$ di un qualsiasi tetravettore k, formiamo i due invarianti I_s e I_t (il tensore metrico è definito come $-g_{00} = g_{11} = g_{22} = g_{33} = 1$) che nel baricentro diventano:

$$(9)' \qquad I_t = -k_\mu u^\mu = k_0\,, \qquad I_s^2(\boldsymbol{k}) = k_\mu k^\mu + I_t^2 = k_1^2 + k_2^2 + k_3^2 = |\boldsymbol{k}|^2\,.$$

Chiamiamo tali quantità « proiezioni » sull'asse del tempo e dello spazio del sistema baricentrico degli impulsi.

Le regole per introdurre i fattori di taglio nell'elemento di matrice della transizione sono: un fattore di taglio spaziale

$$G_s(|\boldsymbol{k}|) = \frac{1}{1 + l^2 I_s^2(\boldsymbol{k})}\,,$$

(dove l è la lunghezza d'onda universale 10^{-14} cm) va introdotta in ogni linea esterna del diagramma; un fattore $G_s^2(|\boldsymbol{k}|)$ in ogni propagatore interno di fermione o di bosone e un fattore di taglio temporale in ogni vertice.

Il fattore di taglio temporale contiene un operatore:

$$g^-[\sum I_t] = \frac{1 - il\sum m}{1 - il\sum I_t}\,,$$

ove $\sum$ è estesa alle particelle assorbite in un vertice, ed un operatore:

$$g^+[\sum I_t] = \frac{1 + il\sum m}{1 + il\sum I_t}\,,$$

in corrispondenza alle particelle emesse nello stesso vertice.

Questi operatori invarianti conservano evidentemente la generale covarianza della teoria, e, come si vedrà in seguito, conservano inoltre l'hermiticità della

(3) G. WATAGHIN: *On the multiple production of mesons and a non local theory of fields* (in corso di pubblicazione).

hamiltoniana e il principio della causalità macroscopica. Nel caso particolare dell'effetto Compton il fattore di taglio relativo al primo diagramma è

$$(10)\quad G_1 = G_s(|\boldsymbol{p}|)G_s(|\boldsymbol{k}|)G_s^2(|\boldsymbol{p}+\boldsymbol{k}|)G_s(|\boldsymbol{p}'|)\,G_s(|\boldsymbol{k}'|)\cdot \\ \cdot g^-[p_0+k_0]g^+[(p+k)_0]g^-[(p+k)_0]g^+[p'_0+k'_0]\,,$$

dove, sempre nell'approssimazione $p_0 \gg m_e$:

$$G_s(|\boldsymbol{p}|) = G_s(|\boldsymbol{k}|) = G_s(|\boldsymbol{k}'|) = G_s(|\boldsymbol{p}'|) = \frac{1}{1+\varrho^2 l^2\omega^2}\,, \qquad G_s(|\boldsymbol{p}+\boldsymbol{k}|) = 1,$$

$$g^\pm[p_0+k_0] = g^\pm[p'_0+k'_0] = \frac{1 \pm ilm_e}{1 \pm il(p_0+k_0)} \simeq \frac{1 \pm ilm_e}{1 \pm 2il\omega}\,, \quad g^\pm[(p+k)_0] = 1\,.$$

Come si vede immediatamente l'inversione dell'ordine temporale dei vertici non altera il contributo dei fattori di taglio nei diagrammi I_a e I_b; esso conduce invece a fattori di taglio differenti nei diagrammi II_a e II_b e precisamente si ha:

$$(11)\quad (\mathrm{II}_a)\quad G_2 = G_s(|\boldsymbol{p}|)G_s(|\boldsymbol{k}|)G_s^2(|\boldsymbol{p}-\boldsymbol{k}'|)\,G_s(|\boldsymbol{p}'|)\,G_s(|\boldsymbol{k}'|)g^-[p_0]\cdot \\ \cdot g^+[(p-k')_0+k'_0]g^-[(p-k')_0+k'_0]g^+[p'_0]\,,$$

$$(12)\quad (\mathrm{II}_b)\quad G_2 = G_s(|\boldsymbol{p}|)G_s(|\boldsymbol{k}|)G_s^2(|\boldsymbol{p}-\boldsymbol{k}|)G_s(|\boldsymbol{p}'|)\,G_s(|\boldsymbol{k}'|)g^-[k_0]\cdot \\ \cdot g^+[(k'-p)_0+p'_0]g^-[(k'-p)_0+p_0]g^+[k'_0]\,.$$

Considerando l'andamento asintotico per ω tendente all'infinito, nell'approssimazione $m_e/\omega \to 0$ e $lm_e \ll 1$ si trova che i fattori di taglio non dipendono dall'inversione temporale dei vertici. In questa approssimazione si ha

$$(13)\quad G_1 \simeq \frac{1}{(1+l^2\omega^2)^4}\cdot\frac{1}{1+4e^2l^2\omega^2}\,,$$

$$(14)\quad G_2 \simeq \frac{1}{(1+l^2\omega^2)^4}\cdot\frac{1}{(1+l^2|\boldsymbol{p}-\boldsymbol{k}'|^2)^2}\cdot\frac{1}{1+l^2\omega^2}\cdot\frac{1}{1+l^2(\sqrt{2\omega^2(1+\cos\theta)}+\omega)^2}\,.$$

Nel calcolare l'elemento di matrice della transizione si deve tener conto che gli stati iniziali sono normalizzati per un flusso incidente (v per cm^{-2} per s), indipendente dai fattori di taglio (v. WATAGHIN, l. c.); pertanto l'introduzione dei fattori di taglio va fatta soltanto negli stati intermedi e in quelli finali. Introducendo dunque nella (2) i fattori G_1 e G_2 normalizzati sul flusso delle particelle incidenti e indicandoli per chiarezza G_{1N} e G_{2N}, la (5) diviene (tenendo

conto che $C_{CM} = D_{CM}$):

$$\overline{X}_{CM} = \frac{m^2}{2K^2} |G_{1N}^2| \sum_{pol.} A_{CM} + \quad (15)$$

$$+ \frac{m^2}{2K'^2} |G_{2N}^2| \sum_{pol.} B_{CM} - \frac{m^2}{2KK'} (\mathrm{Re}\, G_{1N}^* G_{2N}) \sum_{pol.} (C_{CM} + D_{CM}),$$

dove

$$|G_{1N}^2| \simeq \frac{1}{(1 + l^2\omega^2)^4} \cdot \frac{1}{1 + 4l^2\omega^2}, \quad (16)$$

dell'ordine di ω^{-10}

$$|G_{2N}^2| \simeq \frac{1}{(1 + l^2\omega^2)^5} \cdot \frac{1}{[1 + 2l^2\omega^2(1 + \cos\theta)]^4 [1 + l^2(\sqrt{2\omega^2(1 + \cos\theta)} + \omega)^2]}, \quad (17)$$

dell'ordine di ω^{-20} $(\theta \neq \pi)$

$$\mathrm{Re}\, G_{1N} G_{2N} \simeq \quad (18)$$

$$\simeq \frac{\omega^2 [1/\omega^2 + 2l^2 + l^2(1 + \sqrt{2(1 + \cos\theta) + m_e^2/\omega^2})]}{(1 + l^2\omega^2)^5 (1 + 4l^2\omega^2)[1 + 2l^2\omega^2(1 + \cos\theta)]^2 [1 + l^2(\sqrt{2\omega^2(1 + \cos\theta)} + m_e^2 + \omega)]^2},$$

dell'ordine di ω^{-16} $(\theta \neq \pi)$.

L'andamento asintotico della sezione d'urto (1), nel caso non locale, può essere dedotto dall'esame delle formule (15)–(18); escludendo il valore $\theta = \pi$, il secondo processo, che comporta un fattore di taglio dell'ordine di ω^{-20}, diventa trascurabile rispetto al primo che comporta un fattore di taglio dell'ordine di ω^{-10}.

Pertanto nella (15) si deve tener conto soltanto del primo termine e la sezione d'urto (1) diviene

$$\left(\frac{d\sigma}{d\Omega}\right)_{\theta \neq \pi} \simeq \frac{m_e r_0^2}{2\omega^2(1 + \beta)^2} \cdot \frac{1}{(1 + l^2\omega^2)^4 (1 + 4l^2\omega^2)}. \quad (19)$$

Dalla (19) si vede che $d\sigma/d\Omega$ per ω tendente all'infinito tende a zero come ω^{-12}.

Una menzione particolare merita il caso in cui $\theta = \pi$: per questo particolare valore di θ si deve eseguire un'integrazione sull'angolo solido intorno al valore di $\theta = \pi$. In un intorno tale che $|\pi - \theta| \leqslant 1/\omega$ la sezione d'urto differenziale varia ancora come ω^{-12}, poichè il contributo alla sezione d'urto del secondo processo, per direzioni comprese entro l'angolo solido suddetto, risulta asintoticamente dell'ordine di ω^{-14} ed è quindi ancora trascurabile rispetto al primo.

Si conclude che mentre la sezione d'urto locale tende a zero per l'energia baricentrica tendente all'infinito come ω^{-2}, la sezione d'urto non locale varia

asintoticamente come ω^{-12} e a questa contribuisce essenzialmente il primo diagramma dell'effetto Compton.

* * *

Ringrazio sentitamente il prof. G. WATAGHIN per avere suggerito il problema, che è stato parte della tesi di laurea, e per il suo continuo interessamento.

SUMMARY

Our aim is to apply in the case of the Compton effect the non local theory proposed by G. Wataghin and to study the asymptotic behaviour of the differential cross-section by means of this theory,

IL NUOVO CIMENTO Vol. XIII, N. 4 16 Agosto 1959

Spin-Orbit Potential in Pseudoscalar Theory (*).

E. Butkov

Department of Mathematics, McGill University - Montréal

(ricevuto l'11 Maggio 1959)

Summary. — The Levy-Klein method is used to calculate, for pseudoscalar coupling, the spin-orbit potential between two nucleons. The results, carried to two lowest orders in the ratio of meson to nucleon mass, indicate an attractive force for the isotopic spin triplet state and a smaller repulsive force for the singlet state. Quantitative agreement with phenomenological potentials depends, however, on the pair-suppression effects which are still uncertain.

1. – Introduction.

Following recent successes in explaining the nucleon scattering and polarization data with the aid of a velocity-dependent potential ([1-3]), the derivation of such a potential from meson theory has become a subject of increasing interest. Several authors (*e.g.* ([4])) have approached this problem using PS-PV meson theory or its modifications. We propose here a calculation based on the PS-PS theory directly, following the lines developed by Lévy ([5]) and Klein ([6]). The results obtained in this way are expected to depend upon the mechanism of « pair-suppression » and we shall briefly discuss the difficulties caused by this effect, in particular with regard to the relationship with the PS-PV theory.

(*) Part of this work was done while the author was holding a National Research Council of Canada scholarship.

([1]) J. L. Gammel and R. M. Thaler: *Phys. Rev.*, **107**, 291 (1957).
([2]) P. S. Signell and R. E. Marshak: *Phys. Rev.*, **106**. 832 (1957); **109**. 1229 (1958).
([3]) P. S. Signell, R. Zinn and R. E. Marshak: *Phys. Rev. Lett.*. **1**. 416 (1958).
([4]) S. Okubo and R. E. Marshak: *Ann. Phys.*, **4**, 166 (1958).
([5]) M. Lévy: *Phys. Rev.*, **88**, 72, 725 (1952).
([6]) A. Klein: *Phys. Rev.*, **90**, 1101 (1953).

2. – Method and results.

From invariance-considerations it is possible to deduce (4) that only a limited number of types of velocity-dependent potentials can actually occur. We shall confine ourselves to the first power of relative momentum of two nucleons $\boldsymbol{p}$ in which case the potential must be of the spin-orbit type

$$V = V(r) \cdot (\boldsymbol{S} \cdot \boldsymbol{L}) ,$$

where $\boldsymbol{L} = [\boldsymbol{r} \times \boldsymbol{p}]$ and $\boldsymbol{S} = \frac{1}{2}(\boldsymbol{\sigma}_1 + \boldsymbol{\sigma}_2)$.

According to our method of approach the 2-nucleon potential should be expressible as a series in powers of the coupling constant g:

$$V = g^2 V_2 + g^4 V_4 + \ldots .$$

The second-order term V_2 contains a static part and certain velocity-dependent corrections the treatment of which is somewhat ambiguous. According to LÉVY (5) and KLEIN (6) these corrections are equivalent to a contribution to the fourth order static potential. This equivalence is obtained by iterating the Schrödinger equation under the assumption that the velocity-dependent corrections are small compared with the static part. In the treatment of the deuteron-problem where the over-all effect of the potentials upon a wave-function with a rather wide spatial spread is important, this assumption may be very reasonable. This was estimated by BRUECKNER and WATSON (7). These authors pointed out, however, that this argument might not have general validity in the problem of calculating the potential, especially at small distances which is, in fact, the domain of velocity-dependent forces.

In the case of V_2, the velocity-dependent part happens to be not of the spin-orbit type (it is quadratic in $\boldsymbol{p}$) and we need not worry about the difficulty mentioned. We shall have to face the same problem, however, when considering the velocity dependent correction to the fourth-order potential.

Following the work of KLEIN (7) we calculate the fourth order potential from the expression

$$V_4(r) = \frac{g^4}{(2\pi)^6} \int \exp\left[i(\boldsymbol{k}_1 + \boldsymbol{k}_2 \cdot \boldsymbol{r})\right] \cdot \cdot \langle \boldsymbol{p}, -\boldsymbol{p} \,|\, O_4(\boldsymbol{p}, \boldsymbol{k}_1, \boldsymbol{k}_2) \,|\, \boldsymbol{p} - \boldsymbol{k}_1 - \boldsymbol{k}_2, -\boldsymbol{p} + \boldsymbol{k}_1 + \boldsymbol{k}_2 \rangle \, \mathrm{d}\boldsymbol{k}_1 \mathrm{d}\boldsymbol{k}_2 ,$$

(7) K. A. BRUECKNER and K. M. WATSON: *Phys. Rev.*, **92**, 1023 (1953).

involving matrix elements of the operator $O_4(\boldsymbol{p}, \boldsymbol{k}_1, \boldsymbol{k}_2)$ between the initial and final 2-nucleon states. There are 44 contributions to O_4, each of them corresponding to one « irreducible » time-ordered fourth order diagram. The diagrams can be divided into several types, as indicated on Fig. 1.

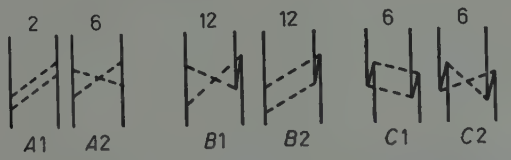

Fig. 1. – Diagrams contributing to the 4-th order potential in PS-PS theory. Number of diagrams of a given type is given at the top of the figure.

A typical contribution to O_4 has the form

$$(-1)^N \frac{[\Gamma_i \Lambda_{\pm}(\boldsymbol{q}) \Gamma_j]^{(1)} [\Gamma_l \Lambda_{\pm}(\boldsymbol{q}') \Gamma_m]^{(2)}}{4\omega_1\omega_2(W-E_1)(W-E_2)(W-E_3)},$$

with the notation closely following that of (7). The structure of O_4 consists, therefore, of operators associated with individual nucleons and of « energy-denominators ».

Evaluating the spin matrix element of O_4 for a nucleon we obtain

$$\frac{1}{2E_s}\left[\frac{(E_p+M)(E_q+M)}{4E_pE_q}\right]^{\frac{1}{2}} \cdot \left\{(E_s \mp M) + (E_s \pm M)\frac{(\boldsymbol{\sigma}\cdot\boldsymbol{p})(\boldsymbol{\sigma}\cdot\boldsymbol{q})}{(E_p+M)(E_q+M)} \mp \frac{(\boldsymbol{\sigma}\cdot\boldsymbol{s})(\boldsymbol{\sigma}\cdot\boldsymbol{q})}{E_q+M} \mp \frac{(\boldsymbol{\sigma}\cdot\boldsymbol{p})(\boldsymbol{\sigma}\cdot\boldsymbol{s})}{E_p+M}\right\},$$

where $\boldsymbol{q}$, $\boldsymbol{s}$ and $\boldsymbol{p}$ are initial, intermediate and final state momenta; upper signs correspond to positive-energy intermediate states and lower signs to negative-energy ones. Isotopic spin matrix elements result in a factor $(3-2\boldsymbol{\tau}_1\cdot\boldsymbol{\tau}_2)$ for $(A1)$, $(B1)$ and a factor $(3+2\boldsymbol{\tau}_1\cdot\boldsymbol{\tau}_2)$ for the remaining ones.

It is now easy to see how the spin-orbit potential arises. Spin matrix elements yield terms with the factor $\boldsymbol{S}\cdot[\boldsymbol{k}_1+\boldsymbol{k}_2\times\boldsymbol{p}]$ and $\boldsymbol{S}\cdot[\boldsymbol{k}_1\times\boldsymbol{k}_2]$. The former factor, when integrated with a function of meson momenta $\boldsymbol{k}_1$ and $\boldsymbol{k}_2$ yields directly a spin-orbit type of potential. The latter factor yields a spin-orbit term when integrated with $(\boldsymbol{p}\cdot\boldsymbol{k}_1)$ or $(\boldsymbol{p}\cdot\boldsymbol{k}_2)$ and a function of $\boldsymbol{k}_1$ and $\boldsymbol{k}_2$. The factors $(\boldsymbol{p}\cdot\boldsymbol{k}_1)$ or $(\boldsymbol{p}\cdot\boldsymbol{k}_2)$ are supplied by expansions in powers of $1/M$ of either the remainder of spin-matrix-elements or the energy-denominators.

We obtain three contributions to the spin-orbit potential from the $\boldsymbol{S}\cdot[\boldsymbol{k}_1+\boldsymbol{k}_2\times\boldsymbol{p}]$ factor. From two-pair diagrams we obtain, from the leading

energy-denominator term (integrals giving rise to our potential are listed in the Appendix):

$$V_4^{(1)} = 6A \frac{1}{x^4} [3H_1(2x) + 2xH_0(2x)], \qquad x = \mu r,$$

where $A = (2\mu/M)^4 (g^2/4\pi)^2 \mu (\boldsymbol{S}\cdot\boldsymbol{L})$ and H_0 and H_1 are «Hankel functions of imaginary argument) as tabulated in [8]. This term was first evaluated by KLEIN.

In our calculation we confine ourselves to fourth order in coupling constant and two lowest orders (fourth and fifth) in powers of $\mu/2M$. In this approximation two-pair diagrams yield another term arising from the velocity-independent correction to the energy-denominators:

$$V_4^{(2)} = 12B \frac{1}{x^6} \Big[x^4 H_0^2(x) + x^4 H_1^2(x) + 3x^2 H_0(x) H_1(x) + 2x^2 H_0^2(x) + 4 \int_x^\infty H_0^2(t) t \, dt \Big]. \qquad B = (\mu/2M) A$$

Next, we get a contribution from one pair diagrams

$$V_4^{(3)} = -24B \frac{1}{x^6} [2(1+x)^2 + x^2] \exp[-2x].$$

We turn now to factors of the type $\boldsymbol{S}\cdot[\boldsymbol{k}_1 \times \boldsymbol{k}_2]$. Combined with velocity dependent corrections to spin matrix elements they yield two terms, both from one pair diagrams:

$$V_4^{(4)} = -24B \frac{1}{x^6} (1+x)^2 \exp[-2x],$$

$$V_4^{(5)} = -8(\boldsymbol{\tau}_1\cdot\boldsymbol{\tau}_2) B \frac{1}{x^6} (1+x)^2 \exp[-2x].$$

Finally, factor $\boldsymbol{S}[\boldsymbol{k}_1 \times \boldsymbol{k}_2]$ can be combined with velocity-dependent corrections to energy-denominators to yield three more terms, two of them from one-pair diagrams

$$V_4^{(6)} = -12A \frac{1}{x^4} [3H_1(2x) + 2xH_0(2x)],$$

$$V_4^{(7)} \approx -6B \frac{1}{x^4} [3x^2 H_0^2(x) + 5x^2 H_1^2(x) + 15xH_0(x)H_1(x) + 14H_1^2(x)] \ (^*),$$

---

[8] E. JAHNKE and F. EMDE: *Tables of Functions* (New York, 1945).

(*) $V_4^{(7)}$ is evaluated approximately. We estimate the error to be $(2 \div 3)\%$ of the overall potential, well within the general accuracy of the method.

and one from no-pair diagrams

$$V_4^{(8)} = 2(3 - 2\boldsymbol{\tau}_1 \cdot \boldsymbol{\tau}_2) B \frac{1}{x^4} [2H_1(x) + xH_0(x)]^2 .$$

We shall now turn to the discussion of the results. First of all there arises the question, mentioned before, of possible « equivalence » of certain velocity-dependent terms and the static terms of higher order. This can possibly affect only the terms $V_4^{(2)}$, $V_4^{(6)}$, $V_4^{(7)}$, and $V_4^{(8)}$. We propose now the view that the « equivalence » should not be invoked in this case. Its validity can be questioned on the grounds mentioned earlier. Secondly, any perturbation-type treatment is carried up to a certain order in the expansion parameter and since the majority of static potentials proposed in the literature are confined to second and fourth order in coupling constant it seems inconsistent to us to propose a velocity-dependent correction modified with reference to higher order static potentials. Finally, within the framework of the adopted formalism, it is not possible to deduce, in a unique fashion, which of the velocity-dependent corrections to the energy-denominators ($V_4^{(6)}$, $V_4^{(7)}$, $V_4^{(8)}$) should be discarded.

The term $V_4^{(8)}$, the only no-pair contribution, deserves, perhaps, a special remark. According to several Japanese authors ([9]) this term should not appear in the potential. The reason is that they use a somewhat different formalism according to which the four « reducible » diagrams (Fig. 2) have to be taken into account, in contrast with Klein's prescription where they are discarded. The contribution from these diagrams exactly cancels $V_4^{(8)}$. We shall not attempt here to discuss the respective merits of these two ways of approach but only mention this fact for the sake of completeness (*).

Fig. 2. – Typical reducible diagrams.

Next and perhaps the most important point to be considered is that of pair-suppression. It is considered to be well-established that the static potentials arising from diagrams with nucleon-antinucleon pairs in the intermediate states should be partly suppressed, presumably to simulate higher-order effects necessarily ignored in the perturbation-type treatments ([11,12]). To estimate the suppression factor one usually performs the Dyson-Foldy transformation ([13])

(*) A recent survey on this topic can be found in reference ([10]).

([9]) S. Okubo: private communication; M. Taketani, S. Machida and S. Onuma: *Progr. Theor. Phys.*, **7**, 45 (1952); S. Okubo: *Progr. Theor. Phys.*, **12**, 603 (1954).

([10]) A. Klein: *Progr. Theor. Phys.*, **20**, 257 (1958).

([11]) K. A. Brueckner, M. Gell-Mann and M. Goldberger: *Phys. Rev.*, **90**, 476 (1953); K. A. Brueckner: *Phys. Rev.*, **91**, 761 (1953).

([12]) A. Klein: *Phys. Rev.*, **95**, 1061 (1954).

([13]) S. D. Drell and E. M. Henley: *Phys. Rev.*, **88**, 1053 (1952).

and uses the equivalence between the diagrams (B) and (C) from Fig. 1 and the diagrams (D) and (E), respectively, from Fig. 3, which are pertinent to the transformed theory. Contributions from the diagrams (D) and (E) should be suppressed according to the meson-pair theory [14] and the numerical factor involved may be estimated, assuming a suitable cut-off.

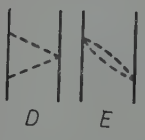

Fig. 3. – Types of diagrams peculiar to the « transformed theory ».

We cannot adopt this approach for two reasons. First of all, meson-pair theory is *a priori* static (in its soluble form) while we are dealing with velocity-dependent forces. Secondly, the correspondence between the nucleon-pair diagrams (B) and (C) in PS-PS theory and meson-pair diagrams (D) and (E) in « transformed theory » breaks down for the spin-orbit potential. We have established this explicitly by performing the calculations in « transformed theory ». For instance, the term arising in the transformed theory from the diagrams of (E) type on Fig. 3 *is not* equal to $V_4^{(1)}$ but to $-V_4^{(1)}$; the combined contribution of (D) and (E) gives, however, a fourth order spin-orbit potential identical to that of PS-PS theory.

Similarly, transformed theory yields contributions from no-pair diagrams which apparently arise in PS-PS theory from one-pair diagrams. It is the γ_5-operator in the transformation that exchanges positive and negative energy states and leads to the usual identification of graphs between the PS-PS and transformed theories. To higher order in $\boldsymbol{p}$ however, the γ_5-operator does not necessarily effect this exchange leading to the more complicated identification for the spin-orbit case.

In view of these considerations it seems most consistent to us to rely upon the PS-PS theory directly in order to estimate pair-suppression effects. According to KLEIN [12] one should replace the coupling constant $g^2/4\pi$ (usually taken as 15) by the value $g_s^2/4\pi$, as defined by DESER, THIRRING and GOLDBERGER [15], which can be obtained from low energy pion-nucleon scattering experiments. According to most recent experimental data this would be equivalent to a suppression factor of about 0.01 per nucleon-pair. Adoption of this value will essentially wipe out the whole spin-orbit potential except for the $V_4^{(8)}$ term which is positive, *i.e.* repulsive, contrary to the experimental data. It should be emphasized, however, that this method of handling the pair-terms is correct only to lowest order in $\mu/2M$ and for the static potential and need not be applicable in our case.

Lacking a clear-cut prescription for treating the pair-suppression effects we

---

[14] G. WENTZEL: *Helv. Phys. Acta*, **15**, 111 (1942); **25**, 569 (1952).
[15] S. DESER, W. E. THIRRING and M. L. GOLDBERGER: *Phys. Rev.*, **94**, 711 (1954).

shall represent our results in the form

$$V_{(S\cdot L)} = \lambda_2 \sum_{i=1}^{2} V_4^{(i)} + \lambda_1 \sum_{i=3}^{7} V_4^{(i)} + V_4^{(8)} ,$$

where λ_1 and λ_2 are the (undetermined) suppression factors for one-pair and two-pair diagrams, respectively. If we compare $V_{(S\cdot L)}$ with the triplet spin-orbit potential required on phenomenological grounds, *e.g.* that of SIGNELL, ZINN and MARSHAK (3) we find that the value $\lambda_1 \approx 0.20 \div 0.25$ will be required, provided that λ_2 is smaller by a factor of 2 or more.

At the same time we obtain a much smaller repulsive potential in the singlet-state which is again consistent with the present evidence (3). We might mention that the suppression factors of this magnitude, namely

$$\lambda_1 = (1 + 3g^2/16\pi^2)^{-1} \approx 0.22$$

and

$$\lambda_2 = (1 + 3g^2/8\pi^2)^{-1} \approx 0.12$$

have been proposed by BRUECKNER (11) on the basis of considerations involving the nucleon propagator suppression and disregarding all other effects.

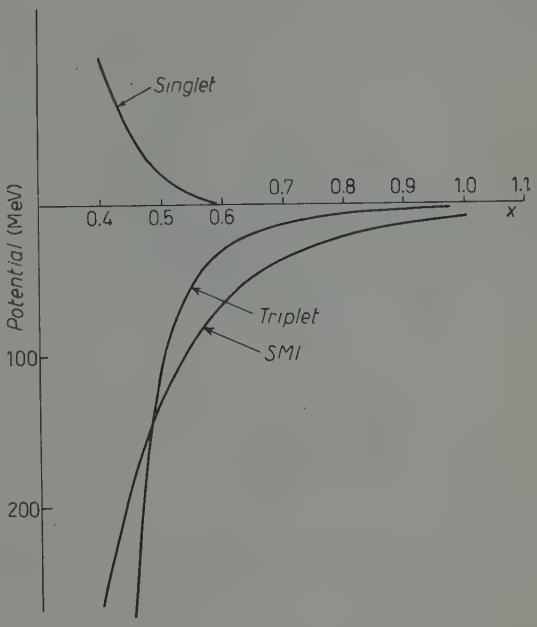

Fig. 4. – Spin-orbit potential $V_{(S\cdot L)}$ with pair-suppression factors 0.22, 0.12 for singlet and triplet states compared with the potential *SM*1 of reference (3).

We have adopted Brueckner's values of λ_1 and λ_2 in Fig. 4 merely for illustrative purposes, without any prejudice as to their theoretical justification.

3. – Conclusion.

In conclusion we must stress the fact that the method of expansions in powers of $1/M$ employed in the evaluation of integrals becomes inapplicable for high momenta of exchanged mesons and these are increasingly important

at small distances. Due to this and other uncertainties our results should be considered mainly qualitative. Nevertheless we believe that our calculations indicate that the spin-orbit potential arising from two-pair diagrams is relatively unimportant (barring the extremely unlikely case that this contribution is suppressed less than that from one-pair diagrams). One pair diagrams yield a much larger contribution which is purely attractive. Due to our lack of knowledge about the precise meaning of pair-suppression mechanism the actual quantitative one-pair contribution must remain uncertain. Since the repulsive no-pair term is numerically much smaller, it will play a significant role only provided the pair suppression is very severe and provided that the no-pair term itself is retained in full strength, which is, however, a somewhat controversial point.

* * *

The author is indebted to Professor E. Lomon for suggesting this investigation and for many discussions. He would also like to thank the members of Applied Mathematics Group at MacGill and Dr. S. Okubo of the University of Rochester for helpful remarks.

Appendix

Integrals giving rise to the spin-orbit terms $V_4^{(1)}$ to $V_4^{(8)}$

$$V_4^{(1)} = -\frac{6ig^4}{(2M)^4(2\pi)^6}\int \frac{\exp[i(\boldsymbol{k}_1+\boldsymbol{k}_2\cdot\boldsymbol{r})]}{\omega_1\omega_2(\omega_1+\omega_2)}\,\boldsymbol{S}\cdot[\boldsymbol{k}_1+\boldsymbol{k}_2\cdot\times\boldsymbol{p}]\,\mathrm{d}\boldsymbol{k}_1\mathrm{d}\boldsymbol{k}_2\,,$$

$$V_4^{(2)} = \frac{6ig^4}{(2M)^5(2\pi)^6}\int \frac{\exp[i(\boldsymbol{k}_1+\boldsymbol{k}_2\cdot\boldsymbol{r})]}{\omega_1\omega_2(\omega_1+\omega_2)^2}\,(\boldsymbol{k}_1+\boldsymbol{k}_2)^2\,\boldsymbol{S}\cdot[\boldsymbol{k}_1+\boldsymbol{k}_2\times\boldsymbol{p}]\,\mathrm{d}\boldsymbol{k}_1\mathrm{d}\boldsymbol{k}_2\,,$$

$$V_4^{(3)} = -\frac{12ig^4}{(2M)^5(2\pi)^6}\int \frac{\exp[i(\boldsymbol{k}_1+\boldsymbol{k}_2\cdot\boldsymbol{r})]}{\omega_1^2\omega_2^2}\,(\boldsymbol{k}_1\cdot\boldsymbol{k}_2)\,\boldsymbol{S}\cdot[[\boldsymbol{k}_1+\boldsymbol{k}_2\times\boldsymbol{p}]\,\mathrm{d}\boldsymbol{k}_1\mathrm{d}\boldsymbol{k}_2\,,$$

$$V_4^{(4)} = \frac{24ig^4}{(2M)^5(2\pi)^6}\int \frac{\exp[i(\boldsymbol{k}_1+\boldsymbol{k}_2\cdot\boldsymbol{r})]}{\omega_1^2\omega_2^2}\,(\boldsymbol{p}\cdot\boldsymbol{k}_2)\,\boldsymbol{S}\cdot[\boldsymbol{k}_1\times\boldsymbol{k}_2]\,\mathrm{d}\boldsymbol{k}_1\mathrm{d}\boldsymbol{k}_2\,,$$

$$V_4^{(5)} = \frac{8i(\boldsymbol{\tau}_1\cdot\boldsymbol{\tau}_2)g^4}{(2M)^5(2\pi)^6}\int \frac{\exp[i(\boldsymbol{k}_1+\boldsymbol{k}_2\cdot\boldsymbol{r})]}{\omega_1^2\omega_2^2}\,(\boldsymbol{p}\cdot\boldsymbol{k}_2)\,\boldsymbol{S}\cdot[\boldsymbol{k}_1\times\boldsymbol{k}_2]\,\mathrm{d}\boldsymbol{k}_1\mathrm{d}\boldsymbol{k}_2\,,$$

$$V_4^{(6)} = \frac{12ig^4}{(2M)^4(2\pi)^6}\int\left\{\frac{\exp[i(\boldsymbol{k}_1+\boldsymbol{k}_2\cdot\boldsymbol{r})]}{\omega_1^3\omega_2^2}+\frac{\exp[i(\boldsymbol{k}_1+\boldsymbol{k}_2\cdot\boldsymbol{r})]}{\omega_1\omega_2^3(\omega_1+\omega_2)}\right\}(\boldsymbol{p}\cdot\boldsymbol{k}_2)\cdot$$
$$\cdot\boldsymbol{S}\cdot[\boldsymbol{k}_1\times\boldsymbol{k}_2]\,\mathrm{d}\boldsymbol{k}_1\mathrm{d}\boldsymbol{k}_2\,,$$

$$V_4^{(7)} = -\frac{6ig^4}{(2M)^5(2\pi)^6}\int\left\{\frac{(\boldsymbol{k}_1+\boldsymbol{k}_2)^2+2\boldsymbol{k}_2^2}{\omega_1^3\omega_2^3}+\frac{2(\boldsymbol{k}_1+\boldsymbol{k}_2)^2}{\omega_1^3\omega_2(\omega_1+\omega_2)^2}\right\}\cdot$$

$$\cdot\exp\left[i(\boldsymbol{k}_1+\boldsymbol{k}_2\cdot\boldsymbol{r})\right](\boldsymbol{p}\cdot\boldsymbol{k}_2)\boldsymbol{S}\cdot[\boldsymbol{k}_1\times\boldsymbol{k}_2]\,\mathrm{d}\boldsymbol{k}_1\,\mathrm{d}\boldsymbol{k}_2\,,$$

$$V_4^{(8)} = \frac{4i(3-2\boldsymbol{\tau}_1\cdot\boldsymbol{\tau}_2)g^4}{(2M)^5(2\pi)^6}\int\frac{\exp\left[i(\boldsymbol{k}_1+\boldsymbol{k}_2\cdot\boldsymbol{r})\right]}{\omega_1^3\omega_2^2(\omega_1+\omega_2)}(\boldsymbol{p}\cdot\boldsymbol{k}_2)\boldsymbol{k}_1\cdot\boldsymbol{k}_2)\boldsymbol{S}\cdot[\boldsymbol{k}_1\times\boldsymbol{k}_2]\,\mathrm{d}\boldsymbol{k}_1\,\mathrm{d}\boldsymbol{k}_2\,.$$

RIASSUNTO (*)

Si usa il metodo di Levy-Klein per calcolare, per l'accopiamento pseudoscalare, il potenziale spin-orbita fra due nucleoni. I risultati, calcolati nei due ordini più bassi del rapporto fra la massa del mesone e quella del nucleone, indicano una forza attrattiva per lo stato di tripletto dello spin isotopico ed una minore forza repulsiva per lo stato di singoletto. L'accordo quantitativo con i potenziali fenomenologici dipende tuttavia dagli effetti della soppressione di coppie i quali sono tuttora incerti.

(*) *Traduzione a cura della Redazione.*

IL NUOVO CIMENTO Vol. XIII, N. 4 16 Agosto 1959

Analysis of the Charge Exchange Reaction $K^+ + p \to K^0 + n$.

C. Ceolin, N. Dallaporta, L. Guerriero, I. Laboragine
G. A. Salandin and L. Taffara

Istituto di Fisica dell'Università - Padova
Istituto Nazionale di Fisica Nucleare - Sezione di Padova

(ricevuto l'11 Maggio 1959)

Summary. — A detailed analysis of the data concerning the reaction $K^+ + p \to K^0 + n$ has been undertaken in order to deduce the behaviour with energy of the total cross-section and the angular distribution of the differential cross-section. It is found that the best fit for the data, corrected for all effects in nuclei, indicate that the total charge-exchange cross-section increases with about the third power of the c.m. momentum. An analysis of the secondary prongs of the K-nucleus events leading to charge-exchange gives indications that the differential cross-section is peaked backward in the c.m. system. These data do not seem to fit with the theoretical formulae based on a $KK\pi$-interaction. Further, different theoretical interpretations are discussed with the aim of seeing if they are adequate to explain the preceding behaviour of the charge-exchange reaction.

1. – Introduction.

During this last year the situation concerning the theoretical interpretation of the strong interactions of the strange particles appears to have gradually grown more complicated with the increasing evidence that different experimental data seem to be incompatible, as first shown by Pais [1], with a number of consequences expected to occur if full symmetries postulated up to now for the scheme of baryon states should have in effect been valid. The simplest and, at the same time, the most fundamental form for this basic

[1] P. A. Pais: *Phys. Rev.*, **110**, 574 (1958); *Phys. Rev.*, **112**, 624 (1958).

symmetrical scheme appears to be the so called doublet approximation which, apart from PAIS, has been already proposed independently in slightly different forms by different authors ([2-4]). This approximation consists essentially in assembling all the baryons into doublets connected between them by the transitions through absorption or emission of different mesons, as indicated in Fig. 1. Now, if one assumes that as a consequence of this scheme, the type of coupling and the interaction constants for all pion interactions are the same, and similarly equal type and strength of coupling occur for the interaction of neutral and charged K's, then one obtains some relations between cross-sections of different reaction processes which may be compared with experience. One of the most striking consequences is that, owing to the doublet approximation with which the Σ^0 and Λ^0 states are represented, mainly

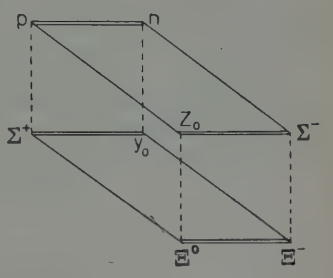

Fig. 1.

$$(1) \qquad Z = \frac{\Sigma^0 + \Lambda^0}{\sqrt{2}}, \qquad Y = \frac{\Sigma^0 - \Lambda^0}{\sqrt{2}},$$

the probability for the following processes turns out to be exactly zero:

$$(2) \qquad \begin{cases} K^+ + n \to K^0 + p\,, \\ K^- + p \to K^0 + n\,, \\ K^- + p \to \Sigma^+ + \pi^-\,, \\ \pi^+ + p \to \Sigma^+ + K^+\,. \end{cases}$$

Now such a consequence is obviously wrong as in fact all these processes are experimentally known and their cross-section does not appear to be of a different order of magnitude from the other similar processes not forbidden by the scheme; therefore the experimental evidence of the violation of the predicted selection rules constitutes the most striking proof that the doublet approximation is by itself insufficient to explain the real situation.

This fact mainly has induced PAIS ([1]) to a further step consisting in the introduction of a perturbation which breaks some symmetries of the doublet approximation and thus allows the forbidden interactions to take place.

To this aim, with the new hypothesis of considering that charged and

([2]) M. GELL-MANN: *Phys. Rev.*, **106**, 1296 (1957).
([3]) J. TIOMNO: *Nuovo Cimento*, **6**, 69 (1957).
([4]) N. DALLAPORTA: *Nuovo Cimento*, **7**, 200 (1958).

neutral K's are of opposite parity, PAIS postulated a parity conserving KKπ interaction which may thus be made qualitatively responsible for the breakdown of the selection rules and the existence of the forbidden reactions.

If such a general idea is true, then is it obvious that the effects of this KKπ-interaction should be most conspicuous in reactions (2); and therefore the behaviour of these symmetry violating reactions appears to be one of the most critical points to study in the present situation for the understanding of the K interaction.

The present paper is intended to be a detailed investigation for the first one of them, *i.e.*:

$$K^+ + n \to K^0 + p \,, \tag{3}$$

for which actually there are already sufficient experimental data to undertake such a work.

The striking fact that the experimental behaviour of this process is quite different from the case of K-proton and K-neutron elastic scattering may be considered as a first indication in agreement with the assumption of PAIS; he himself was induced to calculate the cross-section for this charge-exchange reaction according to the present KKπ-interaction ([1]). The data with which PAIS was able to compare his formulae were however rather scanty, so that no definite impression can be really obtained from this comparison.

A much more extended information from the analysis of the world data on this reaction is now available as appears already from the results communicated at the Geneva Conference ([5]) and from a recent work by GRILLI *et al.* ([5]). Therefore, it was considered worth-while to reanalyze in more detail the whole experimental evidence and compare the results so obtained with PAIS' interpretation.

In Sect. **2** the analysis of the experimental material is presented and the best fit for the behaviour of the total cross-section with energy according to world data is calculated. In Sect. **3** some evidence concerning the angular distribution of process (3) is obtained from the momentum balance of the secondary prongs of the charge-exchange events analyzed in this laboratory. In Sect. **4** a comparison of these results with the curves derived for the KKπ-scheme is presented and a strong disagreement is obtained. In Sect. **5** some other theoretical possible interpretations are examined with the phenomenological aim of selecting those which may be compatible with the main experimental implications.

([5]) Report of the *Annual International Conference on High Energy Physics at CERN*, (1958) p. 171; M. GRILLI, L. GUERRIERO G. A. SALANDIN, D. KEEFE, A. KERNAN, A. MONTWILL: *Nuovo Cimento* **12**, 241 (1959).

2. – Experimental total cross-section.

For the deduction of the behaviour with the energy of the total charge-exchange scattering cross-section the world experimental data from nuclear emulsion concerning the mean free path of inelastic interactions and the ratio $R =$ charge-exchange/no charge-exchange scattering cross-section has been collected. These data are reported in Fig. 2 and 3.

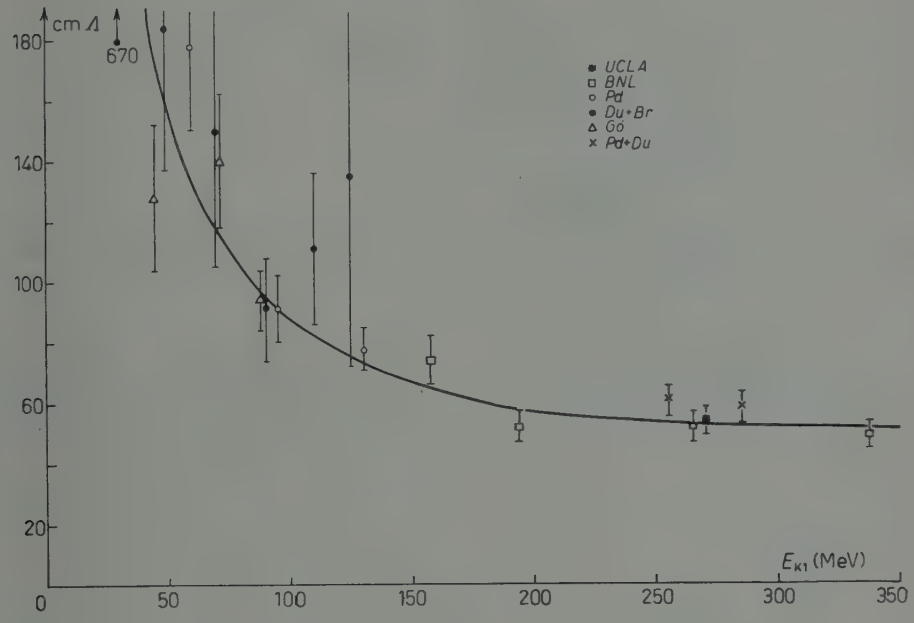

Fig. 2. – Mean free path for inelastic collisions.

In order to obtain the true total cross-section, corrections to the observed mean free path must be made to account for:

a) the respulsive Coulomb potential of about 10 MeV;

b) the shadowing effect of the nuclear matter. To this aim an exponential model for the density of nuclear matter has been used given by:

$$\varrho = \varrho_0 \cdot (1 + \exp[r - r_0]/D)^{-1}\,, \tag{4}$$

in which $r_0 = 10.7 \cdot A^{\frac{1}{3}}$ fermi and $D = 0.56$ fermi.

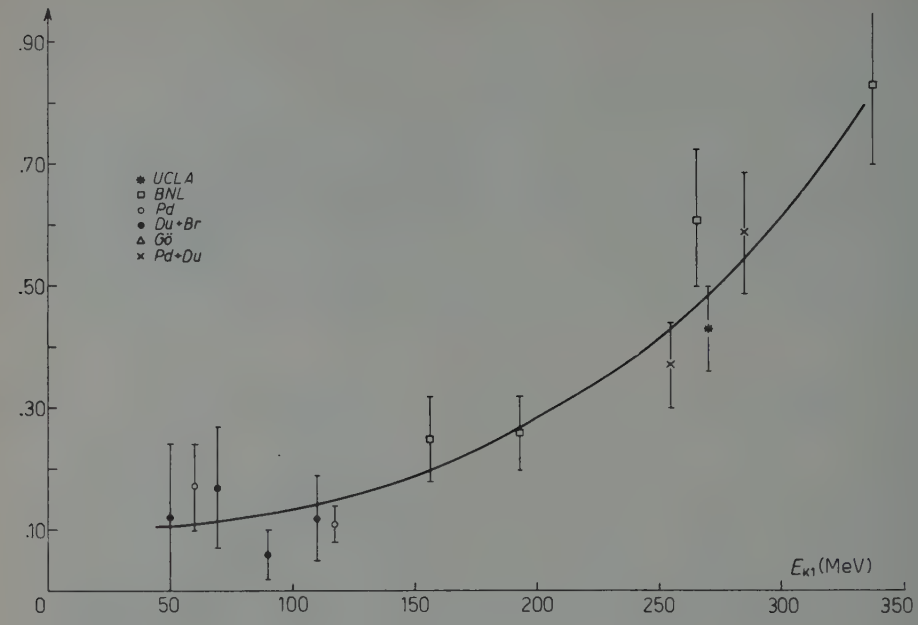

Fig. 3. – Ratio charge exchange/scattering versus primary energy.

c) Furthermore the observed ratio R has to be corrected to take into account the double scattering effects which give an experimental ratio greater than the effective one. The probability of double scattering and the corrected value of R have been calculated according to the adopted nuclear model.

After correction of all these effects one obtains the total charge-exchange cross-section on bound neutron in nuclear matter. The values so obtained are reported in Fig. 4 versus the energy of incoming K.

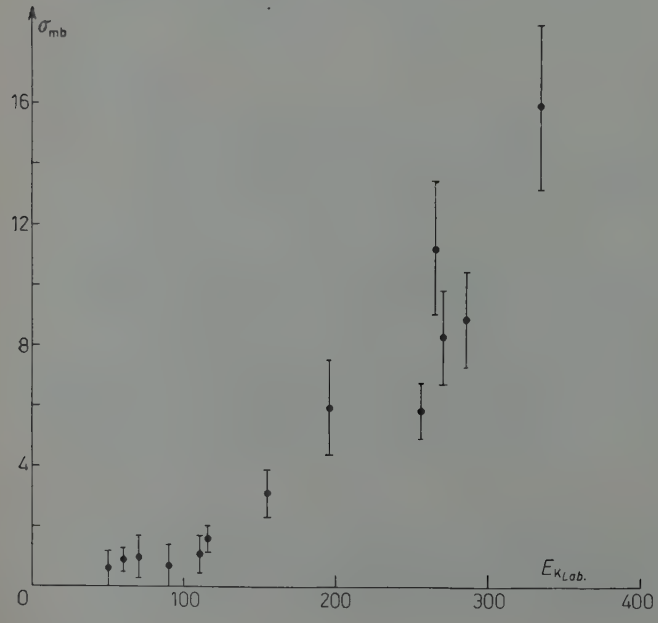

Fig. 4. – Charge exchange cross-section on bound neutron as a function of the energy.

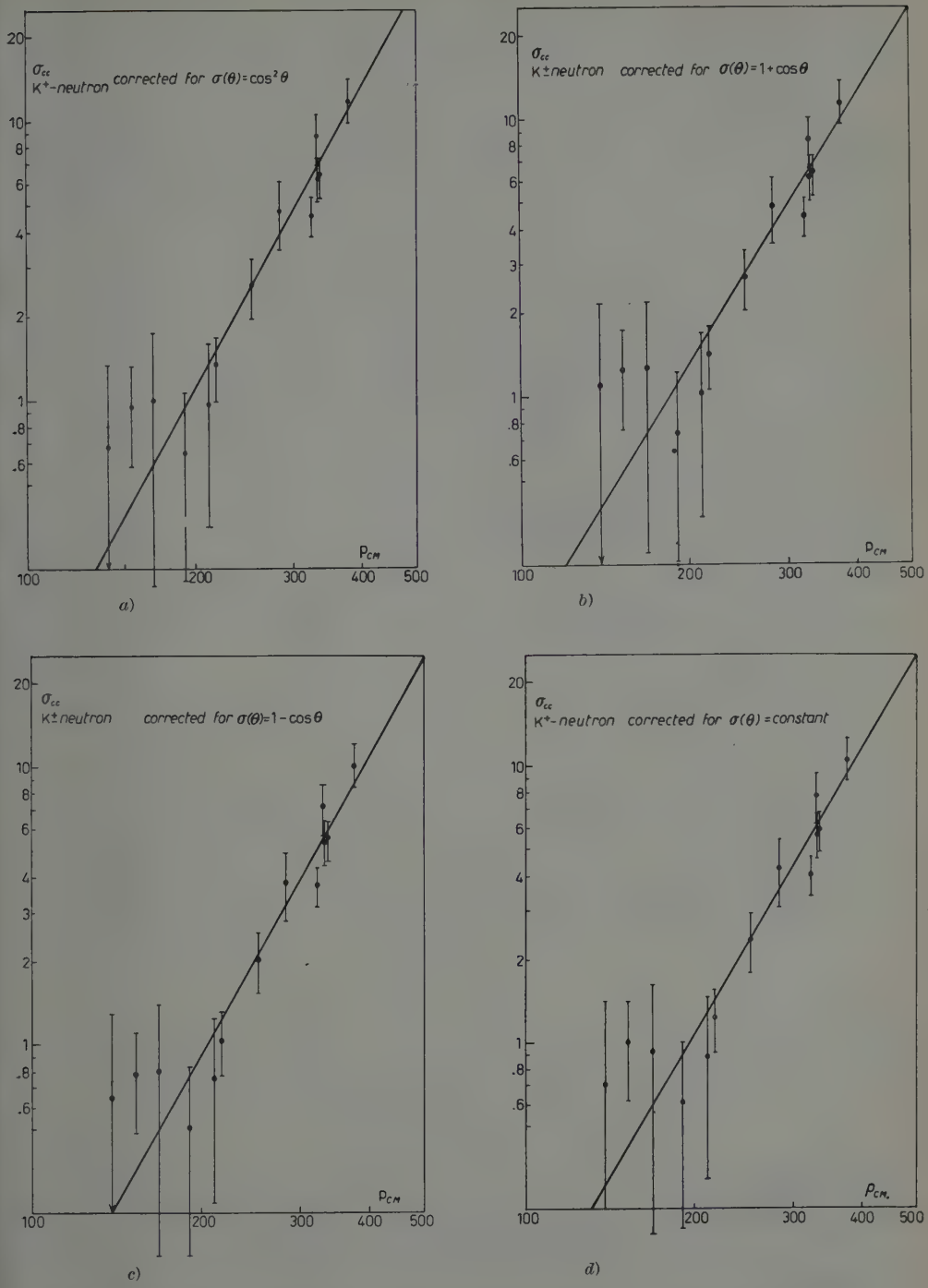

Fig. 5. – Charge exchange cross-section after correction for Pauli principle with different hypotheses on the angular cross-section.

Now, to obtain the true cross-section on a free neutron, we must take into account the effect of the Pauli exclusion principle which cuts off all small momentum transfer scatterings in nuclear matter.

An exact evaluation of such an effect requires the knowledge of the angular cross-section which is presently unknown. However, the very rapid increase of charge-exchange cross-section on bound neutron with energy suggests that probably a P-wave must be predominant in this process. Therefore, tentatively, the Pauli correction has been calculated assuming $\sigma(\vartheta) \propto \cos^2 \vartheta$ and the charge-exchange cross-section thus obtained is indicated in Fig. 5*a*. The increase with energy of this cross-section fits very well a $p^3_{\text{c.m.}}$ dependence.

For reasons which will become apparent in the following Sect., the same correction has been made assuming three other types of angular cross-section, *i.e.* $1 + \cos \vartheta$, $1 - \cos \vartheta$, and constant. The values are indicated in Fig. 5*b*, *c*, *d* respectively.

The values of $p_{\text{c.m.}}$ have been further corrected to take into account the reduction of the K-energy inside the nucleus due to the repulsive potential and the motion of the nucleons which, especially for low energy-K's, favours the higher $p_{\text{c.m.}}$ values.

For each type of angular cross-section we have evaluated with the χ^2-method the most probable value of the $p_{\text{c.m.}}$ power which fits the increase with energy of the total cross-section.

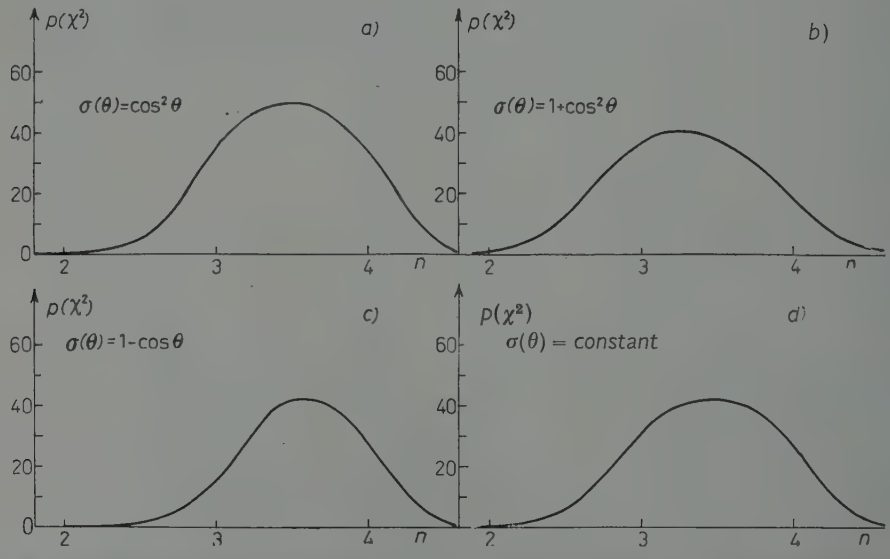

Fig. 6. – Probability distribution of the values of n in the formula $\sigma_{\text{c.e.}} = R p_{\text{c.m.}}$ with different hypotheses on the angular cross-section.

In Fig. 6 *a*, *b*, *c*, *d* the probabilities that the experimental points can derive from a theoretical cross-section $\sigma_{\text{c.e.}} = R p^n_{\text{c.m.}}$ are reported as a function of the

exponent n for the cases of four different Pauli principle corrections. The most probable values of n in this four cases are: $3.55 \pm .70$ for $\sigma(\vartheta) \propto \cos^2 \vartheta$, $3.25 \pm .55$ for $\sigma(\vartheta) \propto 1 + \cos \vartheta$, $3.60 \pm .50$ for $\sigma(\vartheta) \propto 1 - \cos \vartheta$, $3.45 \pm .55$ for $\sigma(\vartheta) = \text{const}$. From these results one can conclude that the increase of the $\sigma_{c.e.}$ with the third power of $p_{c.m.}$ seems rather well established.

Deviations from the most probable values are deduced through a χ^2-method on a purely statistical basis.

3. – Experimental angular distribution.

No indications have been given up to now, as far as we know, concerning the angular distribution of the charge-exchange events owing to the evident impossibility of observing directly the escaping K^0 in the emulsion.

We have thought that a detailed analysis of the secondary prongs of the charge-exchange events may spread some light on this question. Such an analysis has been done only in the energy range between 200 and 305 MeV for the events found in our laboratory.

The method we have used to obtain some indications on this angular distribution consists in measuring the total momentum of all the secondary prongs in the K-nucleus interactions. For the calculation of these momenta it has been assumed that all visible prongs are protons, since previous measurements have shown that this is true for most of the prongs.

The momenta of all visible prongs of a given event were summed vectorially and the resulting momentum $\boldsymbol{\Sigma}_p$ was thus obtained. The total momentum $\boldsymbol{\Sigma}$ transferred to the nucleus differs from that evaluated from the charged prongs only, as if they were protons, by an amount $\boldsymbol{\Sigma}_n$. We have assumed that, although $|\boldsymbol{\Sigma}_p|$ is systematically smaller than the total prong momentum $|\boldsymbol{\Sigma}|$, its direction is symmetrically distributed around the visible momentum and on the average should be:

$$\langle \boldsymbol{\Sigma} \rangle = s \cdot \langle \boldsymbol{\Sigma}_p \rangle ,$$

where s is a coefficient greater than 1 which has to be suitably chosen, therefore, by assuming the momentum of the escaping K as given by:

$$\boldsymbol{p}_2 = \boldsymbol{p}_1 - s \cdot \boldsymbol{\Sigma}_p , \tag{5}$$

the errors on $\boldsymbol{p}_2$ for individual events cancel out on the average, and the angular distribution of p_2, so obtained, differs from the true one only for the smearing effect of this method of evaluation.

Now, in order to determine the number s, we have considered the K-nucleus scattering events and calculated for each of them the ratio s_i of the observed momentum transfer of the K to the total momentum of the visible prongs which should be exactly the value of s for each event. The distribution of this ratio is given in Fig. 7.

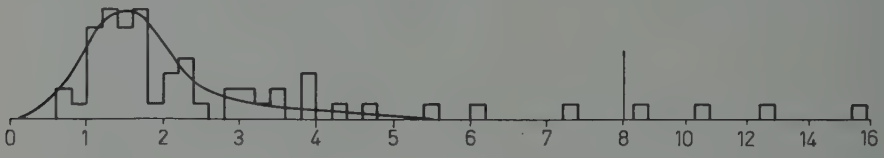

Fig. 7. – Distribution of $|\bar{p}_2 - \bar{p}_1|/\sum \bar{p}$ for scattering events.

K^+ scatterings with recoil were excluded for the impossibility of evaluating with sufficient approximation the momentum of the residual nucleus.

The collided nucleon generally carries most of the transfer momentum; in order that the results obtained with this method for the scattering events should be exactly applicable to the charge-exchange ones, one would like that primary interaction of the K with a nucleon inside the nucleus should give always a proton recoil. Indeed charge-exchange events always yeld a proton recoil, scattering events can give either a proton or a neutron.

Previous measurements have shown however, that the K-neutron scattering cross-section is small in respect to the K proton cross-sections in this energy range. The K-neutron scatterings do not greatly influence the analysis and this fact is confirmed by what follows.

The distribution of Fig. 7 indicates that for most of the events the ratio s_i has a value between 1 and 3. However there are some single events for which this ratio appears to be much larger.

By examination of these special events, it was recognized that in none of these cases a single energetic proton was present, while such energetic protons which are interpreted as the direct recoils of the primary K-nucleon interaction, are generally present in the other events, both scatterings and charge-exchanges.

Therefore, it appears rather probable that the special events with a large value of s_i are direct K-neutron scatterings in which the collided neutron carries most of the transfer momentum.

If we disregard such events, one obtains from Fig. 7 a mean value $s = \bar{s}_i = 2$. We therefore conclude that the momentum of the secondary K may be obtained on the average by:

$$\boldsymbol{p}_2 = \boldsymbol{p}_1 - 2 \cdot \boldsymbol{\Sigma}_p \,.$$

With this assumption the angle ϑ_2 between the escaping and the incoming K can obtained.

In the case of pure scatterings, it is possible to compare the angle ϑ_2 calculated with this prong-method for each event with the angle ϑ_{lab} effectively measured. In Fig. 8*a* we give the distribution of the difference $\vartheta_2 - \vartheta_{lab}$: This distribution turns out to be centered about the value zero with a half width of about 45°. Just for a further check of the method employed, we have plotted in Fig. 8*b* the distribution of the difference $\vartheta_1 - \vartheta_{lab}$ where now ϑ_1 is the angle which would be obtained for the escaping K if calculated with the relation:

$$\boldsymbol{p}_2 = \boldsymbol{p}_1 - \boldsymbol{\Sigma}_p ,$$

that is with $s = 1$ in relation (5), *i.e.* by considering only the momentum of the protons. As in fact was to be expected, it appears then that, all the angles ϑ_1 are underestimated and now the distribution of the differences $\vartheta_1 - \vartheta_{lab}$ is centered around a mean value of about $-40°$.

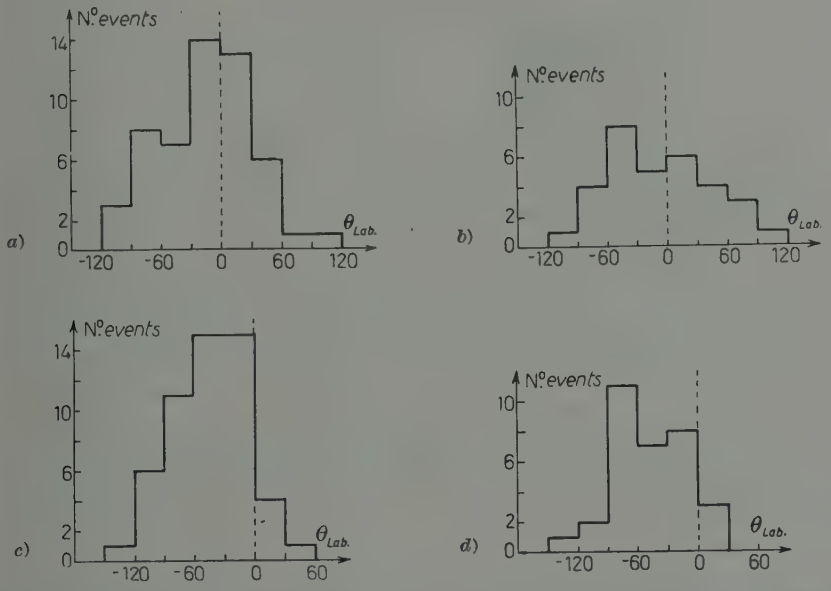

Fig. 8. – Distribution of the difference $\vartheta_2 - \vartheta_{lab}$: *a*) for events without recoil; *b*) for events with recoil. Distribution of the difference $\vartheta_1 - \vartheta_{lab}$: *c*) for events without recoil; *d*) for events with recoil.

Finally in Fig. 8*c* we have plotted the difference $\vartheta_2 - \vartheta_{lab}$ calculated by the same method for those events in which a nucleus recoil is present. This distribution turns out to be also centered on the value zero but with a greater half width than 8*a*, as was to be expected owing to the greater error on the resultant momentum due to the presence of the recoil. A similar distribution for the angles $\vartheta_1 - \vartheta_{lab}$ is given in Fig. 8*d*.

All these different checks clearly indicate that an estimate of ϑ_2 is correct on the average and allows to extend the same method to the case of the charge-exchange events.

In Fig. 9 *a* and *b*, we have plotted therefore the so obtained distributions for the estimated angles ϑ_2 for both cases of the scattering events and respectively of the charge-exchange ones. These two distributions turn out to be rather different. In the lab. system the scatterings appear to be concentrated in the forward hemisphere and the ratio forward/backward is 5.4 ± 2.2 The charge-exchange distribution is much more isotropic and the value of the same ratio is only 1.5 ± 0.6.

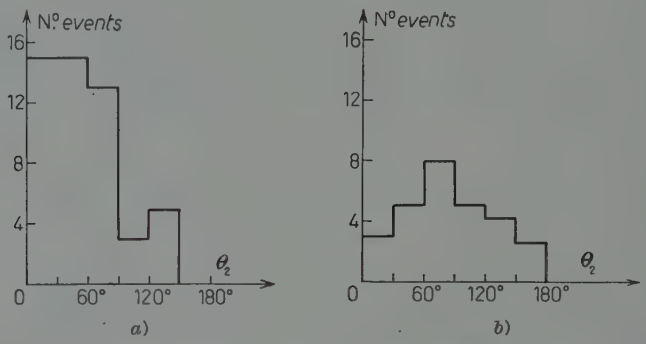

Fig. 9. – Distribution of the angles ϑ_2: *a*) for scatterings; *b*) for charge exchanges.

From this fact it is possible to conclude that the angular cross-section for pure scattering and for charge-exchange must have different shapes. As we know that the scattering cross-section in the center of mass system is rather flat, we must conclude that the charge-exchange cross-section is peaked backwards.

This conclusion obtained by our method is supported by the following independent indications which may be considered as further checks of our results.

a) The mean number of prongs coming out from scattering events and from charge-exchange events is respectively 1.6 and 2.6. It may be remarked that there are practically no cases of charge-exchanges without prongs, while in about $\frac{1}{4}$ of the scattering events only the K is escaping from the interaction.

Of course, scattering events are a mixture of interactions on protons and neutrons, but we know that the K-neutron interaction is less frequent than the K-proton one. Should we even suppose that the frequencies of both processes are equal, then we should expect at most an excess on the average of 0.5 prongs for the case of the charge-exchange always where there is a secondary proton from the primary K-neutron interactions, while in the scatterings the secundary proton occurs only in the K-proton interactions. The fact that

the average excess is higher than 0.5 seems therefore to indicate a higher energy loss in the charge-exchange case and therefore a more backward peaked cross-section for it.

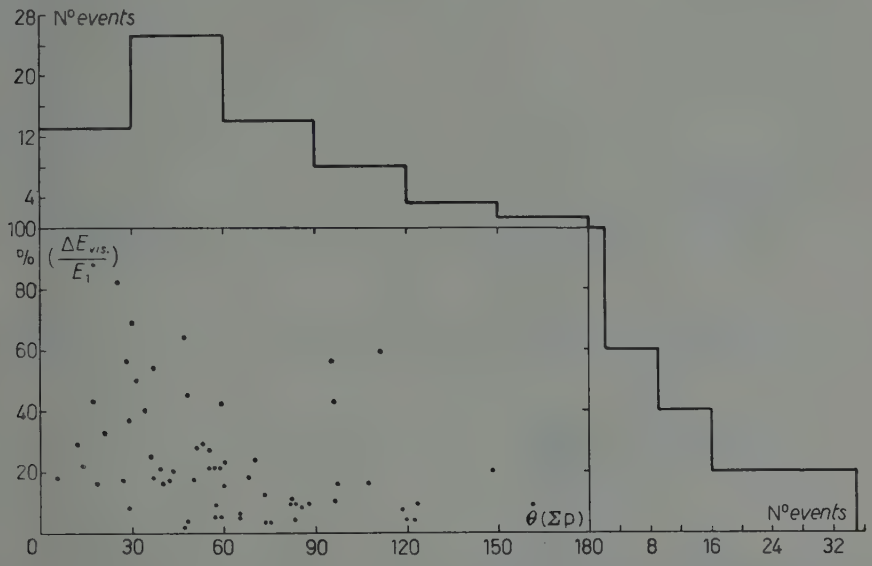

Fig. 10. – Distribution of the visible total energy of the prongs versus the angle of the resultant momentum of the visible prongs $\sum_p p$ for the scatterings.

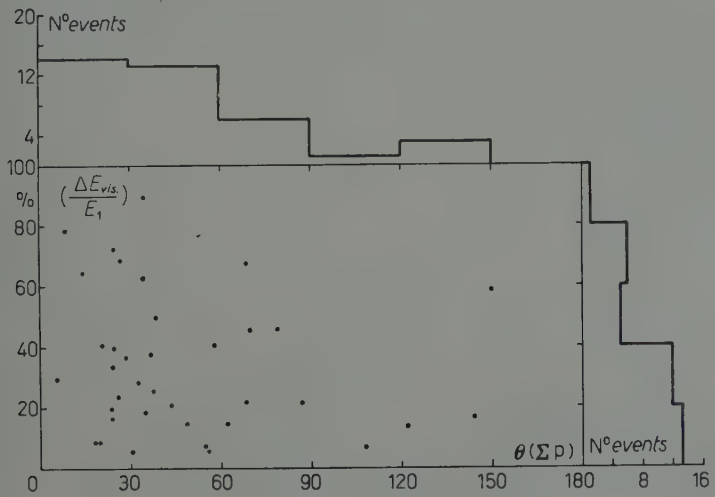

Fig. 11. – The same distribution of Fig. 10 for the charge-exchange.

b) In Fig. 10 and 11 we have plotted the distribution of the visible total energy of the prongs versus the angle of the resultant momentum of the visible

prongs Σ_p for the scattering and the charge-exchange events respectively. We may immediately observe that the charge-exchange events prefer small angles for Σ_p and large energy losses. On the average the visible energy loss for the scattering is 23% and for the charge-exchanges 35%. This difference also may easily be explained if one assumes a backward peaked cross-section for the charge-exchanges.

We may therefore conclude that all the experimental indications, although indirect, point out concordingly to a cross-section for the charge-exchange events peaked backwards, and the fact that this indication is obtained in several independent ways seems to give more strength to this conclusion. It would of course be very desirable that events from other laboratories could be treated in a similar way to reinforce the statistical meaning of our results.

4. – Comparison of the experimental results with the $K\bar{K}\pi$ interaction assumption.

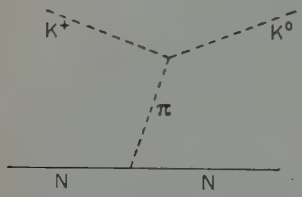

Fig. 12. – Diagram for the $K\bar{K}\pi$ interaction.

We may now compare our experimental cross-section for the charge-exchange process with the formulae given by PAIS [1]. These are deduced according to the diagram of Fig. 12, in which the $K\bar{K}\pi$ interaction Hamiltonian is assumed to be:

$$H_{\text{int}} = f \cdot (2m)[\bar{K}^+ \cdot K^0 \pi^+ + \bar{K}^0 \cdot K^+ \cdot \pi^-] . \tag{6}$$

The formulae (48), (49) in Pais' paper for the differential and total cross-section contain a parameter λ which can take values between $+1$ and -1. The total cross-sections for the three values $+1$, 0 and -1 of the λ parameter are reported in Fig. 13, 14 and 15 and then compared to the experimental behaviour.

As may be seen, for any value of λ there is a rather strong disagreement which is too marked to be attributed to the experimental errors on the total cross-section.

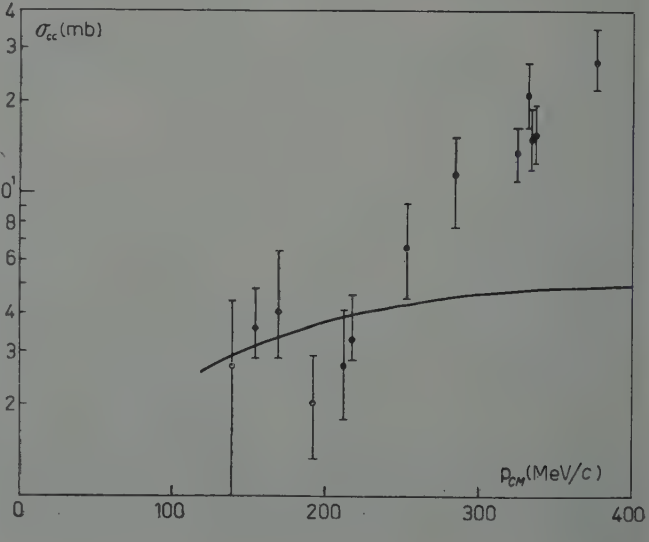

Fig. 13. – Comparison with Pais' theory ($\lambda = +1$).

In Fig. 16 we have next compared the angular distributions in center of mass system according to formula (49) of Pais' paper, with our results for an

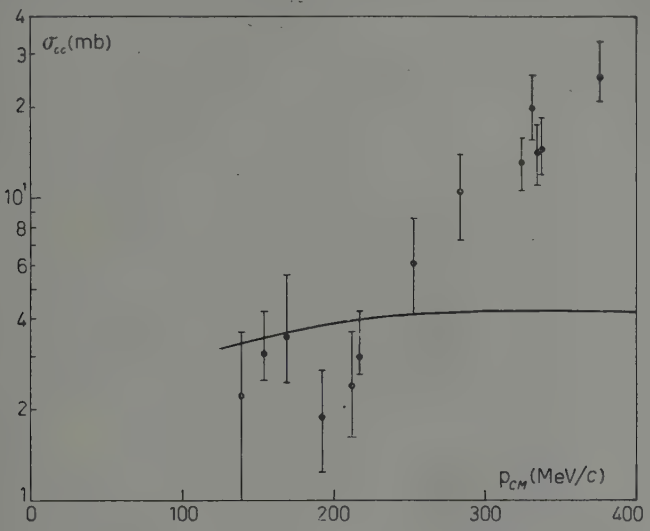

Fig. 14. – Comparison with Pais' theory ($\lambda = 0$).

energy value of 270 MeV, and for the three values of λ: 1, 0 and -1. For all these cases the cross-section turns out to be peaked forward contrarily to our experimental deduction.

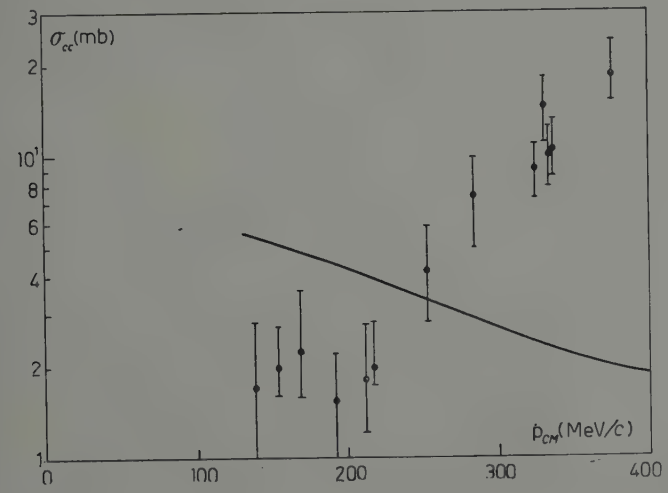

Fig. 15. – Comparison with Pais' theory ($\lambda = -1$).

Assuming the less forward peaked case ($\lambda = -1$), we have therefore calculated the angular distribution which should be expected in the lab. system

For comparison with the experimental results the necessary conditions have been folded in: Fermi motion of the nucleons as well as the smearing introduced by our method.

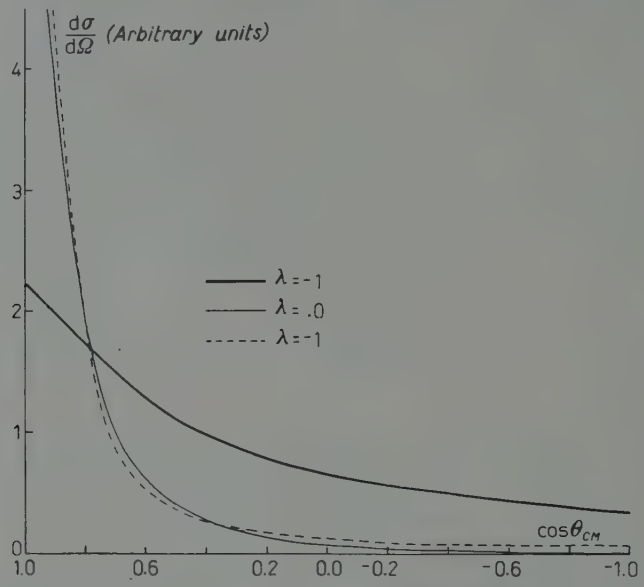

Fig. 16. – Angular cross-section from Pais' theory.

The histograms obtained are given in Fig. 17*a* and *b*. The ratio forward-backward scattering in the first case turns out to be 6.5 and in the second one 3.9, which in both cases is in disagreement with the experimental indications.

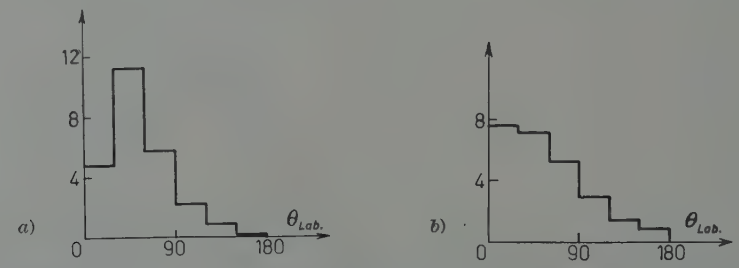

Fig. 17. – *a*) Expected distribution for θ_{lab} of charge exchange with Pais' formule ($\lambda = -1$); *b*) Distribution *a*) smeared for angles ϑ_2.

5. – Theoretical implications.

From the preceding analysis we should be induced to conclude that the KKπ interaction assumption, at least in the approximation used by Pais to derive his formulae, is not adequate to interpret the observed data. We could

then try to discuss which should be the more probable theoretical implications that the actual evidence should require.

The most relevant feature of the data to explain according to our view is the conspicuous increase with energy of the charge-exchange total cross-section in contrast to the almost constant K^+-proton and K^+-neutron cases. A qualitative explanation of this fact in terms of conventional phase-shifts and according to the Gell-Mann-Nishijima theory in which charged and neutral K's are considered as doublets in isotopic spin space, was proposed by GRILLI *et al.* [5]. On the other hand a Tamm-Dankoff calculation of the phase-shifts [6] based on the same theoretical assumption failed completely to reproduce the observed behaviour of the three K-nucleon total cross-sections for any value of the pseudoscalar K-Y-N coupling constants.

Now, the simplest way perhaps to interpret this experimental facts, may be to say that the charge-exchange process goes mainly through a P-wave up to energies of about 350 MeV while, in the same range, it appears rather probable that the K-proton and K-neutron scattering processes are mainly ruled by an S-wave. If these views are true, the failure of the conventional theory becomes quite obvious and we should try to look for some other possibilities of interpretation. Avoiding further approaches considering other pion intermediaries ($KK\pi\pi$ interactions) which have been already proposed by other authors [7,8] and do not appear adequate to explain just the points now mentioned, we may try to proceed in a systematic way by moving from the doublet approximation itself and examining which are the minimum disturbances to impose on it in order to obtain the experimental facts.

The existence of the forbidden reactions (2) which up to now constitutes the main contradiction of the doublet approximation with the experimental evidence, is essentially due to the assumption (1) linking the fictitious doublet states Z and Y with the singlet Λ^0 and the triplet Σ^0. We then first examine the possibilities of leaving in the whole the doublet approximation as it is, and just changing the relations (1). There are already several indications that many of the present difficulties of the scheme may be confined essentially into this mixing of the neutral degenerate states.

Let us therefore assume the following phenomenological relation instead of (1):

$$Z = \frac{\pm a\gamma_5 \Lambda^0 + \Sigma^0}{\sqrt{2}}, \qquad Y = \frac{\pm a\gamma_5 \Lambda^0 - \Sigma^0}{\sqrt{2}}, \tag{7}$$

---

(6) C. CEOLIN, V. DE SANTIS and L. TAFFARA: *Nuovo Cimento*, **12**, 502 (1959).

(7) S. BARSHAY: *Phys. Rev.*, **110**, 743 (1958).

(8) Y. YAMAGUCHI: *Proceedings of the International Conference on Mesons and recently discovered Particles Padua-Venice* (Sept. 1957), part V, p. 42.

expressing essentially the fact that the two final neutral states Λ^0 and Σ^0 are of opposite parity ([9]), and are mixed in different proportions if $a \neq 1$, owing to a possible different renormalization in the cases of scalar and pseudoscalar coupling.

Now, if we choose the sign + in (7) we obtain the following interaction Hamiltonian:

$$(8) \quad H_{\text{int}} = g(\bar{N}_1 \cdot N_2 \cdot K^0 + \bar{N}_1 \cdot N_3 \cdot K^+ + \text{c.c.}) =$$

$$= g\left(\bar{p}\Sigma^+ K^0 + \frac{a}{\sqrt{2}}\bar{n}\gamma_5 \Lambda^0 K^0 - \frac{1}{\sqrt{2}}\bar{n}\Sigma^0 K^0 + \right.$$

$$\left. + \quad \bar{n}\Sigma^- K^+ + \frac{a}{\sqrt{2}}\bar{p}\gamma_5 \Lambda^0 K^+ + \frac{1}{\sqrt{2}}\bar{p}\Sigma^0 K^+ + \text{c.c.}\right),$$

with

$$N_1 = \begin{vmatrix} p \\ n \end{vmatrix}, \qquad N_2 = \begin{vmatrix} \Sigma^+ \\ Y \end{vmatrix}, \qquad N_3 = \begin{vmatrix} Z \\ \Sigma^- \end{vmatrix},$$

which gives pseudo-scalar Λ^0-terms and scalar Σ-terms.

If instead we choose the sign —, we obtain:

$$(9) \quad H_{\text{int}} = g(\bar{N}_1 \gamma_5 N_2 \cdot K^0 + \bar{N}_1 \gamma_5 N_3 K^+ + \text{c.c.}) =$$

$$= g\left(\bar{p}\gamma_5 \Sigma^+ K^0 + \frac{a}{\sqrt{2}}\bar{n}\Lambda^0 K^0 - \frac{1}{\sqrt{2}}\bar{n}\gamma_5 \Sigma^0 K^0 + \right.$$

$$\left. + \quad \bar{n}\gamma_5 \Sigma^- K^+ + \frac{a}{\sqrt{2}}\bar{p}\Lambda^0 K^+ + \frac{1}{\sqrt{2}}\bar{p}\gamma_5 \Sigma^0 K^0 + \text{c.c.}\right),$$

which gives scalar Λ^0-terms and pseudoscalar Σ-terms ([10]).

Now, in order to obtain a predominant S-wave for K-proton scattering we must choose the coefficient « a » such as to reduce the P-wave.

This reduction may be obtained in the limit of a non-relativistic $\boldsymbol{\sigma} \cdot \boldsymbol{k}$ coupling approximation of (8) and (9). However, if we reduce the P-wave in the K-proton scattering, the same reduction should occur in the charge-exchange reaction.

As a further step one can try to reverse the relative parities of the charged to the neutral K's according to Pais' assumption. Starting from (8), one then

---

([9]) S. BARSHAY: *Phys. Rev. Lett.*, **1**, 97 (1958).

([10]) N. DALLAPORTA: *Nuovo Cimento*, **11**, 142 (1959).

obtains for scalar K^+ and pseudoscalar K^0:

$$(10)\quad H_{\text{int}} = g_1 \bar{N}_1 \gamma_5 N_2 K^0 + g_2 \bar{N}_1 \cdot N_3 K^+ + \text{c.c.} =$$

$$= g_1 \left(\bar{p}\gamma_5 \Sigma^+ K^0 - \frac{a}{\sqrt{2}} \bar{n} \Lambda^0 K^0 - \frac{1}{\sqrt{2}} \bar{n}\gamma_5 \Sigma^0 K^0 + \text{c.c.} \right) +$$

$$+ g_2 \left(\bar{n} \cdot \Sigma^- K^+ + \frac{a}{\sqrt{2}} \bar{p}\gamma_5 \Lambda^0 K^+ + \frac{1}{\sqrt{2}} \bar{n} \Sigma^0 K^+ + \text{c.c.} \right),$$

and for pseudoscalar K^+ and scalar K^0:

$$(11)\quad H_{\text{int}} = g_1 \bar{N}_1 N_2 K^0 + g_2 \bar{N}_1 \gamma_5 N_3 K^+ + \text{c.c.} =$$

$$= g_1 \left(\bar{p} \Sigma^+ K^0 + \frac{a}{\sqrt{2}} \bar{n}\gamma_5 \Lambda^0 K^0 - \frac{1}{\sqrt{2}} \bar{n} \Sigma^0 K^0 + \text{c.c.} \right) +$$

$$+ g_2 \left(\bar{n}\gamma_5 \Sigma^- K^+ - \frac{a}{\sqrt{2}} \bar{p} \Lambda^0 K^+ + \frac{1}{\sqrt{2}} \bar{p}\gamma_5 \Sigma^0 K^+ + \text{c.c.} \right).$$

From (10) the K^+-proton scattering and charge-exchange cross-sections are given in the limit of $\boldsymbol{\sigma} \cdot \boldsymbol{k}$ coupling for the pseudoscalar terms and with perturbative approximation by:

$$(12)\quad \sigma(K^+ p\text{-}K^+ p) = \pi g_2^4 \frac{1 + a^4 \cdot (k^4/m_K^4)}{[M_Y - M_N + \omega(k)]^2},$$

$$(13)\quad \sigma(K^+ n\text{-}K^0 p) = \frac{2\pi}{m_K^2} \frac{g_1^2 g_2^2 k^2 \cdot (1 + a^2)}{[M_Y + \omega(k) - M_N]^2}.$$

It is evident that by putting $a \leqslant 1$, while the K^+-proton scattering cross-section is practically flat up to energies for which $k \geqslant m_K$, the charge-exchange cross-section is increasing with k^2. This fact can be considered in agreement with experimental data as far as only these two processes are considered. If instead the K^+-neutron cross-section is examined in this approximation one finds, according to (10):

$$\sigma(K^+ n\text{-}K^+ n) = 4 \cdot \sigma(K^+ p\text{-}K^+ p)$$

contrarily to the experimental results. Should we have deduced similar formulae to (12) and (13) by starting from (11) instead of (10), the K-neutron cross-section should have depended on a P-wave and then should have increased more rapidly than the charge-exchange. Similar results can be obtained also by starting from (9) instead of (8).

From this discussion one can see that there are not sufficient degrees of freedom in the preceding Hamiltonians to account for all the data.

A possibility for further differentiation of the interaction constants may be perhaps obtained in the framework of the scheme proposed by one of us ([10]) in which T conservation is assumed to hold only for pion interactions while for neutral and charged K interactions two other quantum numbers (ω_3 for neutral K's and ζ_3 for charged K's) are conserved. If now these conservation laws are postulated one can easily put different values for the interaction constants in the Hamiltonian (7) of reference ([10]) without disturbing these conservations. Thus with the further assumption (7) of the preceding paper one could obtain an expression of the type:

$$H_{\text{int}} = g_1 \bar{n} \Gamma_1 \Lambda^0 K^0 + g_2 \bar{n} \Gamma_2 \Sigma^0 K^0 + g_3 \bar{p} \Gamma_2 \Lambda^0 K^+ + g_4 \bar{p} \Gamma_4 \Sigma^0 K^+ + \\ + g_\Sigma \bar{n} \Gamma_5 \Sigma^- K^+ + \text{c. c.} \tag{14}$$

where, with an adequate choice of the parities of the different terms and of interaction constants it should be possible to fit the main data.

However, the necessity of introducing so many independent parameters with not sufficient experimental data to test them appears so unsatisfactory that we should rather prefer to look for some quite different possibility of interpretation.

The simplest way left is then to consider a direct two-K interaction process, that is a simultaneous emission or absorption of two K-mesons by a nucleon. That such a kind of interaction should exist seems very probable from the experimentally obtained associated production of K and $\overline{\text{K}}$ at high energies. If now, we further assume according to PAIS that neutral and charged K's are of opposite parity, then the desired general behaviour of the total cross-sections can in some sense be easily obtained in first approximation. In fact, owing to the parity requirements, the two K interaction is, in the case of charged K's, of a scalar type, *i.e.*

$$H_{\text{int}} = \frac{g(4\pi)^{\frac{1}{2}}}{m_K} (\bar{p} p \overline{K}^+ K^+ + \bar{n} n \overline{K}^+ K^+) , \tag{15}$$

and in the case of a charged and a neutral K, of pseudovector type:

$$H_{\text{int}} = \frac{f(4\pi)^{\frac{1}{2}}}{m_K^2} (\bar{p} n \boldsymbol{\sigma} \times \text{grad} (\overline{K}^0 K^+) + \text{c.c.}) , \tag{16}$$

K^+-proton and K^+-neutron scattering differential and total cross-sections are

then obtained in first approximation only with (15) and turn out to be:

$$(17) \quad \frac{d\sigma}{d\Omega}\left(K^+ + \begin{matrix} p \\ n \end{matrix} \to K^+ + \begin{matrix} p \\ n \end{matrix}\right) = \frac{g^2}{m_K^2}, \qquad \sigma\left(K^+ + \begin{matrix} p \\ n \end{matrix} \to K^+ + \begin{matrix} p \\ n \end{matrix}\right) = 2\,\frac{g^2}{m_K^2},$$

while charge-exchange differential and total cross-sections according to (16) are given by:

$$(18) \quad \frac{d\sigma}{d\Omega}(K^+ + n \to K^0 + p) = \frac{f^2}{m_K^4} k^2 (1 - \cos\vartheta), \qquad \sigma(K^+ n \to K^0 p) = \frac{2f^2}{m_K^4} k^2.$$

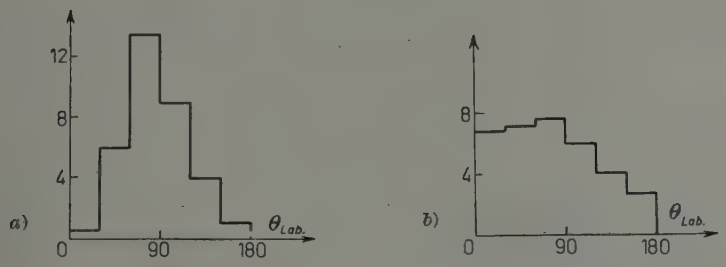

Fig. 18. – *a*) Expected distribution for θ_{lab} of charge exchange with $\sigma(\theta) = 1 - \cos\theta$. *b*) Distribution *a*) smeared for angles θ_2:

These scattering cross-sections remain constant for all energies as seems in fact to be required by the data on high energy scattering ([11]); moreover, as the interaction is of the first order, the sign of the interaction constant may be adapted to fit the sign of the potential.

The charge-exchange cross-section increases with the square of the momentum and is therefore compatible with the experimental evidence. Even its angular dependence of the type $(1 - \cos\vartheta)$ gives a behaviour in qualitative agreement with measurements (Fig. 18 *a* and *b*).

In such an approximation, however, the cross-sections of K-proton and K-neutron scattering turn out to be equal, unless one takes account of higher order diagrams (such as those of Fig. 19) whose consideration, however, should spoil the elementary and straightforward character of the assumptions.

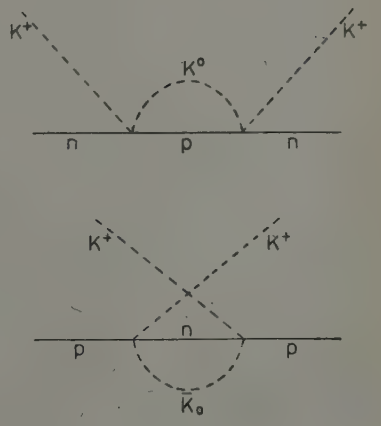

Fig. 19.

([11]) H. C. Burrowes, D. O. Caldwell, D. H. Frisch, D. A. Hill, D. M. Ritson and R. A. Schluter: *Phys. Rev. Lett.*, 2, 117 (1959).

We should therefore conclude that in first approximation this interpretation with a two K interaction does not appear to be worse than most of the other approaches proposed up to now; but this, of course, is far from solving the complicate problem of explaining the general features of the K nucleon interactions.

RIASSUNTO

Un'analisi dettagliata dei dati rigurdanti la reazione di scambio carica $K^+ + n \to K^0 + p$ è stata fatta con lo scopo di ottenere qualche indicazione sull'andamento con l'energia della sezione d'urto totale e sulla distribuzione angolare della sezione d'urto differenziale. È stato trovato che i dati attualmente a disposizione, corretti per tutti gli effetti nel nucleo, indicano che la sezione d'urto totale cresce approssimativamente con la terza potenza dell'impulso nel centro di massa. Un'analisi dai rami secondari degli eventi K-nucleo fornisce anche un'indicazione che, nell'evento studiato, sono preferiti piuttosto i grandi angoli. Questi risultati sembrano in disaccordo con le formule teoriche basate sull'interazione $KK\pi$. Alla fine sono state discusse ulteriori interpretazioni teoriche con lo scopo di cercare di spiegare gli andamenti sperimentali delle sezioni d'urto di scambio carica.

IL NUOVO CIMENTO Vol. XIII, N. 4 16 Agosto 1959

Nuclear Interaction of Heavy Primary Cosmic Radiation.

P. L. Jain

Department of Physics, University of Buffalo - Buffalo, N.Y.

(ricevuto l'11 Maggio 1959)

Summary. — In a stack of 30 nuclear emulsions exposed to cosmic radiation near the geomagnetic equator, 65 tracks of heavy primary nuclei were located. Out of the total 65 tracks of heavy nuclei, 24 exhibited interactions with the nucleons of the emulsion. In 10 of these 24 interactions primary particles break up into fragments of charge —2. The charge of these particles is determined by δ-ray counting and from gap length distribution while the energy per nucleon is found from the relative scattering method and from the opening angle of the fragments.

1. – Introduction.

In part of a stack of nuclear emulsions, 4 inch by 6 inch Ilford G-5 pellicles 400 μm thick, exposed to cosmic radiation near the geomagnetic equator we have observed interactions of some heavy nuclei of primary cosmic radiation. These events were found during regular scanning for an investigation on the charge spectrum of primary cosmic radiation at the top of the atmosphere near the equator.

All the emulsions were scanned along a line parallel to the top edge and on both sides about 1 cm from the edge. All heavy nuclei crossing the scanning line having a projected length of at least 2 mm per plate were accepted and followed through until they left the stack or interacted. If a heavy fragment emerged from an interaction, this fragment was also followed. 65 tracks of heavy nuclei were located which met the above criterion, out of which 24 tracks exhibited interactions.

In general, the interaction of heavy nuclei with the bombarded target nucleus of the emulsion, may be classified into three types.

a) The heavy nucleus, having split up the target nucleus, continues without loss of charge.

b) Part of the incoming nucleus may be sheared off in the collision. The remaining nuclear matter proceeds either as a compact nucleus of reduced charge or is partially or completely dissociated in a narrow shower of penetrating relativistic protons, α-particles and heavy fragments.

c) The heavy nucleus is completely destroyed; this may produce α-particles and a number of shower particles containing protons and mesons collimated in the direction of the incident heavy primary. The target nucleus gives an evaporation star.

It appears that events of type *a*) and *b*) are produced most probably in a glancing collision, where the incoming nucleus does not receive much excitation. In this case there is a greater probability for the occurence of heavier fragments, as there will not be much chance of energy being distributed among the constituent nucleons. Events of type *c*) are produced in a more direct collision with the target nucleus. It is the amount of overlap of nuclear radii which determines the fragmentation probability in an interaction, the more complete the overlap, the more complete the disintegration of the incoming nucleus. Also it appears that the events of type *a*) in which the incident heavy nucleus appears to continue with no loss of charge and of type *b*) in which the fragments of the primary appear with no loss of charge, and with no visible recoil in star production, are really produced by the same physical mechanism and are most probably due to stripping of extended neutrons of either the target or the incident nucleus.

2. – Description of events.

Out of the total 24 events showing interaction one event belongs to type *a*) which makes further secondary interaction and comes under type *b*); 10 events belong to type *b*) and the remaining 14 events to type *c*). In this paper we shall discuss events of type *a*) and *b*) only. Out of 10 events of type *b*) only 8 were considered suitable for analysis and are tabulated in Table I. Out of these 8 events there is one event B_8 in which a primary carbon nucleus breaks up into 3 α's with no sign of star prongs or visible recoil of target nucleus, and thus a charge balance is obtained between the incoming nucleus and its products. We shall call this event a «perfect break-up». Event B_6 is of type *a*) in which a Si nucleus interacts with the target nucleus of the emulsion, the

TABLE I.

Event no.	Primary	Shower particles	Energy from scattering GeV/nucl.	Energy from opening angle GeV/nucl.
B_1	^{12}Mg	$^{9}F + \alpha$ $^{9}F \rightarrow {}^{3}Li + 3\alpha$	12.5	13.4
B_2	^{10}Ne	2α	7.6	9.5
B_3	^{7}N	3α	18.8	17.2
B_4	^{13}A	$^{6}C + 2\alpha$	9.0	10.5
B_5	^{5}B	2α	15.9	17.2
B_6	^{14}Si	5α	11.8	12.0
B_7	^{8}O	4α	8.5	8.9
B_8	^{6}C	3α	13.5	12.1

latter giving a star while the incident Si nucleus appears to continue with no loss of charge. After travelling a distance of about 2 cm in the emulsion it further breaks up into 5 α's.

In the case of event B_7, the primary oxygen nucleus interacts with the hydrogen nucleus of the emulsion and is fragmented into 4 α's and one singly charged track (proton) that was observed at an angle much wider than that containing the jet of fast break up fragments, and that is considered to be the recoil proton. In event B_4, a nucleus of aluminum interacts with the target nucleus and breaks up into 2 α's and a carbon nucleus. The carbon nucleus passes through the whole stack without any further interaction. In events B_2 (Ne), B_3 (N) and B_5 (B) the primary nucleus breaks up into 2 α's, 3 α's and 2 α's respectively, and in each case there were a number of shower particles. In event B_2 one of the α's makes a further interaction and produces a number of shower particles. Another set of small numbers of shower particles was also observed just below the track of the non-interacting α-particle, but in the same direction in which the incident particle was moving. It was apparently due to some neutral particle, perhaps to a neutron separated from the incident nucleus at the interaction of incident heavy primary with the target nucleus of the emulsion. In event B_1 a sodium nucleus breaks up into fluorine and α particle. The fluorine nucleus further breaks up into lithium and 3 α particles with a number of evaporation tracks from the target nucleus.

3. – Charge determination.

A basic problem in nuclear emulsion work with heavy nuclei is to find reliable methods of assigning charges to the primary particles. We have measured charges by two statistically independent methods.

3·1. *δ-ray counting.* – Since the cut-off energy at the equator is greater than 7 GeV per nucleon, all the primary heavy particles entering from the outside have relativistic velocities and their identification is possible by determining δ-ray density.

In calculating δ-rays one has to be careful about the spurious δ-ray density, which arises partly from electron tracks randomly distributed throughout the emulsion and partly from chance configuration of background grains which are interpreted by the observer as δ-rays. The most satisfactory way to set a criterion is to make use of the fact that, in some collisions of fast heavy nuclei with single nucleons in the emulsion, the incident nucleus breaks up completely into singly and doubly charged particles so that it is possible in principle to find the charge of the incident nucleus by adding up the charges of the fragments. However, if one or more of the fragments are singly-charged it is possible that they come from the struck nucleus or that they are mesons produced in the collision. So in a reliable calibration event, all the fragments should be α-particles or heavier nuclei. We have found one such event, B_8, in which a carbon nucleus breaks up into 3 α's only. Fast α-particles were recognized from grain density measurements. All electron tracks containing four or more grains and apparently originating from the track of the primary are counted as δ-rays. For an equatorial stack flown at high altitude, N_δ, the δ-ray density per 100 μm, is given by the relation

$$N_\delta(Z) = aZ^2 + b \,, \tag{1}$$

where b is back ground δ-ray density and a is a constant such that aZ^2 gives the true δ-ray density of charge Z per 100 μm. The background density is not negligible for light tracks and is determined by comparing δ-ray densities of long tracks of relativistic α-particles with δ-ray densities of minimum ionization tracks. The δ-ray density of α-particles is $N_\delta(2) = 0.48$ (δ-rays/100 μm) and of minimum ionization tracks is $N_\delta(1) = 0.27$ (δ-rays/100 μm). Since the true δ-ray density of relativistic α-particles corrected for background must be four times greater than the corrected δ-ray density of minimum ionization tracks, the best relation for the determination of charge from δ-ray count is given as

$$N_\delta(Z) = 0.07\,Z^2 + 0.20 \ \text{(δ-rays/100 μm)} \,. \tag{2}$$

We have used the δ-ray density of event B_8 ($C \rightarrow 3$ α's) as another calibration point to check the relation in equation (2). The measured δ-ray density of event B_8 is 2.69 δ-rays per 100 μm while the above relation in equation (2) gives a value of 2.72 δ-rays per 100 μm.

For higher Z-values, it is not quite safe to use the direct extrapolation relation of δ-ray density as given by equation (2). In Fig. 1, we have shown the δ-ray density relation for different values of Z as measured experimentally

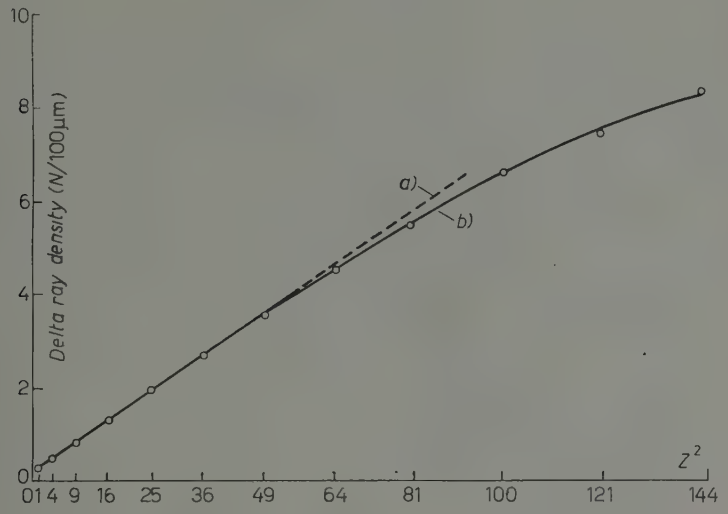

Fig. 1. – δ-ray density *versus* square of the nuclear charge Z. Curve (*a*) is given from the relation $N_\delta = 0.07Z^2 + 0.20$. Curve (*b*) is given from the gap length distribution in tracks of individual relativistic particles.

(curve (*b*)) from tracks whose charge was determined from gap length distribution (discussed below) as well as from charge conservation from break up events and as calculated (curve (*a*)) by the above relation in equation (2).

3·2. *Gap length distribution measurements.* – In order to cross-check the value of charge determination we have used another method based on gap counting and gap length measurements. The length of a gap is the distance between the inside edges of the develop grains. It was shown first by O'Ceallaigh [1] that the distribution in the length of gaps was exponential. Fowler *et al.* [2] showed later that the gap length distribution can be expressed by the formula

$$G_l = g \exp[-g(\alpha + l)], \tag{3}$$

---

(1) C. O'Ceallaigh: *CERN Report* B.S. 11 (1954).
(2) P. H. Fowler and D. H. Perkins: *Phil. Mag.*, **46**, 587 (1955).

where G_l is the density of gaps with length greater than l, α is the average diameter of developed grains, g is a characteristic parameter specifying the ionization that can be obtained by the following formula

$$g = \frac{1}{l_2 - l_1} \log_l \frac{G_{l_1}}{G_{l_2}}. \tag{4}$$

The slope (g) of this distribution is equal to the reciprocal of the average gap length. The choice of l in equation (3) and (4) is important and it is best if l is chosen between 2 and 3 times the mean gap size, $1/g$. Let us consider the expression

$$G_0 = g \exp[-g\alpha]. \tag{5}$$

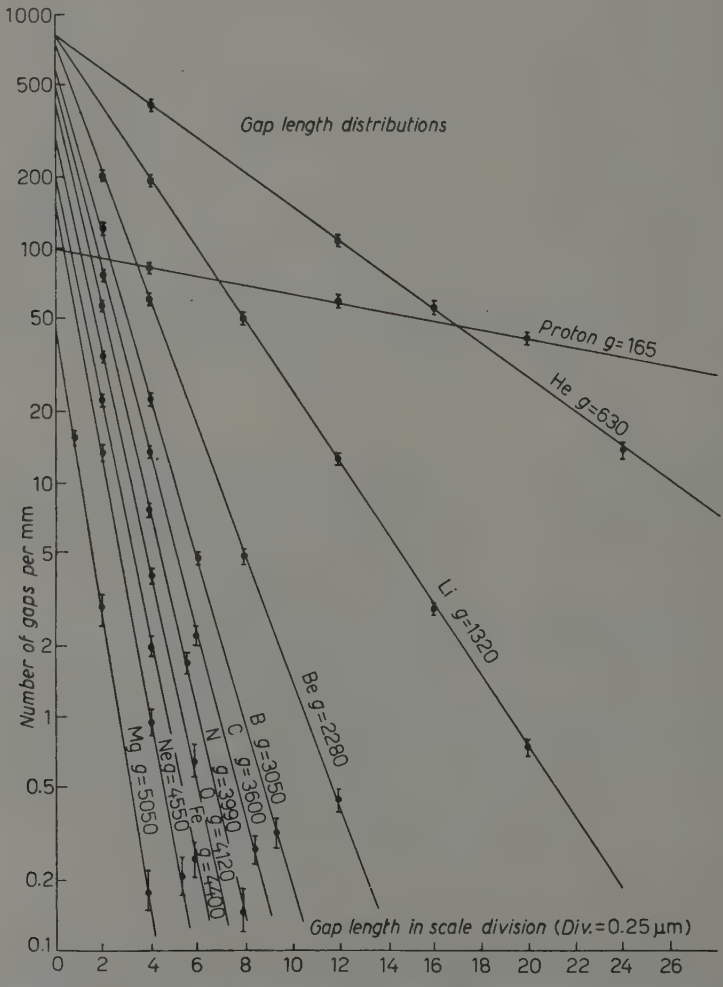

Fig. 2. – Integral gap length distribution in tracks of relativistic cosmic ray particles of different charges.

This is the formula for $l = 0$, *i.e.* for the density distribution of all the resolvable gaps, so that $G_0 = B$, the blob density, the density G of gaps exceeding length l being then given from equations

$$G_l = B \exp[-gl] . \tag{6}$$

This expression is sufficiently accurate for finding the g value if the number of blobs counted is more than about four times the number of large gaps.

Fig. 2 shows the integral gap length distribution observed in the relativistic cosmic ray particles of different charges. The measurements were made on individual flat tracks of particles by means of a microfiler-meter. The lengths of gaps were chosen as an integral multiple of 0.25 μm. If the track dips at an angle θ to the plane of the emulsion, the projected gap length l, as observed in the eye piece, is related to the true length l_t, by $l_t = l \sec\theta$, and in that case the value of g is again given by equation (4) if we multiply it by a factor (2) $\cos\theta$. For our distribution in Fig. 2 we have chosen all flat tracks. For longer gaps the whole track was used whereas for the short gaps only a part of the track was used. Within the limits of experimental errors, the distributions shown in Fig. 2 are exponential. The slopes of all the curves are proportional to the reciprocal of their respective average gap lengths and both these quantities are proportional to Z^2. In Fig. 3, we have plotted g, the exponent of the gap length distribution for relativistic heavy primaries, against Z^2. We see that g tends to a limit as Z increases and hence the specific ionization of the particle becomes very large and the limiting value of g is about 5000/mm. So we see that good charge resolution is possible in the region $1 \leqslant Z \leqslant 9$. If we want to identify an unknown particle for its charge determination, we have to find out its mean gap length, which is equal to $1/g$. To obtain the most accurate value one should measure the length of each individual gap along the track, but this is a very slow and tedious process.

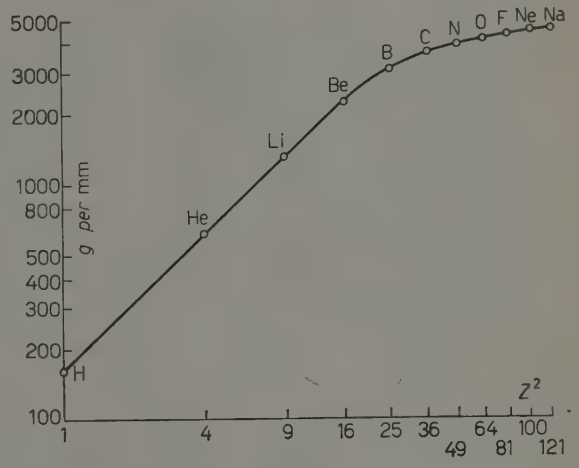

Fig. 3. – The measured values of the coefficient g, observed on individual relativistic particles, plotted against the square of the nuclear charge Z.

Instead we can use either equation (4) or (6). The error involved in finding out the g value by equations (4) or (6) is not greater (2) and this is a very quick method.

4. – Energy determination.

To determine the energy of a fast relativistic particle through nuclear emulsion techniques is a very difficult problem. Multiple scattering techniques will give a wrong value on account of spurious scattering. But here we are dealing with events in which the heavy nucleus breaks up into two or more α-particles or heavier fragments. So one can use track-to-track scattering measurements for finding the energy per nucleon of the primary heavy particles. We have used the following two independent methods for measuring the energy of primary particles.

i) Relative scattering measurements.

ii) Opening angle of the α-particle showers.

One has to be a little careful in the use of method i) for finding out the energy per nucleon of the primary particle, as the effect of spurious scattering and of the distortion in the emulsion cannot be neglected completely. We selected only those events as suitable for this type of measurement which have a distance between the two tracks of not more than 40 μm in any direction. The noise was eliminated by making two sets of measurements on each track with a displacement of 100 μm. The energy values were derived by using the scattering constant $k = 32$ and are given in Table I.

The second independent method used for finding out the energy of the primary particle was from the angle of emission of the secondaries with respect to the direction of the primary. PETERS (3) has given a very simple relation between the angle of emission of α-secondaries and the energy of the primary particle. His formula is based on the assumption that the α-particles are emitted isotropically and with a mean energy of 10 MeV in the center of mass, system. Recently (4) it has been pointed out that the mean energy of the α-particles in the center of mass system increases with the charge of the primary particle and consequently the relation between the energy of the primary particle and the root-mean-square angle, which the nuclear fragments

(3) M. F. KAPLON, B. PETERS, G. T. REYNOLDS and D. RITSON: *Phys. Rev.*, **85**, 295 (1952).

(4) P. H. FOWLER, R. R. HILLIER and C. J. WADDINGTON: *Phil. Mag.*, **2**, 293 (1957).

make with the direction of the incident primary in the laboratory system, as first given by PETERS is modified [5] for different types of nuclei and is written as

$$(7) \qquad \langle\theta_\alpha^2\rangle^{\frac{1}{2}} = \frac{0.050 \pm 0.006}{E}, \qquad \text{for } Z < 6,$$

$$\langle\theta_\alpha^2\rangle^{\frac{1}{2}} = \frac{0.055 \pm 0.006}{E}, \qquad \text{for } 6 \leqslant Z \leqslant 9,$$

$$\langle\theta_\alpha^2\rangle^{\frac{1}{2}} = \frac{0.060 \pm 0.006}{E}, \qquad \text{for } Z \geqslant 10,$$

where $E =$ total energy per nucleon in GeV of the incident nuclei. The above relations are true only in the case of many α-particles, while for the case of a few fragments they will give rise to large fluctuations over the true energy values. Although scattering measurements give the most reliable energy values, yet, as shown in Table I, the difference in the energy values between scattering measurements and the opening angle method is very small in events B_6 and B_7 where there are more fragments than in events B_2, B_5, and B_4 where there are less fragments. One can also determine the value of the energy per nucleon of the primary particle from the angular distribution of shower particles which are produced in the secondary interaction of α-fragments, and will be discussed in paper II.

5. – Conclusion.

We have shown that for determination of the charge of each individual heavy particle one should always use more than one independent method. For relativistic particles, we have used two methods, δ-ray counting and gap length distribution. We also used one independent calibration point from the « perfect break-up » event of a carbon nucleus. It is shown that for higher Z values ($Z > 6$ or 7), the straightforward extrapolation of the δ-ray curve alone is not completely dependable. One can extend these methods of δ-ray counting and gap length distributions at the most up to $Z \sim 10$ or 11. Relative scattering is the most reliable method for finding the energy of relativistic heavy primary, when the primary breaks up into fragments of charge equal to or greater than two.

---

[5] P. L. JAIN, E. LOHRMANN and M. W. TEUCHER: (*Phys. Rev.*) in press.

* * *

We thank Drs. K. E. DAVIS, N. M. DULLER and C. A. RANDALL for sharing with us their plates which were exposed near Guam. We are also very greatful to Dr. E. KERNER of this department for reading the manuscript.

RIASSUNTO (*)

In un pacco di 30 emulsioni nucleari esposte alla radiazione cosmica in prossimità dell'equatore geomagnetico si sono identificate 65 tracce di nuclei primari pesanti. Sul totale di 65 tracce, 24 mostravano interazioni coi nucleoni dell'emulsione. In 10 di queste 24 interazioni le particelle primarie si spezzano in frammenti di carica -2. Si determina la carica di queste particelle col conteggio dei raggi δ e dalla distribuzione della lunghezza dei gap, mentre l'energia per nucleone si trova col metodo dello scattering relativo e dall'angolo di apertura dei frammenti.

(*) *Traduzione a cura della Redazione.*

LETTERE ALLA REDAZIONE

(La responsabilità scientifica degli scritti inseriti in questa rubrica è completamente lasciata dalla Direzione del periodico ai singoli autori)

Collective Excitations of Fermi Gases.

J. GOLDSTONE (*) and K. GOTTFRIED (**)

Universitetets Institut for Teoretisk Fysik - København

(ricevuto il 14 Maggio 1959)

In recent years a rather formidable array of successful but apparently distinct theories of collective motions in Fermi gases have been proposed (1). That most of these methods are actually equivalent within the approximations used can be surmised from the fact that they usually yield identical answers. It is our purpose here to point out that many of the results previously obtained can be retrieved from an approach which is completely elementary (2). The price which must be paid for this simplicity is lack of generality; in particular, the damping of the collective motion is completely beyond the power of this method. We should like to warn the reader at the outset that we have no new results to report, and that the following is, at the very most, a pedagogic contribution to the subject.

Our treatment is based on the time-dependent Hartree-Fock equation. Let $\varrho(t)$ be the density matrix, and $H[\varrho]$ the Hartree-Fock Hamiltonian,

$$\langle q|H[\varrho]|q'\rangle = \langle q|T|q'\rangle + \int \langle qq''|v|q'q'''\rangle \langle q'''|\varrho(t)|q''\rangle \, \mathrm{d}q'' \, \mathrm{d}q''' ,$$

with T the kinetic energy, $\langle qq''|v|q'q'''\rangle$ the antisymmetrized matrix element of the interparticle potential v, and q, q', ... complete sets of single-particle quantum numbers. The equation of motion reads

$$i\frac{\partial}{\partial t}\varrho(t) = [H[\varrho], \varrho(t)] . \tag{1}$$

(*) Present address: CERN, Geneva.

(**) Present address: Physics Dept., Harvard University, Cambridge, Mass.

(1) D. BOHM and D. PINES: *Phys. Rev.*, **92**, 609 (1953); K. SAWADA, K. A. BRUECKNER, N. FUKUDA and R. BROUT: *Phys. Rev.*, **108**, 507 (1957); J. HUBBARD: *Proc. Roy. Soc.*, A **240**, 539 (1957); **243**, 336 (1957); L. D. LANDAU: *Žurn. Eksp. Teor. Fiz.*, **32**, 59 (1957); V. M. GALITSKIJ and A. B. MIGDAL: *Žurn. Eksp. Teor. Fiz.*, **34**, 139 (1958).

(2) After this manuscript was prepared we were shown a preprint by H. EHRENREICH and M. H. COHEN (submitted to *Phys. Rev.*) which also discusses this method and its application to solid-state physics. We should also point out that many of the concepts used by us were previously discussed by J. LINDHARD: *Dan. Mat. Fys. Medd.*, **28**, no. 8 (1954).

The ground state of the system Ψ_0 has the stationary density matrix

$$\varrho_0 = \sum_{n.\,\mathrm{occ.}} |n\rangle\langle n|, \qquad H[\varrho_0]\,|n\rangle = E_n\,|n\rangle\,.$$

Suppose that the system is subjected to an arbitrarily weak external field $W(t)$ which results in the perturbation $\varrho_0 \to \varrho_0 + \varrho_1(t)$, with $\varrho_1(t)$ extremely small. Eq. (1) can therefore be linearized with respect to $\varrho_1(t)$ and $W(t)$. We immediately find that $\varrho_1(t)$ obeys

$$(2)\quad \left[i\frac{\partial}{\partial t} - (E_n - E_{n'})\right]\langle n\,|\,\varrho_1(t)\,|\,n'\rangle = \\ = [\theta(n') - \theta(n)]\Big[\sum_{mm'}\langle nm\,|\,v\,|\,n'm'\rangle\langle m'\,|\,\varrho_1(t)\,|\,m\rangle + \langle n\,|\,W(t)\,|\,n'\rangle\Big]\,,$$

with $\theta(n)=1$ if $|n\rangle$ is occupied in Ψ_0, and zero otherwise.

If the system is extremely large the $|n\rangle$'s are momentum eigenstates $|\boldsymbol{k}\rangle$, and $E_k = (k^2/2m) + V_{\mathrm{ex}}(k)$, with $V_{\mathrm{ex}}(k)$ the one-particle potential arising from the exchange energy. The assumption that v and W are spin-independent local potentials, together with the neglect of the exchange term, reduces (2) to

$$(3)\quad \left[i\frac{\partial}{\partial t} - (E_{\boldsymbol{k}} - E_{\boldsymbol{k}+\boldsymbol{q}})\right]\langle \boldsymbol{k}\,|\,\varrho_1(t)\,|\,\boldsymbol{k}+\boldsymbol{q}\rangle = \\ = [\theta(\boldsymbol{k}) - \theta(\boldsymbol{k}+\boldsymbol{q})]\,\{W_{\boldsymbol{q}}(t) + g\,v(q)\sum_{\boldsymbol{k}'}\langle \boldsymbol{k}'\,|\,\varrho_1(t)\,|\,\boldsymbol{k}'+\boldsymbol{q}\rangle\}\,,$$

where g is the spin-degeneracy.

Putting $W(t) = W\exp[-i\omega t] + \text{h.c.}$, $\varrho_1(t) = \varrho_1 \exp[-i\omega t] + \text{h.c.}$, $\omega > 0$, in (3), we find that

$$(4)\quad \mathrm{Tr}\,(W^{+}\varrho_1) = |W_q|^2\,\frac{S(q\omega)}{1 - g\,v(q)\,S(q\omega)}\,,$$

with

$$S(q\omega) = 2\sum_{\boldsymbol{k}}\frac{\theta(\boldsymbol{k}+\boldsymbol{q})[1-\theta(\boldsymbol{k})]\,(E_{\boldsymbol{k}} - E_{\boldsymbol{k}+\boldsymbol{q}})}{\omega^2 - (E_{\boldsymbol{k}} - E_{\boldsymbol{k}+\boldsymbol{q}})^2}\,.$$

The physical content of eq. (4) can be understood from the following considerations which are independent of the Hartree-Fock approximation. To first order in W the state we are dealing with is

$$\Psi(t) = |0\rangle + \sum_{a\neq 0}|a\rangle\left\{\frac{\langle a\,|\,W\,|\,0\rangle}{\omega - E_a + i\varepsilon}\exp[-i\omega t] - \frac{\langle a\,|\,W^{+}\,|\,0\rangle}{\omega + E_a}\exp[i\omega t]\right\}\,,$$

where $|0\rangle$, $|a\rangle$, are the *exact* eigenstates of the system with excitation energies E_a. Again writing

$$|\Psi(t)\rangle\langle\Psi(t)| = \varrho_0' + (\varrho_1'\exp[-i\omega t] + \text{h.c.}) + 0(W^2)\,,$$

we have

$$(4') \qquad \mathrm{Tr}\,(W^{+}\varrho_1') = \sum_{a\neq 0}\left\{\frac{|\langle a|W|0\rangle|^2}{\omega - E_a + i\varepsilon} - \frac{|\langle 0|W|a\rangle|^2}{\omega + E_a}\right\} \equiv R(\omega)\,.$$

Therefore the poles of $R(\omega)$ give the excitation energies of the system, while

$$-2\,\mathrm{Im}\,R(\omega) = 2\pi\sum_{a\neq 0}|\langle a|W|0\rangle|^2\,\delta(\omega - E_a)\,,$$

is the response, i.e. the total transition probability out of $|0\rangle$ induced by W. As is well known [3], the integral of the response over ω gives the pair correlation function in $|0\rangle$, and therefore this method enables us to find the total energy in the ground state. In fact, (4′) is simply the Feynman propagator

$$-i\int_{-\infty}^{\infty}\langle 0|\,T\left(\exp\left[iHt\right]W^{+}\exp\left[-iHt\right],\,W\right)|0\rangle\,\exp\left[i\omega t\right]\mathrm{d}t\,.$$

Comparing (4) and (4′) we now find that the resonant frequencies of the system are characterized by the momentum $\boldsymbol{q}$ and are the solutions of the secular equation

$$(5) \qquad 1 - g\,v(q)\,S(q\omega) = 0\,.$$

This is precisely the eigenvalue condition discovered by HUBBARD and SAWADA. The spectrum consists of a continuum of single-particle excitations for $|\omega| < (qv_F + q^2/2m)$, v_F being the Fermi velocity, and provided $v(q)$ is repulsive and q not too large, a further isolated root $\omega_{\mathrm{coll}}(q)$ above this continuum. If $v(q) \to q^{-2}$ as $q \to 0$ the isolated root is just the plasma frequency. On the other hand, if $v(q) \to$ const. as $q \to 0$, (short range forces),

$$(6) \qquad \omega_{\mathrm{coll}}(q) \sim qv_F(1 + 2\exp\left[-1/\lambda - 2\right])\,, \qquad \lambda = 2\pi m k_F\,g v(0)\,,$$

in the weak coupling limit ($\lambda \to 0$). This latter solution, which was discovered by LANDAU and which he calls zeroth sound, remains experimentally undetected. If the forces are spin- (or iso-spin)-dependent, the situation is somewhat more complex, because then the separation into direct and exchange terms becomes artificial. Since the collective roots are isolated (i.e., like bound states in ordinary scattering theory) a variational attack using the solutions without exchange as trial functions is feasible.

The connection with Landau's Boltzmann equation can be seen as follows. Rewrite (2) in the coordinate representation:

$$(7) \qquad i\frac{\partial}{\partial t}\langle \boldsymbol{x}|\varrho_1(t)|\boldsymbol{x}'\rangle = \left\{-\frac{1}{2m}\left(\frac{\partial^2}{\partial \boldsymbol{x}^2} - \frac{\partial^2}{\partial \boldsymbol{x}'^2}\right) + V(\boldsymbol{x}) - V(\boldsymbol{x}')\right\}\langle \boldsymbol{x}|\varrho_1(t)|\boldsymbol{x}'\rangle +$$
$$+\langle \boldsymbol{x}|\varrho_0|\boldsymbol{x}'\rangle\int\{v(\boldsymbol{x}-\boldsymbol{y}) - v(\boldsymbol{x}'-\boldsymbol{y})\}\langle \boldsymbol{y}|\varrho_1(t)|\boldsymbol{y}\rangle\,\mathrm{d}^3y\,,$$

---

[3] W. HEISENBERG: *Phys. Zeits.*, **32**, 737 (1931); A. AHIEZER and I. POMERANČUK: *Journ. Phys. USSR*, **11**, 167 (1947); G. C. WICK: *Phys. Rev.*, **94**, 1228 (1954); L. VAN HOVE: *Phys. Rev.*, **95**, 249 (1954); D. PINES and P. NOZIÈRES: *Nuovo Cimento*, **9**, 470 (1958).

where $V(x)$ is the ground state's self-consistent potential, and exchange terms are again deleted. Let $\boldsymbol{x}-\boldsymbol{x}'=\boldsymbol{\xi}$, $2\boldsymbol{r}=\boldsymbol{x}+\boldsymbol{x}'$, $\langle\boldsymbol{x}|\varrho|\boldsymbol{x}'\rangle=\varrho(\boldsymbol{r},\boldsymbol{\xi})$, and $\varrho(\boldsymbol{r},\boldsymbol{k})=\int\exp[-i\boldsymbol{k}\cdot\boldsymbol{\xi}]\cdot\varrho(\boldsymbol{r},\boldsymbol{\xi})\,\mathrm{d}^3\xi$. The Fourier transform of the last term of (7) then reads

$$(8)\quad (2\pi)^{-3}\int\exp[i\boldsymbol{p}\cdot\boldsymbol{r}-\boldsymbol{r}']v(p)\left\{\varrho_0(\boldsymbol{r},\boldsymbol{k}-\tfrac{1}{2}\boldsymbol{p})-\varrho_0(\boldsymbol{r},\boldsymbol{k}+\tfrac{1}{2}\boldsymbol{p})\right\}\varrho_1(\boldsymbol{r}',\boldsymbol{p}',t)\,\mathrm{d}^3p\,\mathrm{d}^3r'\,\mathrm{d}^3p'\simeq$$

$$\simeq i(2\pi)^{-3}\int\exp[i\boldsymbol{p}\cdot\boldsymbol{r}-\boldsymbol{r}']v(p)\frac{\partial}{\partial\boldsymbol{r}'}\varrho_1(\boldsymbol{r}',\boldsymbol{p}',t)\cdot\frac{\partial}{\partial\boldsymbol{k}}\varrho_0(\boldsymbol{r},\boldsymbol{k})\,\mathrm{d}^3p\,\mathrm{d}^3r'\,\mathrm{d}^3p'\,.$$

If the motion is such that only wavelengths large compared to the range of v and the interparticle distance enter, and if $V(x)$ is assumed to be slowly varying, (7) and (8) may be simplified to the transport equation

$$(9)\quad \frac{\partial}{\partial t}\varrho_1(\boldsymbol{r},\boldsymbol{k},t)=\left(-\frac{\boldsymbol{k}}{m}\cdot\frac{\partial}{\partial\boldsymbol{r}}+\frac{\partial V}{\partial\boldsymbol{r}}\cdot\frac{\partial}{\partial\boldsymbol{k}}\right)\varrho_1(\boldsymbol{r},\boldsymbol{k},t)+$$

$$+v(0)\frac{\partial}{\partial\boldsymbol{k}}\varrho_0(\boldsymbol{r},\boldsymbol{k})\cdot\frac{\partial}{\partial\boldsymbol{r}}\int\varrho_1(\boldsymbol{r},\boldsymbol{k}',t)\,\mathrm{d}^3k'\,.$$

Note that for the infinite system in the long wavelength limit (9) is an exact consequence of (3), and therefore Landau's apparently semi-classical treatment is equivalent to the other methods referred to. The solution of (9) in the infinite case is

$$(10)\quad \varrho_1(\boldsymbol{r},\boldsymbol{k},t)=\exp[i(\boldsymbol{q}\cdot\boldsymbol{r}-\omega t)]\frac{\boldsymbol{k}\cdot\boldsymbol{q}\,\delta(k-k_F)}{\omega-\boldsymbol{k}\cdot\boldsymbol{q}/m}\,;$$

interpretation of (10) as a classical distribution function immediately reveals Landau's picture of the motion as a wave on the surface of the Fermi sphere.

In a recent article GLASSGOLD, HECKROTTE and WATSON [4] have employed the Sawada techniques to study collective excitations in nuclear matter. It is shown that when spin and isospin dependent forces are present collective modes can still arise even though the forces are attractive. One of these modes is related to the giant resonance in the photo-effect. It is apparent from the above that these modes are of the zeroth sound type, and are not sound waves in the ordinary sense. Unfortunately it is by no means clear that the simple results found in the infinite case retain an approximate validity in systems as small as atomic nuclei. For in a finite system the single-particle excitation spectrum does not have a sharp upper limit and so, loosely speaking, there will be « damping » of the collective motion even in this lowest order approximation. A study of the finite system can perhaps be based on the transport equation (9), which can be further simplified by taking a Thomas-Fermi distribution for ϱ_0.

* * *

We should like to thank A. BOHR and B. R. MOTTELSON for a number of helpful conversations, and Professor NIELS BOHR for the hospitality of his Institute.

---

[4] A. E. GLASSGOLD, W. HECKROTTE and K. M. WATSON: *Ann. Phys.*, **6**, 1 (1959).

IL NUOVO CIMENTO Vol. XIII, N. 4 16 Agosto 1959

On Mach's Principle.

A. Carrelli

Istituto di Fisica dell'Università - Napoli

(ricevuto il 4 Giugno 1959)

1. The fundamental principles laid down by Mach regarding the meaning of inertia and of absolute motion, summarized by Einstein in the so called *Principle of Mach*, have given rise, as is well known, to lengthy disputes. In view of the importance of the question, any experimental result giving the possibility of a verification of the deductions that may be made from the principle we are considering, is always interesting. Bearing this idea in mind, Cocconi and Salpeter [1] published a paper in which they suggest an experiment capable of proving Mach's statements. The Authors of this study refer to the very essence of the ideas of Mach. In other words, they start from the fact that we are on the Earth which is a part of the Solar System. We therefore occupy a peripheral position in respect of a great mass, that may be considered as being « local », formed by the Galaxy. Owing to this particular position, and precisely as a direct consequence of Mach's principle, the mass of a body should no longer be considered as having a scalar character, whereas a tensorial one should be attributed to it. In other words, according to the said principle, the mass of a body should vary according to whether the movement takes place in the plane of the Galaxy and towards its center, or whether it takes place in a direction at right angles with the plane in question. The Authors of the study that has been published, mention a calculation that aims at giving an estimation of the variation $\Delta m/m$ of the mass that might be met with under such conditions.

They believe that the action F of one mass M upon another might be considered as being proportional to the mass perturbing the mass being studied (the proportionality coefficient being equal to one), moreover they suggest an action inversely proportional to r^{ν}, in which the value of the value of the exponent ν is to be determined, *i.e.* $F=M/r^{\nu}$. It is assumed, of course in an entirely empiric manner, that $\nu=1$ and that $\nu=0.25$, and, for a further position, it is considered that there is a limit to the action that may arrive from distant masses; in other words, that only the action of

[1] G. Cocconi and E. Salpeter: *Nuovo Cimento*, **10**, 646 (1958).

masses contained within a sphere, having a radius R, is perceivable, when $R=cT$ (in which c stands for the velocity of light and T is the inverse to « the Hubble constant »). This magnitude R, in a particular cosmologic theory, is called « radius of the Universe ». In view of the fact that the mentioned theory admits that at a certain initial instant dating back to a certain epoch that is T time away, the entire mass of the Universe was concentrated within an extremely limited volume, and that the gravific action propagates according to a velocity c, it is evident that according to such a set of ideas the action can derive only from the mass contained within a sphere having radius R, when R stands for the radius of the sphere containing all the masses of the world that can exert an influence over a mass on the surface of the Earth. As well as the action of the said mass, which is distributed in all directions, there is the directional action producing the variabilities of m with the direction due to the Galaxy and therefore there will be $\Delta m/m$ different from zero. By means of these positions and of the modern astronomical data regarding sidereal masses it is possible to foresee, according to the value of v, one $\Delta m/m$ equal to 10^{-7} or 10^{-11} respectively for $v=0.25$ or $v=1$.

2. We think that the positions assumed are too arbitrary; however, because of the importance of the problem, the question may be studied from another point of view. In this regard, it must be noted that Mach did not express the quantitative formulation of his thought: EINSTEIN ([2]) believed that Mach's ideas were contained in the theory of generalized relativity. Indeed, by going into further detail, it might be said that the fundamental idea stating that the inertia of a body must grow when inertial masses are drawn nearer to it, is a consequence of gravitational equations ([3]). In his calculations Einstein comes to the conclusion that the effect is very small owing to the smallness of f (the gravitation constant), but he also believes that the effect is basically present, if the generalized theory is considered as being valid.

Einstein does not preoccupy himself trying to establish the law according to which a mass is varied by the presence in the Universe of other masses. In his concept the « Mach action » is already perfectly determined by the field equation. But, no matter how interesting the bulk of considerations developped by Einstein may be, in view of the great interest that a problem of the kind can present, and bearing in mind the uncertainty with which Einstein himself considers the entity of the action that may come from the masses, the best method is that of fixing the experimental limit that may be reached at present for the measuring of a $\Delta m/m$ in regards to the various directions of motion, in connection with the plane of the Galaxy

3. The Authors. mentioned at the beginning of this paper, hereby submit the plan for an experiment exploiting the phenomenon of atomic resonance, by means of the « molecular beam » method; by this method the differences between the lowest energy levels are measured with the greatest approximation. The Authors therefore believe that by means of the « molecular beam » resonance method it is possible to achieve a remarkable precision in the measurements granting the possibility of accepting a $\Delta m/m$ in the realm of 10^{-11}. We also want to add that it is possible to carry out certain experimental tests

([2]) A. EINSTEIN: *The meaning of relativity* (New York, 1955), p. 100.

([3]) W. PAULI: *Teoria della relatività* (Torino, 1958), p. 270.

of an optical character giving the possibility of attaining a high degree of precision. As a matter of fact, the expression of the index of refraction of a substance for a wavelenght region that is distant from the absorption centers might be considered, in the visible zone, as being (for instance in the case of carbon disulphide) the following:

$$(1) \qquad n^2 = 1 + \frac{Ne^2}{m(\nu_0^2 - \nu^2)} .$$

It must be noted, however, that in the above expression one term only is considered as being efficient which is the same as saying that only one absorbing center having a frequency ν_0 and a mass m is effective. For a first approximation, expressions of this kind (1) are valid, for instance, for liquids such as water, alcohol, ether in the visible zone. Having premised the above, let us take a tube, having length l, full of liquid and placed in the same plane as the Galaxy and turned at right angles with its center. Let us also have a beam of polarized light, having its electrical vector inclined at a 45° angle with the plane of the Galaxy, crossing the tube. We may therefore imagine that two different polarized waves are propagated within the tube, having one vector directed at right angles with the plane of the Galaxy and the other directed towards the center of the Galaxy. If there is a difference in the mass of the electrons in consequence of Mach's principle in the two directions, the values of m should also prove different in the two directions, and they should be precisely: m and $m(1 + (\Delta m/m))$. Consequently, the two indexes of refraction, for the two rays being propagated in two directions. shall be different and easy calculations shall result in:

$$n_1 - n_2 = \frac{1}{2} \frac{n_1^2 - 1}{n_1} \frac{\Delta m}{m};$$

depending on the value of $\Delta m/m$ there will be a value for $n_1 - n_2$. The two polarized waves in the two directions at an angle of 90° degrees travel along the tube according to two different phase velocities. And it will be possible to state precisely that at the end of the tube there will be two waves polarized along x and along y and with their vectors given by:

$$E_x = \frac{E_0}{\sqrt{2}} \sin 2\pi \left(\frac{t}{T} - \frac{ln_1}{\lambda} \right);$$

$$E_y = \frac{E_0}{\sqrt{2}} \sin 2\pi \left(\frac{t}{T} - \frac{ln_2}{\lambda} \right).$$

The difference of phase $\Delta\varphi$ is given by:

$$\Delta\varphi = 2\pi \frac{l}{\lambda} (n_1 - n_2) .$$

From this is easy to conclude that when the second nicol is oriented in the same position as the first, the intensity proceeding from it has a certain value I, and when it is oriented at 90° degrees the intensity does not take on a value equal to zero, but instead it takes on a value

$$I(\mathrm{tg}\ \psi)^2 \sim I(\psi)^2 = I \left(\frac{\Delta\varphi}{2} \right)^2 .$$

Knowing the value of $n_1 - n_2$ it is possible to determine theoretically the ratio betwenn the maximun intensity I and the minimum intensity $I(\Delta\varphi/2)^2$. To measure this ratio we should rotate, according to a given angular velocity, the whole system of the tube and nicols that we suppose to be on the plane of the Galaxy, and at right angles with one of its diameters. Because of the rotation the electrical vector of the luminous wawe is to be found, at each revolution, in the two characteristic positions, na-

mely in the plane of the Galaxy and in the perpendicular plane; under these conditions it is evident that the phenomenon of the double refraction disappears as does also, therefore, that of the ellipticity of the light emerging from the second nicol.

If the system is optically perfect, instead of the intensity I we should have zero intensity. We can then measure this periodically variable intensity.

Actually (4) it is possible, with not much difficulty, to measure $\Delta\varphi$ in the range of 10^{-6}, *i.e.* to measure values of $(n_1 - n_2)$ in the range of 10^{-8} and values of $\Delta m/m$ in the range of 10^{-7}.

While proof-reading, Prof. Persico justly reminds me that in the expression of $2\pi\nu_0 = \sqrt{K/m}$ *i.e.* of the frequency of oscillations appears again m.

Supposing at first that K is not influenced by the position of the body, Persico points out the necessity to take account of the variation depending on the presence of m.

The conclusion would be, that for $n_1 - n_2$ one has the following expression:

$$n_1 - n_2 = \frac{1}{2}\,\frac{n_1^2 - 1}{n_1}\,\frac{\Delta m}{m}\,\frac{\nu^2}{\nu_0^2 - \nu^2}\,.$$

This expression is more favourable to put in evidence the variability of the mass if, instead of using liquid, one uses vapour or gas with ν_0 in the visible region, because in that condition the new factor enhances the effect.

(4) J. Bador: *Ann. d. Phys.*, **3**, 33 (1958).

IL NUOVO CIMENTO Vol. XIII, N. 4 16 Agosto 1959

Day to Day Analysis of the Cosmic Ray Diurnal Wave in 1958.

J. F. Steljes

Physics Division, Atomic Energy of Canada Limited - Chalk River, Ontario

(ricevuto il 20 Giugno 1959)

Several cosmic-radiation stations, including the sealevel station at Deep River, Ontario, Canada, B211, are now operating neutron monitors that are sufficiently large to permit day-to-day studies of the diurnal effect. The daily amplitudes and the times of maximum of the 24 h wave for Deep River have been computed throughout 1958 and will be published elsewhere. I.G.Y. data from other stations have also been studied.

Fig. 1, 2 and 3 represent selected periods in March, June and August. The top graph in each figure shows the hourly readings of the Deep River standard neutron monitor in the form of a histogram (1). The thick line drawn through the histogram is the 24 h running average advancing hourly in which the diurnal variation and all its harmonics are suppressed. The second top graph is obtained by subtracting the 24 h running average form the 12 h running average (which retains the first harmonic of the diurnal variation diminished by a factor of $2/\pi$) and multiplying the difference by $\pi/2$. This graph provides a useful qualitative illustration of the behaviour of the diurnal wave.

The lower graphs in the figures show the amplitude and the time of maximum of the 24 h wave calculated by an electronic computer. In performing this calculation, the 24 h running average was first substracted from the raw results. Each day was then considered separately and a sine wave of period 24 h but of variable amplitude and phase was fitted by the method of least squares. Two such calculations were performed one starting the days at midnight U.T. and the other starting at noon U.T. The intermediate points obtained from the second calculation improve the continuity of the results and show the direction of trends more clearly.

The general behaviour of the diurnal wave and its well-known fluctuations of amplitudes and phase (2) are confirmed and shown in more detail. Enhanced oscillations may commence suddenly and cease suddenly. Sometimes enhancement follows a Forbush decrease as was the case on March 25, 1958, but this is by no means a general rule and, as on June 19, oscillations may begin

(1) Paper presented to the I.R.E. Canadian Convention, Toronto, October, 1958. See J. F. Steljes: *Canadian Convention Record of the I.R.E.* (1958). p. 335.

(2) A. M. Conforto and J. A. Simpson: *Nuovo Cimento*, **6**, 1052 (1957).

with no large change of the average flux. The time of the maximum at Deep River in 1958 tends to be in the early afternoon in local time whenever the (Mt. Norikura), Hermanus, Huancayo, and Resolute.

The correlation between stations is illustrated in Figs. 4 and 5 for 39 days

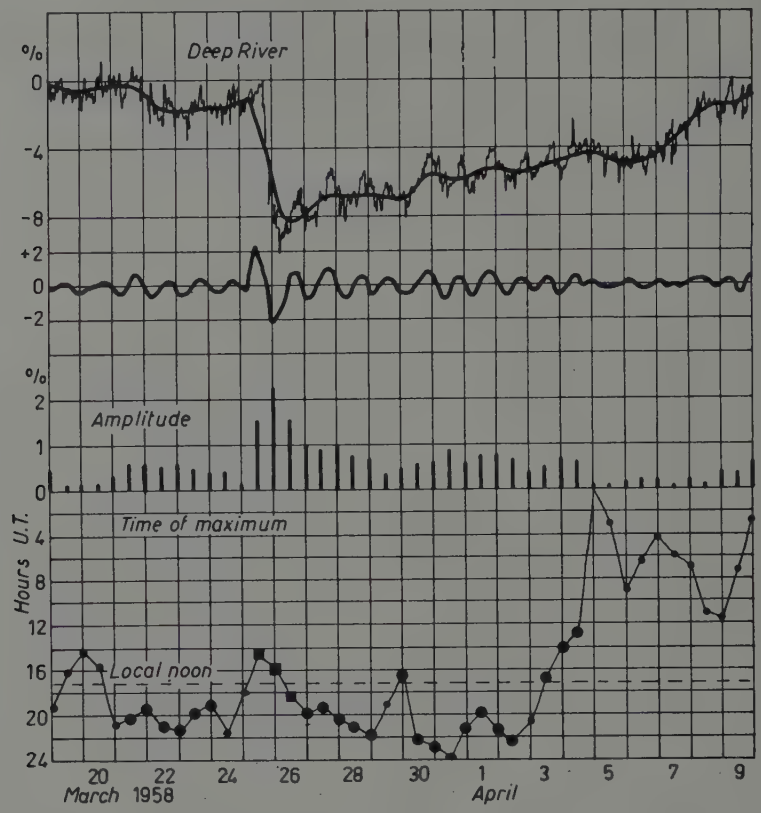

Fig. 1. – The daily variations of the Deep River standard neutron monitor showing enhanced diurnal variations following the Forbush decrease on March 25, 1958. The top graph shows the hourly barometer corrected results in the form of a histogram. The 24 h running average is shown as a heavy line through the middle. The second graph shows the smoothed daily variation obtained as described in the text. The vertical bars show the calculated amplitude of the diurnal component for each day calculated at 12 hourly intervals. The lowest curve shows the time of the maximum of the calculated wave in hours U.T.

amplitude is large. On the other hand, gradual changes of phase, sometimes amouting to the loss (or more often the gain) of a whole cycle, which occur when the amplitude is small, seem to be significant. For example, the shift on April 3 and 4 is found also in the data from Sulphur Mountain, Climax, Tokyo centered on June, 1958. Fig. 4 includes stations that are geographically close together and shows also the data from an ion chamber enclosed in a graphite moderator at Deep River. This ion chamber is sensitive to neutrons of lower energy than the standard neutron monitor. Fig. 5 shows the results from

widely separated stations. Resolute has been included for interest although the phase determinations are unsatisfactory because of the relatively small counting rate.

nearby stations, especially when the amplitude is large. For the more distant stations a correlation is evident, but it is less good. The graphs showing the time of the maximum, which was

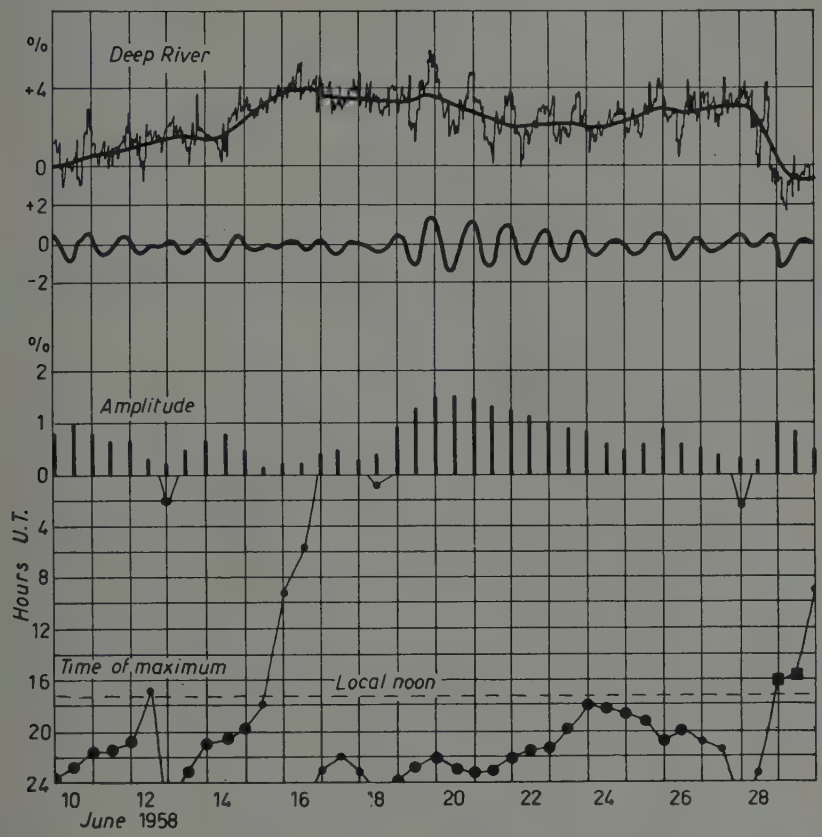

Fig. 2. – Similar curves showing enhanced diurnal variations commencing spontaneously on June 19, 1958.

It is evident from Figs. 4 and 5 that there is a good correlation in the fluctuations of the amplitude of the diurnal wave for nearby stations and that fair world-wide correlation exists. The amplitudes tend to be smaller near the magnetic equator (Huancayo and Tokyo) and near the magnetic pole (Resolute). It is also evident from Fig. 4 that there is a good correlation in the (local) time of maximum of the diurnal wave for

computed in Universal Time, have been displaced vertically in Figs. 4 and 5 so that local noon coincides. The correlation can be still further improved by making the corrections shown in Table I. This indicates, as is known, that the time of maximum of the diurnal wave is a function of latitude, being earlier in the day for the more equatorial stations.

In the vicinity of a sharp Forbush decrease the analysis yields the ampli-

TABLE I. – *Variation of phase in local time with geographical location.*

Station	Geographical location		Weighted average difference in local time of maximum
Resolute	74.7 N	94.9 W	+ 2.5 (?) h
Sulphur Mt.	51.1 N	115.6 W	+ 0.5
Deep River	46.1 N	77.5 W	0.0
Mt. Washington	42.1 N	73.5 W	— 1.0
Climax	39.4 N	106.2 W	— 0.3
Tokyo	35.7 N	137.5 E	— 2.5
Huancayo	12.1 S	74.2 W	— 2.5
Hobart	42.9 S	147.2 E	— 2.0

tude and phase of a sine wave which is the resultant of two waves; one « spuriously » produced by the decrease itself after subtraction of the running average, and another corresponding to the true diurnal variation on that day. If one

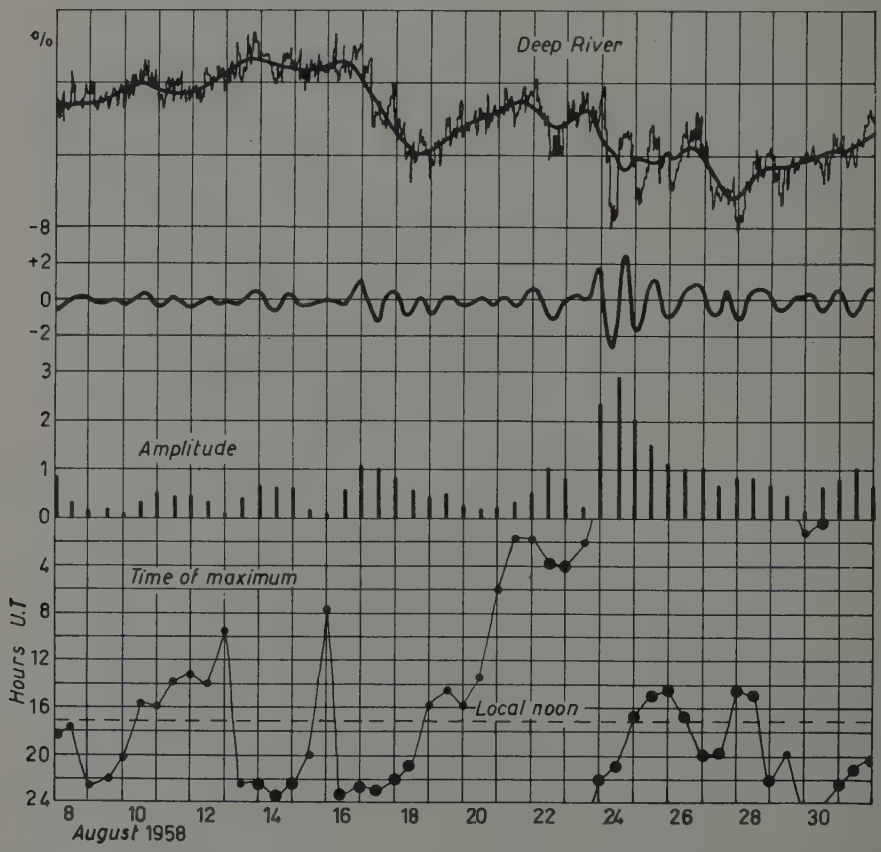

Fig. 3. – Similar curves showing large diurnal variations observed during August, 1958, a period of high magnetic activity.

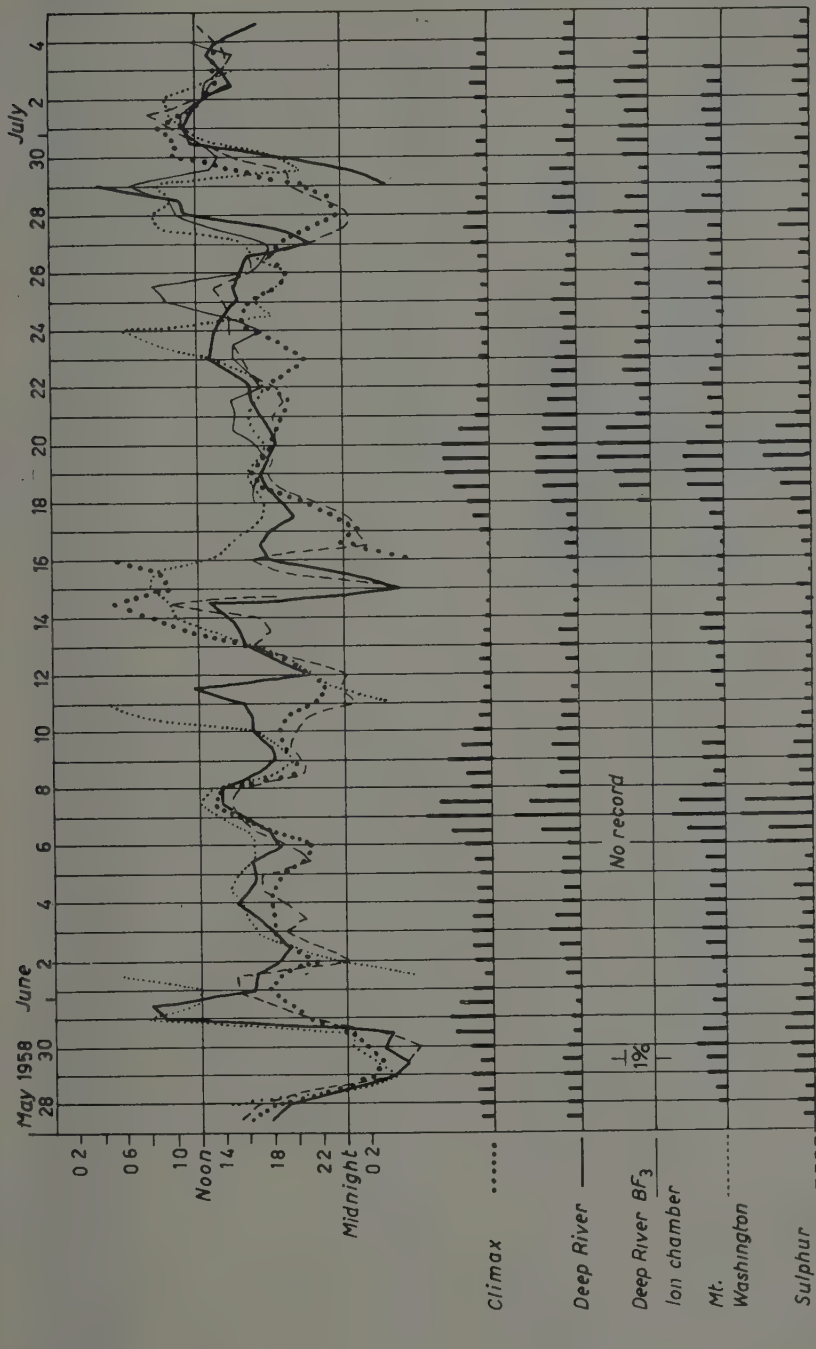

Fig. 4. – The diurnal variation for several nearby IGY stations. The upper part of the figure shows the time of maximum calculated in U.T. A constant is added to the time to make local noon for each station coincide on the graphs. The key to the symbols used is given beside the names in the lower part of the figure, which shows the amplitude in percent at each station.

2433

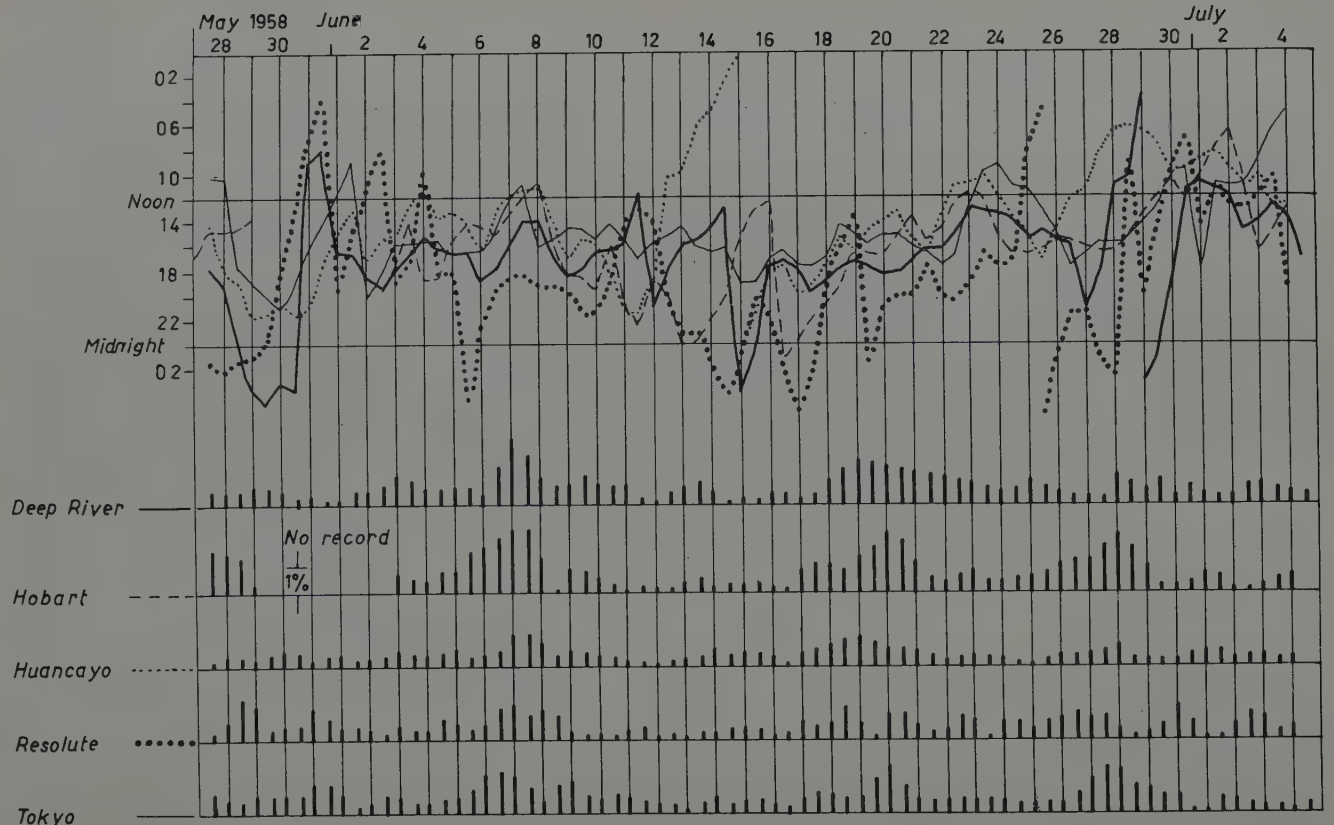

Fig. 5. – The diurnal variation for several, distant IGY stations. The upper part of the figure shows the time of maximum calculated in U.T. A constant is added to the time to make local noon for each station coincide on the graphs. The key to the symbols used is given beside the names in the lower part of the figures, which shows the amplitude in percent at each station.

of these waves is known, the other can be found by vector subtraction. When the spurious wave predominates, all stations show the same time of maximum in Universal Time at about six hours before the steepest part of the decrease which is known to be practically simultaneous over the Earth. When the diurnal effect on the days preceding or following a decrease is large, the time of maximum on the day of the decrease may be displaced implying that a true diurnal effect exists along with the decrease. When a calculation is made for March 25, for instance, the diurnal wave obtained for that day is similar in amplitude and phase to the variations on the following days. Allowance must be made for the different intensities of the Forbush decrease at different latitudes.

The addition of an appreciable diurnal variation having a strong phase dependence on longitude to a general worldwide decrease is responsible for the differing appearance of the Forbush decrease at widely separated stations. The curves shown by McCRACKEN [3] can be explained by assuming that an enhanced diurnal effect began slightly before the advent of the decrease and that the correlation between the enhancement of the daily variation and the decrease is not rigid.

* * *

The writer thanks Dr. H. CARMICHAEL for the benefit of discussion, Miss M. M. HUGHES for computational and graphical assistance, and Dr. J. M. KENNEDY who was responsible for writing the programs for an electronic computer.

[3] K. G. McCRACKEN and N. R. PARSONS: *Phys. Rev.*, **112**, 1798 (1958).

Concerning the Existence of a $\Sigma^- n$ Compound.

E. Gandolfi, J. Heughebaert and E. Quercigh
Istituto Nazionale di Fisica Nucleare - Sezione di Milano

(ricevuto il 30 Giugno 1959)

The programme of the K^- collaboration, this year, includes the study of the details of the interaction at rest of K^--mesons with two or more nucleons in a stack of K-5 emulsions each 600 μm thick, exposed at Berkeley (*). In the course of this work we have carried out measurements of ionization at several points along tracks of Σ-hyperons, of range at emission ⩾ 1 cm (energy ⩾ 56 MeV), to determine their velocity. We have measured 35 Σ-hyperons tracks to date. 33 of them gave good consistency with the calibration, in the limits of the measurement possibilities. Two of them showed an anomalous variation of ionization with path length. These two particles, therefore, warranted closer examination. We chose to concentrate first on that which lay closer to the emulsion plane (dip at emission 6°).

The measurement on the other particle will be reported in the near future.

The particle came from a K^--meson interaction at rest which gave rise to a star of one short black prong and 2 grey prongs. The angle included by the grey prongs was 152°. One of the prongs appeared to be a proton of 81 MeV energy, the other, a singly charged particle, suffered decay into a negative π-meson, after a path length of 22.4 mms. The characteristics of the

Table I.

Primary star				Unknown particle					
Measured mass of K^- primary m_e	Stable particles emitted from K^- star: Nature	Range	Energy MeV	Total path length of particle in emulsion mm	Angle of emission of secondary	Range of secondary mm	Energy of secondary MeV	Sign of secondary	Mass of secondary m_e
(940±80)	Proton P, D, T	21.3 mm 90 μm	81±2	22.4	147° 40′ ±1°	(60.9± 1.8)	(70±1.5)	Negative (ϱ end)	(266±6)

(*) We wish to take this opportunity of thanking the staff at Berkeley for their generous help for this exposure, and Dr. Slater of EFINS, Chicago, who personally made this exposure for the K^- collaboration.

K^--star are therefore those of an interaction of the K^--meson with 2 or more nucleons. In Table I is summarised the information on the K^--star and the decay of the unstable particle.

Careful examination of the track of the particle by two independent observers revealed no single scattering of more than 1° 30′ and no sudden changes in ionization or multiple scattering. The decay point was scrutinized carefully to be sure that the particle was effectively in flight, and that the π-meson secondary arose at this point and was not a casual coincidence of a π-meson crossing the end of the track. The secondary π-meson was followed several times from emission to rest, and vice-versa. Careful search was made at its end for a minimum ionizing particle: none was found. The mass of the π-meson was checked by ionization-range measurements.

Assuming the particle to be a Σ-hyperon, its residual range at decay, deduced from the range and angle of the π-meson secondary is (2.0 ± 0.4) mm. Measurements of gap-length and of scattering at various points along the path of the particle are given in Table II, and compared with the expected values, for a residual range at decay of 2.0 mm, based on a calibration on 15 protons and 3 Σ-hyperons. Also given in the table are measurements on a deuteron. All these tracks come from K^--stars and passed through the same group of plates as the particle in question. All the ionization measurements were made in the central 400 μm of each emulsion.

Gap-length and scattering measurements were performed with a semi-automatic Klausen micrometer [2].

TABLE II.

a) Ionization

Unknown Particle (dip 6°)				Deuteron (dip 16°)			
Residual Range	Value of coefficient « *g* » (*)			Residual Range	Value of coefficient « *g* » (*)		
	Measured	Expected for Σ	Expected for D		Measured	Expected for Σ	Expected for D
0.6 cm	1.18 ± 0.08	0.91 ± 0.02	1.19 ± 0.02	0.9 cm	1.02 ± 0.07	0.70 ± 0.02	0.98 ± 0.02
1.7 cm	0.58 ± 0.04	0.46 ± 0.01	0.63 ± 0.01	1 cm	0.92 ± 0.07	0.64 ± 0.01	0.88 ± 0.02
2.4 cm	0.49 ± 0.03	0.37 ± 0.01	0.51 ± 0.01	1.8 cm	0.59 ± 0.04	0.45 ± 0.01	0.61 ± 0.01
				cm 2.3	0.54 ± 0.04	0.38 ± 0.01	0.52 ± 0.01

(*) « *g* » is proportional to the ionization parameter of Fowler-Perkins [1].

b) Scattering of the unknown particle.

Residual Range	Value of the $p\beta$		
	Measured (MeV/c)	Expected for Σ (MeV/c)	Expected for D (MeV/c)
0.5 cm	99 ± 14	77	94
1.0 cm	139 ± 27	113	138
1.5 cm	186 ± 24	142	174
2.0 cm	197 ± 24	166	204

(1) P. FOWLER and H. PERKINS: *Phil. Mag.*, **46**, 587 (1955).

(2) A. BONETTI, C. DILWORTH, M. LADU and G. OCCHIALINI: *Rend. Acad. Naz. Lincei*, **17** 311 (1954); G. ALVIAL and S. STANTIC: *Nuovo Cimento*, **5**, 1333 (1957); S. COLOMBO, G. GABBA, E. GANDOLFI and E. QUERCIGH: *Comptes Rendus*, 2me *Colloque de Photographie Corpusculaire*, Montréal (1958).

It is clear that our particle has a mass closer to that of the deuteron than that of a Σ-hyperon.

From the variation of gap-length with range, leaving undetermined the residual range, the mass of the particle was calculated, and was found to be,

$$(3\,780 \pm 175)\ m_e\ .$$

The value of the mass from the variation of scattering with range was,

$$(4\,210 \pm 570)\ m_e\ ,$$

(measurement with constant cell).

The weighted mean of these two values is $(3\,817 \pm 167)\ m_e$.

We have therefore a particle of charge 1 of mass approximately twice that of the proton, which decays in flight with emission of a negative π-meson, of energy 70 MeV. Its presence in an interaction of K^--meson leads to an attribution of strangeness -1 and baryonic number 2.

The time of flight of this particle was $2 \cdot 10^{-10}$ s. Using the scheme of the known particles, the most reasonable interpretation of the event is that it is a Σ^--neutron hyperfragment.

Assuming the particle to be a Σ^-n hyperfragment, the total visible energy release in the K^--star is (469 ± 3) MeV. The momentum unbalance being 440 MeV/c, it cannot be taken up by a single neutron, but could be the momentum of recoil of the residual nucleus. Such a recoil, if of an Ag or Br nucleus, would be redily obscured by the star center.

It is, of course, not possible to determine the binding energy of such a compound on a single event. One can obtain only some indication by comparison of the momentum of the Σ-hyperon corresponding to the velocity of the compound, and its momentum given by the dynamics of decay, supposing the decay to have taken place along the line of flight of the compound.

The residual range of the compound is:

(3.3 ± 0.3) mm from gap counting,

(3.0 ± 0.6) mm from constant sagitta,

giving a weighted mean of $(3.24 \pm \pm 0.27)$ mm. This corresponds to a velocity: $\beta = 0.196$, and a momentum of the Σ^--hyperon of (237 ± 5) MeV/c.

A secondary π-meson of (70 ± 2) MeV kinetic energy, emitted at an angle of $147° 40' \pm 60'$, corresponds to a momentum of (235 ± 15) MeV/c of the Σ^--hyperon. Clearly the coincidence of these two values, which would seem to indicate that the Σ^--hyperon decay is little affected by the presence of the neutron, cannot be considered as significant until more examples are available.

The existence of such Σ-hyperon nucleon compounds has been discussed by various authors ([3-5]). The type Σ^-n is expected to be more stable than Σ^+p due to the absence of Coulomb repulsion. BALDO-CEOLIN *et al.* ([6]) have reported an event which they interpret as probable evidence for a Σ^+p compound. There are however alternative interpretations of the event, which the authors discuss.

Estimates ([7,8]) have been made of the probability of formation of hyperon-nucleon compounds in the interaction of K^--mesons with deuterium. Experimental data ([9]) so far have given no evidence for such a compound among 45 events of the type

$$K^- + d \to \Sigma^- + n + \pi^+\ .$$

([3]) W. G. HOLLADAY, quoted by R. G. SACHS: *Phys. Rev.*, **99**, 1573 (1955).

([4]) R. H. DALITZ: *Nucl. Phys.*, **1**, 372 (1956).

([5]) F. FERRARI and L. FONDA: *Nuovo Cimento*, **5**, 1027 (1957).

([6]) M. BALDO-CEOLIN, W. F. FRY, W. D. B. GREENING, H. HUZITA and S. LIMENTANI: *Nuovo Cimento*, **6**, 144 (1957) and *Padua Conference* (1957), page II-96.

([7]) A. PAIS and S. TREIMAN: *Phys. Rev.*, **107**, 1396 (1957).

([8]) T. B. DAY and G. A. SNOW: *Phys. Rev. Lett.*, **2**, 59 (1959).

([9]) R. D. TRIPP: *CERN Conference* (1958).

Compound formation should be easier in K^--interactions with the more closely associated nucleons of the emulsion nuclei. It seems reasonable to look for these events among the K^--multinucleon interactions.

The lifetime of the Σ^-n compound may be the same, or differ from that of the free Σ^+ hyperon. In either case, a contamination of Σ^-n, indistinguishable from normal Σ-hyperon decays if the track is short, could affect the apparent Σ-lifetime, due to the different time in slowing down. This could be connected with the difference in Σ-lifetime as measured in emulsion from that found in hydrogen bubble chamber.

It is possible ([10]) that the interaction with the emulsion nuclei of such Σ^--compounds containing one or more neutrons has already been observed ([11,12]) and interpreted otherwise.

* * *

We are indebted to Dr. H. GREENBERG and Mr. C. WALLER for having made ionization and scattering measurements easier by providing the new K-5 emulsions.

We wish to thank the members of the K^--collaboration, and in particular our colleagues in Milan, who provided the organisation and material on which this work was based. We are very grateful for the close co-operation and guidance of Drs. A. BONETTI and C. DILWORTH, and for the invaluable criticism and direction of Prof. G. OCCHIALINI. Our gratitude goes also to Prof. L. BROWN and to Prof. F. DUIMIO, Dr. F. DELL'ANTONIO, Dr. M. PAURI and Dr. V. AMAR for many helpful discussions. We wish to thank our friends Mr. GARBARI and Mr. GENTILE for their affectionate assistance. Two of us (E.G. and J. H.) wish to thank Prof. P. CALDIROLA for having extended to us the financial assistance and facilities of the Milan Section of the I.N.F.N.

([10]) G. OCCHIALINI: private communication.

([11]) M. M. BLOCK and D. T. KING: *Phys. Rev.*, **97** 1415 (1955).

([12]) Y. EISENBERG: *Phys. Rev.*, **96**, 541 (1954); *Suppl. Nuovo Cimento*, **2**, 484 (1956).

IL NUOVO CIMENTO Vol. XIII, N. 4 16 Agosto 1959

(n, d) Reactions with 14 MeV Neutron Energy.

L. Colli

Istituto di Fisica dell'Università - Milano
Laboratori CISE - Milano

F. Cvelbar (*), S. Micheletti and M. Pignanelli

Istituto di Fisica dell'Università - Milano
Istituto Nazionale di Fisica Nucleare - Sezione di Milano

(ricevuto l'8 Luglio 1959)

In recent measurements with neutrons of 14 MeV, we established the existence of n, d reactions in various nuclei, as announced in a recent paper (1).

An interesting point about these reactions is that they are present in almost all the nuclei studied, with a cross-section of the same order of magnitude as that of the n, p reactions.

It is therefore important to put emphasis on the following point: every time the energy balance makes it possible, the spectra of reactions n, p are certainly contaminated by a quantity of deuterons, when no selection is made between the two types of emitted particles, protons or deuterons.

Under this viewpoint, all previous works (2-5) should be reviewed.

The cross-section and the spectrum for the n, d reaction for deuterons emitted in forward angles have been measured in our laboratory for the elements: ^{27}Al, ^{31}P, ^{32}S, ^{40}Ca, ^{63}Cu, ^{107}Rh.

In this work we are presenting the spectrum for the elements ^{31}P and ^{32}S, which out of all the elements studied

(*) On leave from Jozef Stefan Institut, Ljubljana.

(1) See L. Colli, U. Facchini, I. Iori, G. Marcazzan and A. Sona: under publication on *Il Nuovo Cimento*.

(2) C. Badoni, L. Colli and U. Facchini *Nuovo Cimento*, **4**, 1618 (1956); L. Colli and U. Facchini: *Nuovo Cimento*, **5**, 309 (1957).

(3) R. A. Peck: *Phys. Rev.*, **106**, 965 (1957); H. P. Eubank, R. A. Peck and F. L. Hassler: *Nuclear Physics*, **9**, 273 (1958); H. P. Eubank, R. A. Peck and M. R. Zatrikc: *Nuclear Physics*, **10**, 418 (1959).

(4) G. Brown, G. C. Morrison, H. Muirhead and W. T. Morton: *Phil. Mag.*, **2**, 735 (1957); P. V. March and W. T. Morton: *Phil. Mag.*, **3**, 143, 577 and 1256 (1958).

(5) D. L. Allan: *Proc. Phys. Soc.*, A **70**, 195 (1957); also *Nuclear Physics*, **6**, 464 (1958) and *Nuclear Physics*, **10**, 348 (1959).

have an unexpectedly big cross-section. The spectra are seen in Fig. 1 and 2.

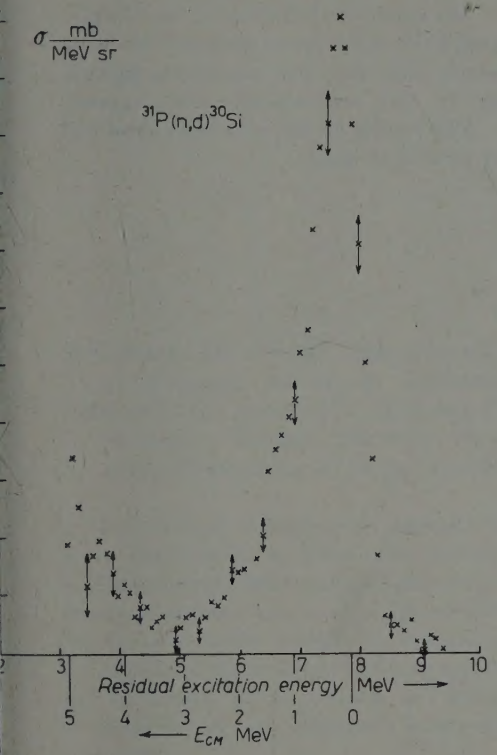

Fig. 1. – Deuteron spectrum from ^{31}P. On the abscissae are shown the proton energy scale and the residual excitation energy scale.

The most remarkable characteristic of these reactions is that they have an intense deuteron line corresponding to the fundamental state of the residual nucleus, in both the elements studied, while a few less intense lines are visible in the case of ^{32}S, corresponding to the excited levels at 1.26, 2.23 and at 3.1 MeV of the residual nucleus ^{31}P. A level seems to be shown also at 0.8 MeV.

This type of spectrum, where the fundamental state is predominant, shows that the n, d reaction proceeds by means of a mechanism of the direct type.

This result can be compared with the predictions of Butler's theory about an n, d reaction of the pick-up type, where the proton is snatched from the nucleus by the incident neutron.

In the two reactions presented in this paper, the transition leading to the

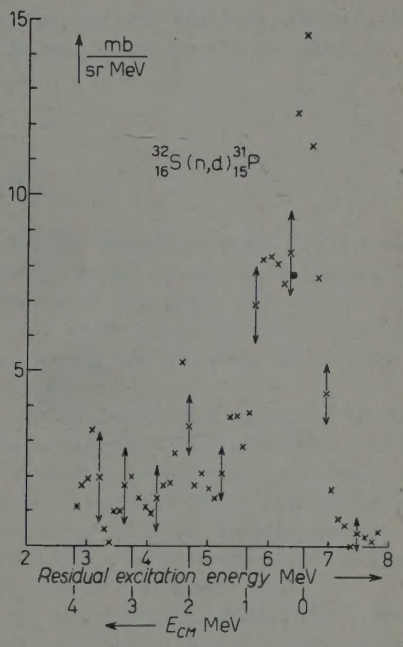

Fig. 2. – Deuteron spectrum from ^{32}S.

fundamental state allows an angular momentum given to the nucleus $l_{min} = 0$ from total angular momentum conservation. Following Butler's theory it should therefore be expected that the reaction should give a high intensity forward.

This is also in excellent agreement with the angular momentum predicted by the shell model for the last proton in both ^{31}P and ^{32}S nuclei. Both of them, following the independent particle description, have in fact the last proton on a s level, giving therefore origin to a pick-up reaction with an $l = 0$ transition allowed.

The very high cross-section for the two fundamental states shows that the single particle reduced width for proton

emission is rather large in this case, that is the ^{31}P and ^{32}S fundamental states can be considered to be made by a core plus one proton. This is quite clear for ^{31}P, which has one s proton after the closed subshell $d\frac{5}{2}$.

^{32}S has two protons; it is indeed interesting to see that the intense peak in ^{32}S is made up of two peaks one at 0 excitation energy and one at 0.8 excitation energy, perhaps corresponding to the two non degenerate states.

The other excited levels of the ^{32}S spectrum have much lower intensity, showing clearly that they are not single particle (or, in this case « single hole ») states.

The results on the other elements will be published soon.

LIBRI RICEVUTI E RECENSIONI

Handbuch der Physik, *Encyclopedia of Physics*, editor, S. FLÜGGE, volume 37/1; Atomi III, Molecole I; Springer - Verlag, Berlino, Gottinga, Heidelberg, 1959, pp. VI-439.

Tre articoli compongono questo volume dell'*Handb. d. Phys.*: un articolo di KUSCH e HUGHES sulla spettroscopia dei raggi atomici e molecolari, un articolo di NIELSEN sulle energie di vibrazione e rotazione delle molecole ed i loro spettri nell'infrarosso, ed un articolo di CRAGGS e MASSEY su le collisioni elettroni-molecole.

L'articolo di KUSCH e HUGHES contiene all'inizio una esposizione della metodologia e quindi espone dapprima la spettroscopia atomica e quindi quella molecolare. L'articolo di NIELSEN è essenzialmente teorico, e dopo una introduzione generale di meccanica quantistica affronta il problema del calcolo delle energie delle molecolepoliatomiche e dei loro spettri nell'infrarosso con le relative anomalie.

Infine l'articolo di CRAGGS e MASSEY tratta dapprima dello scattering elastico ed inelastico di elettroni contro molecole, quindi esamina in dettaglio le particolari eccitazioni di stati di vibrazione e di rotazione e le ionizzazioni di molecole diatomiche e poliatomiche.

I tre articoli si distinguono per la loro completezza e per la cura con cui sono scritti. Riteniamo che per molto tempo serviranno di riferimento per il lavoro degli specialisti in questi importanti campi di ricerca.

R. GATTO

Direttore responsabile: G. POLVANI

Tipografia Compositori - Bologna

Questo fascicolo è stato licenziato dai torchi il 10-VIII-1959

2444